

https://dspace.org/

Green element solutions for inverse groundwater contaminant problems

Onyari, Ednah Kwamboka

2016

http://hdl.handle.net/10539/20616

Downloaded from a DSpace repository. https://dspace.org/

GREEN ELEMENT SOLUTIONS FOR INVERSE GROUNDWATER CONTAMINANT PROBLEMS

Ednah Kwamboka Onyari

A Thesis submitted to the Faculty of Engineering and the Built Environment, University of the Witwatersrand, Johannesburg, in fulfilment of the requirements for the degree of Doctor of Philosophy

JOHANNESBURG, 2016

DECLARATION

I declare that this Thesis is my own unaided work. It is being submitted for the Degree of Doctor of Philosophy in the University of the Witwatersrand, Johannesburg. It has not been submitted before for any degree or examination in any other University.

_____

(Signature of candidate)

_____ day of _____ year _____
day *month* *year*

ABSTRACT

In this work two inverse methodologies are developed based on the Green element method for the recovery of contaminant release histories and reconstruction of the historical concentration plume distribution in groundwater. Unlike direct groundwater contaminant transport simulations which generally produce stable and well-behaved solutions, the solutions of inverse groundwater contaminant transport problems may exhibit non-uniqueness, non-existence and instability, with escalation in computational challenges due to paucity of data.

Methods that can tackle inverse problems are of major interest to researchers, and this is the goal of this work. Basically, the advection dispersion equation which governs the transport of contaminants can be handled by analytical or numerical methods like the Finite element method, the Finite difference method, the Boundary element method and their many variants and hybrids. However, if a numerical method is used to solve an inverse problem the resulting matrix is ill-conditioned requiring special techniques to be employed in order to obtain meaningful solutions. In view of this we explore the Green element method, which is a hybrid technique, based on the boundary element theory but is implemented in an element by element manner. This method is attractive to inverse modelling because of the fewer degrees of freedom that are generated at each node. We develop two approaches, in the first approach inverse Green element formulations are developed, the ill-conditioned matrix that results is decomposed with the aid of the singular value decomposition method and solved using the Tikhonov regularized least square method. The second approach utilizes the direct Green element method and the Shuffled complex evolutionary (SCE) optimization method.

Finally, the proposed approaches are implemented to solve typical problems in contaminant transport with analytical solutions besides those that have appeared in various research papers. An investigation on the capability of these approaches for the simultaneous recovery of the source strength and the contaminant concentration distribution is carried out for three types of sources and they include boundary

sources, instantaneous point sources and continuous point sources. The assessment accounts for different transport modes, time discretization, spatial discretization, location of observation points, and the quality of observation data.

The numerical results demonstrate the applicability and limitations of the proposed methodologies. It is found in most cases that the solutions with inverse GEM and the least squares approach are of comparable accuracy to those with direct GEM and the SCE approach. However, the latter approach is found to be computationally intensive.

I dedicate this work to Trevor and Sophie for a hope and a bright future to come.

ACKNOWLEGEMENT

To start with, I would like to thank God for being my cornerstone and strength throughout this journey.

I am grateful for the opportunity to acknowledge various people who made my study possible. First of all, I offer my sincere gratitude to my supervisor Professor A. E. Taigbenu, who through many discussions provided invaluable input and guided this work. I appreciate his effort and critique that directed and shaped this study. I would also like to thank Professor J. Ndiritu for providing guidance on part of this work.

I am greatly indebted to the University of South Africa, my employer who provided financial support for my studies. In addition, I would like to thank my supervisor Prof A. E. Taigbenu who provided partial funding for my last year of study. This financial support allowed me to concentrate on my studies.

I would like to thank my parents for engraining in me the need for education, and the querying on my progress throughout the study period that urged me to keep going. Last but not least, I would like to thank my husband Dr. E. M. Benecha for his moral support and for his encouraging words when I was in doubt.

TABLE OF CONTENTS

DECLARATION……... ii
ABSTRACT…….. iii
ACKNOWLEGEMENT…….. vi
TABLE OF CONTENTS…… vii
LIST OF FIGURES…….. x
LIST OF TABLES……xv
LIST OF SYMBOLS……...xvi
NOMENCLATURE……..xviii
1 INTRODUCTION…….1
1.1 Background 1
1.2 Study aim and objectives.....3
1.2.1 Study aim..... 3
1.2.2 Study objectives 4
1.3 Thesis outline 4
2 LITERATURE REVIEW……6
2.1 Inverse problems 6
2.1.1 Definition of an inverse problem 6
2.1.2 Inverse problem classification..... 7
2.2 Groundwater flow and contaminant transport in porous media 7
2.2.1 Governing equations..... 7
2.2.2 Initial and Boundary conditions 9
2.3 Categories of the inverse problem.....10
2.3.1 Unknown boundary conditions 10
2.3.2 Unknown initial conditions..... 11
2.3.3 Unknown source strength from point sources..... 12
2.4 Solution techniques of forward contaminant transport 12
2.4.1 Analytical methods 12
2.4.2 Numerical methods 13

2.4.3 Boundary Element formulation for Advection Dispersion Equation ... 17
2.5 Solution techniques for inverse contaminant transport problems 19
2.5.1 Optimization 20
2.5.2 Regularization and stabilization approaches 21
2.5.3 Reversed time approaches 22
2.5.4 Probabilistic methods 23
3 THE GREEN ELEMENT METHOD WITH TIKHONOV REGULARIZATION 27
3.1 Green Element Formulation for 2D direct contaminant transport 28
3.2 Inverse GEM Formulations 32
3.2.1 Formulation 1: Unknown boundary conditions and source strength of point sources 32
3.2.2 Formulation 2: Unknown initial conditions 34
3.3 GEM and the least squares approach 35
3.3.1 Singular value decomposition (SVD) 35
3.3.2 Tikhonov regularization 37
4 THE SHUFFLED COMPLEX EVOLUTIONARY OPTIMIZER AND GEM 41
4.1 Overview of global optimization techniques 41
4.2 Shuffled Complex Evolution optimization method 41
4.2.1 Description of SCE-UA 41
4.2.2 Applications of SCE-UA 44
4.2.3 Further developments of the SCE-UA 46
4.2.4 Choice of the optimization method 47
4.3 The SCE-GEM model 48
4.3.1 Linking GEM model and the SCE-UA optimizer 49
4.3.2 Performance evaluation criterion 50
5 RESULTS AND DISCUSSION 51
5.1 Sensitivity analysis 51
5.1.1 Sensitivity to observation data 51
5.2.1 Sensitivity to spatial discretization 57

5.2 Boundary source problems 64
5.2.1 Test Case 1: 1D problem with a continuous constant source 64
5.2.2 Test case 2: 1D problem with a decaying source 83
5.2.3 Test case 3: 2D steady state problem with a sinusoidal source 93
5.2.4 Test case 4: 2D transient problem with a flux boundary source. 102
5.2.5 Test case 5: 2D transient problem with a flux boundary source 108
5.3 Instantaneous point source problems 113
5.3.1 Test case 1: 2D domain with a single instantaneous source. 114
5.3.2 Test case 2: 2D domain with multiple instantaneous pollutant sources 118
5.4 Continuous point source problems 127
5.4.1 Test case 1: Injection of a pollutant at a point into a uniform steady flow 128
5.4.2 Test case 2: A continuous injection at multiple points into a uniform steady flow 134
5.4.3 Test case 3: Transient continuous point source located at the origin 137
5.5 Case study.....148
5.5.1 Identification of source fluxes using data with measurement error 155
5.5.2 Identification of source fluxes using data with parameter error 159
5.5.3 Identification of source fluxes considering multiple potential sources 160
5.5.4 The influence of time discretization on identification of source fluxes 162
6 CONCLUSIONS & RECOMMENDATIONS……164
REFERENCES……...……...…167
APPENDICES……..….182

LIST OF FIGURES

Figure 2. 1: Direct contaminant transport problem statement. 9
Figure 2.2: Inverse problem statement for contaminant transport. 11
Figure 2.3: 2D computational domain for BEM formulation. 18
Figure 3.1: The L-curve and its properties 39
Figure 4.1: Flowchart of the Shuffled Complex Evolution (SCE-UA) method 43
Figure 5.1: Problem statement for source identification in 1D porous media. 53
Figure 5.2: The estimated source strength with respect to location of observation point. 54
Figure 5.3: The average relative error for the computed source strength with respect to location of observation point. 54
Figure 5.4: The estimated source strength with respect to number of observation data. 56
Figure 5.5: The mean error with respect to the number of observation data. 56
Figure 5.6: Model 1 and exact solutions for the concentration with 5, 10, 20 uniform elements, and 14 non-uniform elements for Case (i): $\boldsymbol{k} = \mathbf{10}$. 59
Figure 5.7: Model 1 and exact solutions for the concentration with 5, 10, 20 uniform elements, and 14 non-uniform elements for Case (i): $k = 40$. 60
Figure 5.8: Mean error for the computed concentration by Model 1 for Case (i). 60
Figure 5.9: Model 1 and exact solutions for concentration with 5, 10 and 20 elements for Case (ii) Test (i). 63
Figure 5.10: Model 1 and exact solutions for concentration with 5, 10 and 20 elements for Case (ii) Test (ii). 63
Figure 5.11: Mean error for the computed concentration by Model 1 Case (ii). 64
Figure 5.12: Model 1 computed source strength for $\boldsymbol{Pe} = \mathbf{50}$ Test Case 1(i). 67
Figure 5.13: Model 1 computed contaminant concentration for $\boldsymbol{Pe} = \mathbf{50}$ of Test Case 1(i). 68
Figure 5.14: Model 2 simulation runs for $\boldsymbol{Pe} = \mathbf{50}$ of Test Case 1(i). 69
Figure 5.15: Model 1 and Model 2 computed solutions of the contaminant source strength for $\boldsymbol{Pe} = \mathbf{50}$ with $\boldsymbol{Cr} = \mathbf{0.5}$ of Test Case 1(i). 70
Figure 5.16: Model 1 and Model 2 solutions for the concentration contaminant fronts for $\boldsymbol{Pe} = \mathbf{50}$ with $\boldsymbol{Cr} = \mathbf{0.5}$ of Test Case (i). 70
Figure 5.17: Mean error for the concentration distribution for Model 1 and Model 2 with $\boldsymbol{Pe} = \mathbf{50}$ of Test Case 1(i). 71
Figure 5.18: Model 1 computed source strengths with different Courant numbers for $\boldsymbol{Pe} = \mathbf{1}$ of Test Case 1 (ii). 72
Figure 5.19: Model 1 computed contaminant concentration fronts for $\boldsymbol{Pe} = \mathbf{1}$ of Test Case 1 (ii). 72
Figure 5.20: Model 2 objective function plot for $\boldsymbol{Pe} = \mathbf{1}$ of Test Case 1 (ii). 73
Figure 5.21: Model 1 and Model 2 computed source strengths for $\boldsymbol{Pe} = \mathbf{1}$ of Test Case 1 (ii). 74
Figure 5.22: Model 1 and Model 2 computed concentration for $\boldsymbol{Pe} = \mathbf{1}$ of Test Case 1 (ii). 74

Figure 5.23: Mean error for the computed concentration by Model 1 and 2 for $\boldsymbol{Pe = 1}$ of Test Case 1 (ii). 75
Figure 5.24: Model 1 computed source strength for $\boldsymbol{Pe = 0.05}$ of Test Case 1 (iii). 76
Figure 5.25: Model 1 computed plume concentration with $\boldsymbol{Pe = 0.05}$ of Test Case 1 (iii). 76
Figure 5.26: The objective function plot for Pe=0.05 of Test Case 1 (iii). 77
Figure 5.27: Model 1 and 2 computed source strength for *Pe*=0.05 of Test Case1 (iii). 78
Figure 5.28: Model 1 and 2 computed concentration distribution for $\boldsymbol{Pe = 0.05}$ of Test Case 1 (iii). 78
Figure 5.29: Mean error for the computed concentration by Model 1 and Model 2 for $\boldsymbol{Pe = 0.05}$ of Test Case 1(iii). 79
Figure 5.30: Model 1 computed source strength with noisy observation data for $\boldsymbol{Pe = 50}$ and $\boldsymbol{Cr = 1.0}$ of Test case 1 (i). 80
Figure 5.31: Model 1 computed concentration distribution with noisy observation data for $\boldsymbol{Pe = 50}$ and $\boldsymbol{Cr = 1.0}$ of Test Case 1 (i). 80
Figure 5.32: Model 1 computed source strength with noisy observation data for $\boldsymbol{Pe = 1}$ and $\boldsymbol{Cr = 1.0}$ of Test case 1 (ii). 81
Figure 5.33: Model 1 computed concentration fronts with noisy data for $\boldsymbol{Pe = 1}$ and $\boldsymbol{Cr = 1.0}$ of Test Case 1 (ii) 81
Figure 5.34: Model 1 computed source strength with noisy observation data for $\boldsymbol{Pe = 0.05}$ and $\boldsymbol{Cr = 1.0}$ of Test Case 1 (iii). 82
Figure 5.35: Model 1 computed concentration with noisy observation data for $\boldsymbol{Pe = 0.05}$ and $\boldsymbol{Cr = 1.0}$ of Test case 1 (iii). 82
Figure 5.36: 1D porous medium with a decaying source. 83
Figure 5.37. The exact and Model 1 solutions for the source strength for $\boldsymbol{Pe = 50}$ of Test case 2. 85
Figure 5.38: The exact and Model 1 computed concentration distribution of $\boldsymbol{Pe = 50}$ of Test Case 2. 85
Figure 5.39. Model 1 estimated source strength for $\boldsymbol{Pe}$ =1 of Test Case 2. 87
Figure 5.40: Exact and Model 1 computed concentration distribution for $\boldsymbol{Pe = 1}$ of Test Case 2. 87
Figure 5.41: Model 2 objective function plot for $\boldsymbol{Pe = 1}$ of Test case 2. 88
Figure 5.42: Model 1 and 2 computed source strength for $\boldsymbol{Pe = 1}$ and $\boldsymbol{Cr = 0.6}$ of Test case 2. 89
Figure 5.43: Model 1 and 2 computed concentration distribution for $\boldsymbol{Pe}$ =1 and $\boldsymbol{Cr = 0.6}$ of Test case 2. 89
Figure 5.44: Mean error for computed concentration by Model 1 and 2 for $\boldsymbol{Pe = 1}$ of Test case 2. 90
Figure 5.45: The exact and Model 1 estimated source strength for $\boldsymbol{Pe = 50}$ of Test case 2 with noisy observation data. 91
Figure 5.46: The exact and Model 1 computed concentration distribution for $\boldsymbol{Pe = 50}$ and $\boldsymbol{Cr = 1}$ of Test case 2 with noisy observation data. 91
Figure 5.47: The exact and Model 1 computed source strength for $\boldsymbol{Pe = 1}$ and $\boldsymbol{Cr = 1}$.0 of Test case 2 with noisy observation data. 92

Figure 5.48: The exact and Model 1 computed concentration distribution for $\boldsymbol{Pe} = \mathbf{1}$ and $\boldsymbol{Cr} = \mathbf{1.0}$ of Test case 2 with noisy observation data. 92
Figure 5.49. Computational domain for Test case 3 (crossed circles indicate observation sampling points). 94
Figure 5.50: Model 2 objective function plot for $\boldsymbol{Pe} = \mathbf{50}$ of Test case 3. 95
Figure 5.51: Model 1 and Model 2 computed source strength for $\boldsymbol{Pe} = \mathbf{50}$ of Test case 3. 95
Figure 5.52 : Concentration contours of Test case 3 for $\boldsymbol{Pe} = \mathbf{50}$. Solid black lines- exact solution, Model 1 solution -blue dash lines and Model 2 solution- grey dash lines. 96
Figure 5.53: The exact, Model 1 and Model 2 computed source strength solutions for $\boldsymbol{Pe}$ =1 of Test Case 3. 97
Figure 5.54: Concentration contours for $\boldsymbol{Pe} = \mathbf{1}$ of Test Case 3. Solid black lines - exact solution, Model 1 solution - blue dash lines and Model 2 solution- grey dash lines. 97
Figure 5.55: Model 2 objective function plot for $\boldsymbol{pe}$ =1 of Test case 3. 98
Figure 5.56: The exact, Model 1 and Model 2 solutions of the source strength, $\boldsymbol{Pe} = \mathbf{0.05}$ of Test case 3. 99
Figure 5.57: Concentration contours of Test case 3 for $\boldsymbol{Pe} = \mathbf{0.05}$. Black solid lines represent the exact solution, the blue dash lines show Model 1 solution, and the grey dash lines represent Model 2 solution. 99
Figure 5.58: Model 2 objective function plot for $\boldsymbol{Pe} = \mathbf{0.05}$ of Test case 3. 100
Figure 5.59: Model 1 computed source strength of $\boldsymbol{Pe} = \mathbf{50}$ of Test case 3 with noisy observation data 101
Figure 5.60 : Model 1 computed source strength for $\boldsymbol{Pe} = \mathbf{1}$ with noisy observation data of Test case 3. 101
Figure 5.61: Model 1 computed source strength of $\boldsymbol{Pe} = \mathbf{0.05}$ with noisy observation data of Test case 3. 102
Figure 5.62: Schematic representation of Test case 4 and 5. 103
Figure 5.63: Plot of Test case 4 (a) exact solution (b) Computed flux by Model 1 using exact measurements, $\boldsymbol{\varepsilon} = \mathbf{0.0}\%$ (c) noisy data, $\boldsymbol{\varepsilon} = \mathbf{0.1}\%$ (d) noisy data, $\boldsymbol{\varepsilon} = \mathbf{0.2}\%$. 105
Figure 5.64: Shows the objective function versus number of simulations for Test case 4. 106
Figure 5.65: Plot of Test case 4 (a) exact flux (b) computed source flux using Model 2. . 106
Figure 5.66: Estimated concentration by Model 1with (a) $\boldsymbol{\varepsilon} = \mathbf{0.0}\%$ (b) $\boldsymbol{\varepsilon} = \mathbf{0.1}\%$ (c) $\boldsymbol{\varepsilon} = \mathbf{0.2}\%$ at time, $\boldsymbol{t} = \mathbf{0}.5$ for Test case 4. 107
Figure 5.67: Mean error for the estimated concentration for Test case 4. 108
Figure 5.68: Plot for Test case 5 (a) exact source flux, (b) Model 1 estimated source fluxes using exact measurements, $\boldsymbol{\varepsilon} = \mathbf{0.0}$ (c) $\boldsymbol{\varepsilon} = \mathbf{0.1}\%$ (d) $\boldsymbol{\varepsilon} = \mathbf{0.2}\%$. 109
Figure 5.69: Plot for the objective function versus the number of simulations for Test case 5. 110
Figure 5.70: Plot showing (a) exact source fluxes (b) Computed source fluxes by Model 2 using exact measurements. 111

Figure 5.71: Estimated concentration by Model 1 with (a) $\boldsymbol{\varepsilon = 0.0\%}$ (b) $\boldsymbol{\varepsilon = 0.1\%}$ (c) $\boldsymbol{\varepsilon = 0.2\%}$ at time, $\boldsymbol{t = 0.5}$. 112
Figure 5.72: Mean error for the computed concentration for Test case 4. 113
Figure 5.73 : Concentration distribution at $\boldsymbol{t = 10}$; graded colour shows the exact plume distribution, and the dashed red line shows Model 1 solution, and the grey colour shows Model 2 solution for Test case 1 with $\boldsymbol{Cr = 1}$. 116
Figure 5.74: Mean error of the computed concentration by Model 1 (in blue) and Model 2 (in red) of Test case 1 with instantaneous sources for various Courant numbers. 117
Figure 5.75: Schematic representation of the aquifer system in Test case 2. The location of the instantaneous sources is shown by the red stars and the sampling points are shown using the red crossed circle. 118
Figure 5.76: Exact, Model 1, and Model 2 computed source strength with exact observation data. 119
Figure 5.77: Contour plots of the concentration distribution at time (t=10). 120
Figure 5.78: Mean error for the computed concentration using Model 1 and 2 with multiple instantaneous sources. 120
Figure 5.79: Exact and computed source strength using noisy observation data for Test case 2. 121
Figure 5.80: Contour plots of the concentration at time $\boldsymbol{t = 10}$. 122
Figure 5.81: The exact in the graded colour and the Model 1 computed concentration with velocity, $\boldsymbol{u = u + 10\%u}$ at time $\boldsymbol{t = 10}$. 123
Figure 5.82: The concentration contours for the exact and computed solutions. 124
Figure 5.83: The exact in the graded colour and the Model 1 computed concentration 125
Figure 5.84: The exact and the computed concentration distribution with velocity and dispersion errors. 126
Figure 5.85: The exact and the computed concentration distribution with velocity, and dispersion errors. 126
Figure 5.86: Exact and computed concentration fronts for velocity, dispersion and both with 10% error along $\boldsymbol{y = 4}$. 127
Figure 5.87: A plot of the objective function versus the number of simulations by Model 2 for Test case 1with point sources. 129
Figure 5. 88: Contour plots of the concentration distribution of Test case 1 simulated with exact observation data. 131
Figure 5. 89: Contour plots of the concentration distribution with error free and 5% observation error. 131
Figure 5.90: A Contour plot of the concentration distribution with velocity errors. 133
Figure 5.91: A contour plot of the computed concentration distribution with dispersion errors. 133
Figure 5.92: Schematic representation of aquifer for Test case 2 with point sources. 135
Figure 5.93: Spatial distribution of contaminant plume of Test case 2 with exact data 136
Figure 5.94: Spatial distribution of contaminant plume of Test case 1 with observation errors 136
Figure 5.95: Computational domain of Test case 3 with a point source. 139

Figure 5. 96: A plot of the objective function versus the number of simulations of Test case 3 in Model 2. 140
Figure 5.97: Model 1 and Model 2 computed source strength of Test Case 3 with point sources. 141
Figure 5.98: Temporal variation of the relative error of the computed source strength by Model 1 and 2 for test case 3. 142
Figure 5.99: The exact concentration distribution is shown in graded colour, the computed solution of Model 1 in red dash line, and the computed Model 2 solution in grey dashed line (a) $\boldsymbol{t = 0.2}$, (b) $\boldsymbol{t = 0.5}$, and (c) $\boldsymbol{t = 1.0}$. 143
Figure 5.100: Temporal variation of the mean relative error of the computed concentration by Mode1 and 2 for test case 3. 144
Figure 5.101: Model 1 computed source strength with time of Test case 3 using noisy observation data. 145
Figure 5.102: Temporal variation of the relative error of the computed source strength for test case 3. 145
Figure 5.103: Model 1 computed concentration distribution at time, $\boldsymbol{t = 1}$ of Test case 3.. 146
Figure 5.104: Temporal variation of the relative error of the computed concentration for test case 3. 147
Figure 5. 105: Schematic representation of the aquifer. 149
Figure 5.106: Concentration distribution contour in the aquifer at various time steps: (a) 3months (b) 12 months. 151
Figure 5.107: Breakthrough curves for observation points γ_2 and γ_1. 153
Figure 5.108: Relative error of computed source fluxes at different time steps. 157
Figure 5.109: Concentration distribution, for the direct solution and computed concentration with $\boldsymbol{\varepsilon = 0}$%, and y $\boldsymbol{\varepsilon = 5}$% (a) 12 months (b) 30 months. .. 158
Figure 5.110: Temporal variation of the mean error for the concentration distribution. ... 159
Figure 5.111: Temporal variation of the mean deviation for the concentration distribution computed with velocity and dispersion errors. 160
Figure 5.112: Relative error of computed source fluxes at different time steps using time discretization $\boldsymbol{\Delta t = 0.25}$. 163

LIST OF TABLES

Table 1.1: Solution techniques for the advection dispersion equation in inverse contaminant transport.....25
Table 5.1: Test scenarios for the analysis of sampling time.....55
Table 5.2: Model 1 computed source strength for unknown boundary for k = 10. 58
Table 5.3: Model 1 computed source strength for unknown boundary for k = 40. 58
Table 5.4: Model 1 computed flux for unknown boundary for k = 10 and k = 40.....59
Table 5.5: Model 1 computed source strength for different element discretizations for case (i). 62
Table 5.6: Model 1 computed source strength for different element discretizations for case (ii). 62
Table 5.7: Computed flux for different element discretizations with ε=0%.....62
Table 5.8: Simulation parameters for Test Case 1 with boundary sources.....65
Table 5.9 : SCE-UA optimization and search termination parameters for Test Case 1. 69
Table 5.10 : SCE-UA optimization and search termination parameters for Test case 2, $\boldsymbol{Pe = 1}$.....88
Table 5.11 : SCE-UA optimization and search termination parameters for all Peclet numbers of Test case 3.....94
Table 5.12: Mean error for the computed concentration using error free and noisy data.....100
Table 5.13: Aquifer parameters and Transport properties for Test case 1 with instantaneous sources. 114
Table 5.14: Test scenario for time discretization using Model 1 of Test case 1 with instantaneous sources.....115
Table 5.15: Test scenario for time discretization using Model 2 of Test case 1 with instantaneous sources.....115
Table 5.16: Computational time (seconds) for Test case 1 with instantaneous sources. 117
Table 5.17: Actual source strengths of the instantaneous sources for Test case 2. 119
Table 5.18: The exact and computed source strengths using randomly perturbed observation data. 121
Table 5.19: Model 1 computed source strength with error in velocity.....123
Table 5.20: Model 1 computed source strength with error in dispersion 123
Table 5.21: Computed source strength with error both in velocity and dispersion. 124
Table 5.22: Computed source strength with opposite error both in velocity and dispersion.....126
Table 5.23: Parameter values used for simulation of the steady state case with point source.....129
Table 5.24: Model 1 and 2 computed source strength for Test case 1 with point source. 130
Table 5.25: Computed source strength with 5% errors in velocity or dispersion.....132
Table 5.26: Computed source strengths by Model 1 and Model 2 for Test case 2.....135
Table 5.27: Computed source strengths by Model 1 while accounting for parameter errors. 137
Table 5.28: Transport parameters used in the simulation of Test case 3.....138
Table 5.29: Flow and transport parameter values 148
Table 5.30: Pumping well rates.....149
Table 5.31: Actual source fluxes for case study.....150
Table 5.32: Case study computed source fluxes by Model 1 and Model 2. 155
Table 5.33: Model 1 computed source fluxes using observation data with random error. 156
Table 5.34: Model 1 computed source fluxes considering parameter errors.....160
Table 5.35: Model 1 computed source fluxes considering multiple potential sources. 161
Table 5.36: Model 1 computed source fluxes using time discretization of Δt=0.25. 162

LIST OF SYMBOLS

∇ Two-dimensional gradient operator in x and y,

Q Contaminant sources or sinks that have a spatial variation

Q_w Sources or sinks in the flow equation

T Transmissivity

K Hydraulic conductivity

S Storativity

h Hydraulic head

C Contaminant concentration

C' Pollution source strength

$\mathbf{V}$ Velocity vector of the transporting medium

u_i Velocity in the x-direction

v_j Velocity in the y-direction

D Hydrodynamic dispersion coefficient

R Retardation factor

μ First-order decay rate coefficient

W_v Recharge volume

η Porosity

b Aquifer thickness

t Time

$\mathbf{n}$ Unit outward pointing normal vector

Ω Computation domain

Γ Boundary

λ	Nodal angle at the source point
q	Flux
L	Aquifer length
α	Regularization parameter
ξ	Amount of observation data
γ	Observation site
PS	Pollutant source

NOMENCLATURE

GEM	Green Element Method
BEM	Boundary Element method
FEM	Finite Element method
FDM	Finite Difference method
SVD	Singular Value Decomposition
SCE-UA	Shuffled Complex evolutionary algorithm
MODFLOW	Modular Three-Dimensional Finite-Difference Groundwater Flow Model
MT3DMS	Modular Transport Three Dimensional Model Simulator
SUTRA	Saturated Unsaturated Transport Model
DRBEM	Dual Reciprocity Boundary Element Method
GA	Genetic Algorithm
ASA	Adaptive Simulated Annealing
QR	Quasi Reversibility
MRE	Minimum Relative entropy
IMSL	International Mathematics and Statistics Library
GCV	Generalized cross validation
NAM	A lumped and conceptual catchment runoff model
MIKE 11	1-dimensional river model
MTD3	Model Transport in 3 Dimensional
MODPATH	Particle Tracking with MODFLOW
SA-SX	Simulated annealing
SCE-GB	Shuffled complex evolutionary- Gradient Based
GBLM	Gradient-based Lavenberg–Marquardt algorithm
MOCOM-UA	Multiobjective Complex Evolution

MCMC	Markov chain Monte Carlo
SCEM-UA	Shuffled Complex Evolution Metropolis
MOSCEM-UA	Multiobjective Shuffled Complex Evolution Metropolis
SP-UCI	Shuffled Complex strategy with Principal Components Analysis
MSCE	Modified Shuffled Complex Evolution

1 INTRODUCTION

In this chapter an introduction to inverse groundwater contaminant transport is given. The discussion starts with a brief background to the problem of groundwater contaminant transport before outlining the problem that is the subject of the current study. The objectives and a brief discussion on the format of the report are given.

1.1 Background

The water quality in an aquifer can degrade due to contaminants that may be released continuously or instantaneously into the subsurface. The former type of release can result from distributed and line sources like landfill sites, mine damps, underground septic tanks, intrusion of salt water from seas and seepage from polluted streams. The latter type may occur due to unintentional spills of toxic substances into groundwater. Contamination may result from a single source or a combination of sources, and because it is often unintentional, it may go undetected for many years, posing many risks to human health and the ecosystem.

Once contamination is detected in an aquifer, it becomes important to monitor, manage and develop a remediation strategy for clean-up. However, because of the huge costs involved for any remediation efforts, it is desired that a concise quantitative understanding of the contaminant characteristics in terms of the source locations, source strengths, number of sources, release duration be known. In most instances, the sources' locations and their characteristics are unknown as records of the release histories of the contaminant sources may not be available, and the originators of the pollution source might have changed over the years. What may be available is the historical distribution of the contaminant at given points within the contaminated aquifer. Thus, it becomes imperative to determine the source characteristics and the plume distribution from limited available data.

This problem of characterizing a contaminant source and reconstructing the historical distribution of a contaminant plume is an inverse problem in

groundwater contaminant transport. Various categories of the inverse problem exist in the literature which include identifying the contaminant source location (Gorelick *et al.,* (1983), Wagner (1992), Mahar *et al*. (2000), Neupauer *et al*. (2000), Neupauer and Wilson (2004)), estimating the number of possible pollution sources (Ayvaz, 2010), estimating the release history (Skaggs and Kabala (1994, 1995), Alapati and Kabala (2000), Sidauruk *et al*. (1998)) and reconstructing the historical distribution of a contaminant (Michalak and Kitanidis (2004), Bagtzoglou and Atmadja (2003)). In this work, the simultaneous recovery of the pollution source strength and the reconstruction of the historical distribution of the concentration plume are addressed.

Mathematical models are widely used in the simulation of groundwater contaminant transport, and when they proceed in a forward modelling fashion, their solutions of the spatial and temporal distributions of the contaminant concentration tend to be uniquely and properly constrained. These forward models are generally stable with well-behaved solution spaces since they are based on the solution of elliptic or parabolic partial differential equations. Their computational challenge arises when advection dominates the contaminant transport process, in which the governing equation is hyperbolic, thereby rendering the differential equation to become "stiff." Although such special cases exist, numerical simulations have been very successful in the field of groundwater modelling.

Unlike direct groundwater contaminant transport simulations which produce generally stable and well-behaved solutions, the solutions of inverse groundwater contaminant transport problems may exhibit non-uniqueness, non-existence and instability (Sun, 1996). Therefore, when inverse modelling is carried out as a result of paucity of the input parameters and the ill-posed nature of the problem, it is generally more challenging and intriguing.

Various numerical methods and their variants have previously been applied to inverse groundwater contaminant transport problems. Examples include the finite difference method (FDM) (Michalak and Kitanidis (2004), Ayvaz (2010), Prakash and Datta (2014)), the finite element method (FEM) (Gorelick *et al.*(1983), Wagner (1992), Datta *et al.*(2009)) and the boundary element method (BEM)

(Lesnic *et al*. (1998), Harrouni *et al.* (1996,1997), Katsifarakis *et al*.(1999)). The methodology proposed in this study is based on the Green element method (GEM) which is founded on the singular integral theory of BEM, but implements the theory in an element-by-element manner (Taigbenu, 1999). GEM has successfully been previously applied to inverse modelling of heat conduction problems (Taigbenu, 2015) and this is the first time it is being applied to inverse groundwater contaminant transport problems.

The GEM formulation followed in this work was recently developed (Taigbenu, 2012) in which a second-order polynomial expression is used to approximate the internal normal fluxes so that only the solution for the concentration or the flux is calculated at external nodes and the concentration at internal nodes. Although this formulation is slightly less accurate than a flux-based one, its ability to generate fewer degrees of freedom per node than the latter makes it more attractive for inverse modelling.

The issue at hand therefore is to develop inverse formulations of GEM that can be used to address inverse contaminant transport problems. However, since solving inverse problems results in ill-conditioned matrices the necessity for regularization is apparent. We therefore explore GEM in conjunction with a regularization approach and an optimization approach.

1.2 Study aim and objectives

1.2.1 Study aim

The main objective of the current research project is to develop inverse GEM formulations for the solution of inverse contaminant transport problems of recovering the release history of contaminant sources and reconstructing the spatial and temporal concentration distribution of the plume.

1.2.2 Study objectives

This goal is achieved through the following specific objectives:

i. To review the direct Green element method formulation for the groundwater contaminant transport problem.
ii. To develop inverse GEM formulations in conjunction with regularization methods for the simultaneous recovery of the release histories of contaminant sources and the reconstruction of the plume's history.
iii. To develop a methodology based on the direct GEM in conjunction with an optimization method to simultaneously recover the release histories of contaminant sources and reconstruct the plume's history.
iv. To demonstrate the use of the developed methods in (ii) and (iii) above on various numerical inverse contaminant transport problems.

1.3 Thesis outline

The previous sections of this chapter explain the purpose and objectives of this study, namely to develop formulations of GEM that solve inverse contaminant transport problems.

In chapter 2 a general introduction is given to inverse contaminant transport. A definition of inverse problems and their classification is provided, and further categorisation of our source identification problem as solved in the remaining chapters of the thesis is presented. An overview of techniques used to solve direct contaminant transport problems is presented. Finally, a brief discussion on inverse techniques that have been implemented to solve inverse contaminant transport problems is presented.

In Chapter 3 we present our first proposed methodology which constitutes of inverse GEM and the singular value decomposition method with the Tikhonov regularized least squares method. Initially, we review the Green element direct formulation for the 2D advection dispersion equation. Later on, we present our inverse GEM formulations for the different inverse problems considered in this

work. Finally, we present how the SVD and Tikhonov regularization approach are used to handle the matrices resulting from the inverse GEM formulation.

In Chapter 4, we present our second proposed methodology which comprises of the direct GEM and the Shuffled complex evolution method. We review the SCE-UA method and give an overview of its applications as well as the modifications of the method. Further on we provide the linkage of GEM and the SCE-UA.

Chapter 5 presents numerical test cases which are solved by the developed methodologies in chapters 3 and 4. Various inverse contaminant transport problems are solved; these include problems with analytical solutions and complex problems that mimic real life problems.

In Chapter 6 the major findings of this study are summarised and the limitations of the study highlighted.

2 LITERATURE REVIEW

2.1 Inverse problems

In recent years, significant developments in solving inverse problems utilizing various solution techniques have been reported. Typical ill-posed problems include numerical differentiation of noisy data (Anderssen and Bloomfield, 1974), the inverse heat conduction problem (Beck, 1985), interpretation of geophysical data (Backus and Gilbert, 1970) and the inverse problem of groundwater hydrology (Yeh, 1986, Neuman, 1973). This thesis deals with the problem of groundwater hydrology and contaminant transport, and thus a detailed discussion is provided in the following sections.

2.1.1 Definition of an inverse problem

Before we can give the definition of an inverse problem, it is crucial to define a direct or a well-posed problem. A problem is considered as well-posed if (1) its solution exists (2) its solution is unique, and (3) its solution is stable (Tikhonov and Arsenin, 1977). A direct problem models a physical phenomenon or a process given the domain in which it acts, the equations that describe the process, the initial and boundary conditions.

On the other hand, an inverse problem is one that either has no solutions in the desired class (non-existence), or has many solutions (non-uniqueness), or the solution procedure is unstable (instability) (Sun, 1996). In the inverse groundwater contamination problem the plume physically exists and thus it should have originated from somewhere. However, mathematically the existence criterion may not be satisfied by the fact that plume concentrations exist. The solution only exists when perfect and consistent models and data that satisfy restrictive conditions are available. Non-uniqueness arises when two or more sets of data lead to the same observations, and thus the exact solution cannot be certainly identified. In addition, since observation error, model structure error, and calculation error always exist in practice, if arbitrarily small errors in the

measurement data lead to indefinitely large errors in the solutions, then the solution cannot be obtained either. This is the problem of instability.

One way to provide numerical stability and uniqueness is to make additional assumptions to turn ill-posed problems into well-posed ones, and this may be achieved by use of stabilization or regularization techniques. These techniques are discussed in Section 2.5 of this thesis.

2.1.2 Inverse problem classification

There are various classifications of the inverse problem. Kabanikhin (2008) has the following inverse classes; retrospective inverse, boundary inverse, continuation inverse, source identification, and coefficient inverse. Sun (1996) classifies inverse problems in groundwater into five types: namely, the identification of parameters, initial conditions, boundary conditions, sinks or sources, and the simultaneous identification of more than one of these components.

In this thesis, the inverse problem is categorized according to the types of sources to be identified, which include identification of (i) boundary conditions (boundary sources) (ii) initial conditions (instantaneous sources) (iii) point sources. In order to explain these categories the formulation of the research problem is discussed.

2.2 Groundwater flow and contaminant transport in porous media

2.2.1 Governing equations

Detailed derivations and discussions on the governing equations for flow and contaminant transport in groundwater systems are available in Freeze and Cherry (1979) and Bear (1972, 1979). The governing equations for two dimensional transient groundwater flow and contaminant transport in the porous medium can be written as (Bear, 1972);

$$\nabla \cdot (T \nabla h) = S \frac{\partial h}{\partial t} + Q_w \tag{2.1}$$

$$T = Kb \tag{2.2}$$

$$\mathbf{V} = \frac{K}{\eta}\nabla h \tag{2.3}$$

$$R\frac{\partial C}{\partial t} = \nabla \cdot (D\nabla C) - \mathbf{V}.\nabla C - \mu C - Q(x, y, t) \tag{2.4}$$

where ∇ is the two-dimensional gradient operator in x and y direction, T is the transmissivity, K is the hydraulic conductivity, S is the storativity, h is the hydraulic head, Q_w represents sources or sinks in the flow equation, C is the contaminant concentration, $\boldsymbol{V} = \boldsymbol{i}u + \boldsymbol{j}v$ is the velocity vector of the transporting medium, D is the hydrodynamic dispersion coefficient, R is the retardation factor, μ is the first-order decay rate coefficient, Q represents sources or sinks that have a spatial variation and can be expressed as $Q = C'W_v/b\eta$, C' represents sources' concentration that have a spatial variation, W_v is the recharge volume, η is the porosity, b is the aquifer thickness, and t is the time dimension.

Equation (2.1 and 2.4) apply to a domain, Ω with the boundary $\Gamma = \Gamma_1 \cup \Gamma_2 \cup \Gamma_3$ subject to initial and boundary conditions, as shown in Figure 2.1. A short discussion on initial and boundary conditions is given because of their physical importance, and relevance to both direct and inverse modelling.

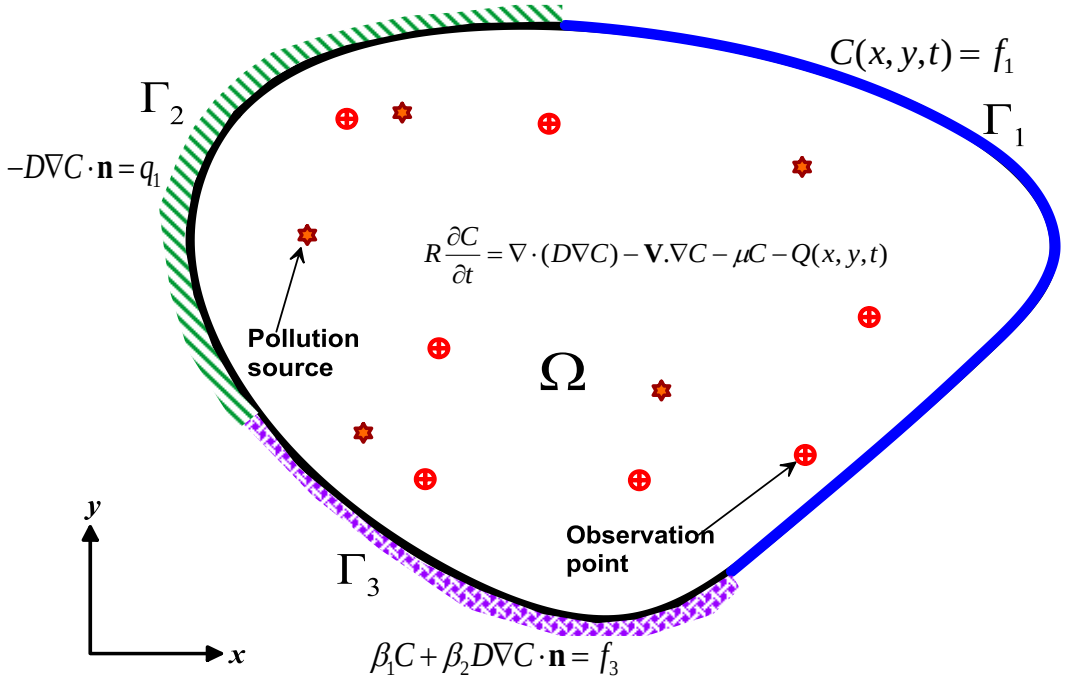


Figure 2. 1: Direct contaminant transport problem statement.

2.2.2 Initial and Boundary conditions

Initial conditions

Initial conditions refer to the hydraulic head or concentration distribution at the instant time $t = 0$ in the domain;

$$C(x,y,t=0) = C_0(x,y) \qquad \text{on } \Omega \tag{2.5}$$

where, $t = 0$ is actually an arbitrary initial time. Equation (2.5) indicates that there exists a concentration of a known function $C_0(x,y)$ in the domain at the initial time.

Boundary conditions

There are three types of boundary conditions which can be imposed on any part of the boundary so that the partial differential equations (2.1 and 2.4) can be solved. The first type of boundary condition gives the hydraulic head or concentration distribution along a part of the boundary (Γ_1), it can be written as

$$C(x,y,t) = f_1 \qquad \text{on } \Gamma_1 \tag{2.6}$$

where f_1 is a known function. This type of boundary condition is referred to as the *Dirichlet boundary condition.* The second type of boundary condition specifies known dispersion flux along a part of the boundary (Γ_2). This can be represented as;

$$-D\,\nabla C.\mathbf{n} = q_1 \qquad \text{on } \Gamma_2 \qquad (2.7)$$

where, q_1 is a known function, and **n** is the unit outward pointing normal vector on the boundary. This type of boundary condition is called the *Neumann boundary condition*. The third type of boundary condition defines the solute transport flux at a part of the boundary surface (Γ_3). It can be written mathematically as;

$$\beta_1 C + \beta_2 D\nabla C \cdot \mathbf{n} = f_3 \qquad \text{on } \Gamma_3 \qquad (2.8)$$

where f_3 is a known function, and β_1, and β_2 are known coefficients. This type of boundary condition is called the *Cauchy boundary condition*. It gives a linear combination of the primary variable and the flux. If the coefficient $\beta 1 = 0$ we have Neumann conditions, whereas if $\beta 2 = 0$ we have Dirichlet conditions.

2.3 Categories of the inverse problem

2.3.1 Unknown boundary conditions

This inverse problem requires the solution of a part of the boundary, Γ_4 where neither the concentration nor its flux is specified. This boundary in essence contains the source of the pollutant. An example of this problem could be a polluted stream that cuts an aquifer, which forms a boundary in the contaminant investigation.

This problem is mathematically under-determined and its solution requires supply of additional data. There are two possible ways to obtain additional data. The first one utilizes additional information available in a Cauchy boundary (Γ_3) since two types of conditions are specified. The second method utilizes additional information from some internal observation points in the domain.

Figure 2.2 shows the schematic of an aquifer with an underspecified boundary (Γ_4) with additional data indicated on the (Γ_3) boundary as well as internal observation points. It should be clear that either of this is utilized in the solution of the inverse problem. Consequently, initial conditions, known boundary conditions, and additional data are used to determine the unknown Γ_4 boundary.

2.3.2 Unknown initial conditions

This inverse problem arises when solving the advection-dispersion Equation (2.4) with initial conditions in Equation (2.5) unknown. An illustration of this is when a hazardous material enters the ground unintentionally through the leakage of a tank, releasing large quantities of contaminants instantaneously. The problem of determining the released amount of the pollutant into the subsurface is an inverse problem. This problem is under-determined and additional information are required for its solution.

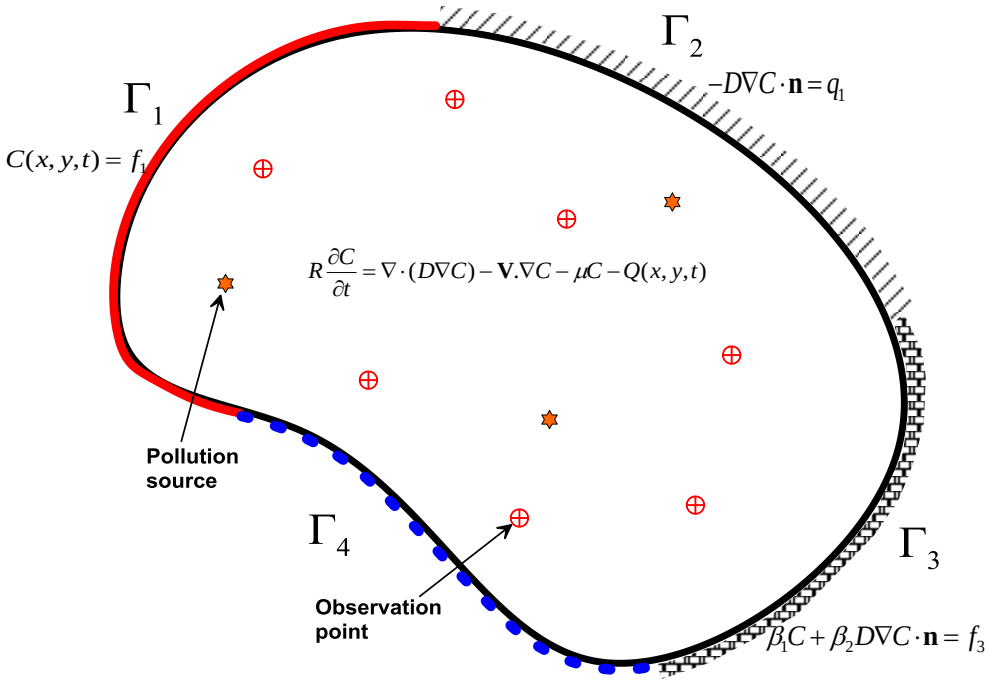


Figure 2.2: Inverse problem statement for contaminant transport.

2.3.3 Unknown source strength from point sources

This inverse problem arises when point sources release an unknown amount of contaminants into the subsurface. The source term in the governing partial differential Equation (2.4) has the strength of these sources unknown. This problem is mathematically under-determined and additional data are required for its solution. Generally, known initial and boundary conditions as well as additional data are utilized for the solution of unknown source strengths in the source term.

In practice this case is more rampant as it arises when contaminants leach from landfill sites, or buried hazardous wastes. It is also important to note that there could be several point sources in the aquifer of which their location and release history are unknown.

2.4 Solution techniques of forward contaminant transport

Solving a forward contaminant transport problem entails finding the spatial and temporal distribution of a contaminant from known system parameters, initial and boundary conditions. The methods of solution may be divided into analytical and numerical.

2.4.1 Analytical methods

Analytical methods can be applied to contaminant transport problems, however their application is limited to problems with homogeneous properties, simple and regular geometry, simple boundary conditions, and constant parameters. Analytical solutions are usually derived from basic physical principles that govern groundwater flow and contaminant transport. The solutions of 1D, 2D, and 3D advection dispersion equations have been investigated in numerous works (Ogata and Banks, 1961; Bear, 1972; Marino, 1974, Van Genuchten, 1981; Domenico, 1987; Batu, 1993; Domenico and Schwartz, 1998). Analytical solutions are mainly used to better understand the mechanism of contaminant transport, predict

the movement of contaminant plumes, and verify the results of numerical modeling.

2.4.2 Numerical methods

Numerical methods generate approximate solutions, but they provide the most powerful and general tools for solving real-life problems. They have proved to be useful in addressing practically realistic problems that have irregular geometries, are in heterogeneous media and non-linear. The techniques that have been used in contaminant transport include Finite Difference Method (FDM), Finite Element Method (FEM), Boundary Element method (BEM) and their variants and hybrids. In this thesis the Green Element method (GEM) is used for solution of the contaminant transport. A brief discussion of these methods and their applications to inverse groundwater hydrology is given in the following sections. Since, these methods have been used widely to solve direct problems, only their applications in inverse groundwater contaminant problems are discussed.

(i) Finite Difference Method (FDM)

The finite difference method approximates differential equations by difference expressions (Dechaumphai, 2010). The FDM is the oldest numerical solution technique, and is widely accepted and used in many engineering applications. The FDM is easily understood and solutions can be conveniently obtained by developing computer programs to perform the numerical calculations. Various commercial software have been developed based on the FDM. In groundwater applications, MODFLOW (Harbaugh and McDonald, 1996) FDM based software is extensively applied.

In inverse contaminant transport, MODFLOW has been used with inverse techniques for source identification, parameter identification, and estimating the historical distribution a contaminant. Tung *et al*. (2003) developed a solution algorithm that combined MODFLOW for forward flow simulations and simulated annealing with the shortest distance method, to determine hydraulic conductivity patterns. Michalak and Kitanidis (2004) used MODFLOW and MT3DMS for the

solution of governing equations with the adjoint and inverse methods to estimate the historical distribution of a contaminant. Ayvaz (2007) proposed an algorithm where the governing equation of groundwater flow was numerically solved using FDM, and the solution was combined with meta-heuristic harmony search algorithm to determine the zonation pattern and the associated transmissivity values. Prakash and Datta (2014) used MODFLOW and MT3DMS for solution of forward flow and solute transport to generate observation measurements, in their study to determine the unknown source flux release history and activity initiation times of sources.

The drawback of the FDM is the difficulty in applying arbitrary boundary conditions, as well as modeling complex geometry.

(ii) Finite Element Method (FEM)

The finite element method was first introduced in the 1950's in the aerospace industry. The FEM discretizes the computational domain of the problem in question into a number of finite elements, and on the nodes the unknowns are determined. The method transforms the differential equations into a set of algebraic equations for each element. The finite element equations from all the elements are combined to form a large set of simultaneous equations. The accuracy of the solution depends on the size and number of elements, and the element interpolation functions in the analysis.

The FEM has been applied in many areas including solid mechanics, heat transfer, fluid dynamics, and electromagnetics, etc. A large collection of software has been developed and widely used for problem solving. In inverse groundwater contaminant transport, SUTRA (Voss, 1984), a software that models saturated-unsaturated, variable density groundwater flow with solute or energy transport, has been used extensively. Gorelick *et al.* (1983) used SUTRA for simulation of flow and solute transport, and combined this model with a nonlinear optimization to obtain release histories of unknown sources. Wagner (1992) used SUTRA to simulate two-dimensional groundwater flow and non-reactive solute transport. The model was combined with an optimization approach to simultaneously

determine unknown parameters and identify sources. Datta *et al*. (2009) used SUTRA for obtaining time varying spatially distributed hydraulic head and solute concentration data. This simulation model was linked externally to algorithms of non-linear programming for source identification with both sources, and flow and transport parameters unknown.

(iii) Boundary Element Method (BEM)

The term Boundary Element Method was first introduced by Brebbia, 1978. The BEM unlike the FDM and FEM discretizes the external surface of a domain into a series of boundary elements. In the boundary element method, a system of discrete equations is obtained from the integral equations by subdividing the boundary into segments over which is prescribed a functional distribution of the dependent variable and the flux (Brebbia, 1978). Variants of the BEM for inhomogeneous partial differential equations to convert domain integrals into boundary integrals have been proposed. One method is the Dual Reciprocity Boundary Element Method (DRBEM), which was proposed by Nardini and Brebbia (1983). The DRBEM divides the solution into two parts; a known particular solution of the inhomogenous partial differential equation and a complementary solution of its homogenous counterpart. The inhomogeneous part is approximated by a series of radial basis functions. The BEM and its many variants are being incorporated into high-speed computer algorithms and being used by the practicing analyst (Banerjee, 1994).

In inverse groundwater hydrology, the BEM has been used in various studies. Lesnic *et al*. (1998) used the BEM for discretizing the partial differential equations for groundwater flow, and combined it with the minimum energy principle to determine the transmissivity of a heterogeneous aquifer from boundary data only. Harrouni *et al*. (1996) used the dual reciprocity boundary element method as the computation tool and genetic algorithms for optimization to investigate a pumping management problem in a homogenous aquifer and a parameter estimation problem in a heterogeneous aquifer. Harrouni, *et al.*(1997a) addressed the inverse problem of groundwater parameter determination as a maximum likelihood (quasi-Newton algorithm) estimation. The study utilized the

DRBEM for the solution of the direct problem and the Quasi Newton method for the unconstrained nonlinear optimization problem. Harrouni, *et al*.(1997b) addressed the problem of aquifer parameter determination by using extended Kalman filtering and DRBEM. Katsifarakis *et al*. (1999) combined the BEM and genetic algorithms to solve three classes of groundwater flow and contaminant transport problems; determination of transmissivities in zoned aquifer, minimization of pumping costs from wells and hydrodynamic control of a contaminant plume by means of pumping and injection wells.

The advantages of the BEM comprise of the fact that only the boundary of the problem requires to be discretized, as compared to the FDM and FEM. This means that the dimension of the problem is reduced by one when using BEM. The disadvantages of the BEM include firstly the large computational time, because the resulting matrix is full. Secondly, fundamental solutions do not exist for all partial differential equations e.g. anisotropic problems, or problems with the governing equation having non-constant coefficients or nonlinear terms.

(iv) Green Element Method (GEM)

The Green Element Method is a hybrid method that is based on the singular integral theory of BEM, but it implements the theory in an element–by-element manner so that it is more efficient and versatile (Taigbenu, 1999). As the Green element method is based on the boundary element theory, the second-order accuracy generally associated with the boundary element method is retained. In this way domain integrations are more easily carried out, medium variations can be readily accommodated and non-linear flow problems are easier to handle. Taigbenu (1999) states that the difficulty in extending the theory of the boundary element method to nonlinear problems stemmed from the fact that the boundary element method was implemented to have "global support", whereas methods like FDM and FEM which proceed in an element-by-element fashion or have "local support" are better able to handle the nonlinearity and variation of medium parameters across elements. The Green element implementation procedure follows that of the finite element method. Thus, the integral representations that

result after applying the standard weighting procedure to the original differential equation in each element are assembled into a summation for all the elements.

The Green Element Method has been used in various fields and applications; its strengths and capability in the solutions of a wide variety of problem have been demonstrated. GEM has been used extensively in the direct groundwater and contaminant transport problems (Taigbenu, 2001a, 2001b, 2003a, 2003c, 2007, Taigbenu and Onyejekwe, 2000). In inverse problems, GEM has been applied to the inverse heat conduction problem to recover temperature, heat flux and heat sources (Taigbenu, 2015). The application of GEM to inverse groundwater contaminant transport problems has not been reported in the existing literature, and it is the objective of this thesis. Chapter three discusses in detail the fundamentals of the GEM and its implementation to solve the inverse groundwater contaminant transport problem.

2.4.3 Boundary Element formulation for Advection Dispersion Equation

The development of the 2D GEM formulation to the research problem begins with the evaluation of the direct solution of the 2D advection dispersion equation. In illustrating the boundary element formulation we consider Figure 2.3 with a domain Ω, and the boundary $\Gamma = \Gamma_1 + \Gamma_2$.

We consider equation (2.4) and the initial and boundary conditions given as;

$$C(r,t_0) = C_0(t) \quad \text{on } \Omega \tag{2.9}$$

I. Dirichlet boundary conditions; $C(r,t) = C_1(t)$ on Γ_1

II. Neumann boundary conditions; $-D\nabla c.\mathbf{n} = q_n(t)$ on Γ_2

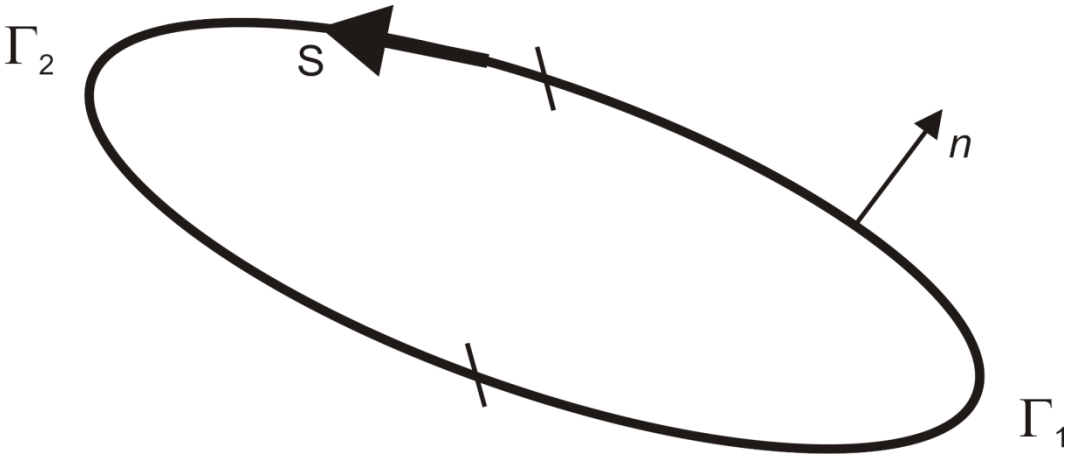


Figure 2.3: 2D computational domain for BEM formulation.

Equation (2.4) can be rewritten as

$$\ell(c) = b_l \tag{2.10}$$

where ℓ stands for a linear differential part, and b_l accounts for all heterogeneity and non-linearity of the transport process. The solution to equation (2.10) is the free-space Green's function or fundamental solution that is utilized in obtaining the integral representation of the transport equation. Considering a homogeneous case, we let equation (2.4) to be rewritten as;

$$D\nabla^2 c = b_l \tag{2.11}$$

where, D is the dispersion coefficient and b_l accounts for advection, transient, and source terms.

$$b_l = u.\nabla c + \frac{\partial c}{\partial t} + Q \tag{2.12}$$

The integral arising from applying Green's identity to equation (2.11) is

$$D\left(\lambda c(i) + \int_{\Gamma}\left[cG^* - G\frac{\partial c}{\partial n}\right]ds\right) + \iint_{\Omega} b_l G dA = 0 \tag{2.13}$$

in which λ is the nodal angle which takes into account the location of the source point ,*i*, the function *G* is the fundamental solution or the solution of the linear operator;

$$\nabla^2 G + \delta(r - r_i) = 0 \tag{2.14}$$

where, $\delta(r - r_i)$ is the Dirac delta function. The Dirac delta function takes a value of zero everywhere except at the source point where it is infinite, however it's integral over the spatial domain is unity. The normal derivative of the fundamental solution is given as $G^* = \partial G / \partial n$. The 1D and 2D fundamental solutions for an isotropic media are given in the equations below (Brebbia, 1978).

$$G = \frac{|x - x_i|}{2} \qquad \text{for 1D} \tag{2.15}$$

$$G = \frac{1}{2\pi} \ln\left(\frac{1}{r}\right) \qquad \text{for 2D} \tag{2.16}$$

where, x_i is the source node and *r* is the distance from the source node to the field node. For 2D, λ=1 when the source is within the domain, λ=0.5 on a smooth boundary, and $\lambda = \theta / 2\pi$ at a corner point with nodal angle θ.

2.5 Solution techniques for inverse contaminant transport problems

Several statistical and deterministic methods have been developed to solve inverse contaminant transport problems. Extensive literature reviews on these methods are provided in Atmadja and Bagtzoglou (2001) and Michalak and Kitanidis (2004). Existing approaches can be roughly classified into four categories, which include optimization approaches, regularization or stabilization methods, backward in time approaches and probability-based approaches.

2.5.1 Optimization

One of the early methods to backtrack a pollutant source was to run forward simulations and check if the solutions agreed with the measured observation data by trial and error (National Research Council, 1990). This method failed because of the non-uniqueness of the solution and the infinite number of possible combinations that could fit the observed data. Optimization techniques when combined with forward simulations, unique best-fitted solutions can be obtained. Some of the optimization techniques that have been employed in inverse contaminant transport can be broadly classified as derivative based, derivative free, and metaheuristic approaches. In this section, we will briefly discuss some of the works that have utilized optimization algorithms in solving inverse contaminant transport problems.

Gorelick *et al*. (1983) proposed the least square regression and linear programming with response matrix approach to identify contaminant sources. The approach was applied to two hypothetical examples to first find the location and magnitude of steady state tracers originating from a leaky pipe, and secondly to identify the location, disposal periods, and disposal fluxes in a transient case. The method assumed transport parameters to be known. In Wagner (1992) an approach was developed to simultaneously estimate hydrogeological parameters and characterise contaminant sources. The model was developed as a non-linear maximum likelihood estimation problem. The approach coupled a two-dimensional groundwater flow and contaminant transport model, and it assumed knowledge of aquifer geometry and zoning of the parameters. A series of works by Mahar and Datta (1997, 2000, and 2001) extended the nonlinear approach and solved various source identification problems. The studies employed the quasi-Newton constrained optimization method. The problem was posed assuming knowledge of the potential source locations and sought to estimate flux releases for a certain period.

Aral *et al.* (2001) proposed the progressive genetic algorithm for identification of contaminant source locations and release histories. To address the problem of

several local minima, Mahinthakumar and Sayeed (2005) proposed a hybrid approach with genetic algorithms and local search strategies for groundwater source identification problems. The algorithms were implemented and tested on a simple 2D problem, and then selected algorithms were implemented for more complex 3D problems. The work evaluated only single source problems and the unknown parameters included the location, size, and strength of the source. In the same line, Singh and Datta (2006) proposed a methodology based on the genetic algorithm. The methodology was tested for combinations of various potential source characteristics including locations, magnitudes, and release periods, data availability and measurement error levels. Identification errors that were obtained using the genetic algorithm (GA) approach were comparably less than those obtained by ANN or classical optimization.

Another optimization approach referred to as applied adaptive simulated annealing (ASA) was proposed by Jha and Datta (2013) to identify multiple contaminant sources in a three dimensional aquifer. The study compared two approaches, the GA and adaptive simulated annealing to identify unknown sources. The ASA solutions were found to converge very closely to the optimal solution using a fraction of the iterations required for a GA. The simulated annealing approach was also used by Prakash and Datta (2014) to simultaneously estimate source flux release history and sources activity initiation times. They considered an illustrative case under transient flow conditions with multiple sources and having different source activity initiation times and missing observation data. The methodology was found to have a potential to be computationally feasible in handling real life unknown groundwater pollution source identification problems.

2.5.2 Regularization and stabilization approaches

A regularization approach alleviates the ill-posed behaviour of the inverse problem through incorporating prior information into the objective function (Sun, 1999). This approach avoids solving the ill-posed problem directly and instead, solves a related well-posed problem whose solution is close in some sense to the solution of the original problem. Skaggs and Kabala (1994) reconstructed the

release history of a groundwater contaminant plume in a 1D homogeneous aquifer that originated from a known single source using Tikhonov regularisation. Liu and Ball (1999) proposed a least square method with a regularization term to estimate a source function. A field scale groundwater experiment at Dover Air Force Base was used for their analysis. Sun *et al.* (2006) formulated the constrained robust least squares (CRLS), such that additional constraints like non-negativity could be imposed. The performance of this methodology was demonstrated through one and two dimensional test problems. Model errors including velocity uncertainty, measurement outlier (data error), and uncertainty in the hydraulic conductivity were considered.

2.5.3 Reversed time approaches

In reverse time approaches, the advection-dispersion equation is solved backward in time. However since the dispersion part is irreversible, the ADE cannot be solved just with negative time steps. Bagtzoglou *et al*. (1992) used the reversed time approach to determine the contaminant's location by random walk particle method. A probabilistic framework was presented to identify contaminant sources in heterogeneous media. Atmadja and Bagtzoglou (2001) enhanced the backward beam equation method to identify contaminant sources in homogenous and heterogeneous media. The enhanced marching jury backward beam method (MJBBM) was found to be robust in handling heterogeneity, and the computational time requirements were reduced.

Skaggs and Kabala (1995) recovered the history of a groundwater contaminant plume using the method of Quasi-Reversibility (QR). They developed a QR solution to a convection-dispersion equation by solving the QR diffusion operator in a moving coordinate system. This method was found to be easier to implement and readily allowed for space and time dependent transport parameters. However, QR results were found to be less accurate when compared to the results obtained from Tikhonov regularisation (Skaggs and Kabala, 1994).

Wilson and Liu (1994) derived expressions for backward in time location and travel time probabilities. They reversed the advective part and kept the dispersion

part. They showed that both location and travel time probabilities could be calculated directly, using a backward in time version of the advection-dispersion modelling.

Neupauer and Wilson (2001) presented the adjoint method as a framework for obtaining the backward-in-time probabilities for multidimensional problems and more complex domain geometries. The numerical implementation of a backward probabilistic model applied in groundwater contaminant is presented in Neupauer and Wilson (2004). In their work they showed that the governing equation for the backward probability model is similar to the governing equation of contaminant transport, thus any numerical code that is used for contaminant transport could be applied to solve for backward location and travel time probabilities. Neupauer and Lin (2006) extended their work and developed a method for conditioning backward location and travel time probability density functions using measured concentrations. They applied the methodology to a single known instantaneous source.

2.5.4 Probabilistic methods

Woodbury and Ulrych (1996) applied a probabilistic approach referred as the Minimum Relative Entropy (MRE) to recover a release history of a contaminant. In this method a source function is discretized into many states, and each state is treated as a statistical variable. The original inverse problem is then transformed to estimate a posteriori joint probability density function for these state variables. For the noise-free data, the MRE was able to reconstruct the plume evolution history indistinguishable from the true data, while for the data with noise, the MRE was able to recover the salient features of the source history.

Snodgrass and Kitanidis (1997) and Michalak and Kitanindis (2003, 2004) developed a geostatistical approach based on Bayesian theory to determine the release history based on the current distribution of a contaminant. In Michalak and Kitanindis (2004) the geo-statistical approach was extended to recover a historical spatial contaminant distribution by implementing an adjoint methodology in a multidimensional and heterogeneous medium.

Table 1.1 gives a summary of the previous studies that have dealt with inverse groundwater contaminant transport problems. The advection dispersion equation for each study and the techniques used to solve the problem are given.

From the foregoing discussion it is clear that there has been progress in solving inverse problems. In this work we explore an optimization approach as well as a regularization approach. Firstly, we develop inverse GEM formulations which result in an ill-conditioned coefficient matrix. In order to compute stable solutions to these systems it is necessary to apply regularization methods. The over-determined matrix is decomposed by the singular value method and regularized by the Tikhonov method. Unlike in the previous studies, the method is extended to two dimensional problems with single or multiple sources. Chapter three discusses the inverse formulation of the Green element method with the Tikhonov regularized least squares method. Secondly, an evolutionary optimization approach, the Shuffled Complex Evolution (SCE-UA) method is applied for source identification. Chapter 4 explains the SCE-UA method and our formulation of the GEM-SCE model for inverse contaminant transport.

Table 1.1: Solution techniques for the advection dispersion equation in inverse contaminant transport.

Reference	Solution techniques	Forward contaminant transport equation	Dimension	Outputs
Gorelick et al (1982)	SUTRA (FEM) with regression and linear programming	$\frac{\partial C}{\partial t} = \frac{\partial}{\partial x_i}\left(D_{ij}\frac{\partial C}{\partial x_j}\right) - \frac{\partial}{\partial x_i}(CV_i) + \lambda C - \frac{C'W}{\varphi b}$	2D, heterogeneous	Location and release history
Wagner B.J. (1992)	SUTRA(FEM) with Non-linear maximum likelihood	$\theta b\frac{\partial C}{\partial t} + \nabla(b\theta VC) - \nabla.(b\theta.D.\nabla C) + qC' + \theta bR = 0$	2D, heterogeneous	Parameter estimation, Source location, Source strength
Skaggs and Kabala (1994)	Analytical solution with Tikhonov regularization	$\frac{\partial C}{\partial t} = D\frac{\partial^2 C}{\partial x^2} - V\frac{\partial C}{\partial x}$	1D, homogenous	Release history
Skaggs and Kabala (1995)	Moving coordinate system- crank Nicolson implicit finite difference scheme with Quasi reversibility.	$\frac{\partial C}{\partial t} = D\frac{\partial^2 C}{\partial x^2} - \frac{\varepsilon\partial^4 C}{\partial x^4}$	1D,homogeneous	Release history
Woodbury and Ulrych (1996)	With minimum relative entropy inversion	$\frac{\partial C}{\partial t} + V\frac{\partial C}{\partial x} - D_x'\frac{\partial^2 C}{\partial x^2} - D_y'\frac{\partial^2 C}{\partial y^2} - D_z'\frac{\partial^2 C}{\partial z^2} + \tau C = 0$	1D, homogeneous	Release history, contaminant history
Alapati and Kabala(2000)	Analytical solution with Non regularized non-linear least squares	$\frac{\partial C}{\partial t} = D\frac{\partial^2 C}{\partial x^2} - V\frac{\partial C}{\partial x}$	1D, homogeneous	Release history-(gradual / catastrophic release)
Mahar and Datta B.(1997,2000, 2001)	MINOS-FDM with embedded optimization	$\frac{\partial(Cb)}{\partial t} = \frac{\partial}{\partial x_i}\left(bD_{ij}\frac{\partial C}{\partial x_j}\right) - \frac{\partial}{\partial x_i}(bCV_i) - \frac{C'W}{\varphi} - \frac{CQ}{\varphi}$	2D, heterogeneous	Estimating unknown magnitude, location, and duration of GW.
Neupauer R. M. and Wilson (2004), Neupaeur and Lin (2006)	MODFLOW+ MT3DMS and Backward probability functions	$\theta\frac{\partial C}{\partial t} = \frac{\partial}{\partial x_i}\left(\theta D_{ij}\frac{\partial C}{\partial x_j}\right) - \frac{\partial}{\partial x_i}(\theta v_i C) + q_I C_I - q_o C$	2D, homogeneous	Contaminant location and source strength

Reference	Solution techniques	Forward contaminant transport equation	Dimension	Output
Bagtzoglou and Atmadja (2003)	Quasi reversibility and Marching Jury backward beam equation	$\frac{\partial C}{\partial t} = \frac{\partial}{\partial x}\left[D(x)\frac{\partial C}{\partial x}\right] - \frac{\partial}{\partial x}[u(x)C]$	1D, homogeneous, heterogeneous	Concentration history
Michalak & Kitanidis (2004)	MODFLOW+ MT3DMS and geostatistical method	$\eta\frac{\partial C}{\partial t} = \frac{\partial}{\partial x_i}\left(\eta D_{ij}\frac{\partial C}{\partial x_j}\right) - \frac{\partial}{\partial x_i}(\eta C V_i) + q_s C_s - q_o C$	2D, heterogeneous	Concentration history
Singh and Datta (2004)	Method of characteristics and Artificial Neural Network	$\frac{\partial (Cb)}{\partial t} = \frac{\partial}{\partial x_i}\left(bD_{ij}\frac{\partial C}{\partial x_j}\right) - \frac{\partial}{\partial x_i}(bCV_i) + \frac{C_s W}{\varepsilon}$	2D, heterogeneous	release history
Singh and Datta (2006)	Method of characteristics and Genetic algorithms	$\frac{\partial (Cb)}{\partial t} = \frac{\partial}{\partial x_i}\left(bD_{ij}\frac{\partial C}{\partial x_j}\right) - \frac{\partial}{\partial x_i}(bCV_i) + \frac{C_s W}{\varepsilon}$	2D, heterogeneous	Location and release history, and release periods
Sun A. Y. *et al*. (2006)	MODFLOW + MT3DMS and Constrained Robust Least Squares and Non-Negative Least Squares	$\frac{\partial C}{\partial t} = \frac{\partial}{\partial x_i}\left(D_{ij}\frac{\partial C}{\partial x_j}\right) - \frac{\partial}{\partial x_i}(CV_i) + \sum\sum z_{mn}\delta(\Omega_m)\delta(T_n), i, j = 1,2,3$	homogeneous	Location and release history
Tamer Ayvaz (2010)	MODFLOW and MT3DMS with statistical pattern recognition Heuristic harmony.	$\frac{\partial (Cb)}{\partial t} = \frac{\partial}{\partial x_i}\left(bD_{ij}\frac{\partial C}{\partial x_j}\right) - \frac{\partial}{\partial x_i}(bCV_i) + \frac{C_s W}{\theta}$	2D, heterogeneous	Location and release history, and number of pollution sources
Tian, N *et al* (2011)	Analytical with Tikhonov regularization and Quantum behaved particle swarm optimization.	$\frac{\partial C}{\partial t} = D\frac{\partial^2 C}{\partial x^2} - V\frac{\partial C}{\partial x}$	1D, homogeneous	Release history
Prakash O., Datta B. (2014)	MODFLOW+ MT3DMS with simulated annealing	$\frac{\partial C}{\partial t} = \frac{\partial}{\partial x_i}\left(D_{ij}\frac{\partial C}{\partial x_j}\right) - \frac{\partial}{\partial x_i}(CV_i) + \frac{q_s}{\theta}C_s - \sum_{k=1}^{N} R_k$	2D, heterogeneous	Release history and activity initiation time

3 THE GREEN ELEMENT METHOD WITH TIKHONOV REGULARIZATION

The objective of this study is to develop a numerical formulation based on the Green Element Method and regularization or optimization techniques for inverse groundwater contaminant transport problems. Two 2-D formulations based on GEM capable of recovering the source release history and reconstructing the historical contaminant distribution are developed. Specific tasks which have been carried out to achieve this include the following:

- development of inverse Green element formulations for the various inverse groundwater contaminant transport problems addressed. These include problems with sources;
    - along the boundary,
    - as unknown initial conditions
    - as point sources
- development and application of the Tikhonov regularized least squares approach for solving the ill-conditioned matrix arising from the inverse Green element formulations.
- linking of the direct Green element method formulation with the Shuffled Complex Evolution method (SCE-UA).

In this Chapter, we discuss the GEM formulation for direct contaminant transport, and then present our inverse GEM formulations. In addition, we discuss inverse GEM with the Tikhonov regularized least squares approach. The direct Green element method and the Shuffled complex evolutionary method are discussed in Chapter 4.

3.1 Green Element Formulation for 2D direct contaminant transport

Most applications of GEM in solving groundwater flow and contaminant transport to date have focused on direct well-posed problems (Taigbenu, 2001a, 2001b, 2003a, 2003c, 2007; Onyejekwe *et al*. 2001). The direct formulation of the Green element method, which follows the BEM theory explained in section 2.4.3, but implemented in an element by element manner, is discussed in this section. This direct formulation forms the basis for the inverse formulations developed herein. We consider the advection dispersion Equation (2.4) and the initial and boundary conditions Equations (2.5-2.8), (restated here as equations (3.1-3.5) for easy of reference).

$$\nabla \cdot (D\nabla C) = R\frac{\partial C}{\partial t} + \mathbf{V} \cdot \nabla C + \mu C + Q(x, y, t) \tag{3.1}$$

Subject to;

$$C(x, y, t = 0) = C_0(x, y) \qquad \text{on } \Omega \tag{3.2}$$

$$C(x, y, t) = f_1 \qquad \text{on } \Gamma_1 \tag{3.3}$$

$$-D\,\nabla C.n = q_1 \qquad \text{on } \Gamma_2 \tag{3.4}$$

$$\beta_1 C + \beta_2 D\nabla C \cdot \mathbf{n} = f_3 \qquad \text{on } \Gamma_3 \tag{3.5}$$

Expressing equation (3.1) as a Poisson type equation, so that the fundamental solution to the Laplace differential operator can be applied, we obtain;

$$\nabla^2 C = -\nabla \ln D.\nabla C + \frac{1}{D}\left(\mathbf{V}.\nabla C + R\frac{\partial C}{\partial t} + \mu C + Q(x, y, t) \right). \tag{3.6}$$

Letting $\vartheta = \ln D$, and $\varphi = 1/D$, Equation (3.6) can be represented as

$$\nabla^2 C = -\nabla \vartheta.\nabla C + \varphi\left(R\frac{\partial C}{\partial t} + \mathbf{V}.\nabla C + \mu C + Q(x, y, t) \right). \tag{3.7}$$

The Green's second identity with two functions U and V is written as;

$$\iint_{\Omega}\left(U\nabla^2 V - V\nabla^2 U\right)dA = \int_{\Gamma}\left(U\nabla V - V\nabla U\right).\mathbf{n}ds\,. \tag{3.8}$$

If we set U to C and V to G, we obtain

$$\iint_{\Omega}\left(C\nabla^2 G - G\nabla^2 C\right)dA = \int_{\Gamma}\left(C\nabla G - G\nabla C\right).\mathbf{n}ds\,. \tag{3.9}$$

We transform Equation (3.7) into an integral one by applying the Green's second identity in Equation (3.9) and utilize the free space Green's function from the solution of $\nabla^2 G = \delta(r - r_i)$ in the infinite space. The integral equation is thus given as;

$$\begin{aligned} &-\lambda C_{(r_i)} + \int_{\Gamma}\left(C\nabla G.\mathbf{n} + G\nabla C.\mathbf{n}\right)ds + \\ &\iint_{\Omega} G\left[-\nabla\vartheta.\nabla C + \varphi\left(\mathbf{V}.\nabla C + R\frac{\partial C}{\partial t} + \mu C + Q(x,y,t)\right)\right]dA = 0 \end{aligned} \tag{3.10}$$

The boundary and domain integrals in Equation (3.10) are similar to those obtained from the boundary element formulation as described in section 2.4.3. Unlike in the boundary element method where only the boundary is discretized, in the Green element method elements are used to discretize the computational domain. On these elements, basis functions of the Lagrange family are prescribed for interpolating the quantities C, q, ϑ and φ, that is $C \approx N_j C_j$ (where N_j are linear interpolating functions). The discrete element equation for each element, e, is given as;

$$-\lambda^e C^e_{(r_i)} + \sum_{e=1}^{M}\left[\begin{aligned} &\int_{\Gamma^e}\left(C\nabla G + G\nabla C\right).\mathbf{n}ds + \\ &\iint_{\Omega^e} G\left[-\nabla\vartheta.\nabla C + \varphi\left(\mathbf{V}.\nabla C + R\frac{\partial C}{\partial t} + \mu C + Q(x,y,t)\right)\right]dA \end{aligned}\right] = 0 \tag{3.11}$$

where M is the total number of polygon elements, and Γ^e and Ω^e are the boundary and the domain of the e^{th} element. Introducing the Lagrange approximations into equation (3.11) and rearranging gives;

$$\sum_{e=1}^{M} R_{ij}C_j + L_{ij}q_j + S_{ijk}\vartheta_j C_k + T_{ijk}\vartheta_j C_k + U_{ijkl}\varphi_j u_k C_l + Y_{ijkl}\varphi_j v_k C_l)$$
$$+ W_{ijk}\varphi_j\left(R\frac{\partial C_k}{\partial t} + \mu C_k\right) + F_{ij}Q_j = 0 \qquad (3.12)$$

Where, $q = -\partial C/\partial n$ is the normal contaminant flux, $Q = C_s W_v / b\eta$ and the elemental matrices are given as

$$R_{ij} = \int_{\Gamma^e} N_j \nabla G_i \cdot \mathbf{n}\, ds - \delta_{ij}\lambda,$$

$$L_{ij} = \int_{\Gamma^e} G_i N_j ds,$$

$$S_{ijK} = \iint_{\Omega^e} G_i \frac{\partial N_j}{\partial x}\frac{\partial N_k}{\partial x} dA,$$

$$T_{ijk} = \iint_{\Omega^e} G_i \frac{\partial N_j}{\partial y}\frac{\partial N_k}{\partial y} dA$$

$$U_{ijkl} = \iint_{\Omega^e}\left[G_i N_j N_k \frac{\partial N_l}{\partial x}\right] dA,$$

$$Y_{ijkl} = \iint_{\Omega^e}\left[G_i N_j N_k \frac{\partial N_l}{\partial x}\right] dA \qquad (3.13)$$

$$W_{ijk} = \iint_{\Omega^e} G_i N_j N_k dA,$$

The expression for the matrix F_{ij} resulting from the contribution of contaminant sources, depends on whether they are distributed or point sources. For each point source, the expression is given as;

$$F_{ij} = \varphi(r_j)\ln(r_j - r_i) \tag{3.14}$$

where, $\varphi(r_j)$ is the reciprocal of the dispersion coefficient that is evaluated at $r_j = (x_j, y_j)$. For distributed sources, the expression is given as;

$$F_{ij} = \varphi(r_j)\iint_{\Omega^e} \ln(r - r_i)N_j dA \tag{3.15}$$

The elemental integrations in Equation (3.13) together with the forcing term Equation (3.14) and/or (3.15) are done analytically. Aggregating the discrete element Equation (3.11) for all elements used to discretize the computational domain gives a matrix equation of the form

$$E_{ij}C_j + L_{ij}q_j + W_{ij}R\frac{dC_j}{dt} + F_{ij}Q_j = 0 \tag{3.16}$$

The temporal derivative term is approximated by a finite difference expression: $dC/dt \approx [C^{(2)} - C^{(1)}]/\Delta t$. Applying the generalized finite difference scheme with a weighting factor, θ to Equation (3.16) yields

$$\left(\theta E_{ij} + R\frac{W_{ij}}{\Delta t}\right)C_j^{(2)} + \left(\omega E_{ij} - R\frac{W_{ij}}{\Delta t}\right)C_j^{(1)} +$$
$$\theta L_{ij}q_j^{(2)} + \omega L_{ij}q_j^{(1)} + \theta F_{ij}Q_j^{(2)} + \omega F_{ij}Q_j^{(1)} = 0 \tag{3.17}$$

where, the superscripts 1 and 2 refer to t_1 as the previous time and the current time, $t_2 = t_1 + \Delta t$, respectively, with a time step of Δt, while $\omega = 1 - \theta$ (values vary between 0 and 1). It is noted that different values of θ give rise to various schemes; a scheme with $\theta = 0$ is referred to as the fully explicit scheme, that with $\theta = 0.5$ the Crank-Nicholson scheme, that with $\theta = 0.67$ the Galerkin scheme, and finally that with $\theta = 1$ the fully implicit scheme.

Equation (3.17) can be condensed to a matrix equation, which is represented as:

$$\mathbf{Aw} = \mathbf{b} \tag{3.18}$$

where

$$\mathbf{A} = \begin{bmatrix} \left(\theta E_{ij} + R\dfrac{W_{ij}}{\Delta t}\right) \\ \theta L_{ij} \end{bmatrix} \quad \text{and} \quad \mathbf{w} = \begin{Bmatrix} C_j^{(2)} \\ q_j^{(2)} \end{Bmatrix} \tag{3.19}$$

The matrix **A** (M × N) is referred to as the global coefficient matrix, with **M** being the number of nodes in the computational domain which is the same as the number of discrete equations generated, while **w** (N x 1) is a vector of nodal unknowns, where *C* or *q* is determined for external nodes and *C* for the internal nodes at the current time. The matrix **b** (M x 1) is the vector of known quantities comprising the initial data, prescribed boundary conditions, and the forcing term.

3.2 Inverse GEM Formulations

The inverse GEM formulations developed in this section are based on the aforementioned direct formulation. The unknowns in the inverse problem determine how the computation of the coefficient matrix will be handled. Two inverse formulations have been developed and are discussed in the following sections.

3.2.1 Formulation 1: Unknown boundary conditions and source strength of point sources

This formulation requires the recovery of the strength of boundary sources and/or point sources in the groundwater system. The problem is posed such that a part of the boundary (Γ_4) has unknown boundary conditions as well as the forcing term which represents point sources in equation (3.14) has the source strength unknown.

In this formulation, Equations (3.6 to 3.16) hold like in the direct problem. Thus, applying the finite difference approach to equation (3.16), we can obtain;

$$\left(\theta E_{ij} + R\frac{W_{ij}}{\Delta t}\right)C_j^{(2)} + \theta L_{ij} q_j^{(2)} + \theta F_{ij} Q_j^{(2)} = \left(R\frac{W_{ij}}{\Delta t} - \omega E_{ij}\right)C_j^{(1)} - \omega L_{ij} q_j^{(1)} - \omega F_{ij} Q_j^{(1)} \qquad (3.20)$$

where, $C_j^{(2)}$ and $q_j^{(2)}$ contain the concentration and flux of the unknown boundary, and $Q_j^{(2)}$ represents the unknown forcing term. These terms are taken in the direct problem to be known but they are sought terms in this formulation. Equation (3.20) is condensed into a matrix similar to Equation (3.18). The difference in the inverse matrix is the known and unknowns quantities.

$$\mathbf{Px} = \mathbf{s} \qquad (3.21)$$

where,

$$\mathbf{P} = \begin{bmatrix} \left(\theta E_{ij} + R\frac{W_{ij}}{\Delta t}\right) \\ \theta L_{ij} \\ \theta F_{ij} \end{bmatrix} \quad \text{and} \quad \mathbf{x} = \begin{Bmatrix} C_j^{(2)} \\ q_j^{(2)} \\ Q_j^{(2)} \end{Bmatrix} \qquad (3.22)$$

where **P** is an M×N ill-conditioned matrix, with M being the number of nodes in the computational domain which is the same as the number of discrete equations generated, and N represents the number of unknowns which are *C* and/or *q* at external nodes including the *contaminant source strength as well as the flux along the unknown boundary* (Γ_4), *C* at internal nodes and *the contaminant point source strengths, Q*. The vector **x** represents the unknown quantities that should be calculated and **s** represents known quantities which consists of the terms in the right hand side of Equation (3.20) as well as the contributions from the available concentration measurements.

3.2.2 Formulation 2: Unknown initial conditions

This formulation seeks to determine the source strengths of instantaneous contaminant sources. The governing Equation (3.1) is solved with known initial and boundary conditions in Equations (3.2-3.5), with the aim of determining the unknown source strengths and the spatial and temporal contaminant distribution. In this case Equation (3.6 to 3.13) applies without the forcing term. The elemental approximations in Equation (3.13) are aggregated for all elements to give a matrix equation of the form

$$E_{ij}C_j + L_{ij}q_j + W_{ij}R\frac{dC_j}{dt} = 0 \tag{3.23}$$

Applying finite differencing to Equation (3.23), we obtain;

$$\left(\theta E_{ij} + R\frac{W_{ij}}{\Delta t}\right)C_j^{(2)} + \theta L_{ij}q_j^{(2)} - \left(\omega E_{ij} + R\frac{W_{ij}}{\Delta t}\right)C_j^{(1)} - \omega L_{ij}q_j^{(1)} = 0 \tag{3.24}$$

The third term in Equation (3.24) with $C_j^{(1)}$ is usually taken in the direct problem to be known but for this inverse problem, there are a number of locations (F) where it has to be calculated at time, $t = 0$. All known boundary and initial data and concentration measurements at observation points are incorporated into equation (3.24) to give a condensed matrix similar to equation (3.21);

$$\mathbf{Px} = \mathbf{s} \tag{3.25}$$

where,

$$\mathbf{P} = \begin{bmatrix} \left(\theta E_{ij} + R\frac{W_{ij}}{\Delta t}\right) \\ \theta L_{ij} \\ -\left(\omega E_{ij} + R\frac{W_{ij}}{\Delta t}\right) \end{bmatrix} \text{ and } \mathbf{x} = \begin{Bmatrix} C_j^{(2)} \\ q_j^{(2)} \\ C_j^{(0)} \end{Bmatrix} \tag{3.26}$$

The unknowns in this matrix **P** include the concentration, *C* and/or flux *q* at external nodes, *C,* at internal nodes *and the unknown contaminant source strength at time, t=0*. The vector **x** represents the unknown quantities that should be calculated and **s** is a vector of known quantities in equation (3.24) as well as the contributions from the available concentration measurements. In practice, concentration measurements may contain measurement errors. In this work, we examine the influence of observation measurement errors on the numerical solutions by perturbing randomly the measured or observed concentration according to this relationship

$$\tilde{C}_n = C_n\left[1 + \varepsilon \times RAN(n)\right] \tag{3.27}$$

Where, ε is the noise level, and *RAN* are random numbers that are generated using the IMSL program routine RNNOR in FORTRAN, and $\tilde{C}_n$ is the perturbed value of the observed concentration C_n.

3.3 GEM and the least squares approach

The inverse formulations described above result in ill-conditioned and over-determined matrices. Being over-determined, they can be solved by the least squares method, and being ill-conditioned, they are regularized by the Tikhonov regularization method. We develop a methodology where the matrices are decomposed using the singular value decomposition method and are solved by the least squares method with Tikhonov regularization. A detailed discussion of these methods is provided in the following sections.

3.3.1 Singular value decomposition (SVD)

The singular value decomposition method is used to facilitate the decomposition of the linear system of equations resulting from solving the inverse contaminant transport problems in Equations (3.21 and 3.25) (restated here as Equation (3.28) for easy of reference).

$$\mathbf{Px} = \mathbf{s} \tag{3.28}$$

The matrix **P** is ill-conditioned, and the right hand side **s** may be contaminated by an error, ε, which may arise from observation measurement errors. The SVD decomposes the matrix **P** which is an $(\mathbf{M}\times\mathbf{N})$ with $\mathbf{M}\geq\mathbf{N}$ into the following form;

$$\mathbf{P}=\mathbf{U}\mathbf{D}\mathbf{V}^{T} \tag{3.29}$$

where, **U** is an orthogonal (**M** x **M)** matrix, such that $\mathbf{U^{T}U}=\mathbf{UU^{T}}=\mathbf{I_{m}}$, **V** is an orthogonal (**N x N**) matrix, such that $\mathbf{V^{T}V}=\mathbf{VV^{T}}=\mathbf{I_{n}}$ (**I** is an identity matrix). **D** is an (M x N) matrix, containing zeros outside the diagonal and non-negative numbers (the singular values, ψ_i) on the diagonal, represented as;

$$\mathbf{D}=\begin{bmatrix}\psi_1 & & & 0\\ & \psi_2 & & \\ & & .. & \\ 0 & & & \psi_m\end{bmatrix} \tag{3.30}$$

The column vectors $\{uu_i\}$ of **U** are called left-singular vectors, while the row vectors $\{vv_i\}$ of **V** are called right-singular vectors. The diagonal elements $\{\psi_i\}$ of **D** are the singular values, sorted in decreasing order, such that $\psi_1\geq\psi_2\geq\psi_3\geq...\psi_m\geq 0$, uu_i and vv_i are the i^{th} column of the matrices **U** and **V**, respectively. Computing the SVD consists of finding the eigenvalues and eigenvectors of $\mathbf{PP}^{T}$ and $\mathbf{P}^{T}\mathbf{P}$. The columns of **U** are eigenvectors of $\mathbf{PP}^{T}$ and the rows $\mathbf{V}^{T}$ are the eigenvectors of $\mathbf{P}^{T}\mathbf{P}$. The SVD has a powerful property of compressing the information contained in **P** into the first singular vectors which are mutually orthogonal and their importance rapidly decreases after the first columns or rows. The singular value range can be defined using a condition number, *C*

$$C\equiv\frac{\max\psi}{\min\psi} \tag{3.31}$$

As the value of C becomes larger the problem becomes more ill-conditioned, and as $C\rightarrow\infty$ the matrix becomes strictly singular. The boundary between well-posed

and ill-posed is not clearly given, however generally an acceptable range for the condition number is $C \leq 10^3$.

If we now attempt to solve the inverse problem in Equation (3.28) by the least squares method, the Euclidian norm $\|\mathbf{Px} - \mathbf{s}\|^2$ is minimized to give the solution for the unknowns **x**

$$\mathbf{x} = \left(\mathbf{P}^T\mathbf{P}\right)^{-1}\left(\mathbf{P}^T\mathbf{s}\right) \tag{3.32}$$

Equation (3.32) can be rewritten as;

$$\mathbf{x} = \sum_{i=1}^{J_R} \frac{uu_i^{tr}\mathbf{s}}{\psi_i} vv_i \tag{3.33}$$

in which, J_R is the rank of the matrix **P**. The small non-zero singular values ψ_i cause difficulties such as instability in the solution for **x**. If the matrix **P** is considered as a noisy representation, the small non-zero singular values can be replaced with exact zeros. The unique solution then is given as;

$$\mathbf{x} = \sum_{i=1}^{N} \frac{uu_i^{tr}\mathbf{s}}{\psi_i} vv_i = \mathbf{P}^{+}\mathbf{S} \tag{3.34}$$

where, $\mathbf{P}^{+}$ is the pseudoinverse or the Moore-Penrose inverse of the matrix **P**, and is referred to as the truncated SVD (TSVD) solution. In other instances a regularised approach may be used in conjunction with the SVD. This is the approach followed in this Thesis, a regularization technique referred to as the Tikhonov regularization method is employed.

3.3.2 Tikhonov regularization

Regularization techniques are used to stabilize inverse problems (Engl *et al*., 1996). The Tikhonov regularization method is the most commonly used scheme and has been adopted in this study. Considering the ill-conditioned linear Equation (3.28), the Tikhonov regularized solution; $\mathbf{x}_\alpha$ is defined as the solution to the following least squares problem:

$$\min_{X}\left\{\left\|\mathbf{Px}-\mathbf{s}\right\|^{2}+\alpha^{2}\left\|\mathbf{Ix}\right\|^{2}\right\}. \tag{3.35}$$

Regularization is necessary when solving inverse problems because the simple least squares solution, when α=0, is dominated by contributions from data errors and rounding errors. The regularization parameter (α) controls the weight given to the minimization of the semi-norm $\left\|\mathbf{Ix}\right\|$ of the solution relative to minimization of the residual norm $\left\|\mathbf{Px}-\mathbf{s}\right\|$. The solution to Equation (3.33) is given as;

$$\mathbf{x}(\alpha)=\sum_{i=1}^{N}\frac{\psi_i}{\alpha^{2}+\psi_i^{2}}uu_i^{tr}\mathbf{s}vv_i \tag{3.36}$$

The factor $\psi_i/(\alpha^2+\psi_i^2)$ serves to dampen the contribution of the small singular values. The choice of the regularization parameter is very crucial to obtaining meaningful solutions. Various methods have been proposed for selecting the regularization parameter and they include; the L-Curve (Hansen,1992), Generalized cross validation (Craven *et al.* (1979), Golub *et al.* (1979)), and the discrepancy principle (Goncharskii *et al.* (1972)). In this work, we utilize the L-curve method.

L-Curve

The L-curve method was suggested by Hansen (1992). It is a continuous curve consisting of all the points $\left(\left\|\mathbf{Px}_{\alpha}-\mathbf{s}\right\|,\left\|\mathbf{Ix}_{\alpha}\right\|\right)$ for $\alpha\in[0,\infty)$. It is a log-log plot of the norm of a regularized solution against the norm of the corresponding residual for all values of the regularization parameter. It shows the compromise between the perturbation error and the regularization error (over-smoothing). A suitable regularization is the one corresponding to a regularized solution near the corner of the L-curve, at which both errors are minimized. The "corner" is where the curvature of the L-curve is maximum (see Figure 3.1), and it can be expressed as (Hansen, 1992);

$$k=2\frac{\hat{\rho}'\hat{\eta}''-\hat{\rho}''\hat{\eta}'}{\left((\hat{\rho}')^{2}+(\hat{\eta}')^{2}\right)^{3/2}} \tag{3.38}$$

where, $\eta = \|\mathbf{x}_\alpha\|^2$, $\rho = \|\mathbf{P}\mathbf{x}_\alpha - \mathbf{s}\|^2$, $\hat{\eta} = \log\eta$, $\hat{\rho} = \log\rho$. The first and second derivatives of η and ρ are given as $\hat{\eta}', \hat{\rho}', \hat{\eta}'', \hat{\rho}''$ respectively (Hansen, 2000).

Hansen (1992) demonstrated that under certain assumptions the L-curve is similar to both the GCV and the discrepancy principle. Whenever the GCV finds a good regularization parameter, the corresponding solution is located at the corner of the L-curve. However, the L-curve is able to filter out correlated errors and obtain a good regularization parameter, as compared to the GCV that mistakes correlated errors to be part of a signal, thus influencing the choice of the regularization parameter.

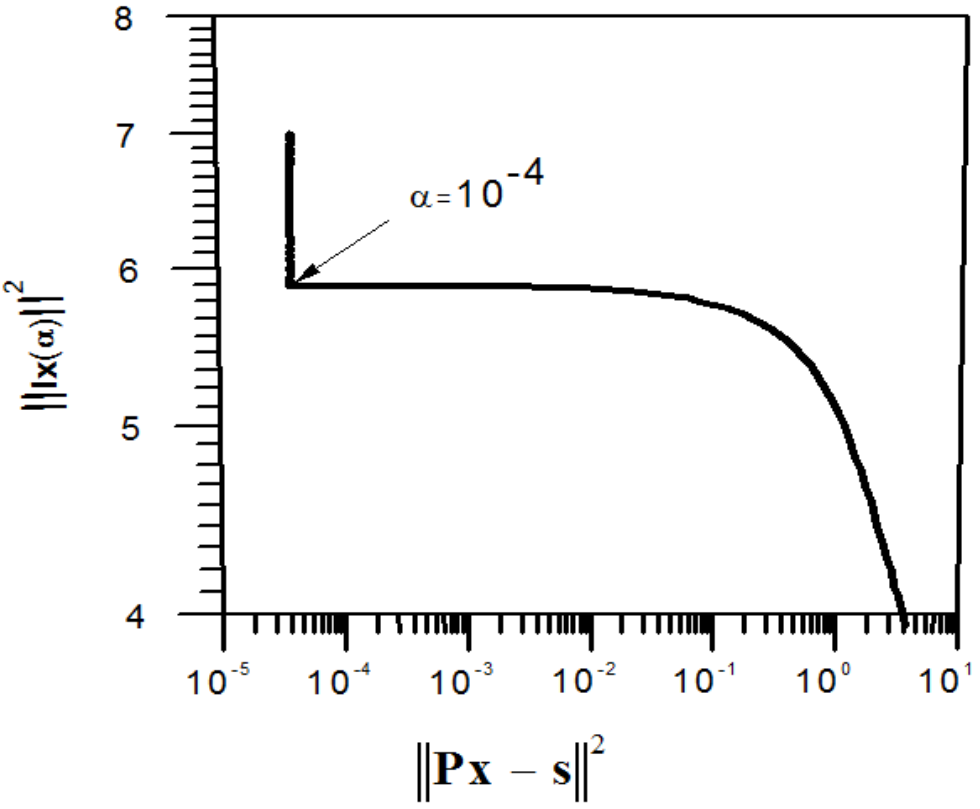


Figure 3.1: The L-curve and its properties

Hansen (2000) pointed out two limitations of the L-curve which include the reconstruction of very smooth exact solutions and the asymptotic behaviour as the problem size increases. Brezinski *et al*. (2008) pointed out that there are many cases where the L-curve exhibits more than one corner or no corner at all.

In this work the L-curve method is implemented to determine the regularization parameter. The code that was developed allowed for automatic determination of the regularization parameter, and the best parameter was used to compute the inverse solution. For transient problems, the regularization parameter was determined at every time step.

4 THE SHUFFLED COMPLEX EVOLUTIONARY OPTIMIZER AND GEM

This chapter discusses the Shuffled Complex Evolution (SCE) optimization method used in this study. A brief overview of global optimization techniques and the SCE as well as a description of the linkage of the numerical model and the optimizer are given. Finally, the criterion used to assess the performance of the method is discussed.

4.1 Overview of global optimization techniques

Global optimization is applicable in many fields including engineering, science, and economics. Solomatine *et. al*. (1999) identified global search techniques that have been applied in hydrology and grouped them into: space covering techniques, random search methods, multiple local search methods, and evolutionary algorithms. Of interest in this work are evolutionary techniques which mimic natural evolution processes and are capable of solving very large and complex problems. Examples in this category include genetic algorithms, differential evolution, particle swarm optimization, and the Shuffled Complex Evolution (SCE). This last method, the SCE is employed in this work and thus a detailed discussion is given in the following sections.

4.2 Shuffled Complex Evolution optimization method

4.2.1 Description of SCE-UA

The SCE-UA algorithm was developed at the University of Arizona (Duan *et al*., 1992) to deal with challenges faced when dealing with global optimization problems. The initial study of this algorithm identified five major characteristics that complicate catchment model calibration (a typical global optimization problem), which include the following:

i. many regions of attraction to which the search can converge to,
ii. numerous local minima,
iii. roughness of the objective function surface,
iv. varying degrees of sensitivity for the parameters, and
v. the non-convex shape of the response surface near the true solution.

To address these challenges, four concepts were synthesised that have proved effective for global optimization which include combination of deterministic and random or probabilistic approaches (Gomulka,1978), systematic evolution of complex points spanning the parameter space in the direction of global improvement (Price, 1978, 1983,1987), competitive evolution (Holland,1975) and complex clustering (Torn,1978). In essence, the Shuffled Complex Evolution method combines the best features of the controlled random search algorithms, with the competitive evolution concept, and the concept of complex shuffling.

The SCE-UA generates a population of possible solutions to the problem and divides this population into a number of sub-populations (complexes or communities). Based on a statistical 'reproduction' process the simplex geometric shape is used to direct the search. The downhill simplex method (Nelder and Mead, 1965) is then used to evolve each complex for a set number of evolutions. The improved solutions from the complexes are then shuffled to enable the exchange of 'good traits' among the complexes. The ability of this technique to escape local regions of attraction in a search space is taken care of by the process of shuffling and reformulation of new complexes. The resulting complexes are evolved and shuffled repeatedly until the set criterion for terminating the search is met. The process of complex shuffling and competitive evolution embodied in the algorithm ensures that the information contained in the sample is efficiently and thoroughly exploited and does not become degenerate (Duan *et al*., 1993). The details of the SCE algorithm are summarized in Figure 4.1.

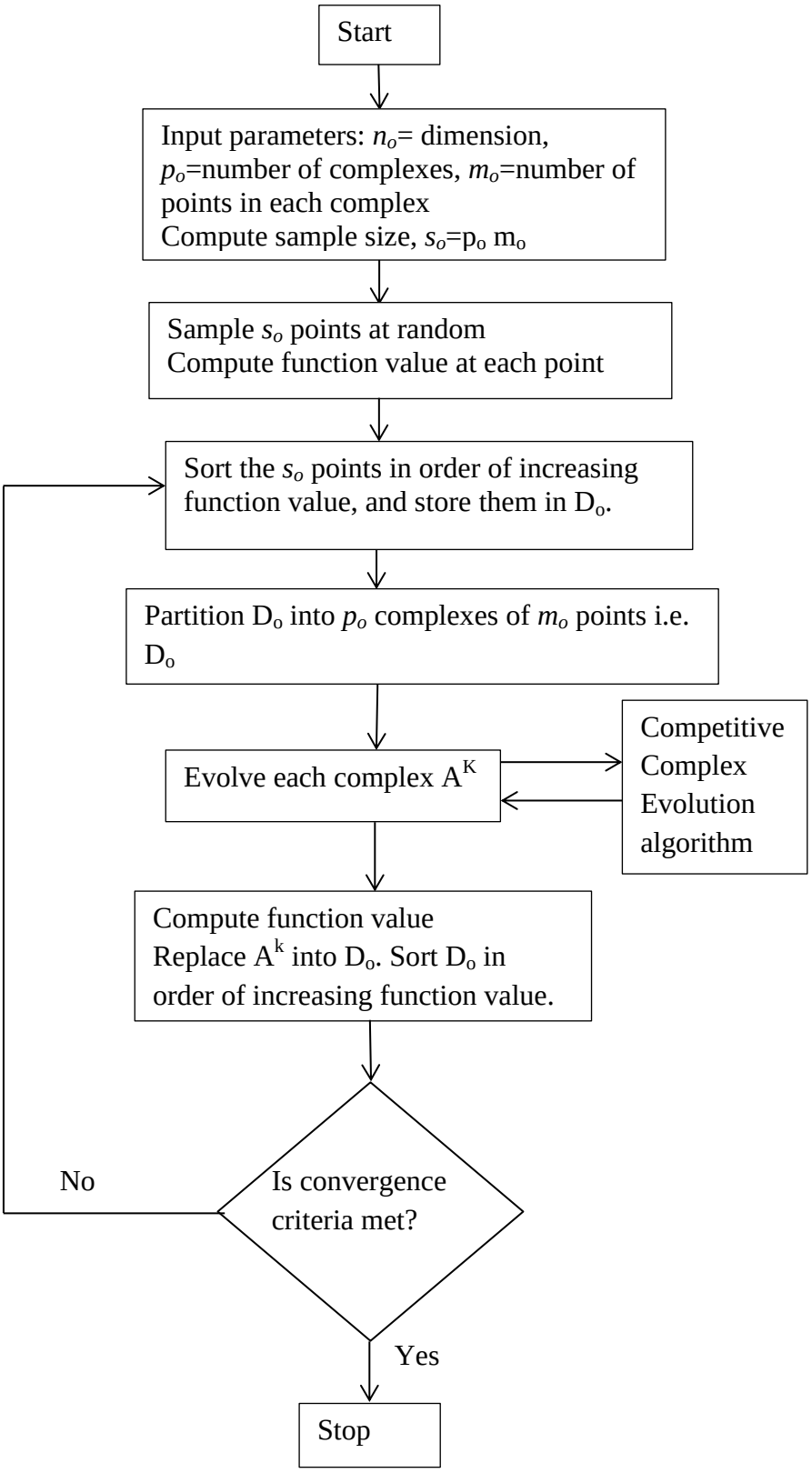


Figure 4.1: Flowchart of the Shuffled Complex Evolution (SCE-UA) method (adapted from Duan *et al.*, 1992, 1993).

The Competitive Complex Evolution (CCE) method is used to evolve each complex. Each point of a complex is taken as a probable 'parent', thus has the ability to participate in reproducing an 'offspring'. A stochastic scheme is used to construct subcomplexes which function like a pair of parents. The idea of competitiveness in forming of subcomplexes allows the stronger to survive and breed offspring than the weaker; this expedites the search towards promising regions. Detailed literature on CCE can be found in Duan *et al*, 1992. In order to utilize the SCE algorithm in Figure 4.1, a number of parameters have to be determined. Duan *et al.* (1994) presented suitable values for the user-specified parameters as a function of the number of parameters (n_o) to be optimized. These parameters include the:

- number of points in each complex (m_o) = ($2n_o$+1),
- number of points to select in complex (q_o) = (n_o+1),
- number of consecutive offspring generated by each sub-complex (α_{opt}) =1
- number of evolution steps taken by each complex (β_{opt}) =m_o.

If these values are used in the optimization, the number of complexes (p_o) will be the only parameter that remains to be determined.

4.2.2 Applications of SCE-UA

The SCE-UA method has been extensively applied in calibration of various models with demonstrative positive results. SCE-UA has been used for calibration of rainfall-runoff models, which include the Sacramento model (Sorooshian *et al*., 1993; Gan *et al*., 1997; Yapo *et al*., 1998; Ajami *et al*., 2004,), the Tank model (Tanakamaru and Burges,1996; Cooper *et al*., 1997), NAM/MIKE 11 model (Madsen, 2000), and the Xinanjiang model (Gan *et al*.,1997, Zhijia *et al.*, 2013,). In groundwater, Contractor and Jenson (2000) employed the SCE-UA for calibration of a finite element groundwater flow model. Bell *et al.* (2002) applied SCE-UA for optimization of parameters of a contaminant transport model for assessing a landfill liner design. Eusuff and Lansey (2004) calibrated groundwater flow modelling tools MODFLOW, MTD3 and MODPATH in the development of

a soil aquifer treatment management model. He *et al*. (2007) used SCE-UA to calibrate a groundwater prediction model for a coastal plain in Japan.

Comparisons of the SCE-UA to other global and local search algorithms in hydrology in model calibration have been carried out. Thyer *et al.* (1999) compared the performance of two probabilistic global optimization methods, the SCE-UA and the three phase simulated annealing algorithm (SA-SX). These algorithms were applied to calibrate a model using data from two Australian catchments that have low and high runoff yields. The algorithms were found to have a similar efficiency for the low-yielding catchment, but SCE-UA was almost twice as robust. For the high yielding catchment the robustness of the algorithms was similar but SCE-UA was six times more efficient than SA-SX. Ndiritu and Daniell (2001) compared an improved GA with the SCE-UA and noted that SCE-UA outperformed the improved GA on two of the three optimization problems that they investigated. Hence, they concluded that SCE-UA could be preferred for rainfall-runoff model calibration and for other unfamiliar continuous variable problems. Wang *et al.* (2010) compared SCE, SGA and µga in parameter calibration of a grid based distributed rainfall runoff model. All the methods performed well in calibration; however, SCE was more robust and had best performance in verification.

The SCE-UA has been applied in inverse groundwater modelling problems. Agyei and Hatfield (2006) compared three algorithms SCE-UA, Shuffled Complex Evolution-Gradient Based (SCEGB), and gradient-based Lavenberg–Marquardt algorithm (GBLM) for estimation of parameters in a coupled numerical groundwater flow and contaminant transport model. The parameters that were estimated include the hydraulic conductivity tensor, vertical hydraulic conductivity through a confining bed, longitudinal and transverse dispersivities, and the aquifer porosity. Using perfect observation data the SCE and SCEGB were successful in identifying the global optimum and predicting all model parameters, while GBLM failed to identify the optimum. In simulations with observation corrupted with noise, SCE and SCEGB outperformed the GBLM by

having more accurate parameter estimates. However, SCEGB was found to be more computationally efficient when compared to SCE-UA.

4.2.3 Further developments of the SCE-UA

The Shuffled Complex Evolution method is widely used in hydrology and has proved to be a robust and efficient global optimization algorithm, as discussed in Section 4.2.2. However SCE-UA, is limited when dealing with multiobjective problems, parameter uncertainties, and high dimension problems. In the quest for improvement and further development of the method, several modifications have been reported in a number of studies. To deal with multiobjective problems, Yapo *et al.*, 1998 developed the Multiobjective Complex Evolution (MOCOM-UA) method using the concepts of complex shuffling and downhill Simplex evolution from SCE-UA and the concept of Pareto dominance (Goldberg, 1989). This method is efficient in estimating Pareto solutions, but it is limited by clustering solutions into a region and converging prematurely (or sometimes fails to converge) for large numbers of parameters and strongly correlated performance criteria (Gupta *et al.*, 2003).

In order to account for uncertainties in hydrological parameters, Vrugt *et al*. (2003a) developed a Markov chain Monte Carlo (MCMC) approach named the Shuffled Complex Evolution Metropolis (SCEM-UA). The method follows the SCE-UA procedure except that the Metropolis scheme replaces the simplex scheme as the search kernel, and the algorithm does not subdivide the complex into sub-complexes during the generation of offspring. However, this method is limited to single objective problems. In a follow up study, Vrugt *et al*. (2003b) modified the SCEM-UA by developing the Multiobjective Shuffled Complex Evolution Metropolis (MOSCEM-UA) method which incorporates the modified strength Pareto dominance technique and the Metropolis algorithm. The MOSCEM-UA method generates a fairly uniform approximation of the entire Pareto, as compared to MOCOM-UA. However, it is best suited for hydrologic model calibration applications that have small parameter sets and small model evaluation times (Tang *et al.*, 2006).

To overcome the population degeneration problem which arises when the search process degenerates into a subspace thereby missing the potential of exploring the full parameter space especially in high dimensional or complex problems, Chu *et al*. (2010) improved the SCE-UA by developing the Shuffled Complex strategy with Principal Components Analysis (SP-UCI). This method outperforms the SCE-UA technique by retrieving better parameter values, being more robust, and better delineating the uncertainty distributions of model parameters. However the SP-UCI technique has been found to converge prematurely, and to get stuck in a local basin of attraction on the way to the global minimum of a posterior distribution in complex and multimodal search spaces (Laloy and Vrugt, 2012). In the same line, Mariani *et al*., 2011 developed the Modified Shuffled Complex Evolution (MSCE), by combining the Downhill Simplex search strategy with a differential evolution method. The method is less susceptible to premature convergence and less likely to be stuck in local optima in some of the benchmark problems.

4.2.4 Choice of the optimization method

From the foregoing discussion the SCE-UA is found to perform satisfactorily compared to other methods in calibration of rainfall-runoff models and groundwater models, as well as in inverse groundwater flow and transport. However, some weaknesses have been pointed out and several modifications of the method have been developed. The inverse contaminant problem addressed in this study is a single objective problem, and does not consider uncertainties; therefore the SCE-UA modifications that consider these challenges may not be suited for our case. The approaches that address the degeneration problem, which include SP-UCI and MSCE offer promising capabilities but have been pointed to fail in some cases. We therefore, employ the classical SCE-UA approach in this Thesis.

4.3 The SCE-GEM model

The numerical simulator, GEM is used to compute the governing equations of flow and contaminant transport, see Section 3.1 for details. The SCE-UA technique is implemented with the objective to search for a feasible set of the unknown parameters that minimize deviations between the estimated and the observed concentrations of the pollutant at selected observation locations, and estimated and known boundary conditions. To achieve this objective, the method minimizes the weighted sum of the squares of the differences between the calculated and the measured concentration values, and the estimated and known boundary conditions. The optimization model thus can be written as:

Minimize

$$J_{\min} = \frac{1}{N_t}\sum_{t=1}^{N_t}\left\{\begin{array}{l}\sum_{m=1}^{N_\gamma}\left[C^{cal}(x_m,y_m,t) - C^{meas}(x_m,y_m,t)\right]^2 \\ + \sum_{i=1}^{N_z}\left[C_i^{cal}(t) - C_i^{meas}(t)\right]^2\end{array}\right\} \tag{4.1}$$

Subject to

$$C^{'(L)} \le C^{'} \le C^{'(U)} \tag{4.2}$$

$$q^{(L)} \le q \le q^{(U)} \tag{4.3}$$

where, the superscripts *cal* and *meas* refer to the calculated and the measured or given values, respectively. N_t is the total number of simulation time steps, $C^{cal}(x,y,t)$ is concentration estimated by the model corresponding to m^{th} location and t^{th} time step. The first part of the functional refers to the N_γ internal points where the concentration measurements are available and the second part refers to the Cauchy boundary segment (Γ_3). It is crucial to note that in this formulation the Γ_3 boundary with N_z nodes where both the Dirichlet and Neumann conditions are known, only one type of condition is specified. For instance, if the concentration is prescribed, the functional then evaluates the deviation between the calculated and the prescribed fluxes. On the other hand, a boundary (Γ_4) where neither data on the primary variable nor the flux is available, the optimizer is used to predict

one of the variables so as to compute the other variable. The constraints in Equations (4.2 and 4.3) basically provide the lower and upper bounds to ensure that practically acceptable ranges are considered for the source strength (either concentration or flux). Therefore, the Shuffled Complex Evolution optimization approach solves Equation 4.1 subject to Equation 4.2 or 4.3, when linked to the direct GEM for contaminant transport simulation.

4.3.1 Linking GEM model and the SCE-UA optimizer

Both the numerical model and the optimizer used in this study have been coded using the same platform Microsoft PowerStation FORTRAN. The direct GEM formulation followed in this work was recently developed and coded by Taigbenu (2012), while the SCE-UA optimizer used was coded by Ndiritu (2009) for automatic calibration of a rainfall-runoff model. The linkage between GEM and SCE-UA was first developed in Taigbenu and Ndiritu (2011), where the methodology was applied to steady state heat conduction problems. In the present study, we develop the GEM-SCE model for transient problems. This section gives a brief discussion on how the numerical model and the optimization model are linked.

The numerical and the optimization model are directly linked through exchange of information. The simulation model determines the number of unknowns referred to as decision variables, while the optimizer determines a set of parameters within the allowable range for these decision variables. The numerical model uses these parameters to simulate the contaminant transport problem and compute an objective function. The optimizer picks the computed objective function as the value corresponding to the set of parameters provided, completing a single simulation. Basically, several simulations are done until the stopping criterion is achieved. Repeated calls to the transport simulator GEM are required for obtaining the objective functions that the SCE needs for the Competitive Complex Evolution.

Stopping criteria

It is essential to use an apt stopping criterion for the optimization algorithm to stop at the right time without compromising the reliability of finding the global optimum while using minimum computational resources. We have adapted three stopping criteria checked at each generation for SCE in this work. That is, the evaluation stops when one of the following criteria is arrived:

i. The epoch objective function changes less than a given specified value,
ii. A maximum number of user-specified epochs is attained,
iii. A minimum value of the objective function is reached.

4.3.2 Performance evaluation criterion

In order to measure the performance of the proposed simulation-optimization model, the mean error of the estimated concentration to the actual concentration is evaluated. The mean error (ME) for each time step for all nodes can be defined as:

$$\text{Mean Error (\%)} = \frac{1}{M}\sqrt{\frac{\sum_{i=1}^{M}\left(C^{cal}-C^{meas}\right)^2}{\sum_{i=1}^{M}\left(C^{meas}\right)^2}}\times 100 \qquad (4.4)$$

where, the superscripts *cal* and *meas* refer to the calculated and the measured or given values of the concentration, and M refers to the total number of nodes.

5 RESULTS AND DISCUSSION

In this chapter numerical test cases are used to demonstrate the computation capability of the formulations developed in the preceding chapters. The two inverse GEM formulations described in Chapter 3 are employed as follows; **Formulation 1** of **Section 3.2.1** is used for problems with sources along the boundary as well as point sources in **Sections 5.1, 5.2, 5.4 and 5.5**, **Formulation 2** of **Section 3.2.2** is applied to instantaneous sources in **Section 5.3**. We refer to these formulations of inverse GEM with Tikhonov regularized least square as **Model 1**. The formulation of direct GEM with the Shuffled complex evolution developed in Chapter 4 is referred as **Model 2**. We utilize typical test cases in contaminant transport which have analytical solutions, as well those that have appeared in many research papers to assess the potential of our proposed methodologies. A sensitivity analysis is conducted to show the performance of the methodology.

5.1 Sensitivity analysis

To evaluate the performance and capability of the developed methods for contaminant source identification, a sensitivity analysis is carried out on observation data and spatial discretization.

5.1.1 Sensitivity to observation data

The quality and quantity of observation data inevitably influence the accuracy of the estimated source strength in the source identification problem. In this section, we evaluate factors associated with observation data, which include the amount of observation data, ζ and the observation site, γ. In the literature various efforts to design an optimal monitoring network have been reported. For two and three dimensional domains, Mahar and Datta (1997), Yeh *et al*. (2007), and Jha and Datta (2013) showed that in essence an observation network should be located in the resultant direction of flow downstream of the pollutant sources, and that the network should be able to capture the contaminant plume. Sun *et al*. (2006) provided necessary conditions for source identifiability which include; firstly, for

any source to be identified, at least one observation point should respond to the source, and secondly, in the observation system no pair of sources being identified should result in identical responses. Li and Mao (2011) considered a 1D domain and showed that there exists a given number of observation points to guarantee a solution, and that too few measurements render the problem not easily identifiable while more information do not improve the solution considerably. The study indicated as well that when an observation site is closer to the source location better estimates can be obtained.

In this work we investigate a classical transient one-dimensional contaminant transport problem that arises as a result of advection and dispersion of a contaminant with source strength, *C'* that is continuously released from a boundary. The aquifer is homogeneous with a uniform velocity field in the *x*-direction. This problem is governed by Equation (2.4) with no decay (μ=0) and no external sources (Q = 0). For a conservative pollutant, the exact solution is given by Ogata and Banks (1961) as,

$$C(x,t) = \frac{C'}{2}\left\{ erfc\left(\frac{x-ut}{2\sqrt{Dt}}\right) + \exp\left(\frac{ux}{D}\right) erfc\left(\frac{x+ut}{2\sqrt{Dt}}\right)\right\}. \qquad (5.1)$$

We consider the domain shown in Figure 5.1 and utilize Model 1 for the sensitivity analysis. The inverse problem requires determining the source strength, *C'*. It is solved in a 2D grid [L, 10^3] which is only discretized in the *x*-direction. To minimize the influence of the imposed no-flux condition on the top and bottom boundaries on the 1-D solution, the boundaries are kept as far apart from each other in the *y* direction by an arbitrary dimension of 10^3. The left boundary that contains the source has the unknown strength (Γ_4), while the right boundary is a Dirichlet boundary, the upper and lower boundaries are no flux boundaries.

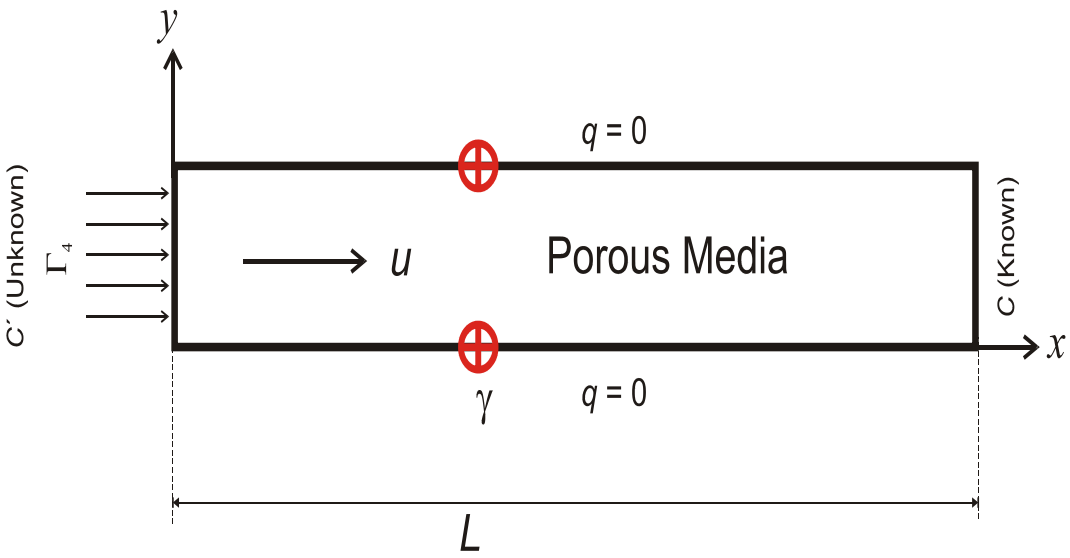


Figure 5.1: Problem statement for source identification in 1D porous media.

The following parameters were utilized in the simulations; $u = 1, D = 2.5, \Delta x = 0.125, L = 5, \Delta t = 0.125, \varepsilon = 0.01$ and the total simulation time, $t_f = 1.25$. Numerical tests were performed to evaluate the influence of observation locations on source identification, and five locations were evaluated, $\gamma = 0.125$, $\gamma = 1$, $\gamma = 1.5$, $\gamma = 2.5$, and $\gamma = 4.5$. Note that the observation location γ represents the *x*-value in a 1D problem. The L-curve method was used to determine the regularization parameter at every time step. A range for the regularization parameter was between 1.03×10^{-5} and 4.04×10^{-8}.

Figure 5.2 shows the computed source strength for different locations of observation points, while Figure 5.3 shows the average relative error for the computed source strength with respect to location of observation point. It is observed that the accuracy of the computed source strength is better when the observation site, γ is closer to the source location, but the accuracy reduces as the location moves away from the source. The average relative error in Figure 5.3 for the estimated source strength indicates better estimates when the source location is within $\gamma \leq 1$, but the error increases steadily for values $\gamma > 1$.

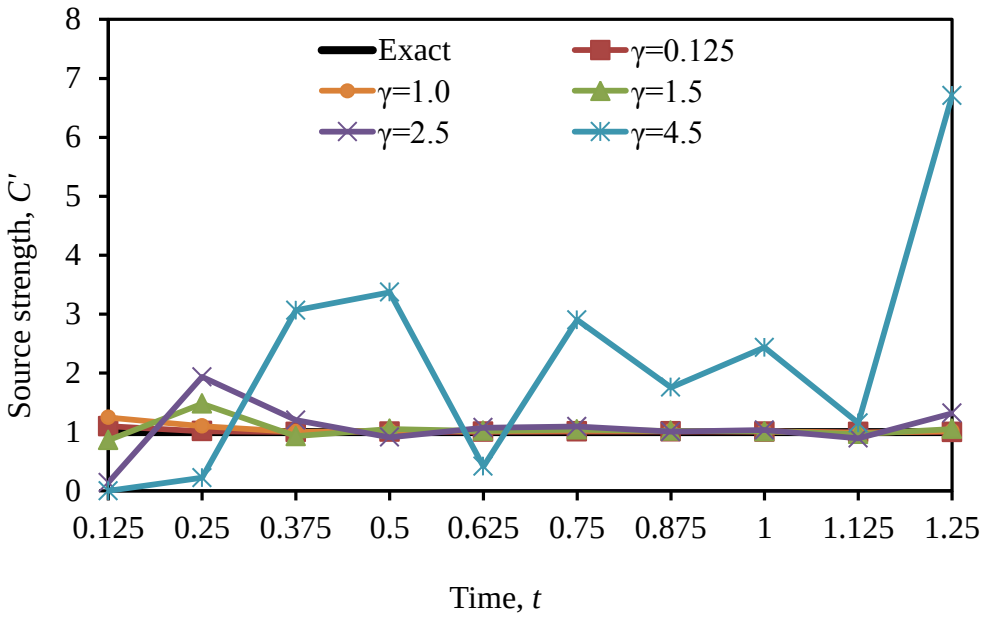


Figure 5.2: The estimated source strength with respect to location of observation point.

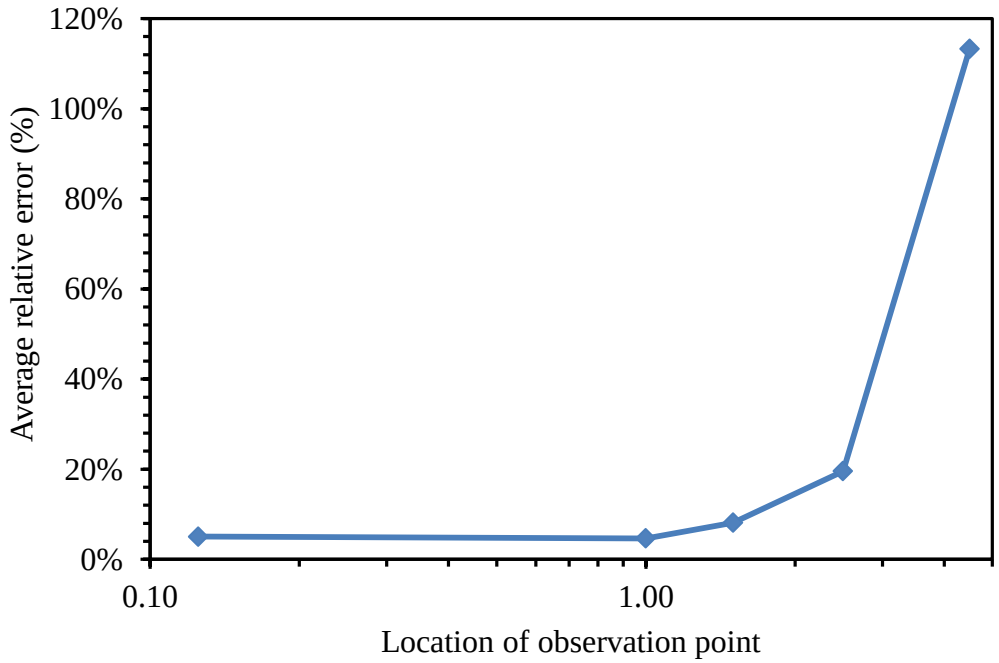


Figure 5.3: The average relative error for the computed source strength with respect to location of observation point.

To evaluate the influence of the amount of observation data, ζ, which is equal to the number of time steps multiplied by the number of observation points, numerical tests were carried out as shown in Table 5.1. The parameters used in the previous simulation were utilized and the sampling location was taken at $\gamma = 0.125$. Figure 5.4 shows the estimated source strength for the four runs. It is observed that Run 1 gave excellent results compared to Run 2, 3 and 4. In Run 2 sampling starts after the first three time steps, implying that additional information from the observation points is only received starting the 4^{th} time step. It is therefore observed that when the measurements are taken after the plume has evolved; the source strength is not estimated until at least some measurement is recorded.

Figure 5.5 shows the average relative error for the computed source strengths in the various runs. It is observed that the error is highest in Run 4 because additional information is only provided at the last time step. The error reduces with increase in the amount of observation data, and thus Run 1 gives the least error as all the time steps have information to support the inversion problem. It can be deduced that limited temporal observation data will certainly influence source recovery.

Table 5.1**: Test scenarios for the analysis of sampling time.**

Run number	Sampling time, t_s
Run 1	All time steps
Run 2	$4\Delta t$, $5\Delta t$, $6\Delta t$, $7\Delta t$, $8\Delta t$, $9\Delta t$, $10\Delta t$
Run 3	$6\Delta t$, $7\Delta t$, $8\Delta t$, $9\Delta t$, $10\Delta t$
Run 4	$10\Delta t$

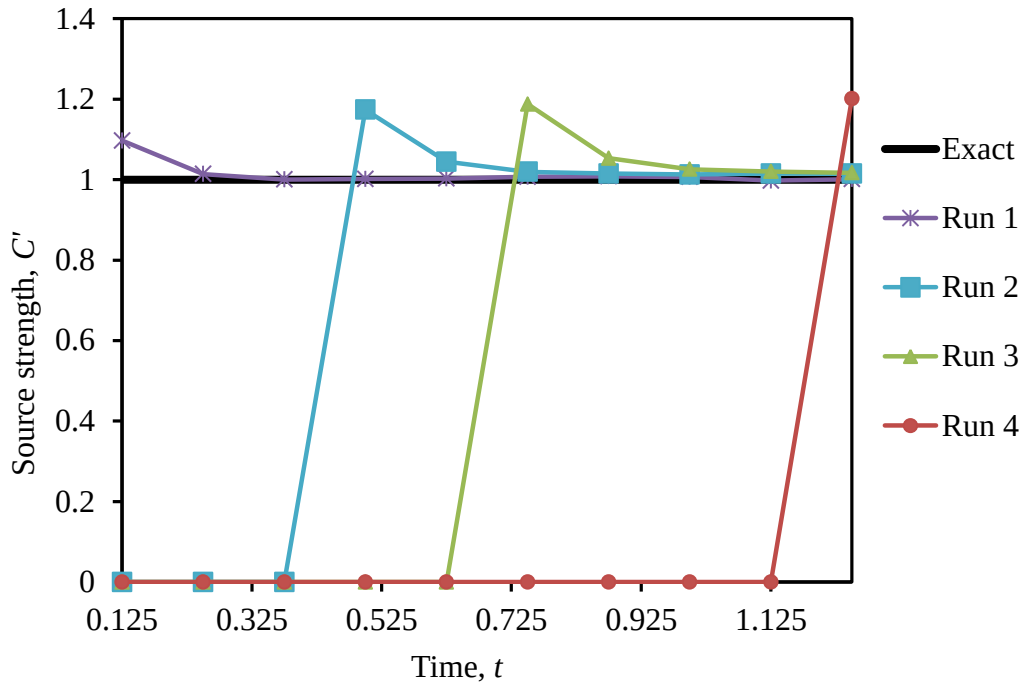


Figure 5.4: The estimated source strength with respect to number of observation data.

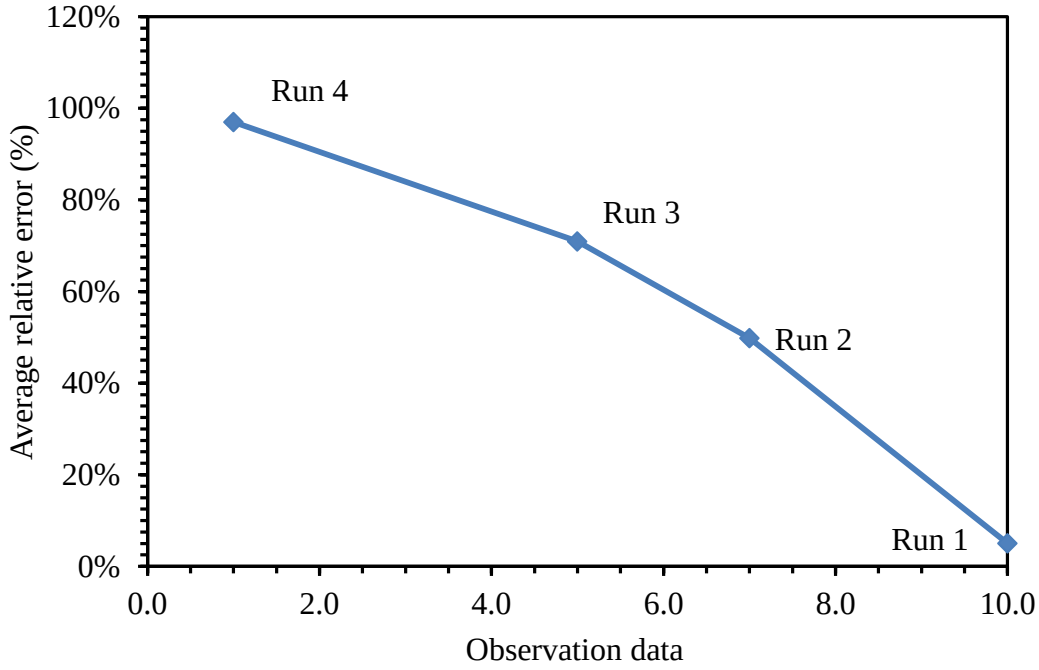


Figure 5.5: The mean error with respect to the number of observation data.

5.2.1 Sensitivity to spatial discretization

Case (i) 1D Steady case with variable velocity

This is a 1-D steady transport case with a variable velocity in the *x*-direction. It is governed by Equation (2.4) with $\mu = 0$ and $Q = 0$. In the direct formulation, Dirichlet boundary conditions are provided along $x = 0$ and $x = 1$ as $C = C_0$, and $C = C_1$ respectively (Popov and Power, 1999, Natalini and Popov, 2004, Taigbenu, 2007). The velocity field in the *y*-direction is zero while in the *x*-direction is given as;

$$u = \ln\frac{C_1}{C_0} + k\left(x - \frac{1}{2}\right) \tag{5.2}$$

Taking the hydrodynamic dispersion coefficient as unity, the analytical solution is given as:

$$C = C_0 \exp\left\{\frac{k}{2}x^2 + \left(\ln\frac{C_1}{C_0} - \frac{k}{2}\right)x\right\}. \tag{5.3}$$

The first derivative of Equation (5.3) is given as;

$$\frac{dc}{dx} = \left(kx + \left(\ln\frac{C_1}{C_0} - \frac{k}{2}\right)\right) * C_0 \exp\left\{\frac{k}{2}x^2 + \left(\ln\frac{C_1}{C_0} - \frac{k}{2}\right)x\right\} \tag{5.4}$$

in which, the values of *k* represent the mode of transport.

In this work, this example is simulated in a 2-D rectangular domain $[1,10^3]$ as an inverse problem in which the boundary along $x = 0$ is a Γ_4 boundary where the concentration and flux are unknown, while the boundary along $x = 1$ is a Dirichlet boundary where *C* is specified. The upper and lower boundaries of the computational domain are no flux boundaries. The computational domain is discretized uniformly into 10, 20 and 40 rectangular elements. A non-uniform discretization of 14 elements is also employed in order to capture the steep gradient of the concentration profile close to $x = 0$. The lengths of these rectangular elements in the *x*-direction are: 0.025, 0.025, 0.025, 0.025, 0.05, 0.05,

0.1, 0.1, 0.1, 0.1, 0.1, 0.1, 0.1 and 0.1. Additional information in terms of observed concentration data for this problem are provided on the top and bottom boundary at $\gamma = 0.1$, and at all time steps.

Two modes of transport are evaluated by taking the values of k as 10 and 40 for dispersion dominant and advection dominant transport cases respectively. The value of C_0=300 and C_1=10. The computed source strengths on the boundary along x=0 for k=10 and k=40 are given in Table 5.2 and Table 5.3 respectively. It is seen that Model 1 gives better prediction of the source strength for the less convective case k=10 than the more convective case k=40. For both cases, the accuracy of Model 1 solutions is enhanced with increase in the number of uniform elements incorporated in the simulations. However, using 14 non-uniform elements produces solutions with accuracy comparable to those with 20 and 40 uniform elements. The computed source strengths using observation data with 5% randomized errors are slightly higher than the error free. The error relative to exact source strength is highest for 10 elements in both cases.

Table 5.2: Model 1 computed source strength for unknown boundary for $\boldsymbol{k = 10}$.

Exact source strength (x=0)	No. of elements	$\boldsymbol{\varepsilon = 0\%}$			$\boldsymbol{\varepsilon = 5\%}$		
		Inverse solutions			Inverse solutions		
		$C'(x=0)$	Relative error (%)	α	$C'(x=0)$	Relative error (%)	α
300	10	266.1398	11.2867	8.11×10^{-4}	271.511	9.4963	5.83×10^{-4}
300	20	294.8619	1.7127	3.84×10^{-4}	300.840	0.28	8.11×10^{-4}
300	40	299.5846	0.1385	1.50×10^{-4}	305.6718	1.8906	5.38×10^{-5}
300	14 (non-uniform)	299.3021	0.2326	2.13×10^{-4}	305.3529	1.7843	9.29×10^{-5}

Table 5.3: Model 1 computed source strength for unknown boundary for $\boldsymbol{k = 40}$.

Exact source strength ($x = 0$)	No. of elements	$\boldsymbol{\varepsilon = 0\%}$			$\boldsymbol{\varepsilon = 5\%}$		
		Inverse solutions			Inverse solutions		
		$C'(x=0)$	Relative error (%)	α	$C'(x=0)$	Relative error (%)	α
300	10	137.4342	54.1886	3.06×10^{-4}	140.2280	53.2573	2.67×10^{-4}
300	20	276.4327	7.8558	1.06×10^{-4}	282.0936	5.9688	3.29×10^{-5}
300	40	299.7404	0.0865	5.38×10^{-5}	305.8966	1.9655	1.50×10^{-5}
300	14 (non-uniform)	299.4816	0.1728	7.84×10^{-5}	305.5922	1.8641	4.75×10^{-5}

The solutions for the flux q are presented in Table 5.4 for the two convective cases. As earlier observed with the computed solution of the source strength, the solution of the flux $q(x = 0)$ with 14 non-uniform elements is comparable to that with 40 uniform elements. The concentration profiles for $k = 10$ and $k = 40$ from Model 1 simulations are presented with their exact solutions in Figures 5.6 and 5.7, and their errors relative to the exact solution are presented in Figure 5.8. The discretization of 10 elements gives the worst estimate of the concentration distribution as well as high errors relative to the exact concentration distribution.

Table 5.4: Model 1 computed flux for unknown boundary for ***k* = 10** and ***k* = 40**.

Convective value k =10				Convective value k = 40		
Exact flux	**Model 1** $q\ (x = 0)$ solutions			Exact	**Model 1** $q\ (x = 0)$ solutions	
	No. of elements	**ε = 0%**	**ε = 5%**		**ε = 0%**	**ε = 5%**
-2520.36	10	-2233.073	-2278.859	-7020.36	-3215.198	-3281.017
-2520.36	20	-2476.393	-2527.447	-7020.36	-6468.565	-6601.559
-2520.36	40	-2516.576	-2568.632	-7020.36	-7014.522	-7159.004
-2520.36	14 (non-uniform)	-2512.364	-2563.877	-7020.36	-7007.563	-7151.008

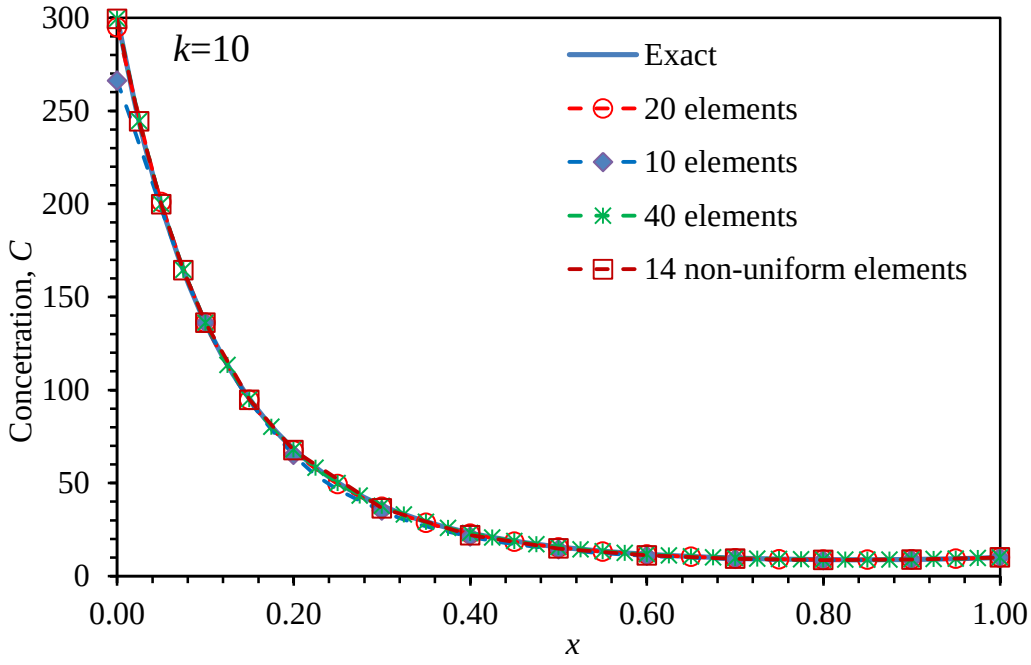


Figure 5.6: Model 1 and exact solutions for the concentration with 5, 10, 20 uniform elements, and 14 non-uniform elements for Case (i): $k = 10$.

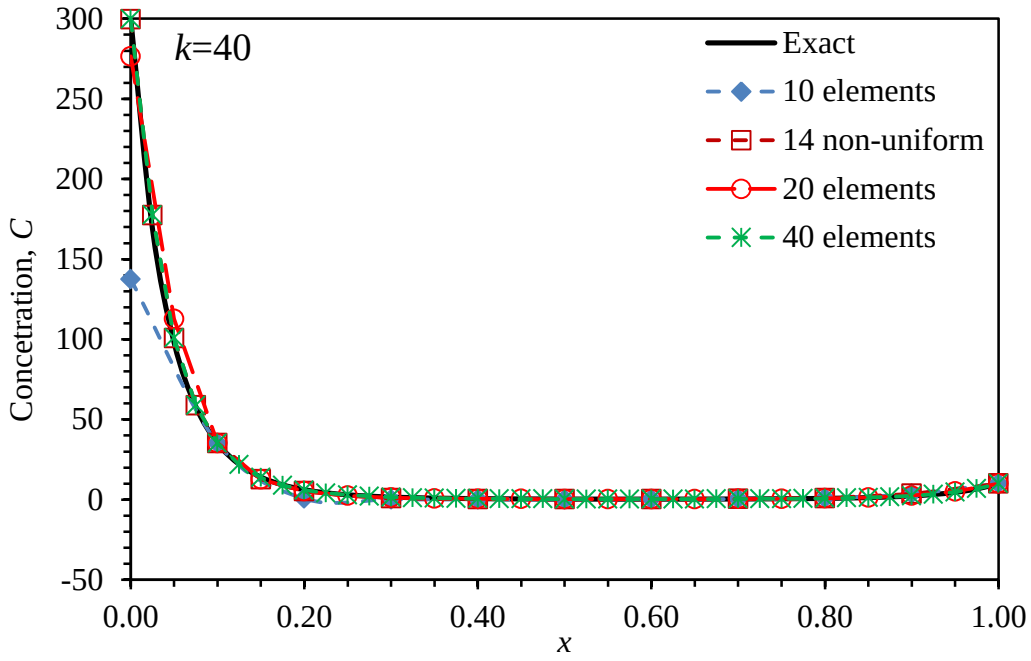


Figure 5.7: Model 1 and exact solutions for the concentration with 5, 10, 20 uniform elements, and 14 non-uniform elements for Case (i): k = 40.

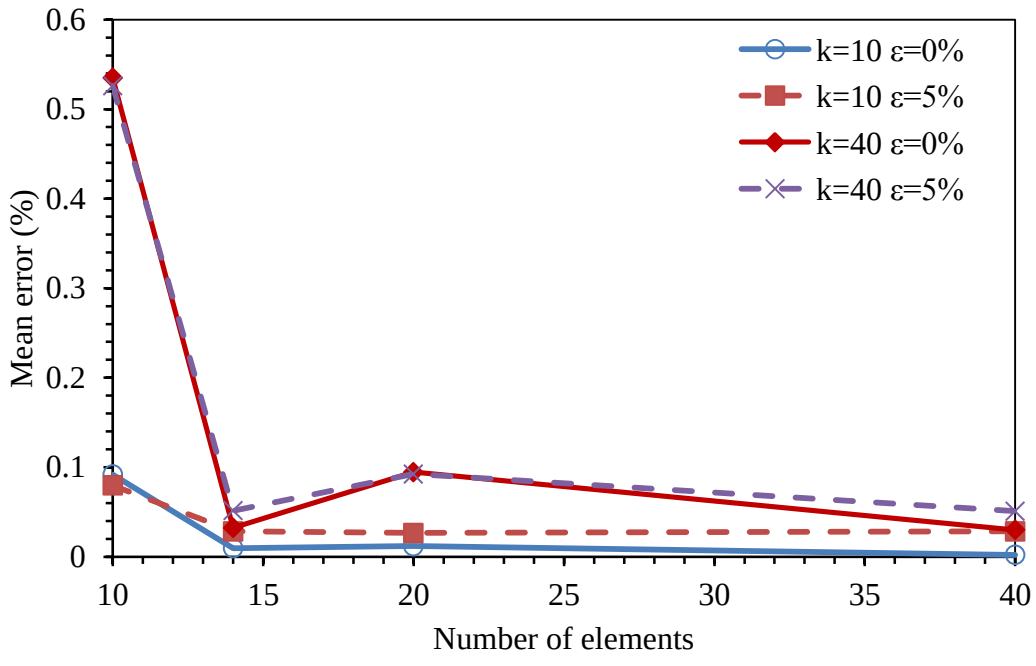


Figure 5.8: Mean error for the computed concentration by Model 1 for Case (i).

Case (ii) 1D inverse steady convection-diffusion problem with constant velocity

This is a simple one dimensional convection-diffusion problem with Dirichlet boundary conditions, at x=0, and x=1, given as $C(x=0) = 1$ and $C(x=1) = 2$ respectively. The velocity is uniform in the x-direction and is taken as u=5 and the dispersion coefficient is taken as unity. The analytical solution to this problem is given in Qiu *et al.* (1998) as;

$$C = 2 - \frac{1 - e^{u(x-1)}}{1 - e^{-u}} \tag{5.5}$$

The inverse problem is analysed in a two dimensional rectangular domain $[1,10^3]$ with no flux imposed on the top and bottom boundaries. The boundary along $x = 1$ is taken as a Dirichlet boundary where the concentration is specified, the boundary along $x = 0$ is an unknown boundary, referred to as Γ_4 boundary. Two cases are considered to assess the influence of available measured concentration data in the computation of the solution. In Test (i) the concentration is given at $\gamma = 0.2$ and $\gamma = 0.8$, in Test (ii) at $\gamma = 0.6$ only. The computational domain is discretized into 5, 10 and 20 uniform elements. The computed source strength along the unknown boundary $x = 0$ is given in Table 5.5 and Table 5.6 for Test (i) and Test (ii) respectively. The results indicate good prediction by Model 1 of the source strength at the Γ_4 boundary ($x = 0$).

It is also observed that the error relative to the exact source strength is higher when the observation data is perturbed randomly with 5% error in both Test (i) and Test (ii). The concentration profiles for Test (i) and Test (ii) are respectively presented in Figures 5.9 and 5.10 for the three discretization used in the GEM simulations. The computed results for the solution with 10 and 20 elements are in excellent agreement with the exact solution. However, the solution with 5 elements is unable to correctly capture the concentration profile close to the boundary $x = 1$ because of the inability of the coarse discretization to correctly capture the higher gradient of the concentration profile.

Table 5.5: Model 1 computed source strength for different element discretizations for case (i).

Exact C' (x=0)	No. of elements	Model 1 solutions Case (i)					
		$\varepsilon = 0\%$			$\varepsilon = 5\%$		
		C' (x = 0)	Relative error (%)	α	C' (x = 0)	Relative error (%)	α
1.000	5	1.0117	1.17	2.61×10^{-3}	1.0193	1.93	2.61×10^{-3}
1.000	10	1.0025	0.25	2.14×10^{-3}	1.0204	2.04	1.85×10^{-3}
1.000	20	1.0003	0.03	1.45×10^{-3}	1.0207	2.07	8.11×10^{-4}

Table 5.6: Model 1 computed source strength for different element discretizations for case (ii).

Exact C' (x = 0)	No. of elements	Model 1 solutions Case (ii)					
		$\varepsilon = 0\%$			$\varepsilon = 5\%$		
		C' (x = 0)	Relative error (%)	α	C' (x = 0)	Relative error (%)	α
1.0000	5	1.0005	0.05	2.25×10^{-5}	1.0103	1.03	2.61×10^{-5}
1.0000	10	1.0006	0.06	2.04×10^{-5}	1.0105	1.05	2.49×10^{-5}
1.0000	20	1.0006	0.06	2.25×10^{-5}	1.0104	1.04	1.94×10^{-5}

The flux along $x = 0$ is well estimated in all the cases as shown in Table 5.7. The relative error for the computed solutions is presented in Figure 5.11, where they indicate a decrease with increase in the number of elements. Furthermore, the relative error is smaller for Test (i) than Test (ii), and this is due to the higher number of available data and their location. The computed concentration with 5% observation error has higher mean error.

Table 5.7: Computed flux for different element discretizations with ε=0%.

Exact	Model 1 solutions		
q (x = 0)	No. of elements	Case (i) q (x = 0)	Case (ii) q (x = 0)
0.0339	5	0.0404	0.0805
0.0339	10	0.0306	0.0352
0.0339	20	0.0333	0.0336

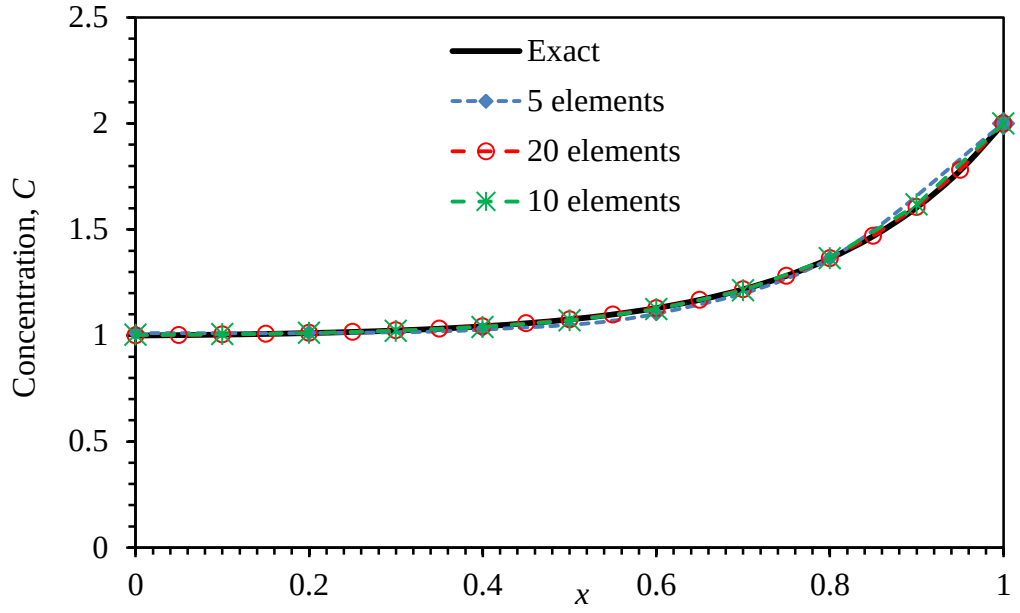


Figure 5.9: Model 1 and exact solutions for concentration with 5, 10 and 20 elements for Case (ii) Test (i).

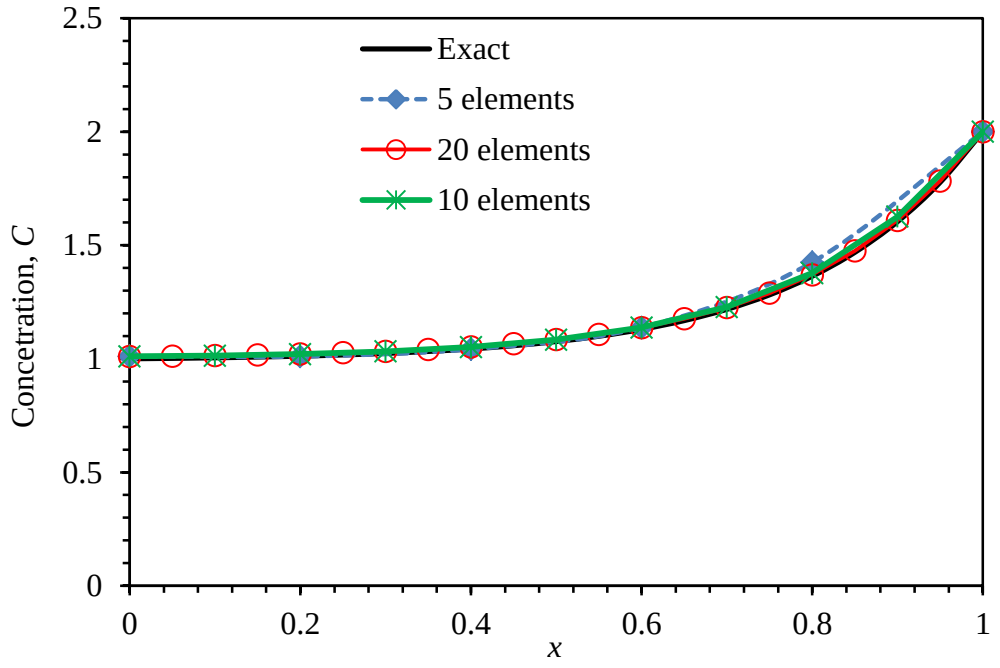


Figure 5.10: Model 1 and exact solutions for concentration with 5, 10 and 20 elements for Case (ii) Test (ii).

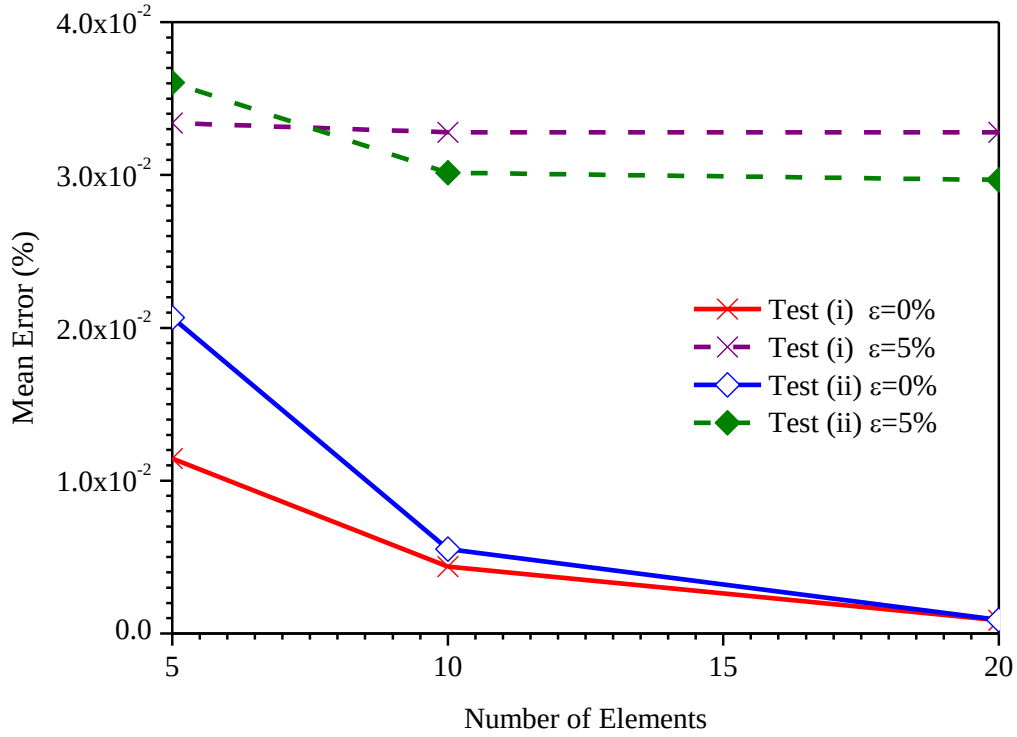


Figure 5.11: Mean error for the computed concentration by Model 1 Case (ii).

5.2 Boundary source problems

In this section, Model 1 and Model 2 are used to perform numerical tests. Five test cases are evaluated; the first three test cases determine the source strength of a concentration boundary while accounting for different transport modes, time discretization, and observation errors. The last two cases determine the source strength of a flux boundary while considering observation errors.

5.2.1 Test Case 1: 1D problem with a continuous constant source

This example is the classical transient one-dimensional contaminant transport problem that arises as a result of advection and dispersion of a continuous contaminant source of strength, *C'* of infinite duration by a uniform velocity field ($\boldsymbol{V} = \boldsymbol{i}u$) and in a homogenous medium. In a real life situation, this case may occur when a polluted river cuts an aquifer and there is stable, uniform, one-dimensional flow in the aquifer. For the conservative transport case with no decay ($\mu = 0$) and absence of external sources ($Q = 0$), the exact solution is given in Equation (5.1).

Posed as an inverse problem, the strength of the contaminant source, C' is unknown. A 2-D rectangular domain is used for the GEM simulations. On the top and bottom boundaries of the domain, a no-flux condition is prescribed, and the lateral extent in the x-direction for the right boundary, L, is set as a Dirichlet boundary. Along the left boundary ($x = 0$) the source concentration and flux are not known so that it is a Γ_4 boundary. The initial concentration everywhere in the domain is zero.

Numerical solutions are assessed for three cases or types of transport.

- Case (i) represents an advective dominant transport with a Peclet number ($Pe = u\Delta x/D$) of 50.
- Case (ii) represents marginal advection dominant transport of $Pe = 1$.
- Case (iii) is a dispersion dominant one with $Pe = 0.05$.

The simulation parameters of these three transport cases are given in Table 5.8. The influence of the time step on the numerical solutions is assessed for three values of the Courant number, $Cr = u\Delta t/\Delta x$, namely $Cr = 1.0$, $Cr = 0.5$ and $Cr = 0.1$. The sampling location for concentration measurements for $Pe = 50$ and 1 is at $\gamma = 0.025$ and for $Pe = 0.05$ the observation point is located at $\gamma = 0.125$. The values of the regularization parameter, α, are obtained by the L-curve.

Table 5.8: Simulation parameters for Test Case 1 with boundary sources.

Transport case	***Pe***	***D***	***u***	**Δx**	***L***
Advection dominant (i)	50.0	0.0005	1.0	0.025	1.0
Marginal advection (ii)	1.0	0.025	1.0	0.025	1.0
Dispersion dominant (iii)	0.05	2.5	1.0	0.125	5.0

(i) Advection dominant transport

With the exact value of the concentration source $C' = 1$ for all times, it's computed value at various times for the advection dominant case (i) is presented in Figure 5.12. From Figure 5.12, it is observed that there is correct prediction of the strength of the contaminant source by Model 1 for $t > 0.08$. At early times the

numerical solutions oscillate about the exact value with the simulation of $Cr = 1.0$ exhibiting the least amount of oscillation compared to those with $Cr = 0.1$ and 0.5. It should be pointed out that unlike in direct numerical modelling with GEM of contaminant transport where the value of the Courant number, *Cr*, influences the numerical stability (Taigbenu, 1999), in inverse modelling its value plays a dual role of influencing the numerical stability and determining the frequency at which data are available to the numerical scheme from the observation points. With respect to the latter role, because the transport process with $Pe = 50$ is predominantly advection driven, the Model 1 simulation with $Cr = 0.1$ takes about 10 time steps before information of the concentration from the pollution source along $x = 0$ becomes available at the two observation points along $\gamma = 0.025$, hence the wild oscillations of the numerical results at the early simulations times, but at later times information of the concentration is frequently available for the numerical calculations as the plume passes this point.

Conversely, the Model 1 simulation with $Cr = 1.0$ takes only one time step before concentration information from the pollution source is available at the two observation points along $\gamma = 0.025$ hence the more subdued oscillations at early times, but information of the concentration is less frequently available for the numerical calculations at later times. Thus, the Model 1 simulation with $Cr = 1.0$ gives better prediction of the source strength at early times than that with $Cr = 0.1$, and conversely at later times. However, it should be pointed out that it is difficult to ascertain whether these two influences of *Cr* on the overall solution are conflicting or complementing, and which influence is more significant for any contaminant transport mode. The Model 1 solutions for all *Cr* values correctly predict the concentration strength at later times. The discrepancy at *t*=0 and the early times is also caused by discontinuities from the zero initial conditions to the constant releases of $C' = 1$. The average relative error for all times for the computed source strength was obtained as 10.37%, 9.46%, and 4.72% for $Cr = 0.1$, $Cr = 0.5$, and $Cr = 1.0$ respectively.

The exact and numerical solutions for the concentration fronts at various times are presented in Figure 5.13, and it shows that the solutions for the contaminant front

are more dispersed with $Cr = 1.0$ and $Cr = 0.5$ than with $Cr = 0.1$, while the latter has trailing oscillations which are not observed for $Cr = 0.5$ and $Cr = 1.0$. The mean error for the computed concentration for $Cr = 0.1$, $Cr = 0.5$, and $Cr = 1.0$ is 0.1942%, 0.2111%, and 0.2196% respectively.

The Model 2 optimization and search termination parameters are given in Table 5.9 for Test Case 1(i). It is of paramount importance to note that the number of decision variables increases with increase in the time steps. The convergence behaviour of the objective function for five runs with different random seeds is shown in Figure 5.14. The minimised objective function was obtained as 9.930×10^{-4}. The objective function values for the 5 runs were identical suggesting very effective optimization. A single run with averagely 70 000 simulations took 54089.12 seconds to compute optimal solutions, while Model 1 took 11.40 seconds for the same problem.

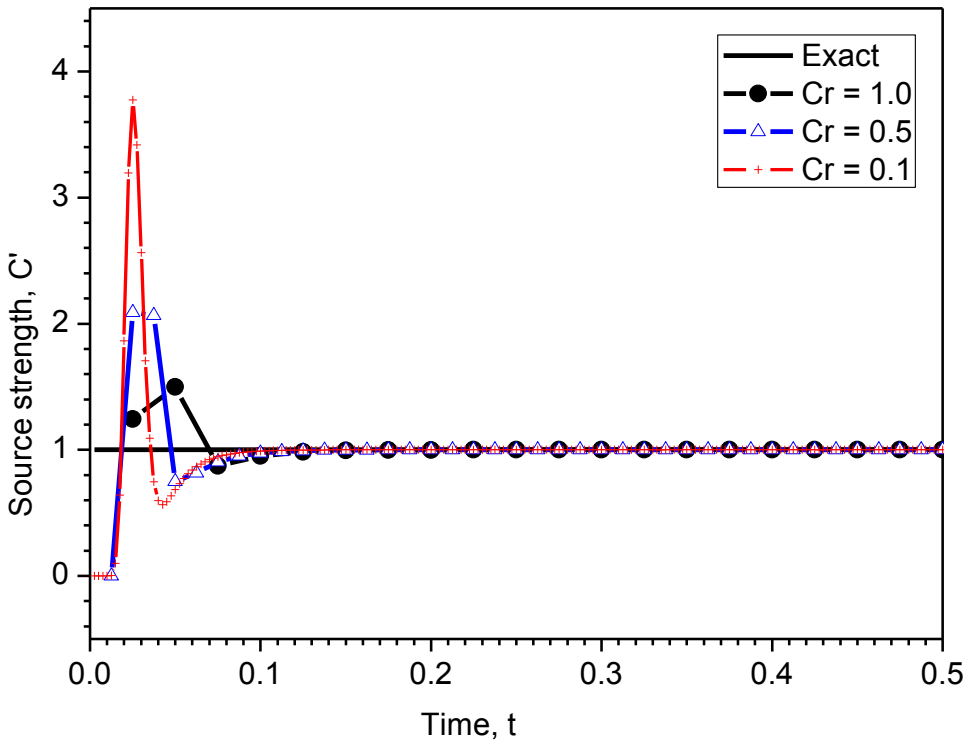


Figure 5.12: Model 1 computed source strength for $Pe = 50$ Test Case 1(i).

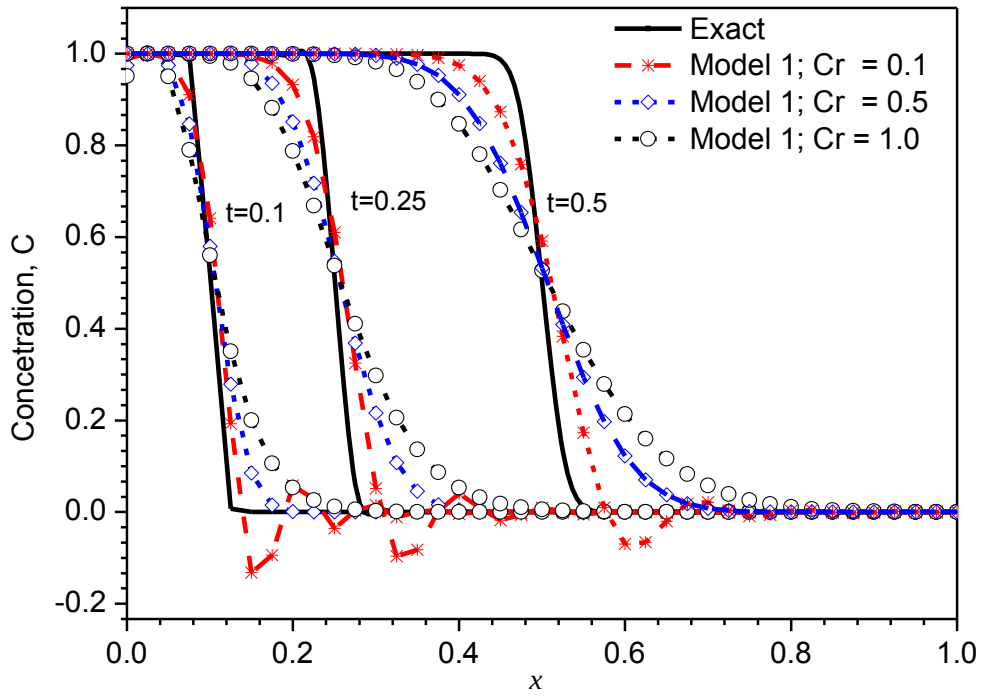


Figure 5.13: Model 1 computed contaminant concentration for $Pe = 50$ of Test Case 1(i).

It is observed from Figure 5.15 that Model 1 and Model 2 compute the source strength accurately after time t>0.08, while an oscillatory behaviour is exhibited in the early times. The computed concentration distribution is given in Figure 5.16, with both models producing more dispersed fronts than the exact. The mean error relative to the exact solution for the concentration distribution is shown in Figure 5.17 and both methods perform equally. It is therefore observed that the computational effort required by Model 2 is much higher than Model 1 for the same results.

Table 5.9 : SCE-UA optimization and search termination parameters for Test Case 1.

Description of parameter	**Notation**	**Peclet, $Pe = 50$ and $Pe = 1$**	**Peclet, $Pe = 0.05$**
Number of decision variables	n_o	40	16
Number of complexes	p_o	10	10
Number of points in each complex	m_o	81	33
Sample size	s_o	810	330
Number of points to select in complex	q_o	41	17
Optimization parameter	α_{opt}	1	1
Optimization parameter	β_{opt}	81	33
Minimum value of the objective function	minmax	0.001	0.001
Maximum number of epochs for termination	maxepoch	100	100
Change in epoch objective function prompting termination	conv	0.005	0.005
Spacing of epochs in checking for convergence	iconv	10	10

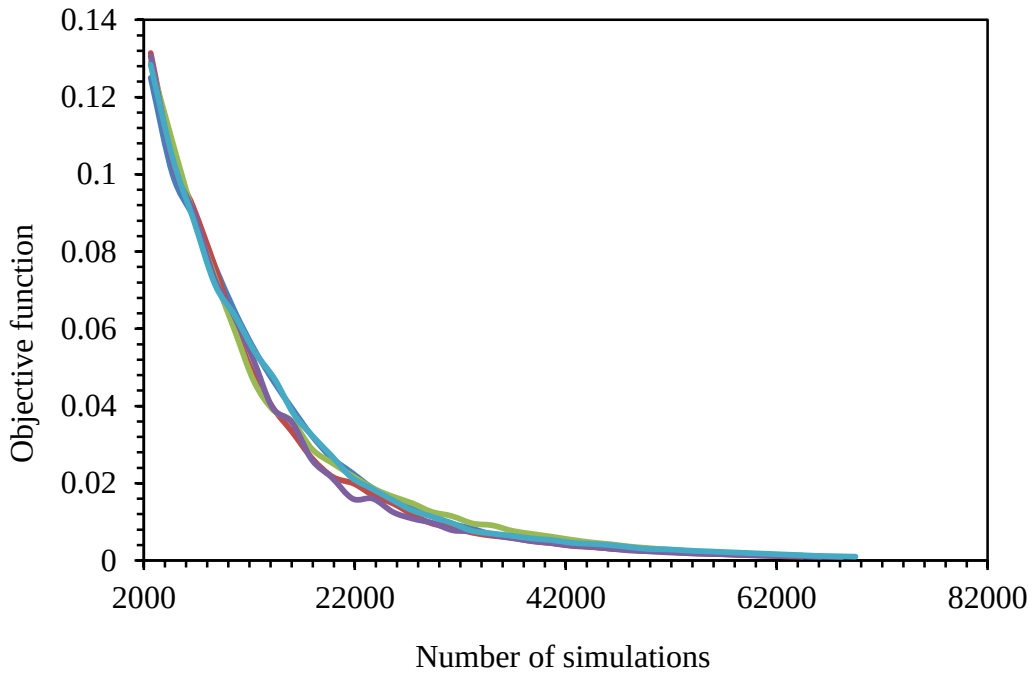


Figure 5.14: Model 2 simulation runs for $Pe = 50$ of Test Case 1(i).

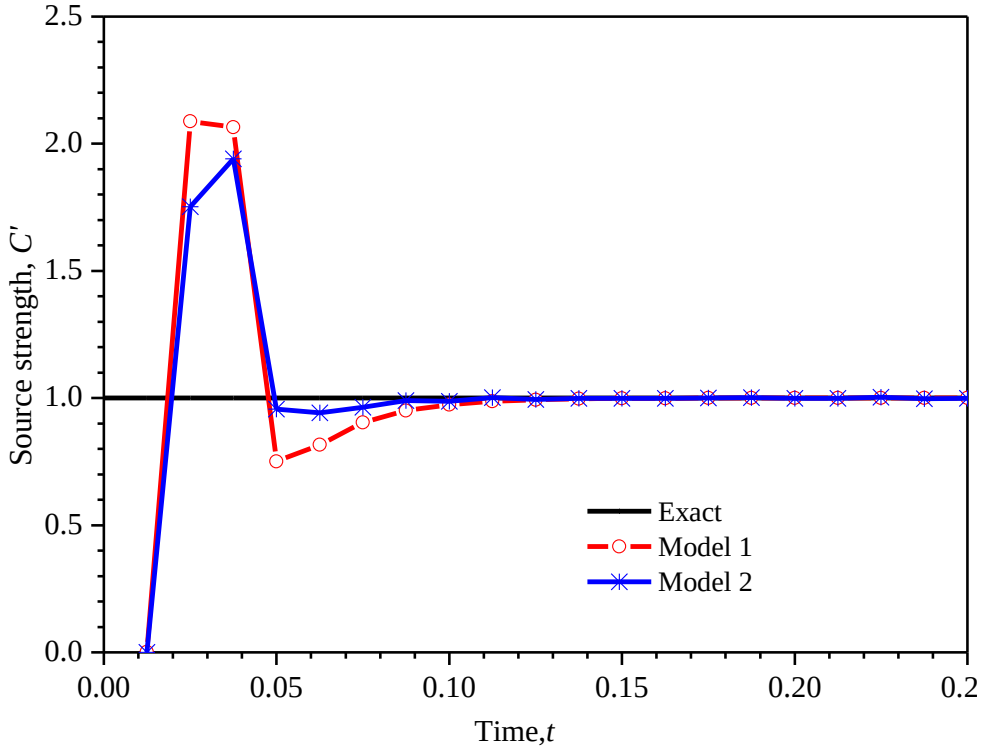


Figure 5.15: Model 1 and Model 2 computed solutions of the contaminant source strength for $Pe = 50$ with $Cr = 0.5$ of Test Case 1(i).

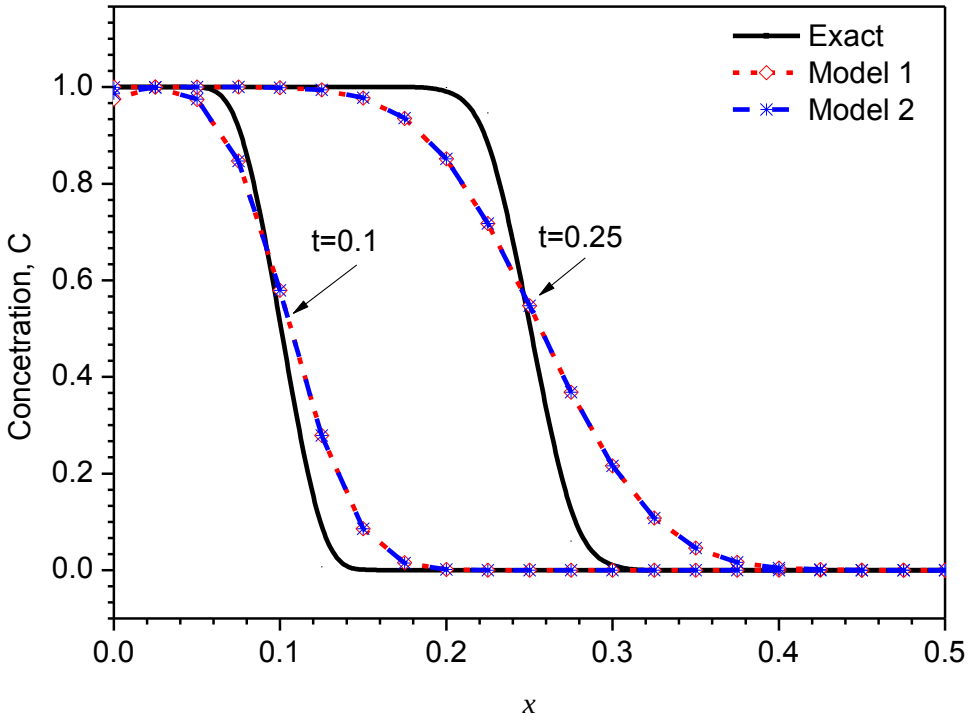


Figure 5.16: Model 1 and Model 2 solutions for the concentration contaminant fronts for $Pe = 50$ with $Cr = 0.5$ of Test Case (i).

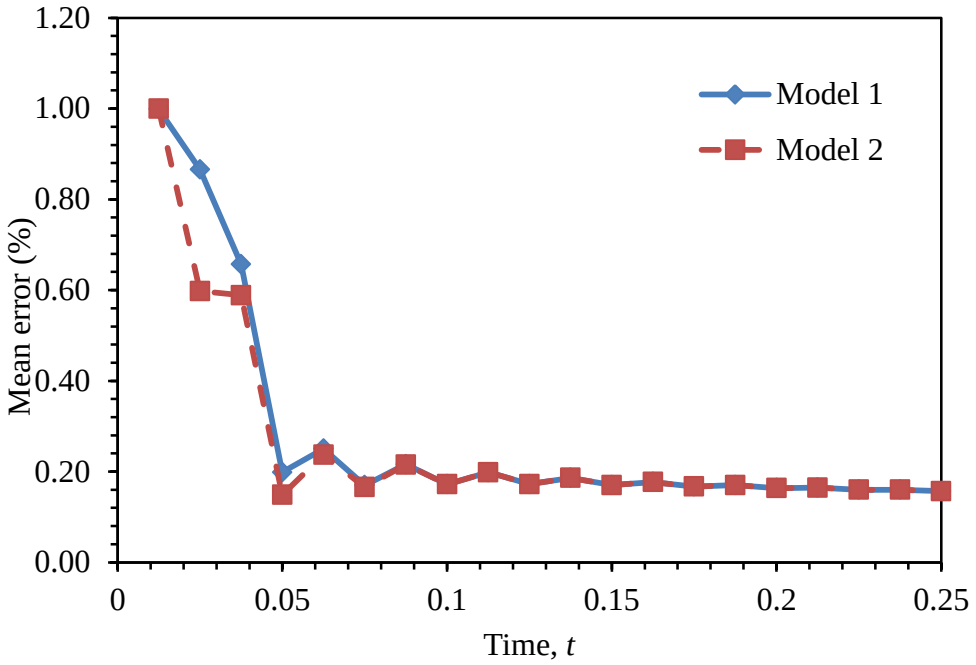


Figure 5.17: Mean error for the concentration distribution for Model 1 and Model 2 with $Pe = 50$ of Test Case 1(i).

(ii) Marginal advection transport

For the transport case (ii) of marginal advection ($Pe = 1$), the Model 1 computed source strength is presented in Figure 5.18. The source strength is correctly predicted for $t > 0.08$. Because this contaminant transport case is more dispersive than the previous one, the spread of the contaminant plume is larger thus information at the observation point closest to the source is readily available. Furthermore, the numerical solutions do not exhibit oscillations as in case (i) because the observation points have information of the concentration at small times in case (ii) than case (i), and from results of direct modeling, this transport case has better numerical stability characteristics than the advection-dominant case (i) [Taigbenu,1995]. The exact and Model 1 solutions of the computed concentration distribution of the contaminant are shown in Figure 5.19. The results with Cr=0.1 give slightly better prediction of the contaminant front than $Cr = 0.5$ and $Cr = 1.0$. The mean error for the computed concentration for $Cr = 0.1$, $Cr = 0.5$, and $Cr = 1.0$ were obtained as 0.017%, 0.042%, and 0.072% respectively.

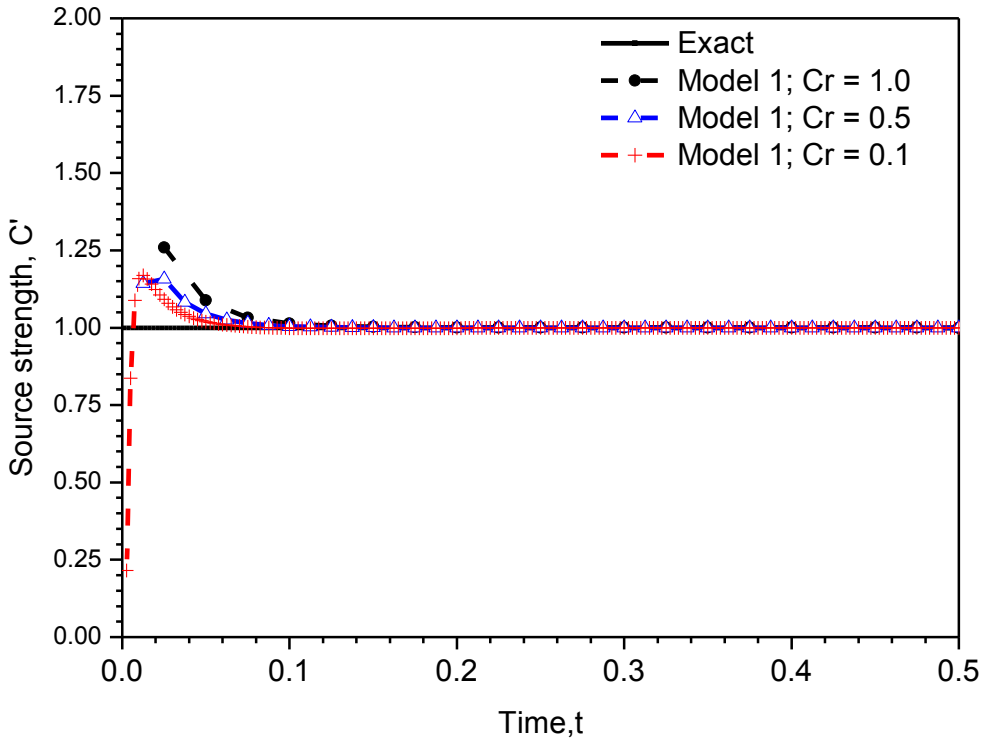


Figure 5.18: Model 1 computed source strengths with different Courant numbers for $Pe = 1$ of Test Case 1 (ii).

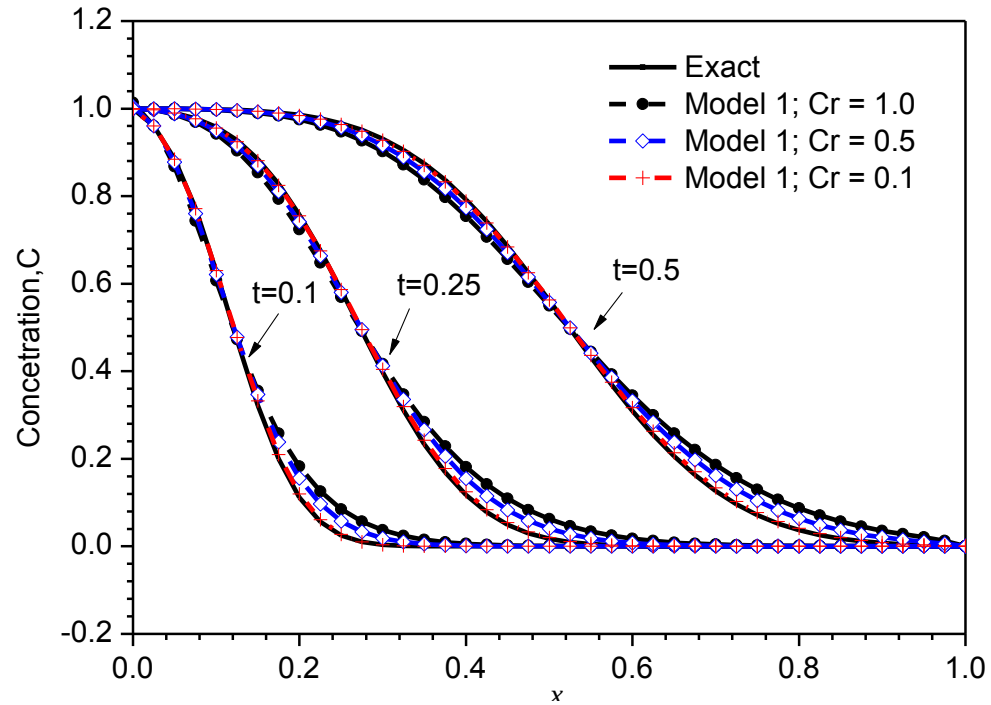


Figure 5.19: Model 1 computed contaminant concentration fronts for $Pe = 1$ of Test Case 1 (ii).

The Model 2 parameters and the termination criteria used in this simulation are the same as for $Pe = 50$, see Table 5.9. Several runs with different random seeds were carried out and a minimized objective function of 9.991×10^{-4} was obtained as shown in Figure 5.20. On average a run for this case took 46 000 simulations, and the simulation time for a single run is 7701.15 seconds compared to 1.39 seconds for Model 1. It is observed from Figure 5.21 that the results from Model 1 and Model 2 are largely the same; however, the former converges quicker to the exact source strength than the latter. The historical distribution of the concentration is given in Figure 5.22 and the recovered concentrations from both models are identical. The mean error for the computed concentration solutions to the exact is shown in Figure 5.23. Model 1 has higher errors at early times but then the errors of both models decrease thereafter.

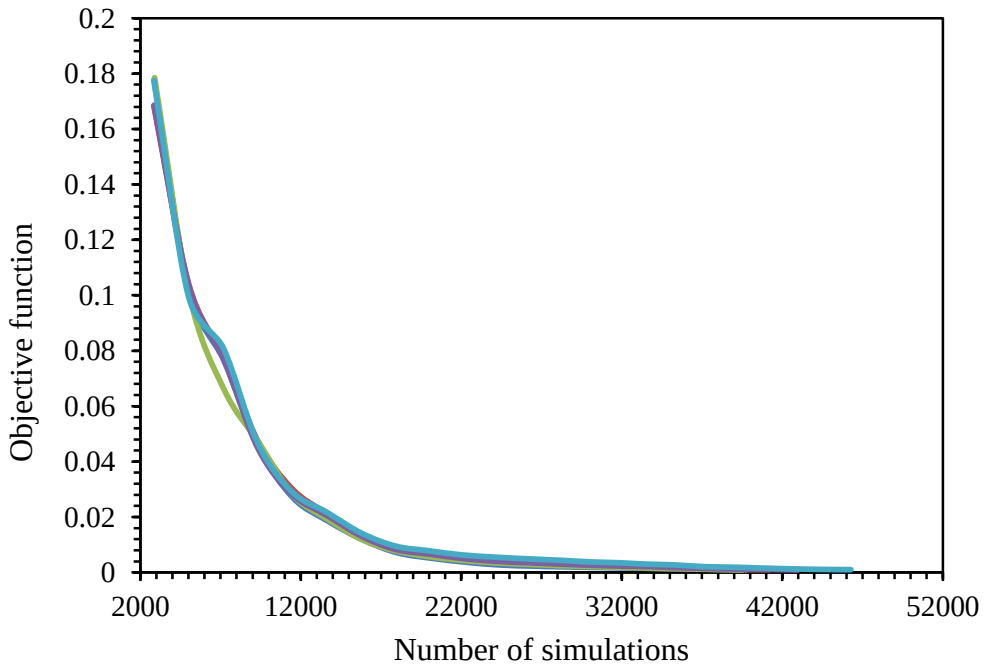


Figure 5.20: Model 2 objective function plot for $Pe = 1$ of Test Case 1 (ii).

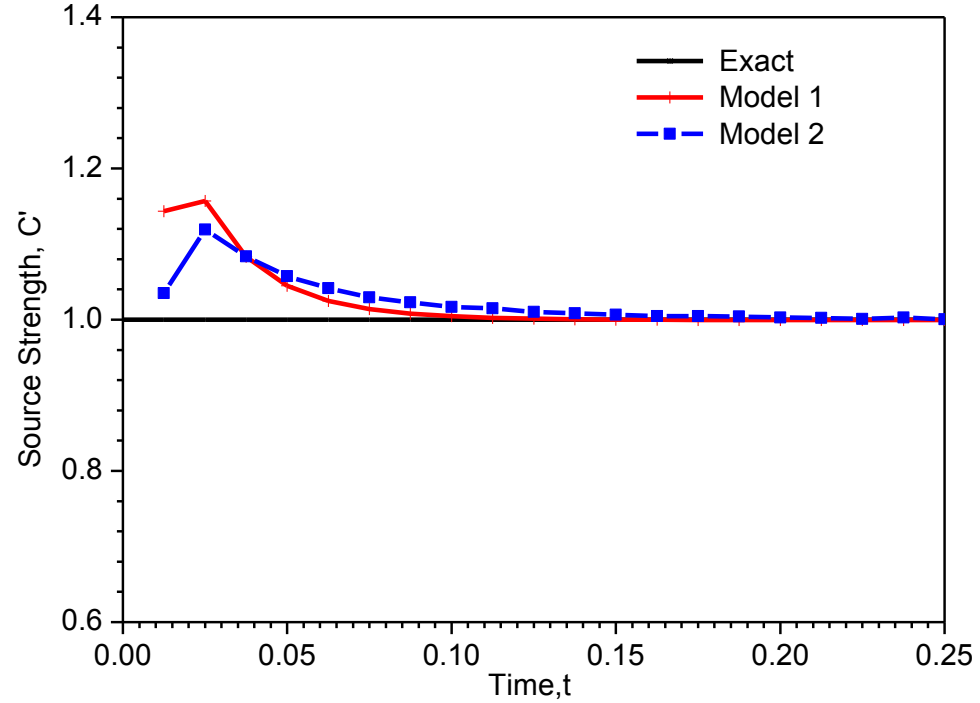


Figure 5.21: Model 1 and Model 2 computed source strengths for $Pe = 1$ of Test Case 1 (ii).

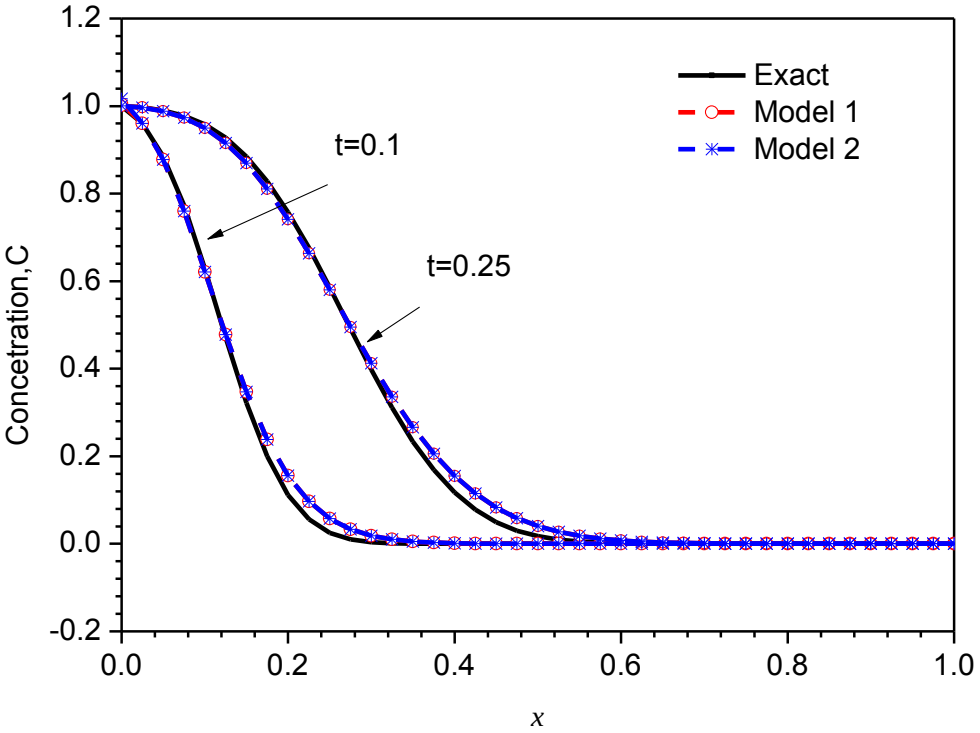


Figure 5.22: Model 1 and Model 2 computed concentration for $Pe = 1$ of Test Case 1 (ii).

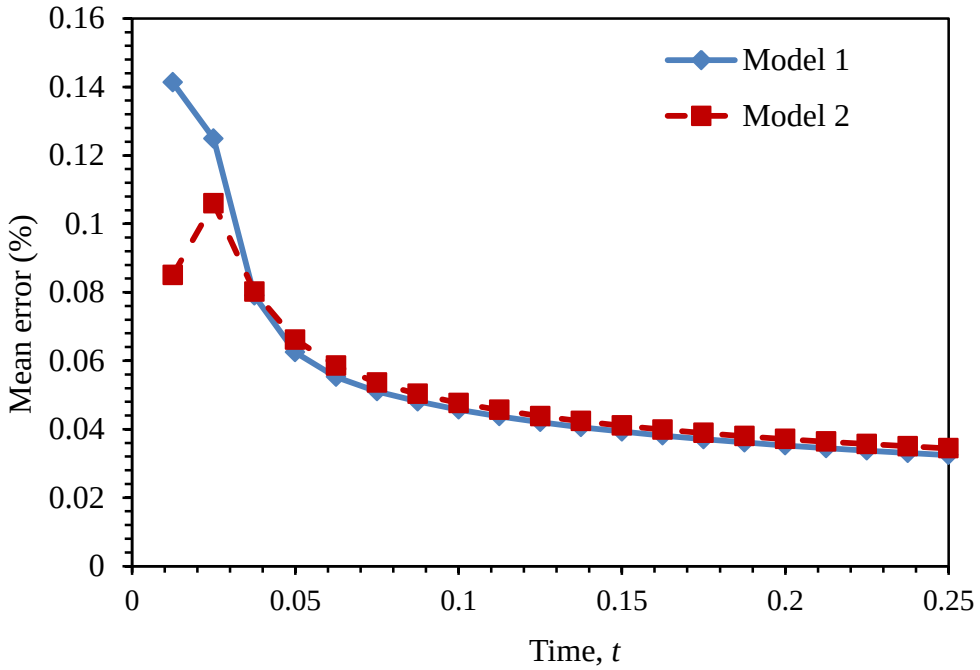


Figure 5.23: Mean error for the computed concentration by Model 1 and 2 for $Pe = 1$ of Test Case 1 (ii).

(iii) Dispersion dominant transport

For the dispersion dominant transport case (iii) with $Pe = 0.05$, the source strength is predicted accurately except for the first time step when $Cr = 1.0$ and $Cr = 0.5$ and for the first three time steps when $Cr = 0.1$ (Figure 5.24). For the same reasons alluded to earlier with the previous transport case (ii), the information at the observation point closest to the source is readily available even at small time steps thus better approximations of the source strength and the historical distribution are obtained. One feature of the numerical solutions in Figure 5.24, also observed for the advection-dominant, and marginal advection transport is that the simulations with $Cr = 0.1$ give the best prediction of the pollution source strength at later times. Figure 5.25 shows the contaminant fronts at times $t = 0.125, 0.25$ and 0.5 for all Courant numbers. The Model 1 solution of the contaminant front with *Cr*=0.1 is excellent and slightly better than that with $Cr = 0.5$ and $Cr = 1.0$. The mean errors for the computed concentration with $Cr = 0.1, 0.5,$ and 1.0 are 0.073%, 0.084%, and 0.096% respectively.

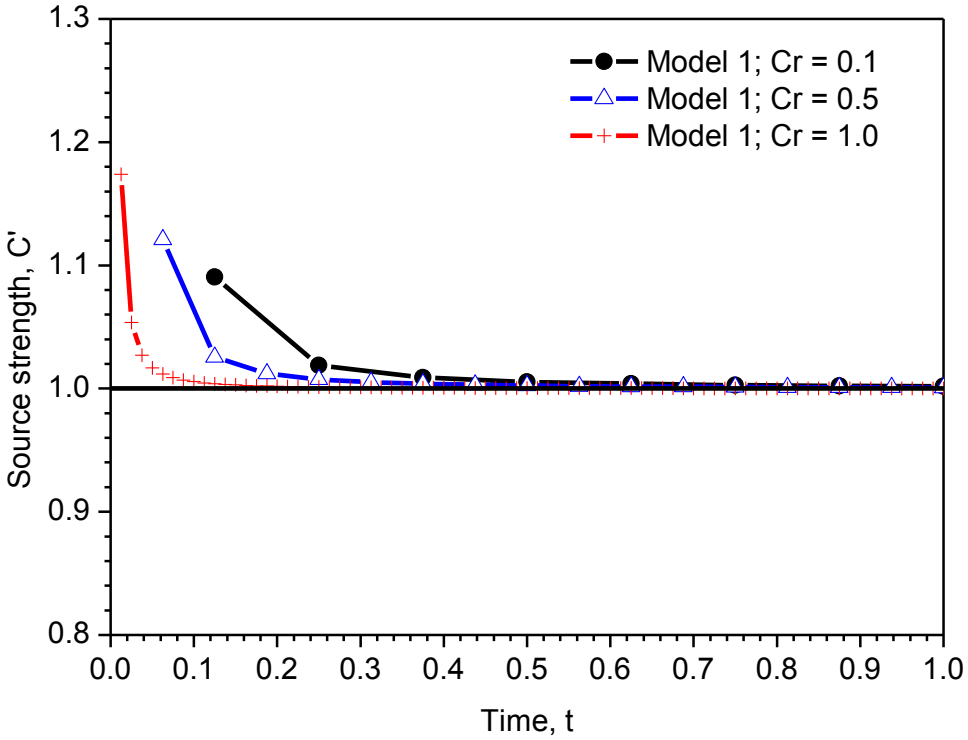


Figure 5.24: Model 1 computed source strength for $Pe = 0.05$ of Test Case 1 (iii).

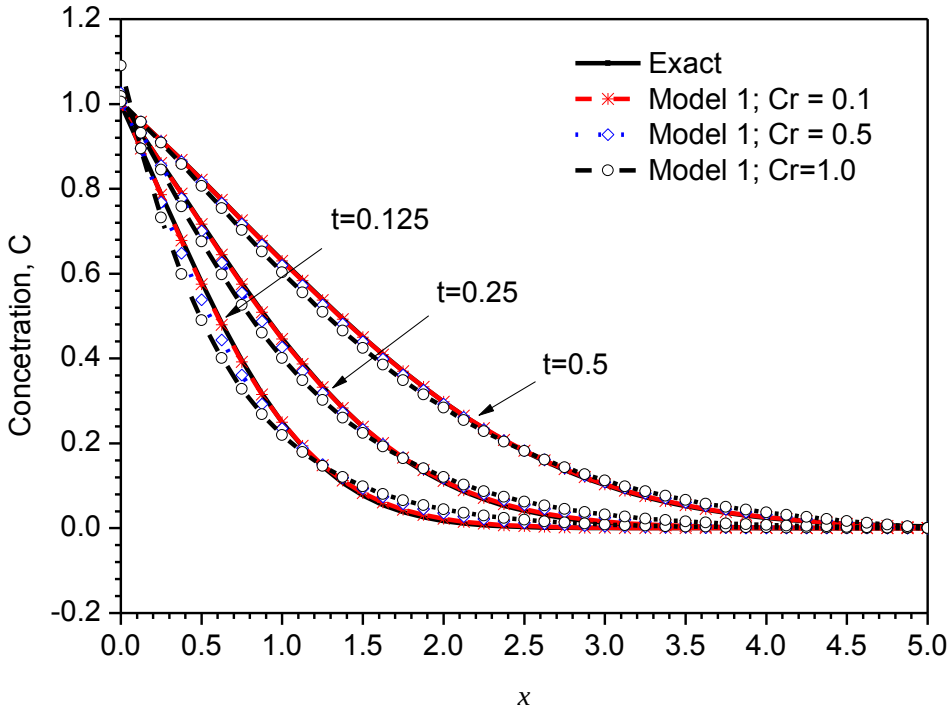


Figure 5.25: Model 1 computed plume concentration with $Pe = 0.05$ of Test Case 1 (iii).

Simulation parameters for Model 2 with $Pe = 0.05$ are given in Table 5.9. An objective function of 8.411×10^{-4} was obtained from a number of simulation runs as shown in Figure 5.26. An average run with approximately 15,000 simulations took 245.61 seconds compared to 2.71 seconds for Model 1. The computed source strength in Figure 5.27 is estimated excellently by both Models 1 and 2. There is agreement in the predicted concentration distribution by both models (see Figure 5.28). The mean error relative to the exact concentration in Figure 5.29 shows that both models perform equally and satisfactorily for this case.

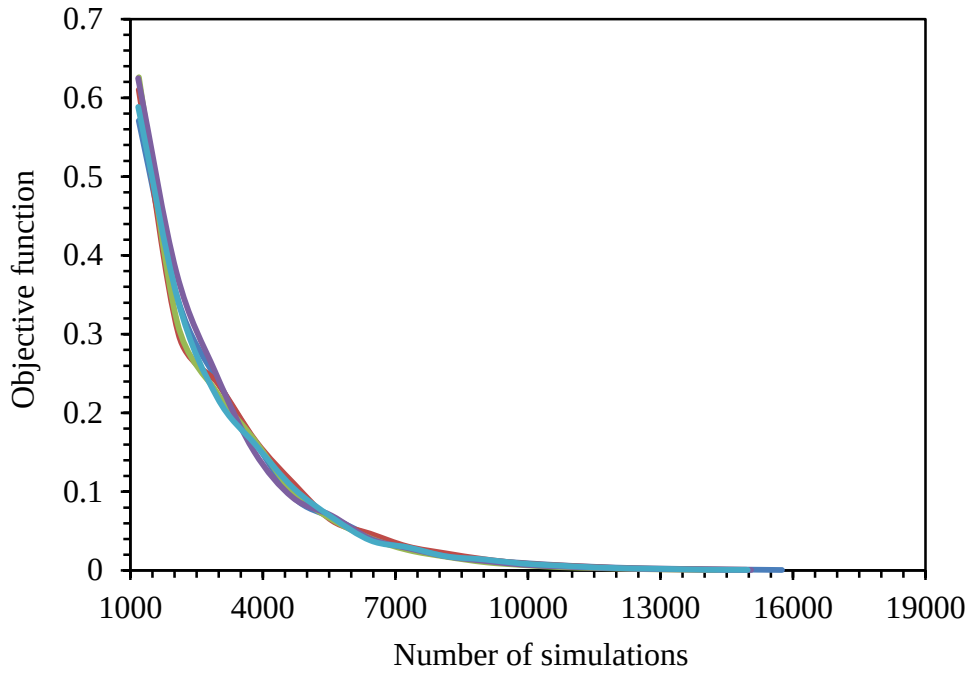


Figure 5.26: The objective function plot for Pe=0.05 of Test Case 1 (iii).

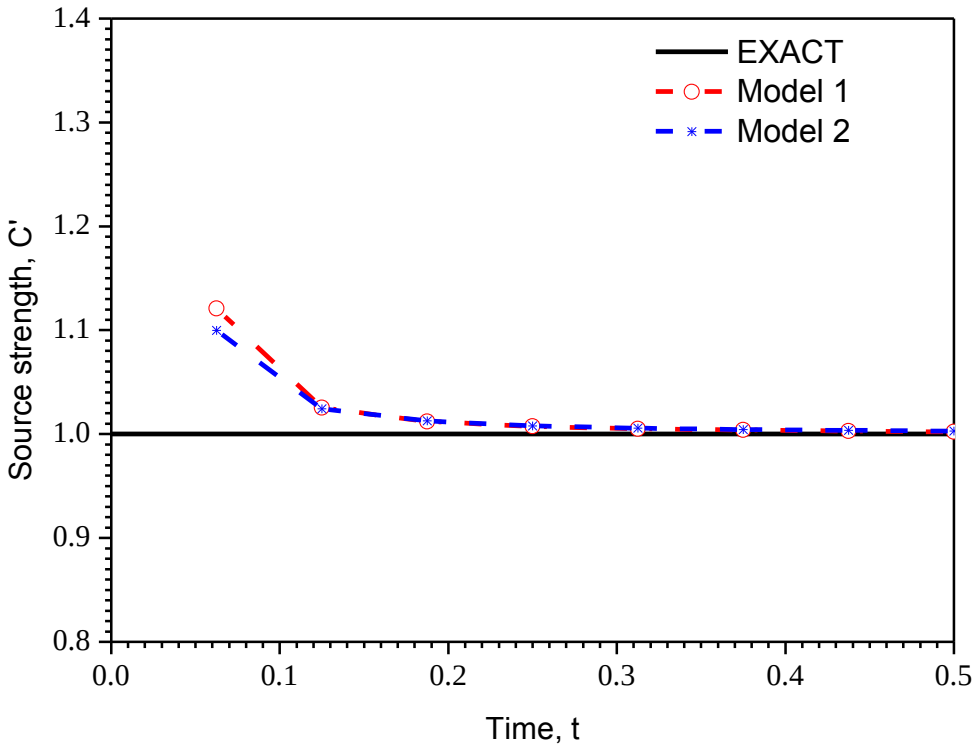


Figure 5.27: Model 1 and 2 computed source strength for *Pe*=0.05 of Test Case1 (iii).

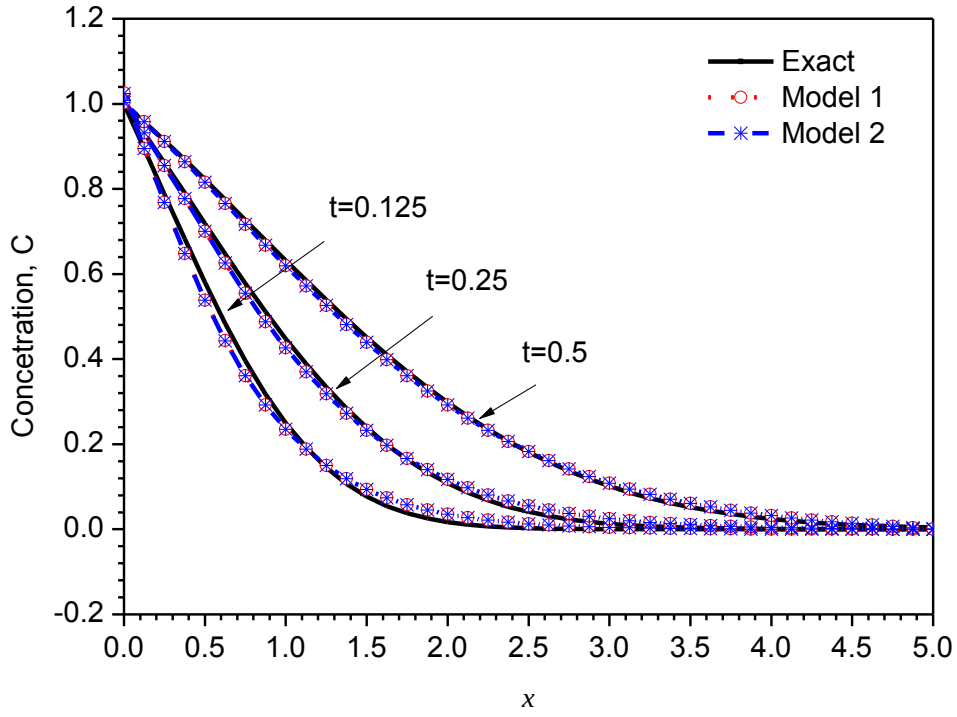


Figure 5.28: Model 1 and 2 computed concentration distribution for $Pe = 0.05$ of Test Case 1 (iii).

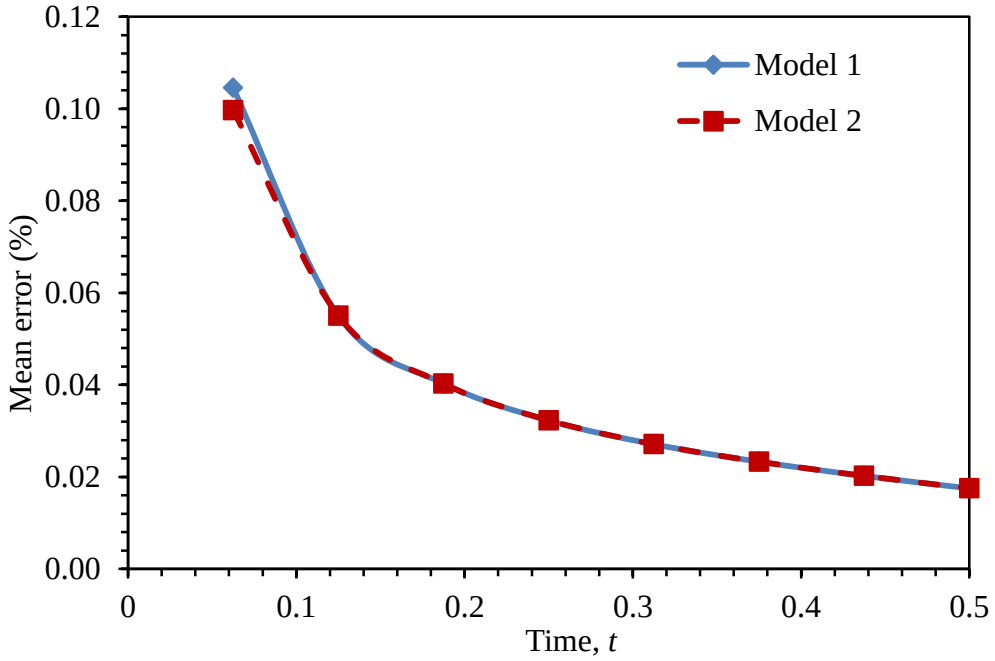


Figure 5.29: Mean error for the computed concentration by Model 1 and Model 2 for $Pe = 0.05$ of Test Case 1(iii).

(d) Random error in the observation data of Test case 1

To investigate the influence of observation errors on source recovery, observation data were randomly perturbed with noise levels of $\varepsilon = 1\%$, 3%, and 5% using Equation 3.27. The simulation data were kept same as for the error free case in Table 5.8. The Model 1 solutions for the source strength and the concentration distribution for $Pe = 50$ are presented in Figure 5.30 and 5.31, $Pe = 1$ are presented in Figure 5.32 and 5.33, while $Pe = 0.05$ are presented in Figure 5.34 and 5.35 for various noise levels. The estimated solutions give a good prediction of the contaminant source strength at noise level of 1% but oscillate about the exact solution at noise levels of 3% and 5%. A good prediction of the contaminant concentration was obtained in all cases, for $Pe = 50$ the predicted concentration matched the computed with $\varepsilon = 0$, while for $Pe = 1$ and $Pe = 0.05$ the estimated concentration matched the exact solution. Generally, it is observed that observation errors do not influence the computed concentration distribution.

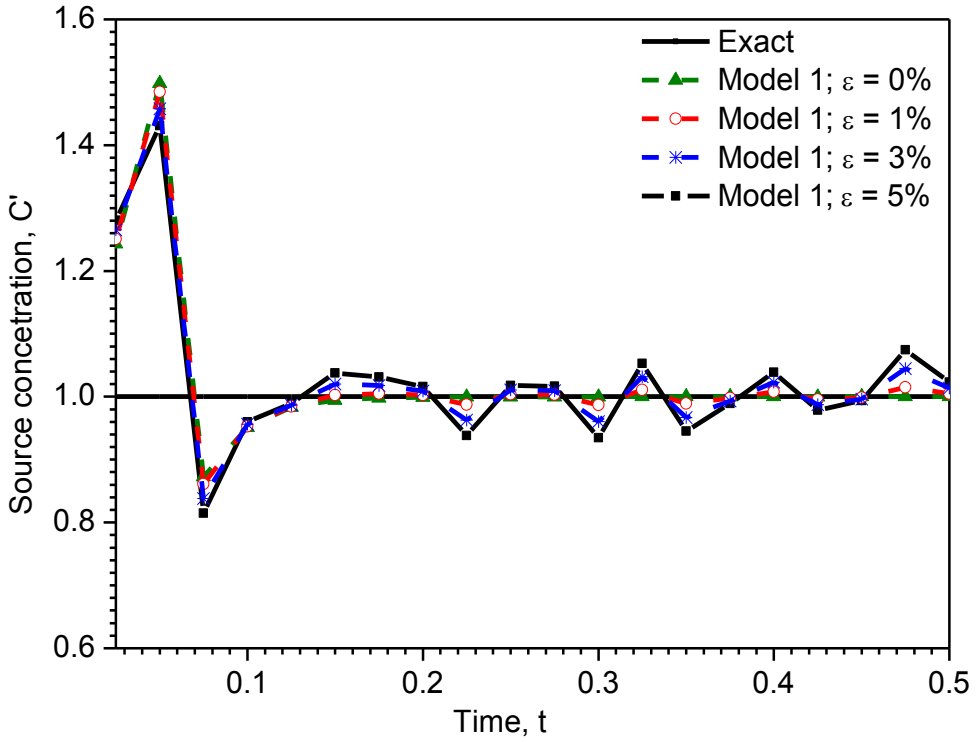


Figure 5.30: Model 1 computed source strength with noisy observation data for $Pe = 50$ and $Cr = 1.0$ of Test case 1 (i).

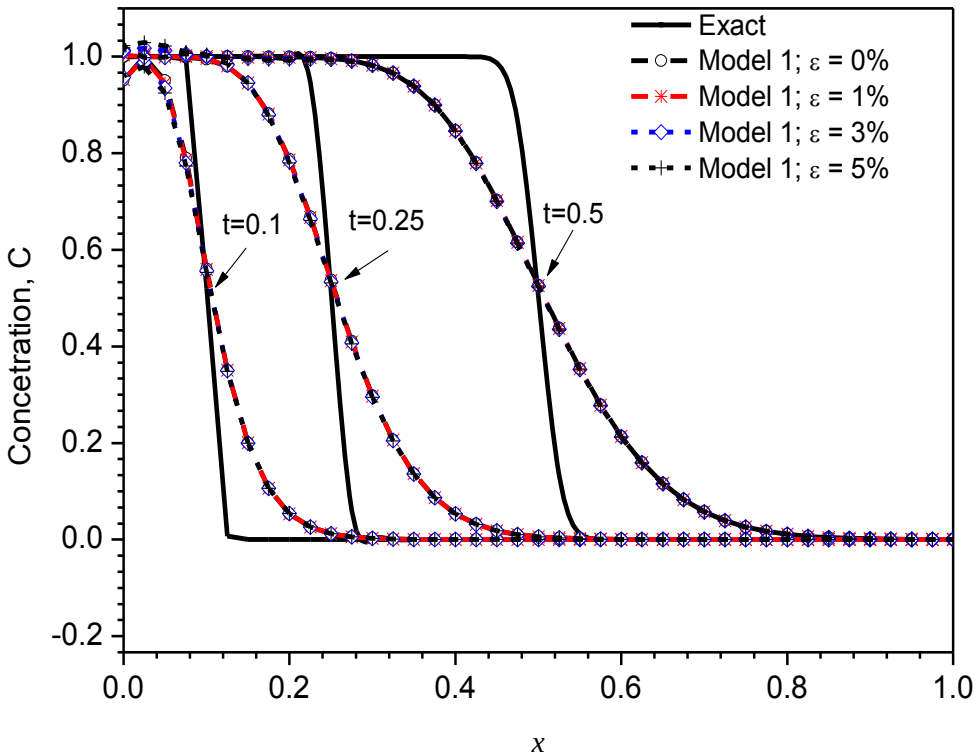


Figure 5.31: Model 1 computed concentration distribution with noisy observation data for $Pe = 50$ and $Cr = 1.0$ of Test Case 1 (i).

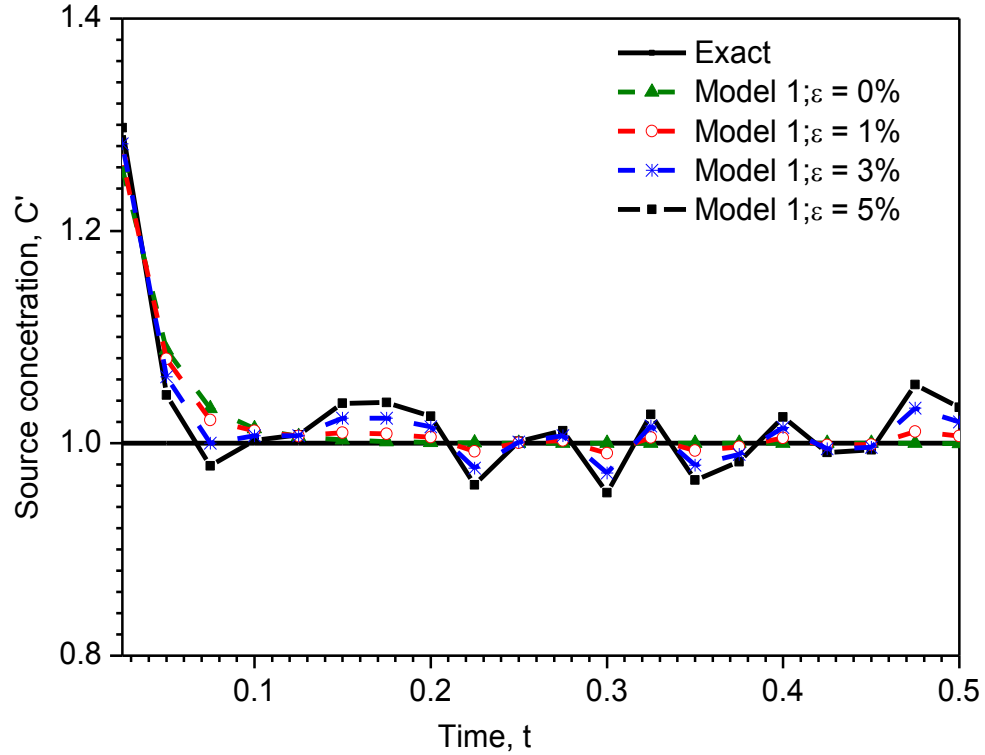


Figure 5.32: Model 1 computed source strength with noisy observation data for $Pe = 1$ and $Cr = 1.0$ of Test case 1 (ii).

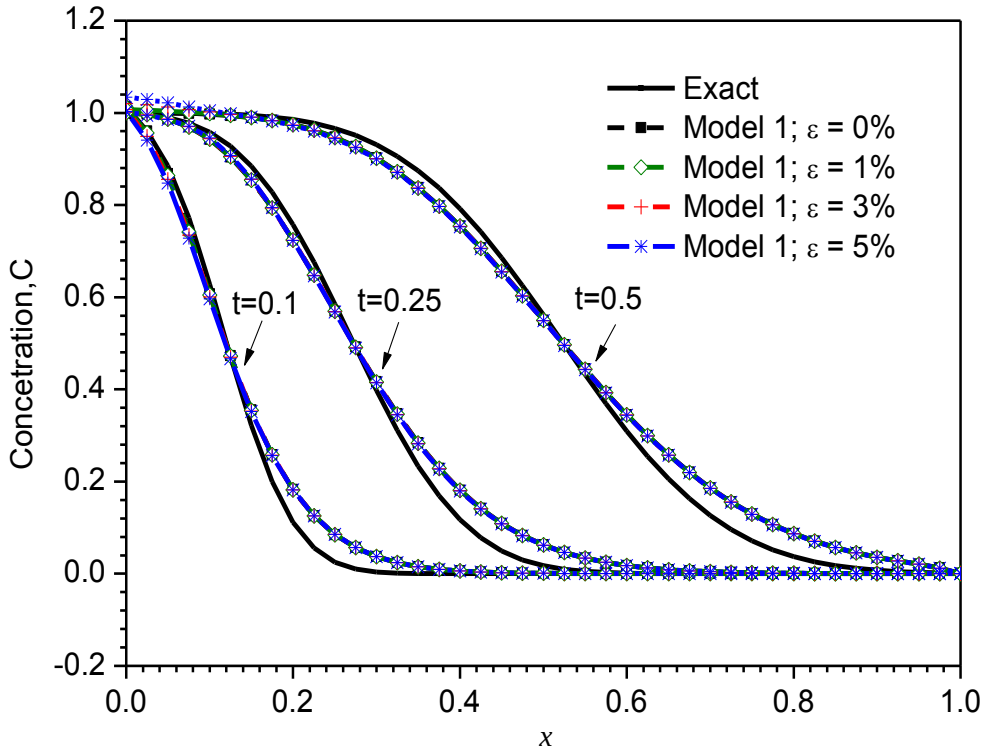


Figure 5.33: Model 1 computed concentration fronts with noisy data for $Pe = 1$ and $Cr = 1.0$ of Test Case 1 (ii).

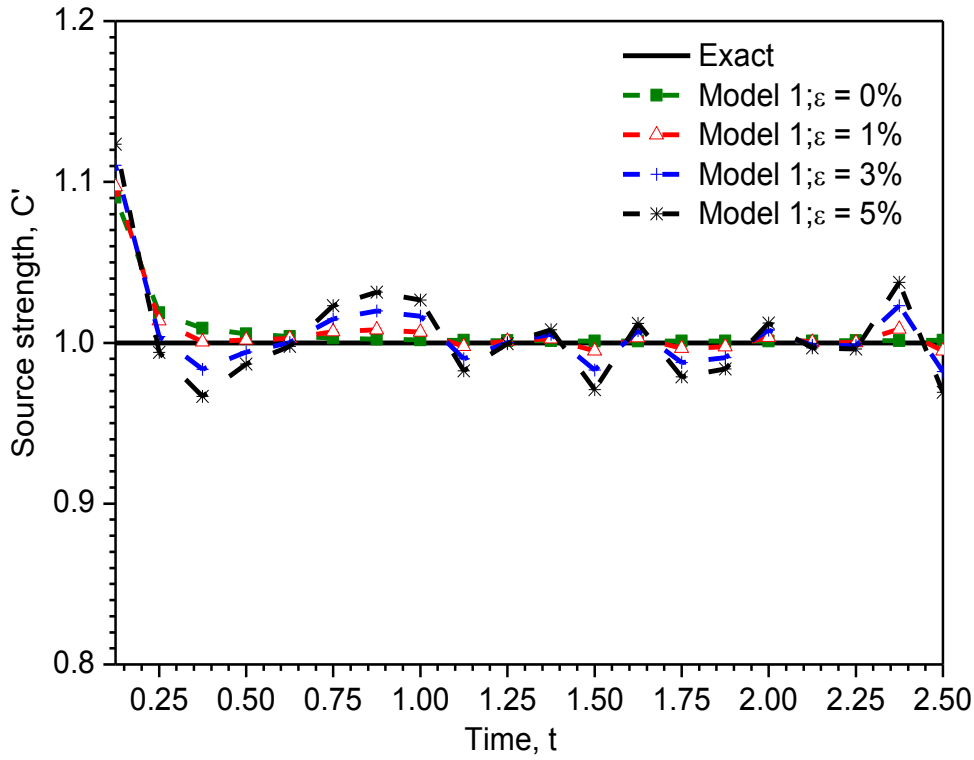


Figure 5.34: Model 1 computed source strength with noisy observation data for $Pe = 0.05$ and $Cr = 1.0$ of Test Case 1 (iii).

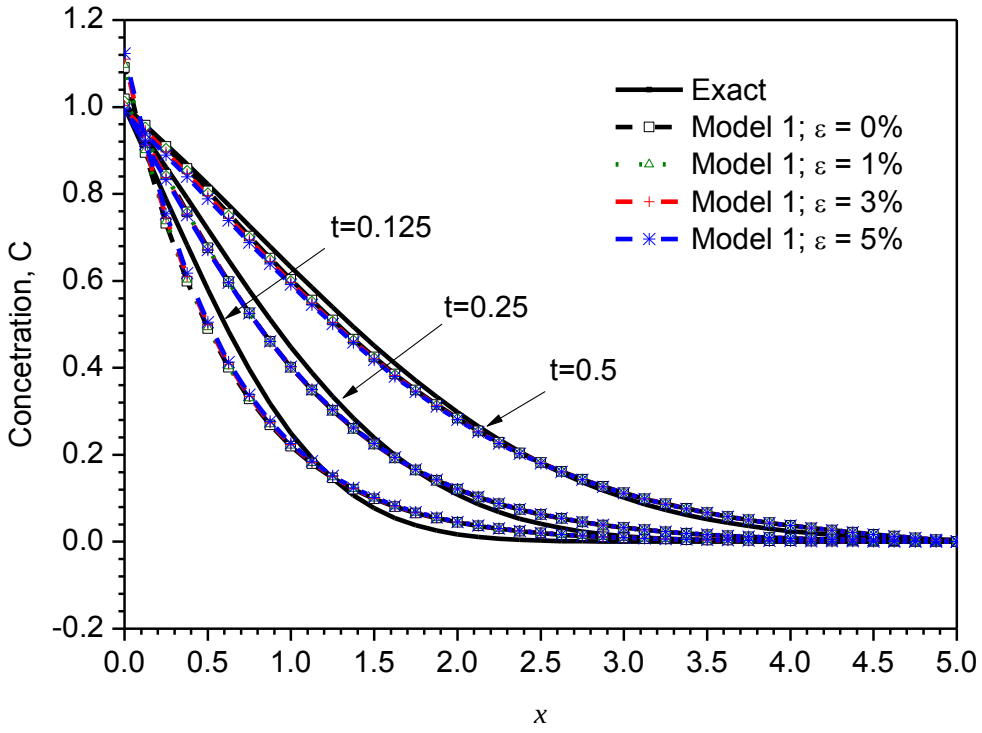


Figure 5.35: Model 1 computed concentration with noisy observation data for $Pe = 0.05$ and $Cr = 1.0$ of Test case 1 (iii).

5.2.2 Test case 2: 1D problem with a decaying source

This test case is a 1-D problem with a decaying contaminant source that is introduced into a homogeneous and isotropic aquifer. It is governed by the advection dispersion Equation (2.4) with R =1, μ = 0, Q = 0. The velocity flow field is uniform in the x-direction, $\boldsymbol{V} = \boldsymbol{i}u$. The initial and boundary conditions for the direct problem shown in Figure 5.36 are given as:

$$\begin{aligned} &C(x,0) = 0;\ x \geq 0 \\ &C(0,t) = C' e^{\Theta t};\ t > 0 \\ &\mathrm{C}\,(L,t) = 0;\ t \geq 0 \end{aligned} \tag{5.6}$$

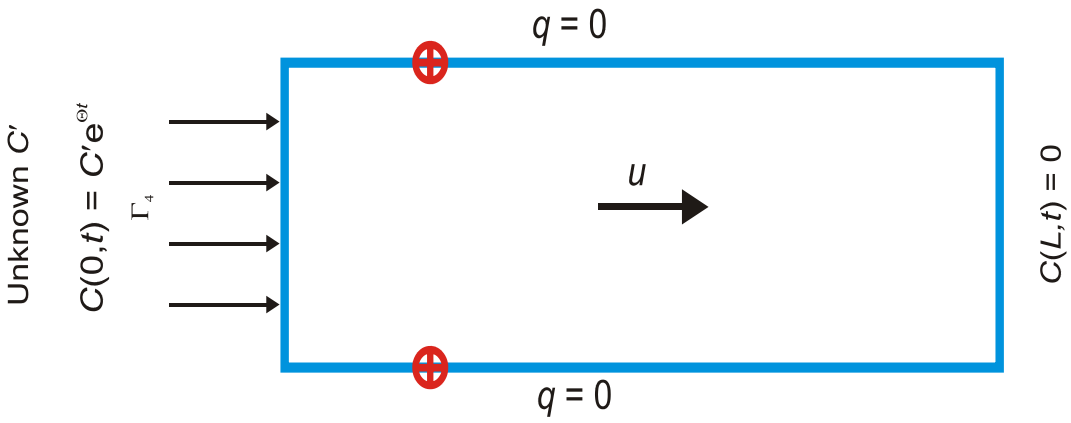


Figure 5.36: 1D porous medium with a decaying source.

The analytical solution is given in Mariño, 1974 as;

$$C(x,t) = \frac{C' e^{\Theta t}}{2} \left\{ \begin{aligned} &\exp\left[\frac{x(u-\phi)}{2D}\right] erfc\left(\frac{x-\phi t}{2\sqrt{Dt}}\right) + \\ &\exp\left[\frac{x(u+\phi)}{2D}\right] erfc\left(\frac{x+\phi t}{2\sqrt{Dt}}\right) \end{aligned} \right\} \tag{5.7}$$

in which, Θ is a constant, positive, or negative, and $\phi = \left(u^2 + 4D\Theta\right)^{1/2}$

Inverse modeling of this example is carried out in a finite 2-D rectangular domain and requires the calculation of the variable source concentration along x=0, while the right boundary is specified as a Dirichlet boundary and the top and bottom

boundaries are no-flux boundaries. A value of Θ = -1.0 is used in the exact solution. Two modes of transport are evaluated, namely;

- advection dominant transport with $Pe = 50$ ($D = 0.12$, $u = 6.0$, and $\Delta x = 1.0$),
- equal dispersion-advection transport with $Pe = 1$ ($D = 6.0$, $u = 6.0$, and $\Delta x = 1.0$).

There are two observation points where concentration measurements are available on the top and bottom boundaries along $\gamma = 1.0$ The influence of the time step on the numerical solution is examined for Courant numbers, $Cr =$ 0.1, 0.5, and 1.0.

(a) Advective dominant transport

Figure 5.37 shows the computed source strength with time for $Pe = 50$. As in the previous case and for the reasons explained earlier, the Model 1 solutions for the source strength oscillates about the exact values for small times $t < 0.5$, and the Model 1 simulation with $Cr = 1.0$ gives the best estimate of the source strength, while that with $Cr = 0.1$ out-performs the others at later times. The estimated and exact solutions of the spatial distribution of the concentration plume are shown in Figure 5.38. The Model 1 solution with $Cr = 0.1$ better captures the steep concentration fronts than with $Cr = 0.5$ and 1.0 but it under-predicts the concentration profile just downstream of the front. The average mean error for the computed concentration for $Cr = 0.1, 0.5$, and 1.0 is 0.317%, 0.343%, and 0.362% respectively.

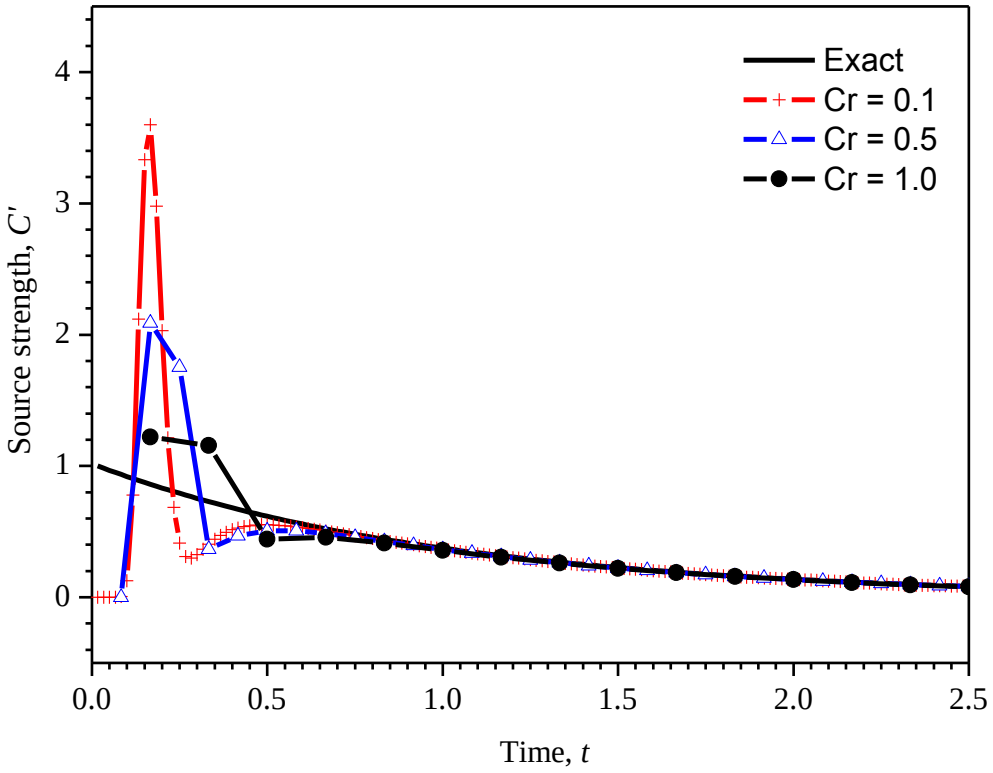


Figure 5.37. The exact and Model 1 solutions for the source strength for $Pe = 50$ of Test case 2.

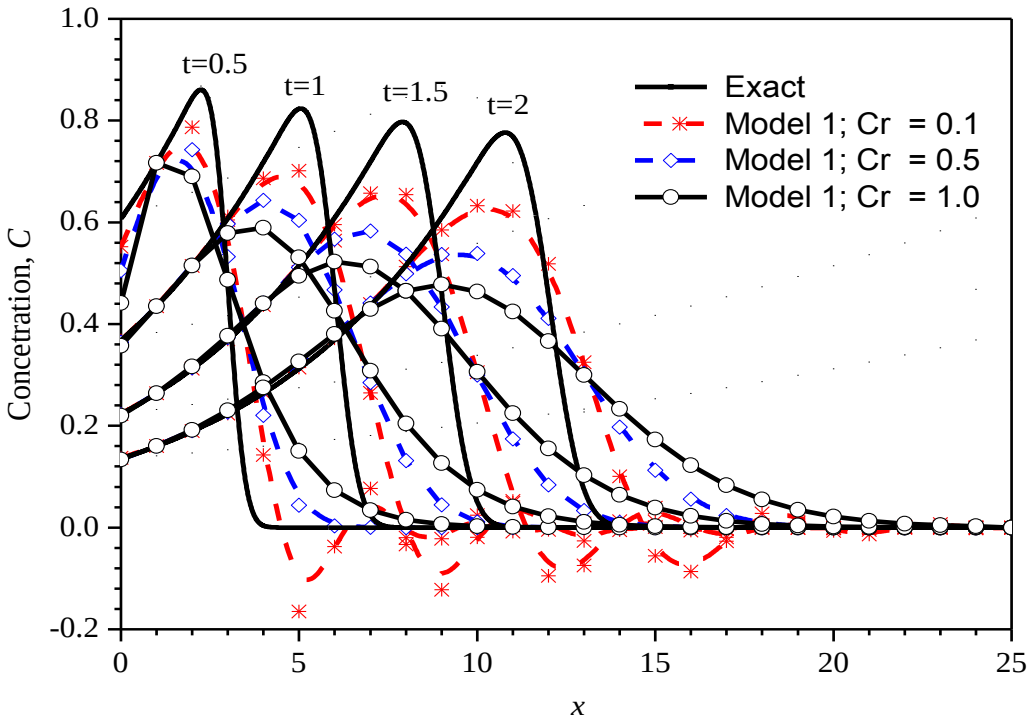


Figure 5.38: The exact and Model 1 computed concentration distribution of $Pe = 50$ of Test Case 2.

(a) Equal dispersion-advection transport

For the equal dispersion-advection transport case, the exact and Model 1 solutions of the source strength are shown in Figure 5.39. The source strength is excellently estimated by Model 1 except at early times. Furthermore, the concentration profiles at various times are presented in Figure 5.40 which shows that the inverse solutions with $Cr = 0.1$ are the most accurate with mean error of 0.027% compared with those of $Cr = 0.5$ and 1.0 with mean error of 0.066%, and 0.114% respectively.

The equal advection-dispersion case (ii) is evaluated by Model 2 using the parameters given in Table 5.10. The number of unknowns is two along $x = 0$, and the time discretization results in 25 time steps, thus the number of decision variables in this case is $n = 50$. The objective function obtained for Model 2 is 9.228×10^{-4} as shown in Figure 5.41, where the average number of simulations per run was about 120,000. With this number of simulations the computation time obtained for Model 2 was 3729.13 seconds, while Model 1 required 0.36 seconds.

The computed source strength and the concentration distribution by Model 1 and Model 2 compared the exact solution for $Cr = 0.6$ are presented in Figures 5.42 and 5.43 respectively. The results for the source strength from both models are virtually the same and improve with time. For the concentration distribution both models underestimate the peak and the front is more dispersed. The mean error of the computed concentration for both Model 1 and Model 2 is observed to decrease with increase in time.

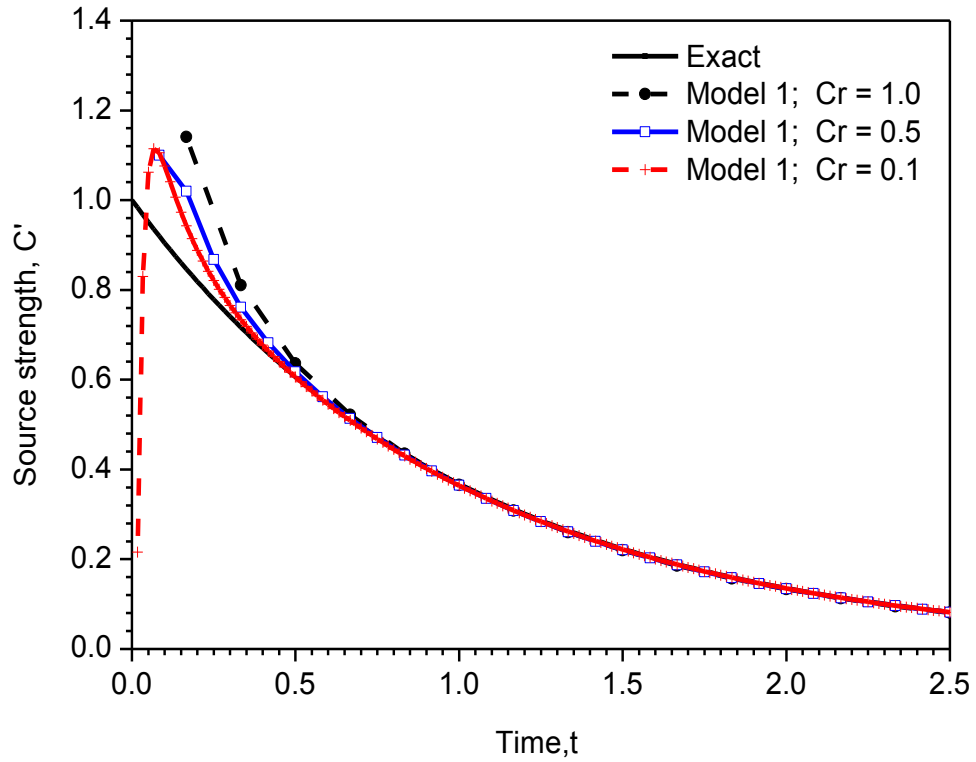


Figure 5.39. Model 1 estimated source strength for Pe =1 of Test Case 2.

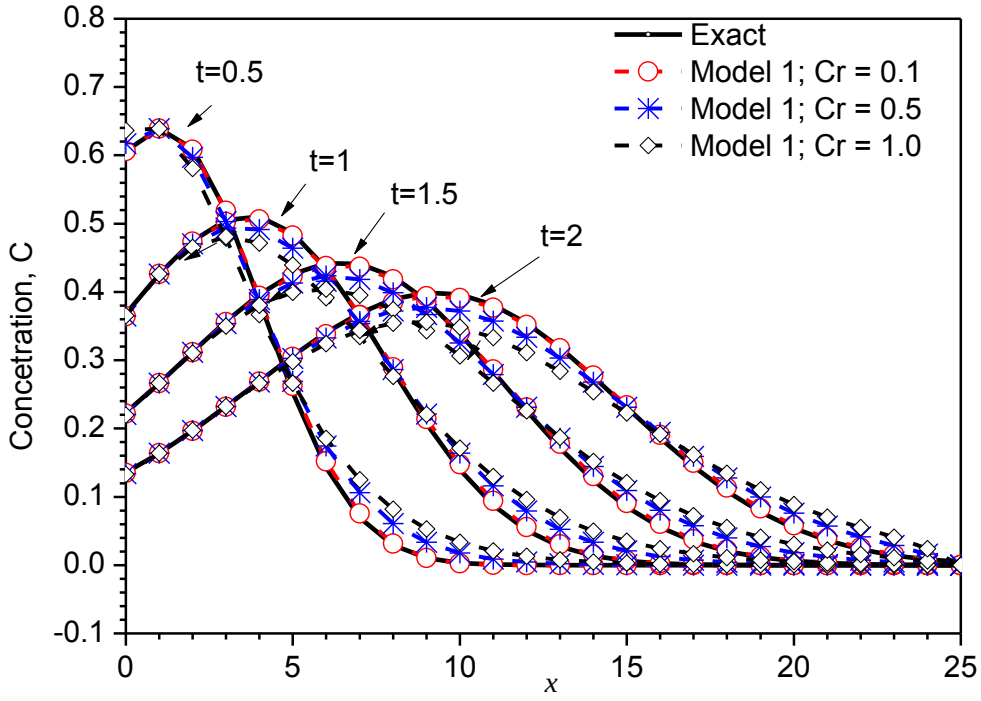


Figure 5.40: Exact and Model 1 computed concentration distribution for Pe = 1 of Test Case 2.

Table 5. 10 : SCE-UA optimization and search termination parameters for Test case 2, $Pe = 1$.

Description of parameter	**Notation**	**Peclet, $Pe = 1$ (Value)**
Number of decision variables	n_o	50
Number of complexes	p_o	10
Number of points in each complex	m_o	101
Sample size	s_o	1010
Number of points to select in complex	q_o	51
Optimization parameter	α_{opt}	1
Optimization parameter	β_{opt}	101
Minimum value of the objective function	minmax	0.001
Maximum number of epochs for termination, maxepoch	maxepoch	100
Change in epoch objective function prompting termination	conv	0.005
Spacing of epochs in checking for convergence	iconv	10

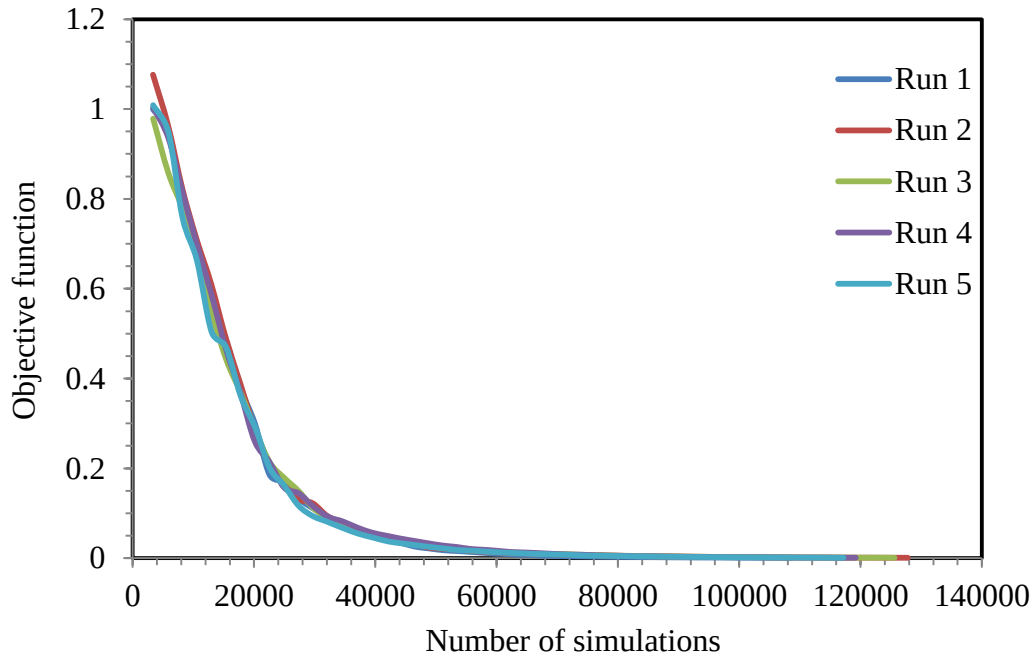


Figure 5.41: Model 2 objective function plot for $Pe = 1$ of Test case 2.

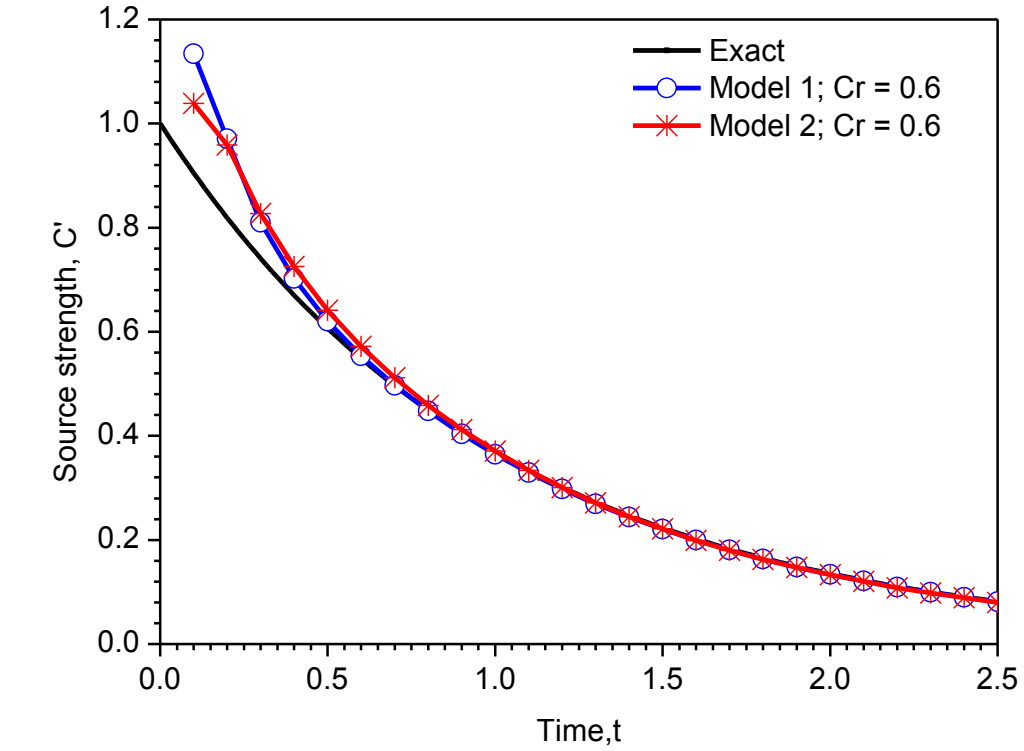


Figure 5.42: Model 1 and 2 computed source strength for $Pe = 1$ and $Cr = 0.6$ of Test case 2.

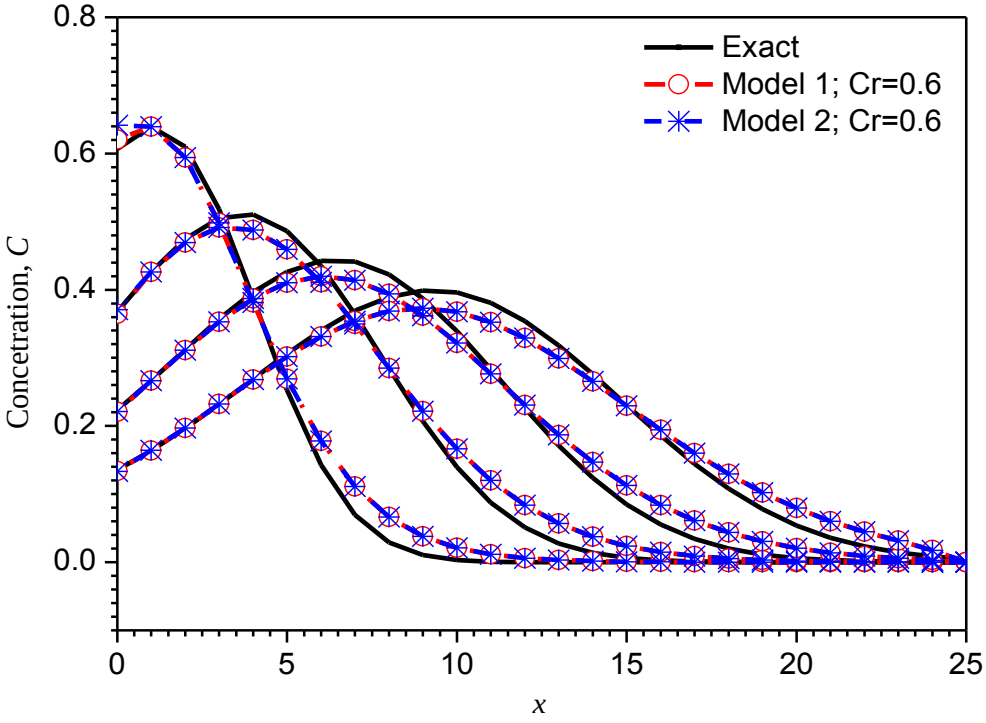


Figure 5.43: Model 1 and 2 computed concentration distribution for $Pe = 1$ and $Cr = 0.6$ of Test case 2.

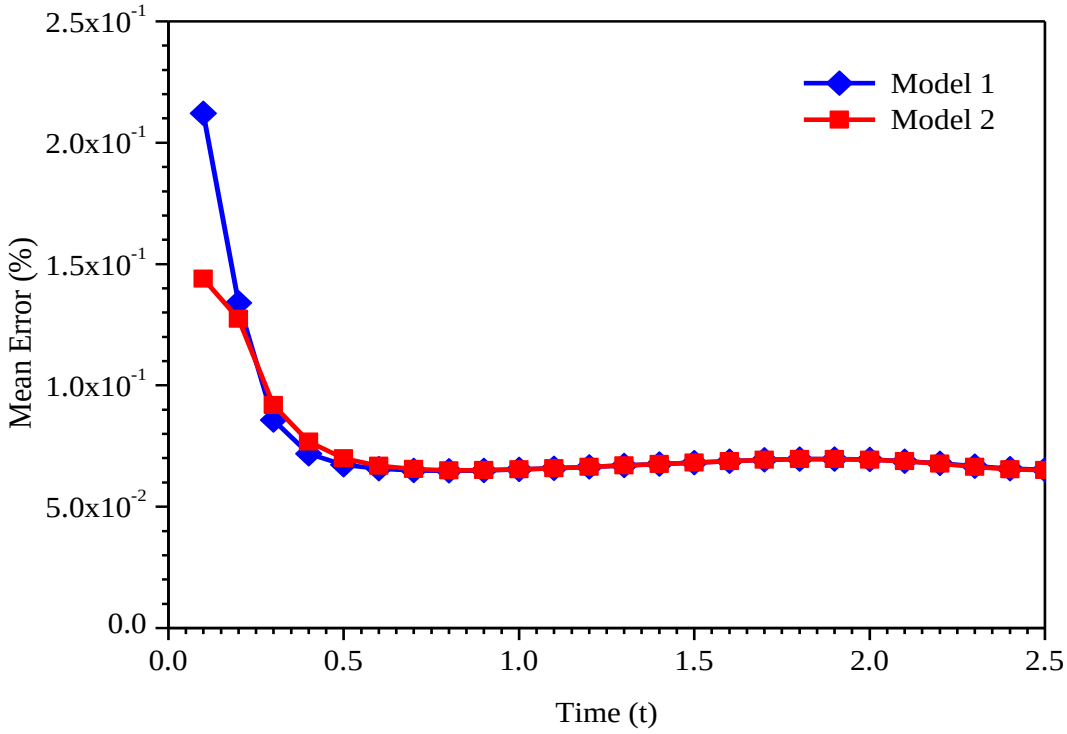


Figure 5.44: Mean error for computed concentration by Model 1 and 2 for $Pe = 1$ of Test case 2.

Random error in observation data of Test case 2

The concentration data at observation points were perturbed with noise levels of $\varepsilon = 1\%$, $\varepsilon = 3\%$, and $\varepsilon = 5\%$. The other simulation parameters and data were kept same as for the error free case. The Model 1 solutions for the source strength and the historical distribution with Peclet *Pe*=50 are presented in Figure 5.45 and 5.46, while *Pe*=1 are presented in Figure 5.47 and 5.48 for various noise levels. Both the recovered source strength and the concentration distribution are not significantly influenced by the noisy observation data. The estimated concentration distribution with noisy observation data match the estimated solutions with ε= 0% for both *Pe*=1 and *Pe*=50.

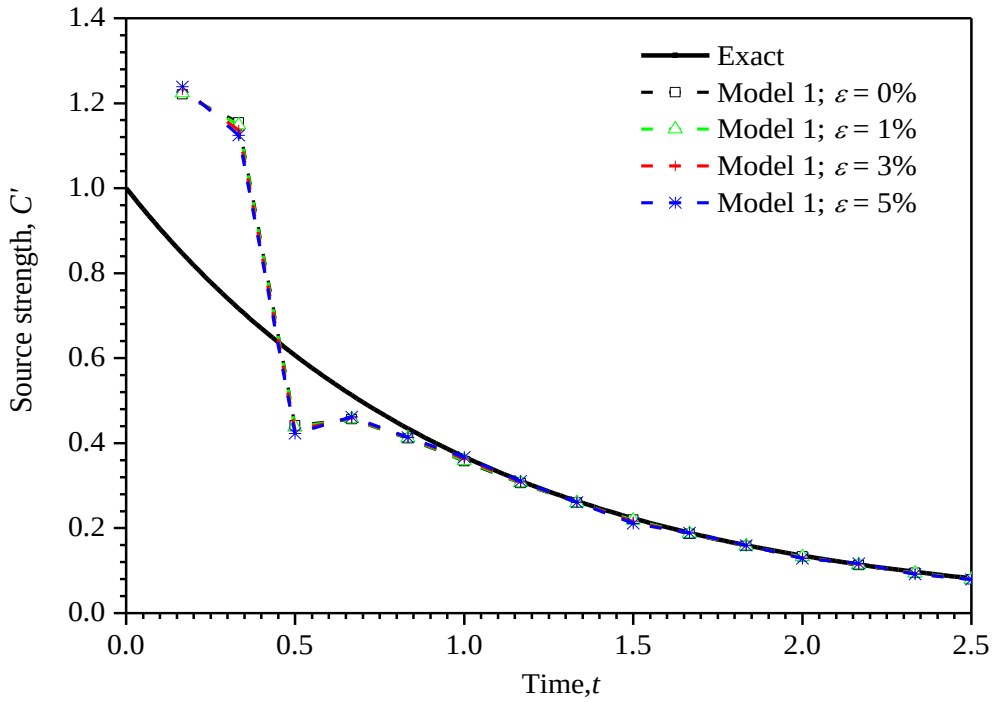


Figure 5.45: The exact and Model 1 estimated source strength for $Pe = 50$ of Test case 2 with noisy observation data.

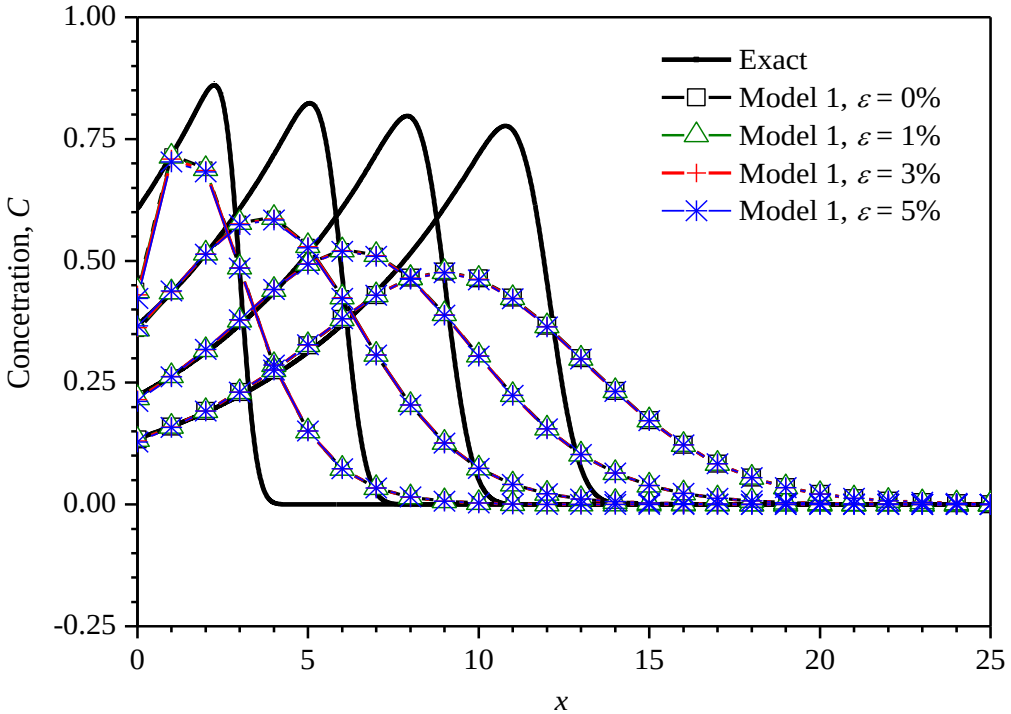


Figure 5.46: The exact and Model 1 computed concentration distribution for $Pe = 50$ and $Cr = 1$ of Test case 2 with noisy observation data.

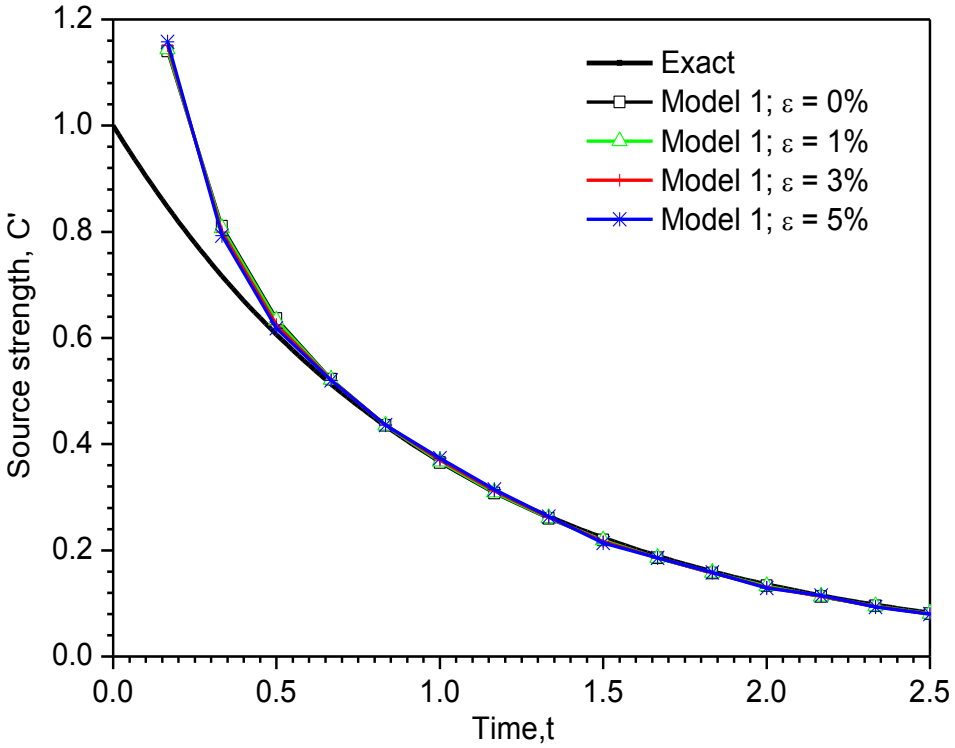


Figure 5.47: The exact and Model 1 computed source strength for $Pe = 1$ and $Cr = 1.0$ of Test case 2 with noisy observation data.

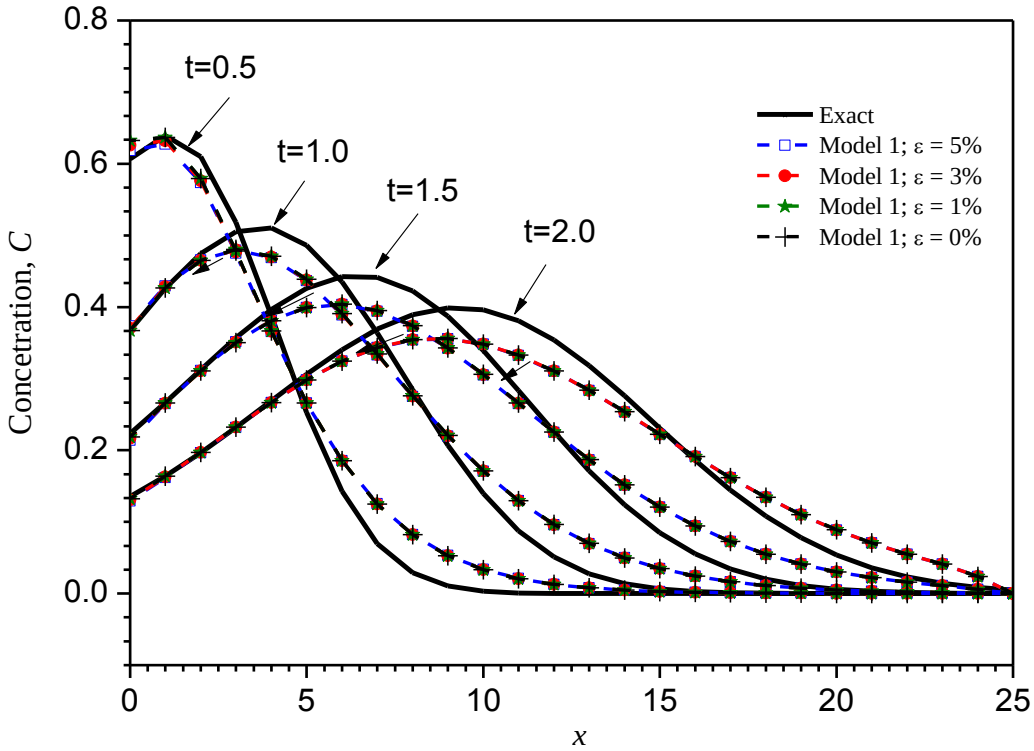


Figure 5.48: The exact and Model 1 computed concentration distribution for $Pe = 1$ and $Cr = 1.0$ of Test case 2 with noisy observation data.

5.2.3 Test case 3: 2D steady state problem with a sinusoidal source

This test case represents steady contaminant transport in a 2-D square domain that is governed by the advection dispersion Equation (2.4) with R=0, μ=0, Q=0 and **V**=**i***u*. For the direct problem, solved by Qiu *et al*., 1998, all the boundaries have Dirichlet boundary conditions. The left boundary along x=0 has a sinusoidal concentration distribution C' (0, y) =sin (πy) while all other boundaries have a zero concentration value. The analytical solution to this problem is given as:

$$C(x,y) = \frac{e^{m_1(1-x)} - e^{m_2(1-x)}}{e^{m_1} - e^{m_2}} \sin(\pi y) \tag{5.8}$$

Where, $m_1 = \frac{1}{2}\left(\sqrt{u^2 + 4\pi^2} - u\right)$ and $m_2 = -\frac{1}{2}\left(\sqrt{u^2 + 4\pi^2} + u\right)$ (5.9)

The first order derivatives along the boundaries are given as;

$$\frac{\partial c}{\partial x} = \frac{-m_1 e^{m_1(1-x)} + m_2 e^{m_2(1-x)}}{e^{m_1} - e^{m_2}} \sin \pi y$$

$$\frac{\partial c}{\partial y} = \frac{e^{m_1(1-x)} + e^{m_2(1-x)}}{e^{m_1} - e^{m_2}} \pi \cos \pi y \tag{5.10}$$

Posed as an inverse problem, this test case is simulated by considering the boundary along x=0 as a Γ_4 boundary where neither the concentration nor the flux is known, and the boundary along $x = 1.0$ is set as a Neumann boundary where only q is specified. On the top and bottom boundaries the concentration values are set to zero. Three transport cases are evaluated with Peclet values of $Pe = 50$, 1 and 0.05. The computational domain [1×1] is discretized into 100 uniform square elements, and the dispersion coefficient is taken as unity, while a uniform velocity u is chosen to be 500, 10, and 0.5 for the three transport cases. Figure 5.49 shows the computational domain with boundary conditions and the nine observation points (N_γ) located along $x = 0.1$. The parameters that were used in Model 2 to evaluate this test case for all Peclet numbers are given in Table 5.11.

The objective function for Model 2 with $Pe = 50$ was found to be 9.239×10^{-4} as shown in Figure 5.50.

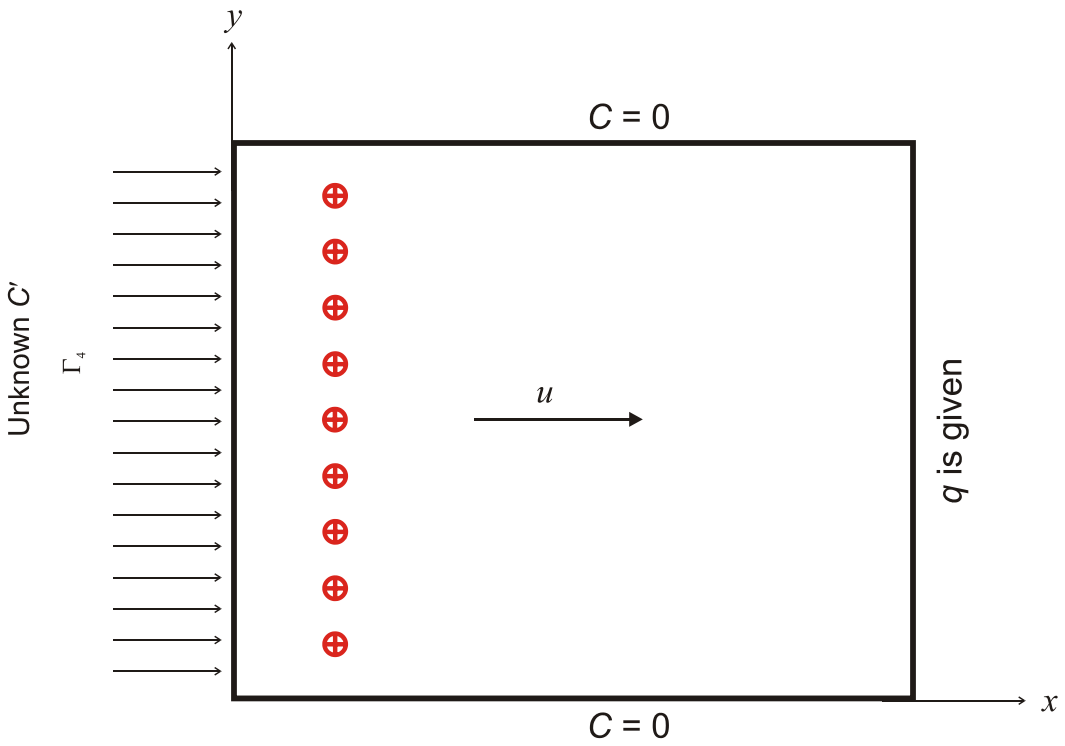


Figure 5.49. Computational domain for Test case 3 (crossed circles indicate observation sampling points).

Table 5.11 : SCE-UA optimization and search termination parameters for all Peclet numbers of Test case 3.

Description of parameter	Notation	Parameter Value
Number of decision variables	n_o	9
Number of complexes	p_o	10
Number of points in each complex	m_o	19
Sample size	s_o	190
Number of points to select in complex	q_o	10
Optimization parameter	α_{opt}	1
Optimization parameter	β_{opt}	19
Minimum value of the objective function	minmax	0.001
Maximum number of epochs for termination, maxepoch	maxepoch	100
Change in epoch objective function prompting termination	conv	0.005
Spacing of epochs in checking for convergence	iconv	10

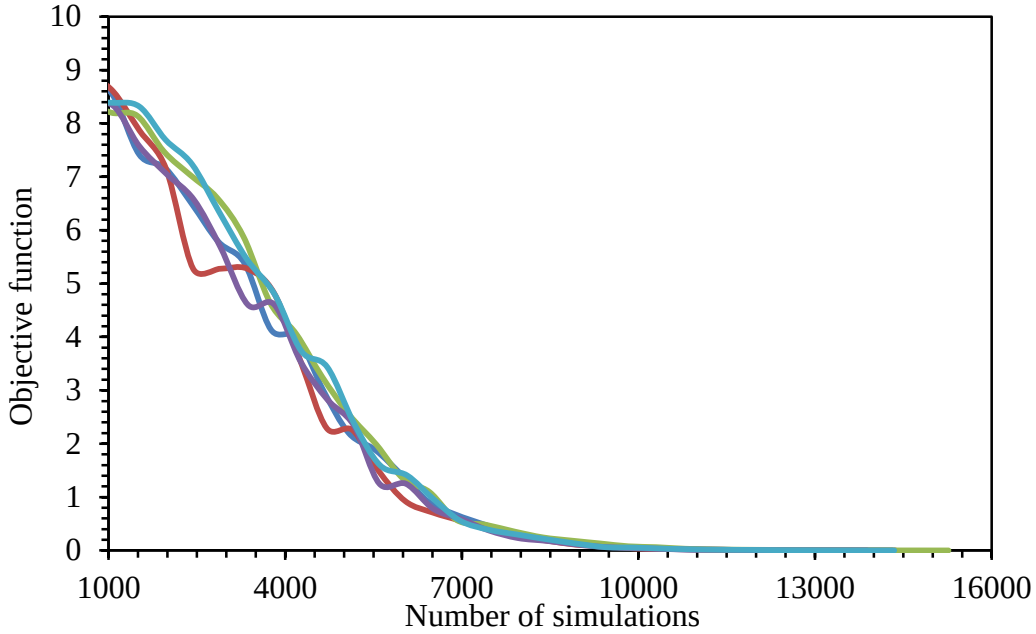


Figure 5.50: Model 2 objective function plot for $Pe = 50$ of Test case 3.

The exact and the computed source strengths for error free observation data for the advection dominant transport case of $Pe = 50$, are given in Figure 5.51. Model 1 predicts the source strength excellently while Model 2 under-predict the source strength. The reason for this would be that Model 2 gets trapped in a local minimum in the search for a global minimum.

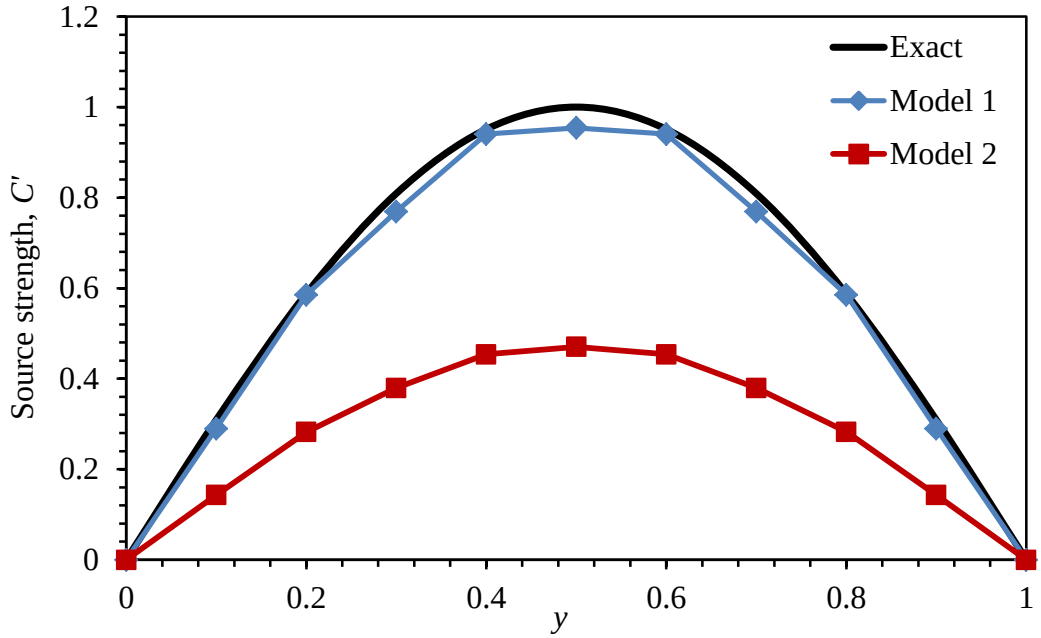


Figure 5.51: Model 1 and Model 2 computed source strength for $Pe = 50$ of Test case 3.

Figure 5.52 shows the contours of the concentrations, the steep concentration gradient in the vicinity of $x = 1$, which exhibits a 'boundary-layer' phenomenon because of the advection dominance of the transport, is correctly captured by Model 1 and Model 2, however oscillations are observed with amplitudes increasing in Model 2. Considerable amount of instability is observed in both solutions. Furthermore, the computation time for Model 2 was 201.40 seconds compared to 1.89 seconds for Model 1.

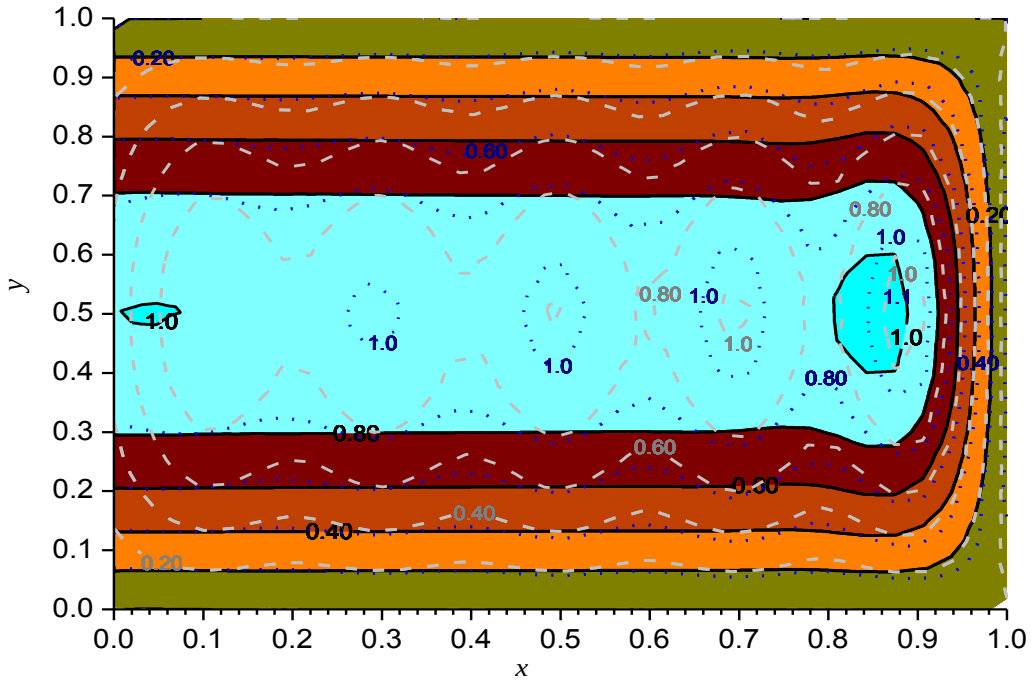


Figure 5.52 : Concentration contours of Test case 3 for $Pe = 50$. Solid black lines- exact solution, Model 1 solution -blue dash lines and Model 2 solution- grey dash lines.

The exact and computed source strength for the marginal advection transport case of $Pe = 1$ is presented in Figure 5.53. The results from Model 1 and Model 2 are indistinguishable and correctly reproduce the exact source strength, implying that, with reduced advection and reduced concentration gradient in the vicinity of $x = 1$, the computed results improve. The computed spatial distributions of the concentration and the exact solution are shown in Figure 5.54. Both methods correctly reproduce the exact solution. For Model 2 the objective function was found as 9.2759×10^{-4} as shown in Figure 5.55. The mean error for Model 1 was

obtained as 1.37% while that for Model 2 as 1.47%, indicating comparable approximations by Model 1 and 2. The computation time for Model 1 was obtained as 0.12 seconds compared to 243.90 seconds for Model 2.

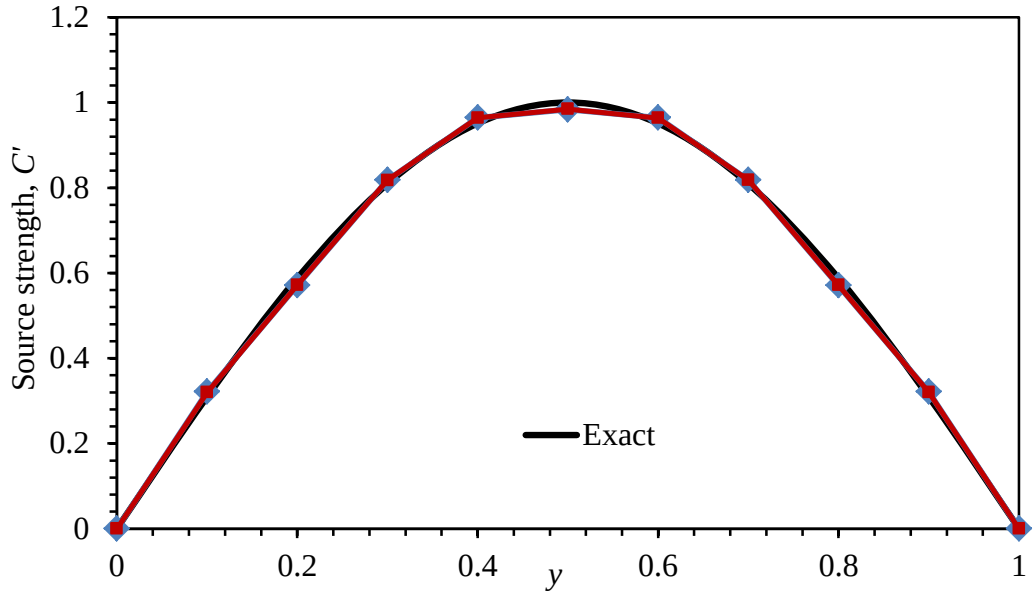


Figure 5.53: The exact, Model 1 and Model 2 computed source strength solutions for Pe =1 of Test Case 3.

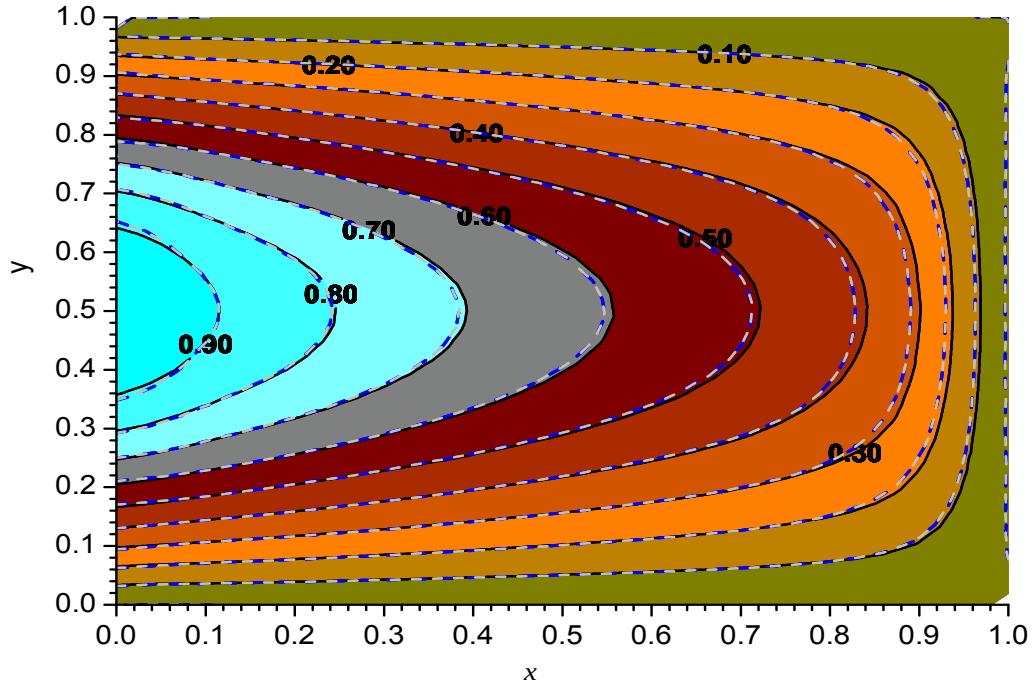


Figure 5.54: Concentration contours for $Pe = 1$ of Test Case 3. Solid black lines - exact solution, Model 1 solution - blue dash lines and Model 2 solution- grey dash lines.

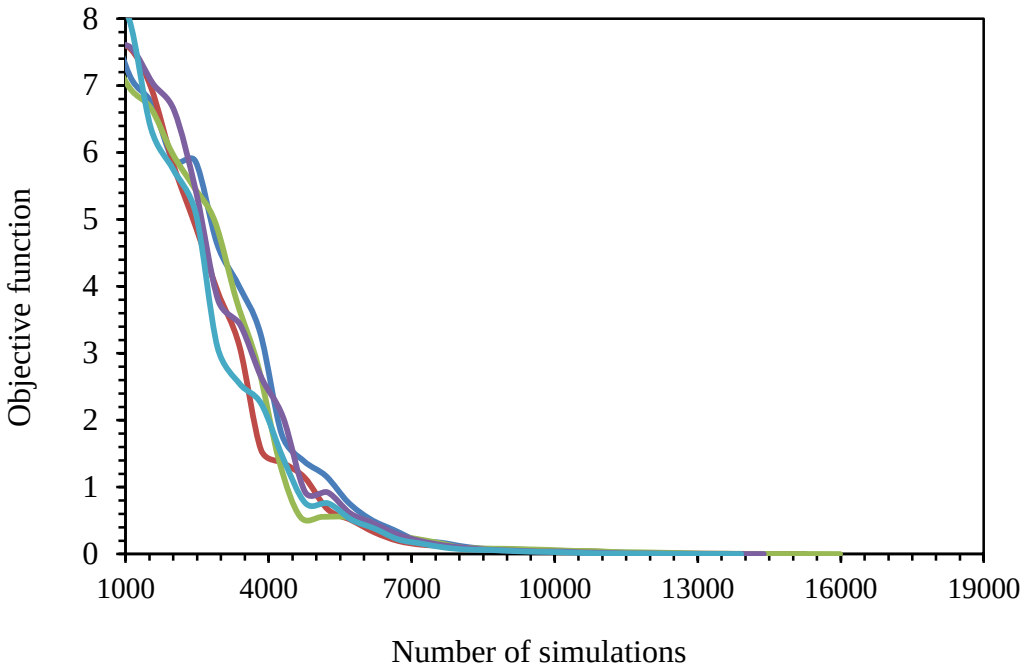


Figure 5.55: Model 2 objective function plot for pe =1 of Test case 3.

Figure 5.56 shows the exact solution with the Model 1 and Model 2 computed source strengths for the dispersion dominant transport case of $Pe = 0.05$. There is very good agreement between the exact, Model 1 and Model 2 solutions. The contour plots of the computed concentration distribution and the exact solution are presented in Figure 5.57; there is a good agreement with Model 1 and 2 solutions. The obtained objective function for Model 2 was 9.537×10^{-4} as shown in Figure 5.58. The computation time for Model 1 was 0.9 seconds compared to 257.50 seconds for Model 2.

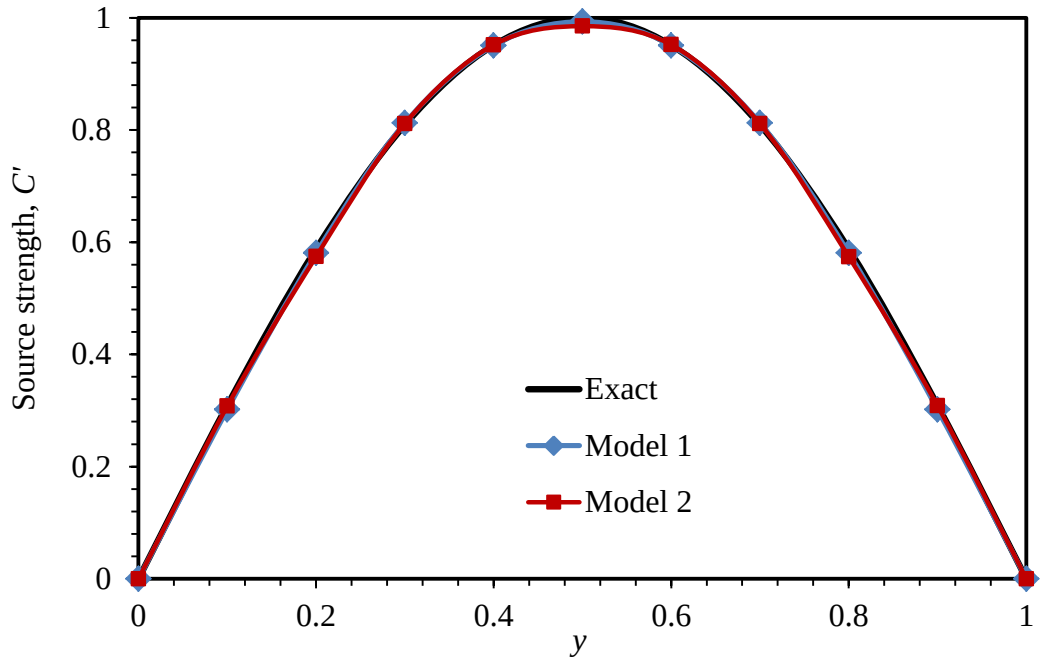


Figure 5.56: The exact, Model 1 and Model 2 solutions of the source strength, $Pe = 0.05$ of Test case 3.

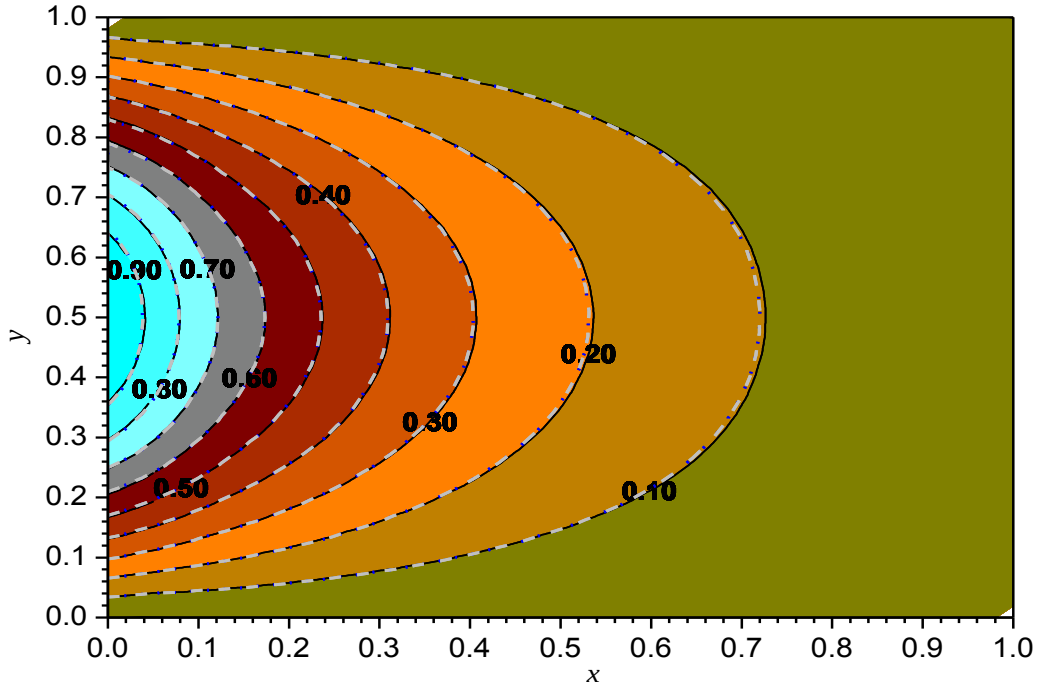


Figure 5.57: Concentration contours of Test case 3 for $Pe = 0.05$. Black solid lines represent the exact solution, the blue dash lines show Model 1 solution, and the grey dash lines represent Model 2 solution.

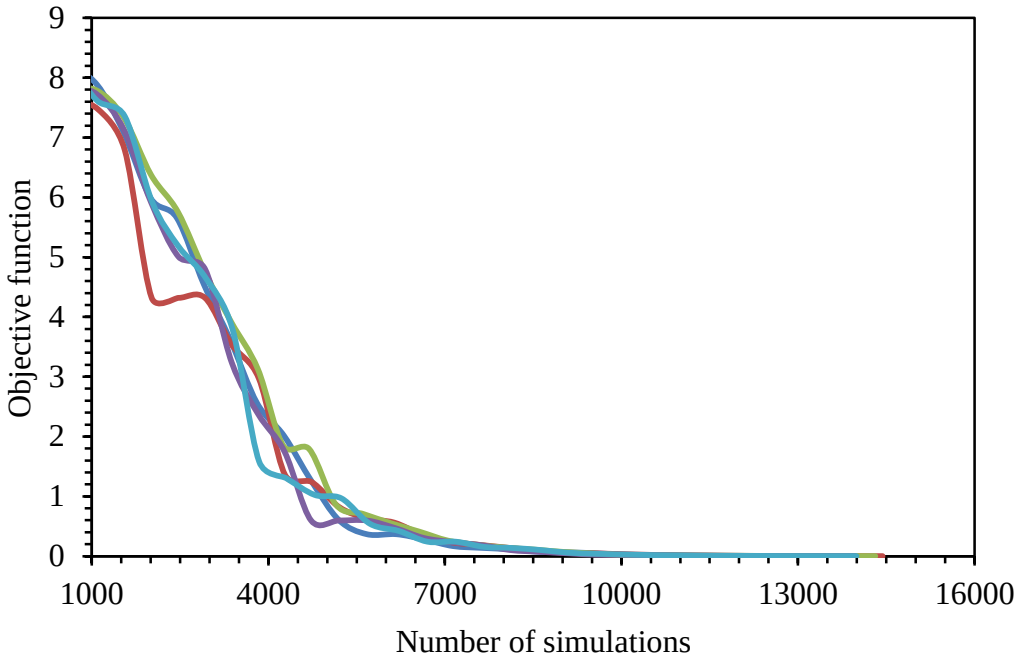


Figure 5.58: Model 2 objective function plot for $Pe = 0.05$ of Test case 3.

Random errors in observation data of Test case 3

The influence of observation errors on source recovery of this case was evaluated by randomly perturbing concentration data with noise levels of ε=1%, ε=3%, and ε=5%. The Model 1 solution for the computed source strength with noisy data for *Pe* = 50 is presented in Figure 5.59, *Pe* = 1 in Figure 5.60, and *Pe* = 0.05 in Figure 5.61. The computed solutions give a good prediction of the contaminant source strength at noise level of 1% but small deviations from the exact solution at noise levels of 3% and 5% are observed in all cases. The mean error for the computed concentration is provided in Table 5.12, it is observed that the advective case is estimated with higher relative error as compared to the marginal and dispersive cases. Again, the mean error increases with increase in the observation data errors.

Table 5.12: Mean error for the computed concentration using error free and noisy data.

Pe	**Mean error (%)**			
	$\boldsymbol{\varepsilon = 0\%}$	$\boldsymbol{\varepsilon = 1\%}$	$\boldsymbol{\varepsilon = 3\%}$	$\boldsymbol{\varepsilon = 5\%}$
50	0.0989	0.0993	0.101	0.104
1	0.0148	0.0157	0.0231	0.0336
0.05	0.00787	0.0132	0.0339	0.0558

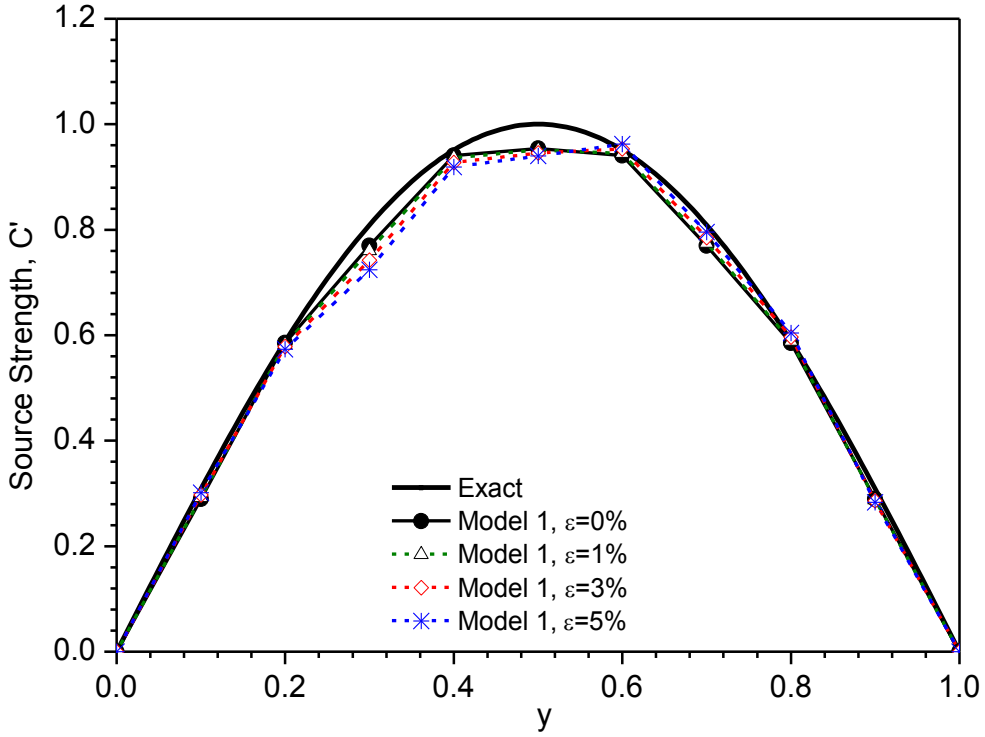


Figure 5.59: Model 1 computed source strength of $Pe = 50$ of Test case 3 with noisy observation data

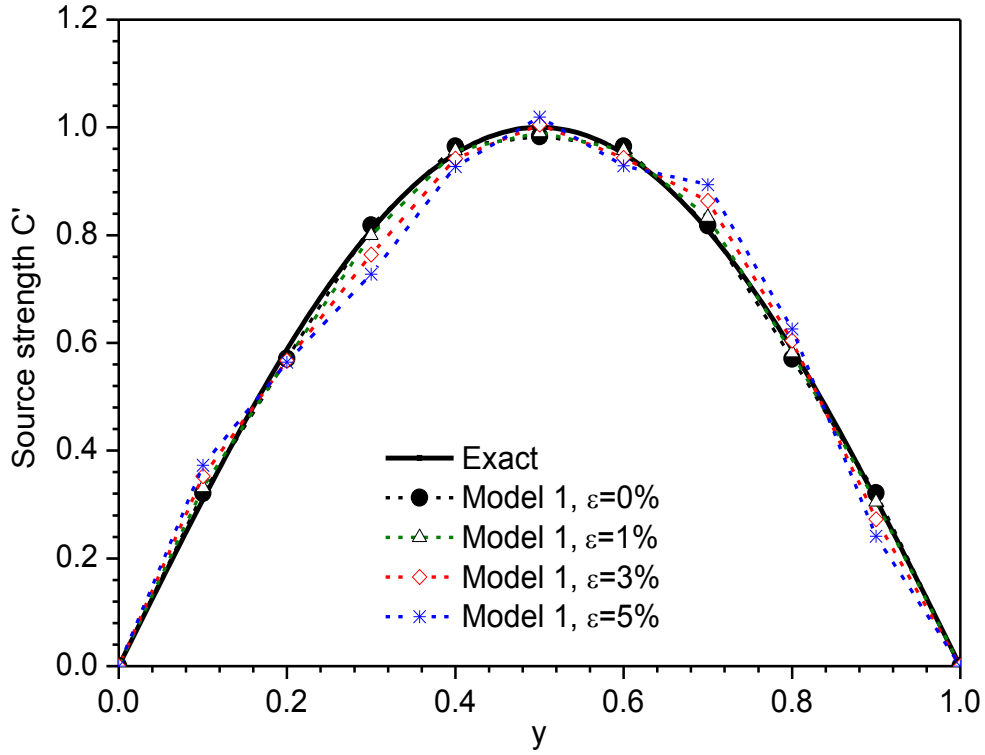


Figure 5.60 : Model 1 computed source strength for $Pe = 1$ with noisy observation data of Test case 3.

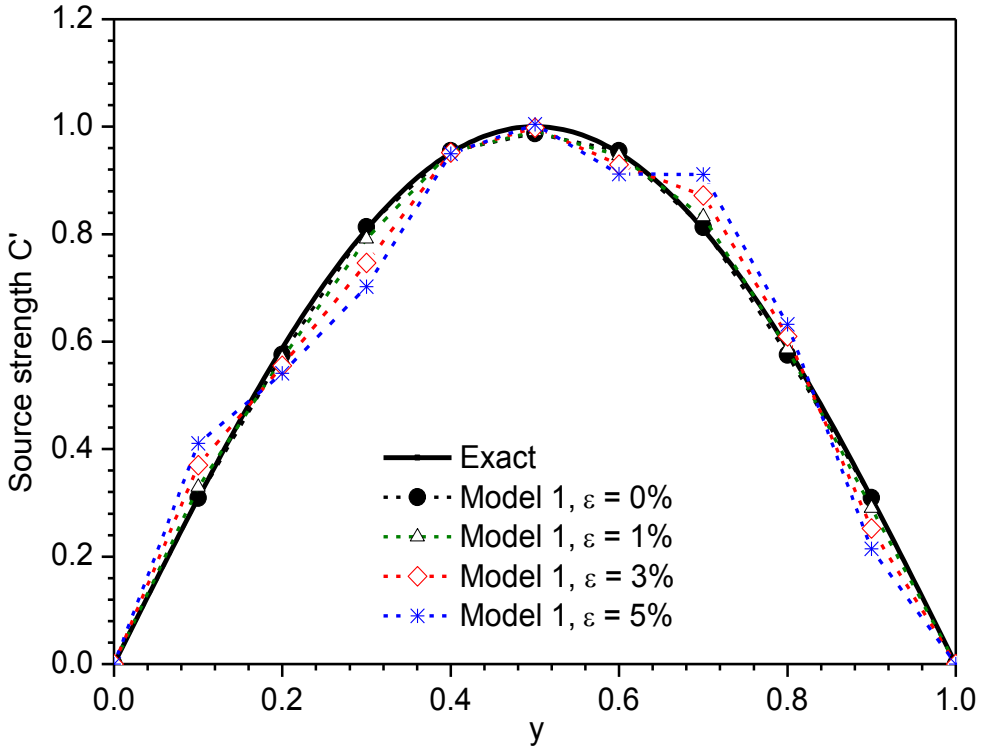


Figure 5.61: Model 1 computed source strength of $Pe = 0.05$ with noisy observation data of Test case 3.

5.2.4 Test case 4: 2D transient problem with a flux boundary source.

This is a 2D dimensionless case, which has been solved by Huang *et al*. (2008). In this work we consider a finite, isotropic, homogeneous aquifer of thickness, $b = 1$ and length, $L = 1$. The flow is assumed to be steady in the *x*-direction with an average pore velocity, $u = 0.01$. The contaminant source is located at the top boundary within the section L_2-L_1, as shown in Figure 5.62. This problem is formulated as follows;

$$R\frac{\partial C}{\partial t} = \nabla \cdot (D\nabla C) - \mathbf{V}.\nabla C - \mu C \tag{5.11}$$

$$C(x, y, t = 0) = 0,\ 0 < x < L, 0 < y < b \tag{5.12}$$

$$\frac{\partial C(0, y, t)}{\partial x} = 0,\ 0 < y < b,\ t > 0 \tag{5.13}$$

$$\frac{\partial C(1,y,t)}{\partial x} = 0\,,\ 0 < y < b\,,\ t > 0 \tag{5.14}$$

$$\frac{\partial C(x,0,t)}{\partial y} = 0\,,\ 0 < x < L\,,\ t > 0 \tag{5.15}$$

$$\frac{\partial C(x,1,t)}{\partial y} = q(x,t)\,,\ \begin{Bmatrix} q(x,t) & 0.15 \le x \le 0.3 \text{ and } y = 1.0 \\ 0 & \text{elsewhere} \end{Bmatrix} \tag{5.16}$$

$$q(x,t) = 7.0 + \left[20x \times \sin\left(\frac{2\pi t}{t_f} \right) \right];[0.15 \le x \le 0.3],\ t_f=0.5 \tag{5.17}$$

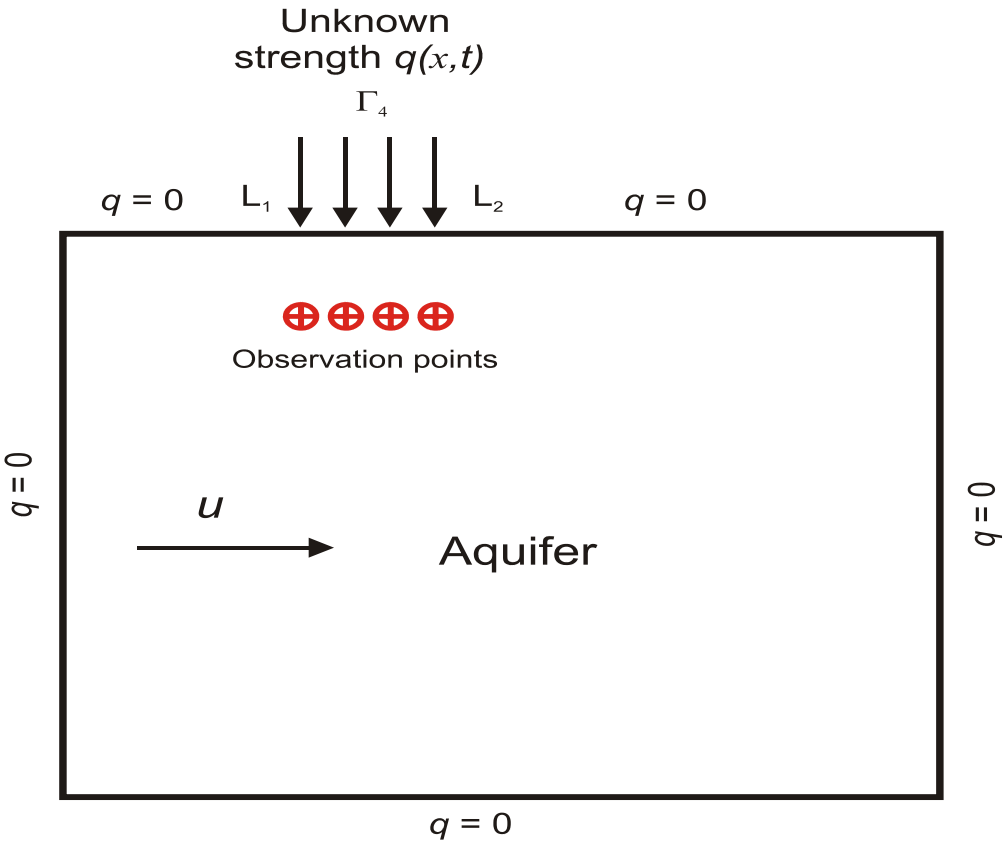


Figure 5.62: Schematic representation of Test case 4 and 5.

To inversely determine the space time dependent unknown flux release function $q(x,t)$ for the aquifer we utilize known initial and boundary conditions as well as additional data from observation points. There is no prior information on the functional form to the inverse. The following parameter values are used for

simulation $L1 = 0.15, L2 = 0.3, D = 1.0, R = 1.0, \mu = 0.0$. The GEM space and time discretization are taken as $\Delta x = 0.05$, $\Delta y = 0.05$, and $\Delta t = 0.01$.

In this work we consider an isotropic case as compared to the original work in Huang *et al.*, 2008 where anisotropic case was evaluated. As discussed in Section 5.1 the influence of observation points on the recovery of the unknown source plays a critical role. The flow in the *x*-direction is same as in the *y*-direction, thus having observation points very close to the bottom of the aquifer will not provide adequate information for the inversion. We therefore, locate our observation points close to the source at $y = 0.9$ between $x = 0.15$ and $x = 0.3$, a total of 4 observation points were sufficient for the inversion.

Figures 5.63 (a), (b), (c), and (d) show the exact and the estimated fluxes by Model 1. The estimated fluxes are computed using exact measurements with $\varepsilon = 0\%$, and measurements with observation error of $\varepsilon = 0.1\%$, and $\varepsilon = 0.2\%$. It should be noted that the amount of error introduced in observation data is smaller than the previous cases, because of the sensitivity of the flux to observation errors (Taigbenu, 2015). It is found that the computed fluxes using exact measurements are excellent, when compared to the exact fluxes. On the other hand, the influence of noise on the concentration (primary variable) is amplified on the contaminant flux, such that the estimated flux exhibits oscillations. The average relative errors between the true flux and the computed fluxes were obtained as 0.035%, 0.139%, and 0.266% for observation data with ε=0.0%, $\varepsilon = 0.1\%$, and $\varepsilon = 0.2\%$ respectively.

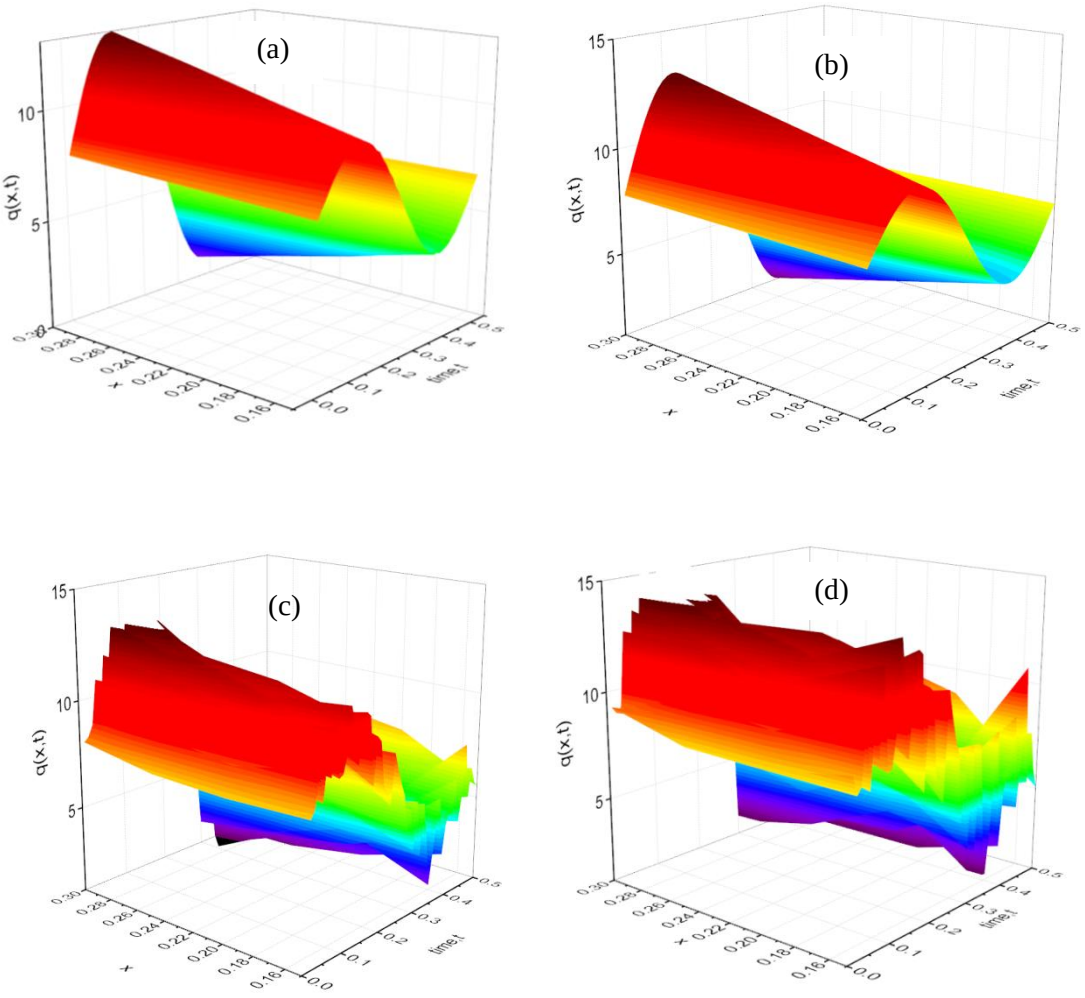


Figure 5.63: Plot of Test case 4 (a) exact solution (b) Computed flux by Model 1 using exact measurements, $\boldsymbol{\varepsilon = 0.0\%}$ (c) noisy data, $\boldsymbol{\varepsilon = 0.1\%}$ (d) noisy data, $\boldsymbol{\varepsilon = 0.2\%}$.

Model 2 simulation parameters for this test case include $n = 200, p = 10, m = 401, q_c = 201, \beta_{opt} = 401$, and α_{opt} =1. Figure 5.64 shows the minimized objective function that was obtained as 1.6×10^{-3} after approximately 706000 simulations. The computed flux by Model 2 is shown in Figure 5.65, it is seen that the trend is correctly captured; however the smoothness of the function is not correctly captured. The average error for the computed flux by Model 2 relative to the exact flux was obtained as 28.444%, which is much higher that 0.035% for Model 1. Furthermore the computation time for Model 2 was 27328.75 seconds compared to 19.72 seconds in Model 1.

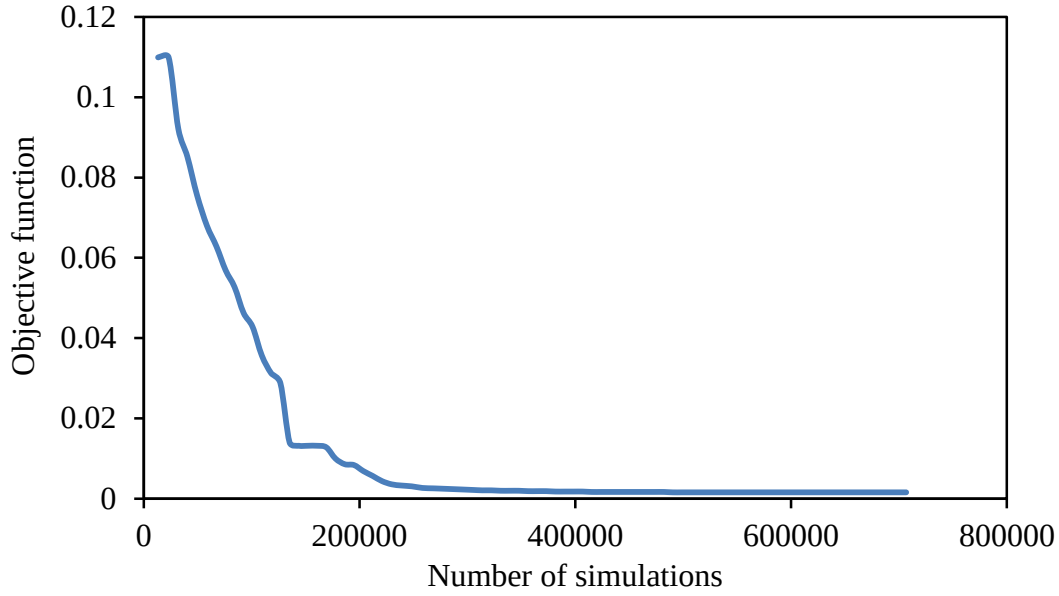


Figure 5.64: Shows the objective function versus number of simulations for Test case 4.

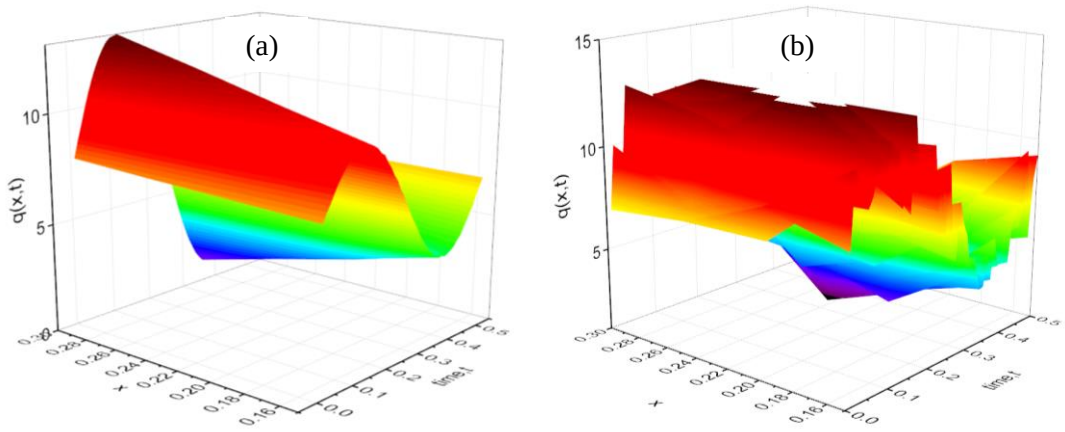


Figure 5.65: Plot of Test case 4 (a) exact flux (b) computed source flux using Model 2.

Figures 5.66 (a), (b), and (c) show the computed concentration distribution at time, $t = 0.5$ using Model 1 with exact observation data, and observation data with $\varepsilon = 0.1\%$ and $\varepsilon = 0.2\%$ respectively. It is seen that the computed concentration is indistinguishable for the three cases, thus it can be concluded that the spatial and temporal concentration distribution is not significantly influenced by noise in observation data. Figure 5.67 shows the error for the computed concentration relative to the exact concentration in all cases and it is observed that the error increases with increase in noise levels, but generally the error is below 0.0016% which implies a good recovery of the plume.

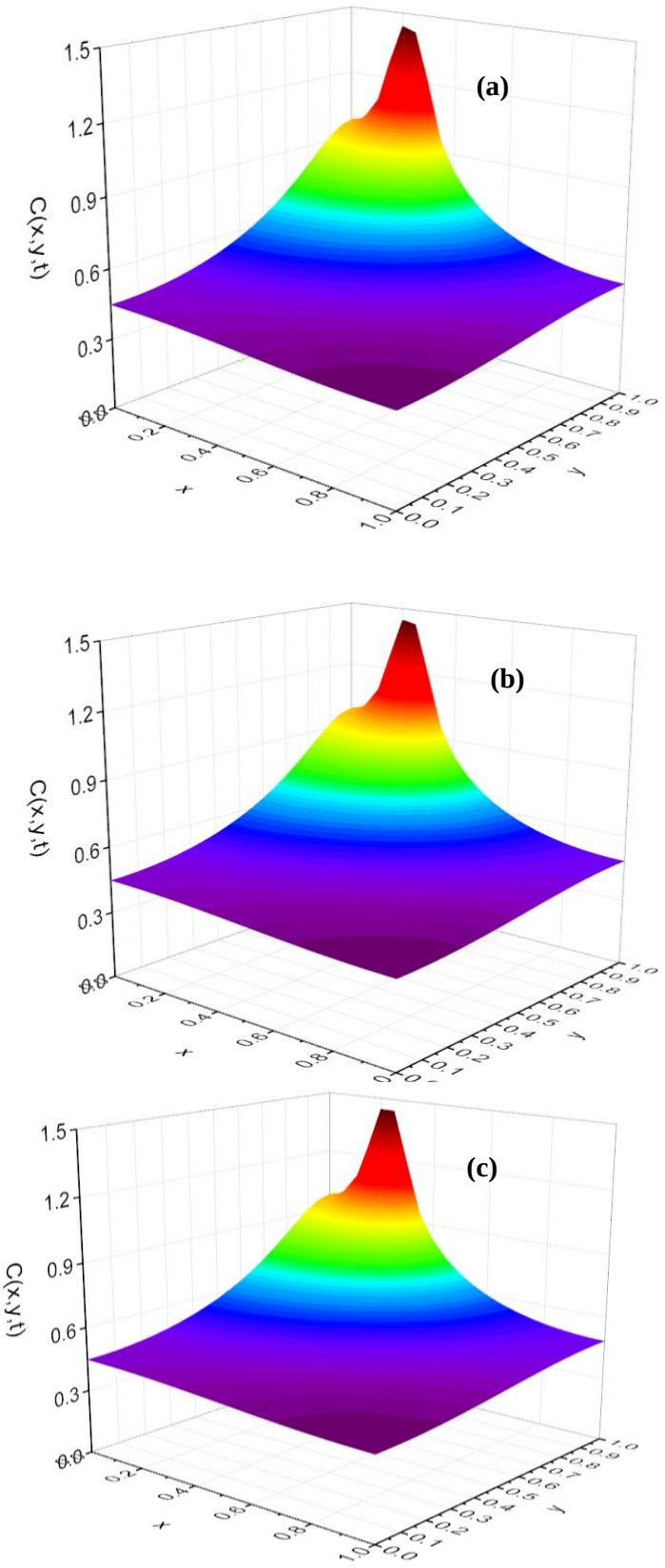


Figure 5.66: Estimated concentration by Model 1with (a) $\boldsymbol{\varepsilon = 0.0}$% (b) $\boldsymbol{\varepsilon = 0.1}$% (c) $\boldsymbol{\varepsilon = 0.2}$% at time, $\boldsymbol{t = 0}$.5 for Test case 4.

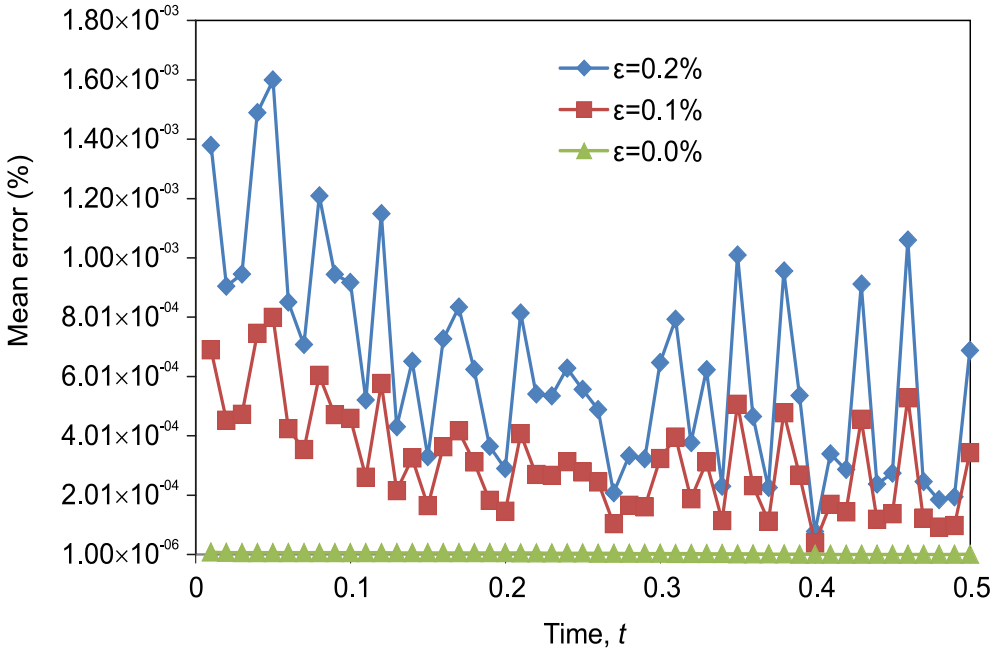


Figure 5.67: Mean error for the estimated concentration for Test case 4.

5.2.5 Test case 5: 2D transient problem with a flux boundary source

The system parameters used in the numerical calculations of this case are the same as in Test case 4. The space and time dependent contaminant release function $q(x, t)$ for this case is assumed as the following function;

$$q(x,t) = \begin{cases} 10x & 0 \le t \le 0.1 \\ 20x & 0.1 < t \le 0.2 \\ 30x & 0.2 < t \le 0.3 \\ 40x & 0.3 < t \le 0.5 \end{cases} \tag{5.18}$$

This case is more arduous since the contaminant release function has discontinuities. The inverse simulation is carried out using error free measurements $\varepsilon = 0\%$, and measurements with noise levels of $\varepsilon = 0.1\%$ and $\varepsilon = 0.2\%$. Figures 5.68 (a), (b), (c), and (d) show the exact and the computed source fluxes using Model 1. The computed flux $q(x,t)$ for all cases is not accurate at the early times, largely because of the discontinuous nature of the problem. Additionally, an oscillatory behaviour is exhibited by the estimated flux

with noisy observation concentration data. The estimated source fluxes are obtained with average relative errors of 4.512%, 11.004%, and 18.461% for error free data, and the cases with $\varepsilon = 0.1$ % and $\varepsilon = 0.2\%$ respectively. As expected this case is more rigorous with discontinuities and it performs poorly compared to Test case 4. It is also observed that noisy observation data has a significant influence on the computed fluxes.

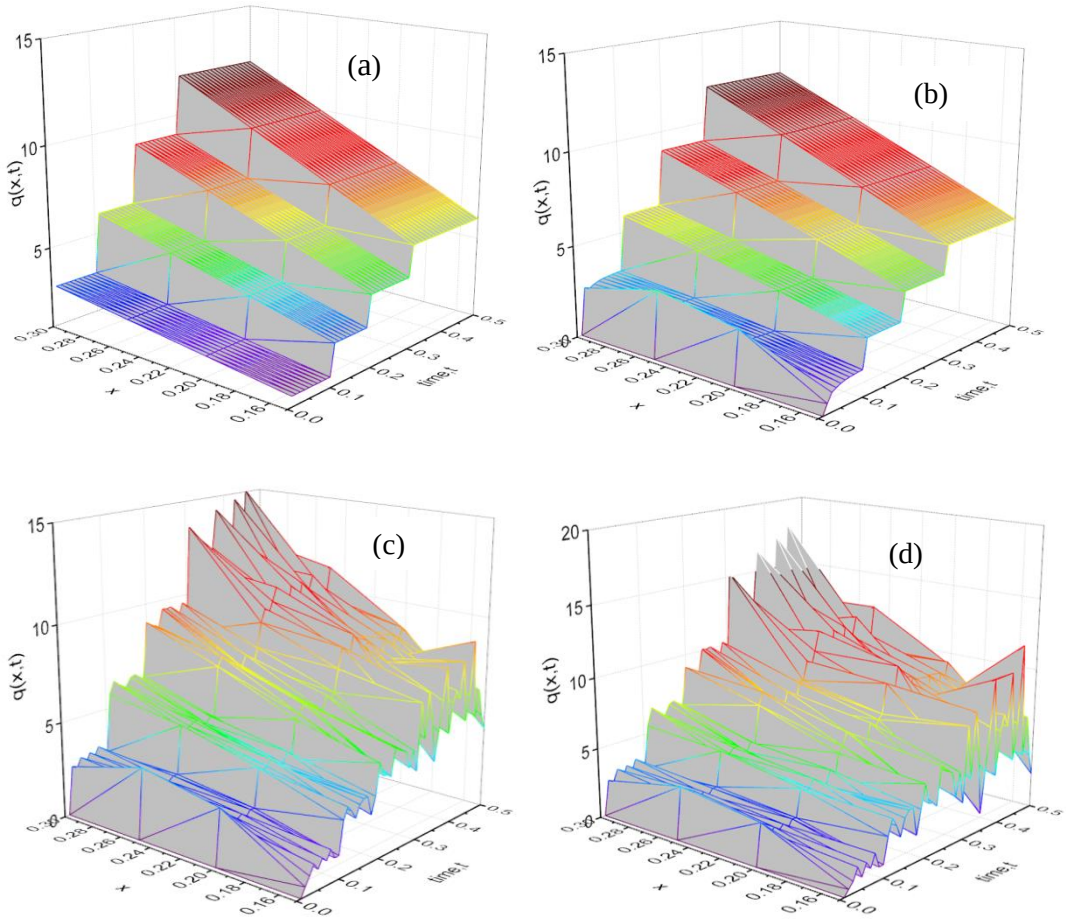


Figure 5.68: Plot for Test case 5 (a) exact source flux, (b) Model 1 estimated source fluxes using exact measurements, $\boldsymbol{\varepsilon = 0.0}$ (c) $\boldsymbol{\varepsilon = 0.1}$% (d) $\boldsymbol{\varepsilon = 0.2}$%.

Model 2 was used in this case to estimate the source fluxes and the following simulation parameters were assumed $n_o = 200, p_o = 10, m_o = 401, q_o = 201, \alpha_{opt} = 1$and $\beta_{opt} = 401$. The minimised objective function was obtained as

2.9×10^{-3} after 514178 simulations, as shown in Figure 5.69. A single run with this number of simulations was carried for 15091.12 seconds.

Figure 5.70 shows the exact source flux and the computed source flux using Model 2. The computed source flux when compared to the exact solution; is observed that the trend is captured well; however, the smoothness of the function is not preserved in the inverse solution. The average relative error for the computed flux to the exact is 29.674% which is higher compared to 4.512% for error free observation in Model 1. Generally, Model 1 performs better when using error free observation data.

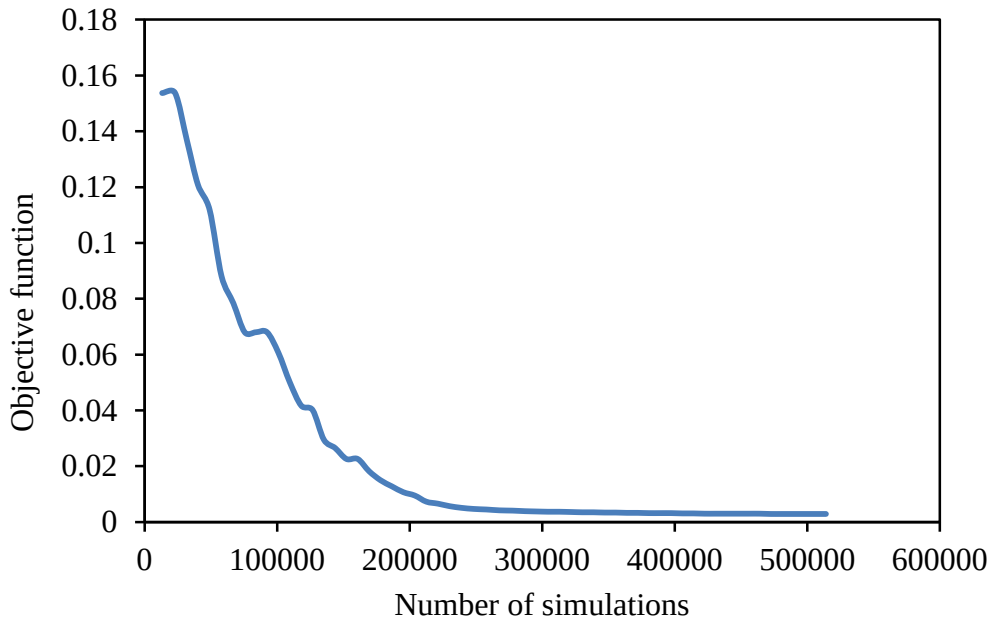


Figure 5.69: Plot for the objective function versus the number of simulations for Test case 5.

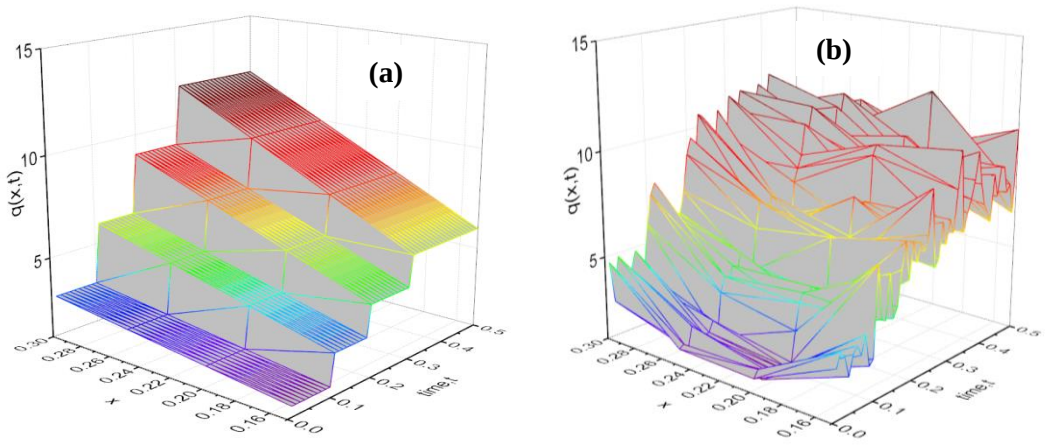


Figure 5.70: Plot showing (a) exact source fluxes (b) Computed source fluxes by Model 2 using exact measurements.

Figures 5.71 (a), (b), and (c) show the recovered concentration by Model 1 with exact data and noisy data of $\varepsilon = 0.1\%$, and $\varepsilon = 0.2\%$. From the figures it is observed that the recovered concentration is not significantly influenced by noisy observation data, as there is an indistinguishable match. Figure 5.72 shows the mean error for the computed spatial concentration that is under $3.5\times10^{-3}\%$, indicating a good estimate of the plume distribution by the exact and noisy observation data. Another observation is that the magnitude of the mean relative errors increases with increase in observation errors.

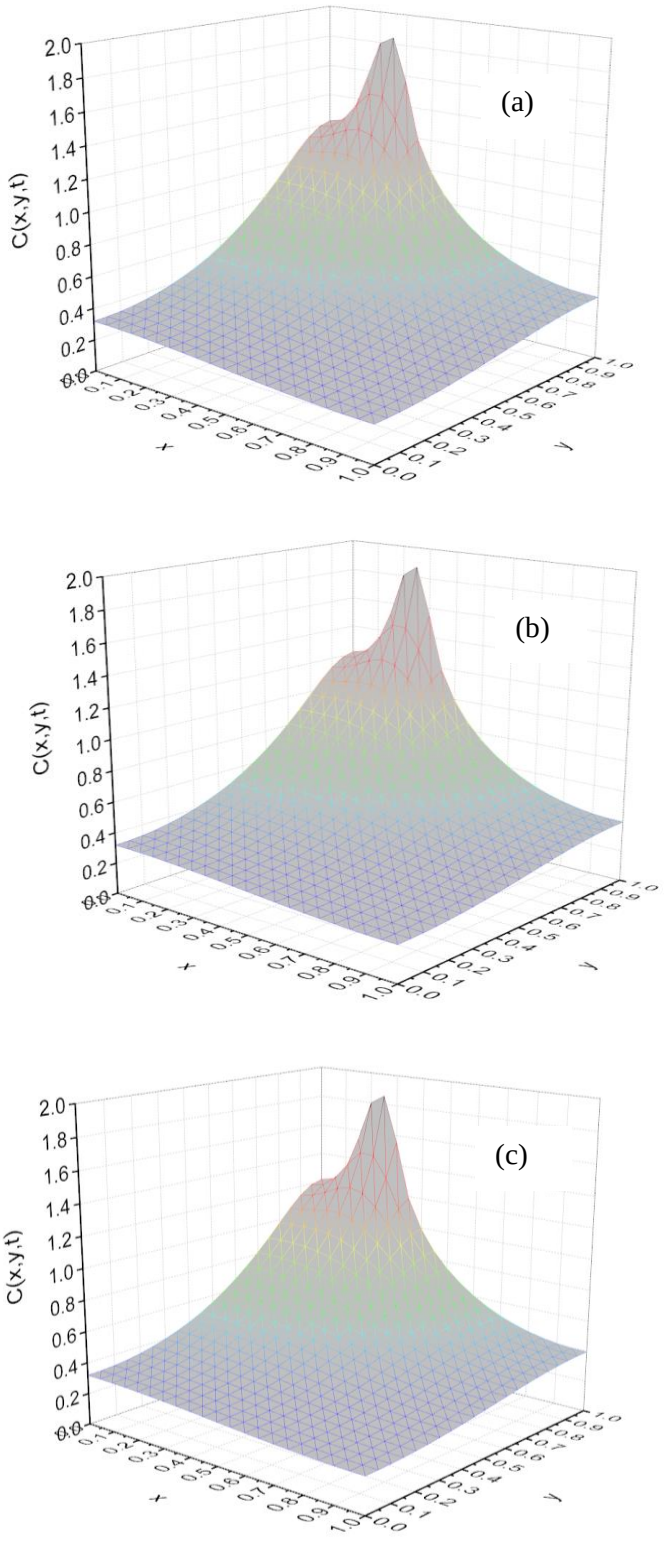


Figure 5.71: Estimated concentration by Model 1 with (a) $\varepsilon = 0.0\%$ (b) $\varepsilon = 0.1\%$ (c) $\varepsilon = 0.2\%$ at time, $t = 0.5$.

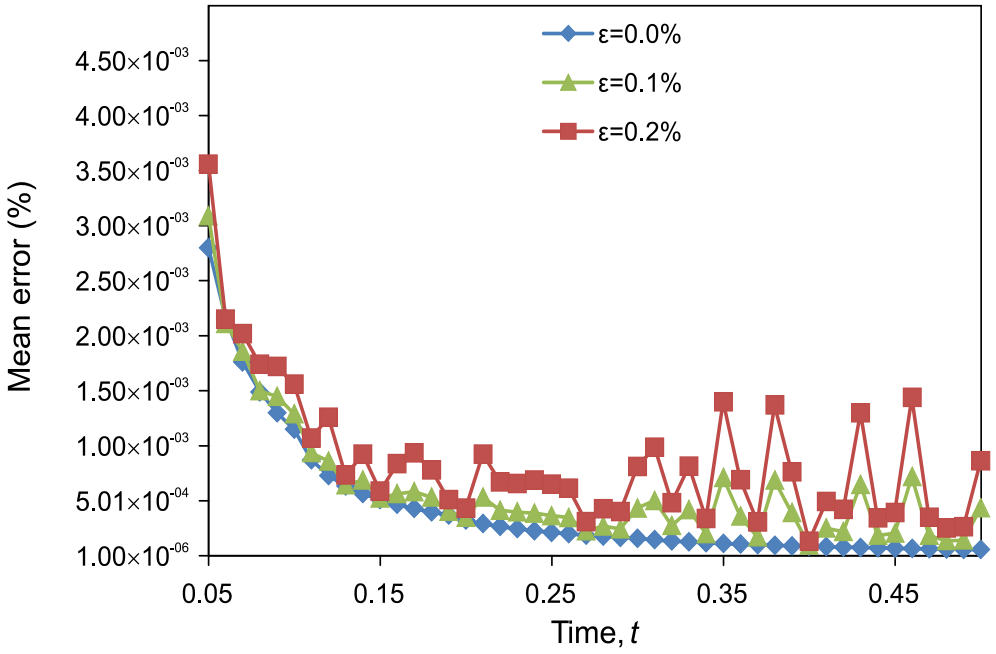


Figure 5.72: Mean error for the computed concentration for Test case 4.

5.3 Instantaneous point source problems

In this section, numerical simulations are carried out using two 2D transient test cases. The first test case has a single instantaneous source with unknown source strength. It seeks to determine the source strength while accounting for the location of observation points, and time discretization. The second case has multiple sources (active and non-active) and it examines the simultaneous recovery of the source strength and the historical distribution, under observation and parameter errors. The test cases have analytical solutions that are used for benchmarking our solutions.

The analytical solution for the concentration distribution from instantaneous sources in a 2-D homogeneous aquifer under a uniform flow velocity in the *x*-direction is known and given in Bear, 1972 as:

$$C(x,y,t)=\sum_{m=1}^{F}\frac{C'}{4\pi tD}\exp\left[-\frac{(x-x_m-ut)^2}{4Dt}-\frac{(y-y_m)^2}{4Dt}\right] \tag{5.19}$$

where C' is the concentration of the pollution source that is instantaneously injected into the aquifer at (x_m, y_m), while F is the number of instantaneous sources.

5.3.1 Test case 1: 2D domain with a single instantaneous source.

In this case a conservative pollutant is instantaneously injected at time t=0 at the position (x=5.0, y=4.0). The pollutant is advected in the x-direction and equally dispersed longitudinally and transversely through the aquifer. The simulation is carried out in a 2-D rectangular domain [50×10] with Dirichlet boundary conditions prescribed on all boundaries. The flow velocity and the dispersion coefficient have unit values. Table 5.13 presents the pollutant and GEM simulation parameters. Two rows of observation points, both perpendicular to the direction of flow are deployed. Two cases are examined, namely;

- Case (i) observation points are located on all nodes along $x = 6.25$ and $x = 20$ except at the boundaries.
- Case (ii) observation points are located on all nodes along $x = 7.5$ and $x = 20$ except at the boundaries.

The influence of the Courant number, $Cr = u\Delta t/\Delta x$ is evaluated by having three different time discretizations i.e. $\Delta t = 0.625$, $\Delta t = 0.9375$, and $\Delta t = 1.25$. The fully implicit scheme with $\theta = 1$ is used in the GEM simulations. The parameters that are used for simulation in Model 2 are $n_o = 1$, $p_o = 10$, $m_o = 3$, $q_o = 2$, α_{opt} =1, and β_{opt} =3. It is worth noting that although this case is a transient case, the source strength, C', is only determined at time, $t = 0$, thus the decision variables are equal to the number of pollution sources.

Table 5.13: Aquifer parameters and Transport properties for Test case 1 with instantaneous sources.

Parameter	Parameter value
Spatial discretization, Δx, Δy	1.25, 1
Source concentration, C'	100
Dispersion coefficient, D	1
Velocity,u	1
Time step, $\Delta t_1, \Delta t_2, \Delta t_3$	0.625, 0.9375, 1.25

Tables 5.14 and 5.15 show the computed pollutant source strengths by Model 1, and Model 2 respectively. From Table 5.14 it can be seen that Model 1 estimates the source strength for case (i) with higher accuracy compared to case (ii), and a small time step with $Cr = 0.5$ gives better estimates than $Cr = 0.75$ and $Cr = 1.0$. The relative error for the computed source strength increases with increase in Courant number in case (i) and case (ii). Table 5.15 shows the computed source strength, the minimised objective function, J_{min}, and the error relative to the exact solution by Model 2. It is observed that Model 2 under predicts the pollution source strength in case (i) and case (ii) except for case(ii) with Cr=1.0. The computed source strength by Model 2 in case (ii) is estimated with higher accuracy compared to case (i), and a smaller $Cr = 0.5$ gives better estimates for case (i). It is therefore recognized that the location of observation points as well as time discretization do influence source identification.

Table 5.14: Test scenario for time discretization using Model 1 of Test case 1 with instantaneous sources.

Cr	Case (i)			Case (ii)		
	C'	Relative Error (%)	α	C'	Relative Error (%)	α
0.5	97.885	2.115	$2.61\text{x}10^{-5}$	107.633	7.633	$2.61\text{x}10^{-5}$
0.75	89.493	10.507	$2.61\text{x}10^{-5}$	136.895	36.895	$2.61\text{x}10^{-5}$
1	79.042	20.958	$2.61\text{x}10^{-5}$	142.714	42.714	$1.94\text{x}10^{-5}$

Table 5.15: Test scenario for time discretization using Model 2 of Test case 1 with instantaneous sources.

Cr	Case (i)			Case (ii)		
	C'	J_{min}	Relative error (%)	C'	J_{min}	Relative error (%)
0.50	87.306	2.02×10^{-2}	12.694	91.443	2.26×10^{-2}	8.557
0.75	82.971	3.942×10^{-2}	17.029	97.522	4.96×10^{-2}	2.478
1.00	77.253	6.29×10^{-2}	22.747	102.093	8.15×10^{-2}	2.093

The computed concentration for case (i) with $Cr = 1.0$ is presented as a contour plot in Figure 5.73. It is observed that the concentration distribution is correctly predicted by Model 1, while Model 2 depicts a trailing plume. Figure 5.74 shows the mean error for the computed concentration by both Models 1 and 2 which reduces with time, however Model 1 consistently has lower error compared to Model 2. The computational time for Models 1 and 2 is given in Table 5.16, it is seen that Model 2 requires more time for computation than Model 1.

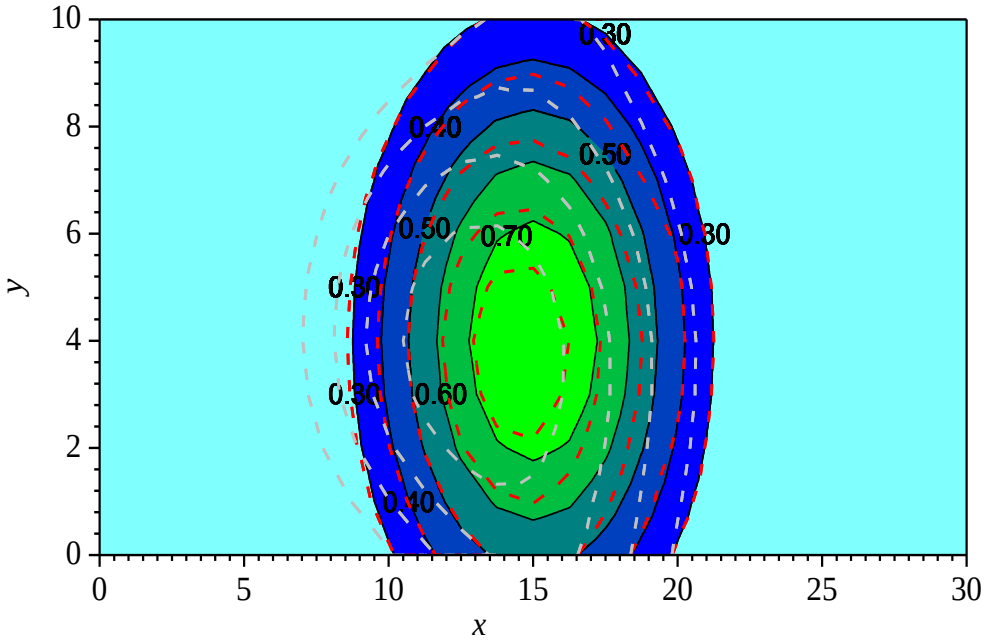


Figure 5.73 : Concentration distribution at $t = 10$; graded colour shows the exact plume distribution, and the dashed red line shows Model 1 solution, and the grey colour shows Model 2 solution for Test case 1 with $Cr = 1$.

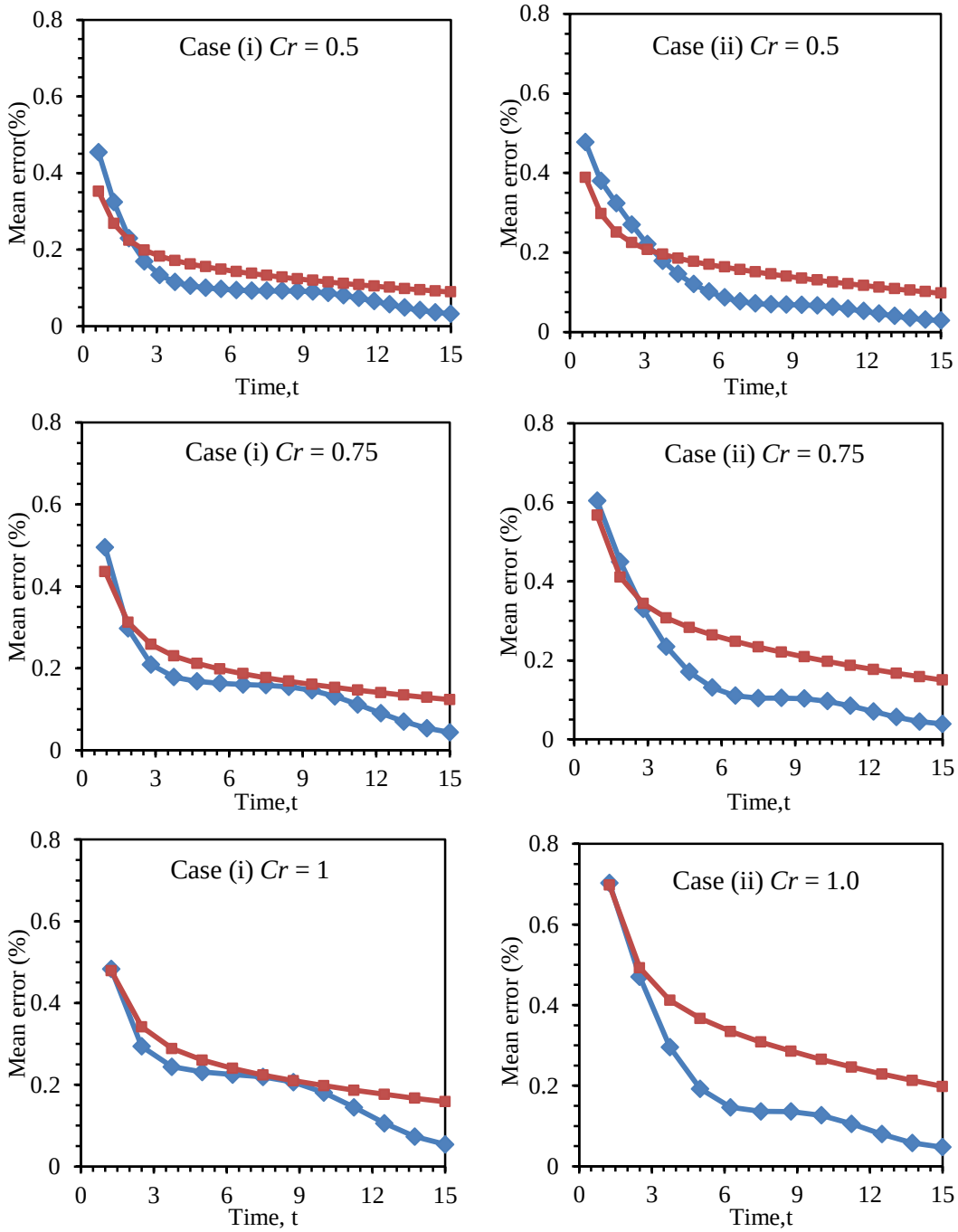


Figure 5.74: Mean error of the computed concentration by Model 1 (in blue) and Model 2 (in red) of Test case 1 with instantaneous sources for various Courant numbers.

Table 5.16: Computational time (seconds) for Test case 1 with instantaneous sources.

Cr	Time for simulation of Case (i)		Time for simulation of Case (ii)	
	Model 1	Model 2	Model 1	Model 2
0.50	21.41	68.47	38.24	62.18
0.75	14.43	69.27	14.22	79.49
1.00	11.00	64.73	11.23	55.28

5.3.2 Test case 2: 2D domain with multiple instantaneous pollutant sources

In this case, five conservative pollutants positioned at $(x = 5.0,\ y = 1.0)$, $(x = 5.0,\ y = 4.0)$, $(x = 5.0, y = 7.0)$, $(x = 8.75, y = 4.0)$, and $(x = 8.75, y = 6.0)$ are injected instantaneously at time t=0. The actual source strengths for these sources are given in Table 5.17, and are utilized in Equation (5.19) to determine the concentration distribution at the observation points, as well as the boundary conditions, however they are unknown in the inverse problem. It is important to note that three of these sources are active while the remaining two are dummy sources. This problem is solved in a rectangular domain of [50×10], which is discretized into elements of $(\Delta x = 1.25 \times \Delta y = 1)$, the hydrodynamic dispersion, and the velocity in the x-direction have unit values. Dirichlet boundary conditions are specified on all boundaries. The sampling points γ for concentration are located on the nodes along x=6.25, and x=11.25. A uniform time step, Δt = 0.625, and the fully implicit scheme with θ=1 are used in the GEM simulation. The parameters used in Model 2 simulation are $n_o = 5, p_o = 10, m_o = 11, q_o = 6, \alpha_{opt} = 1$, and $\beta_{opt} = 11$. Figure 5.75 shows the schematic representation of the problem, as well as the sampling points.

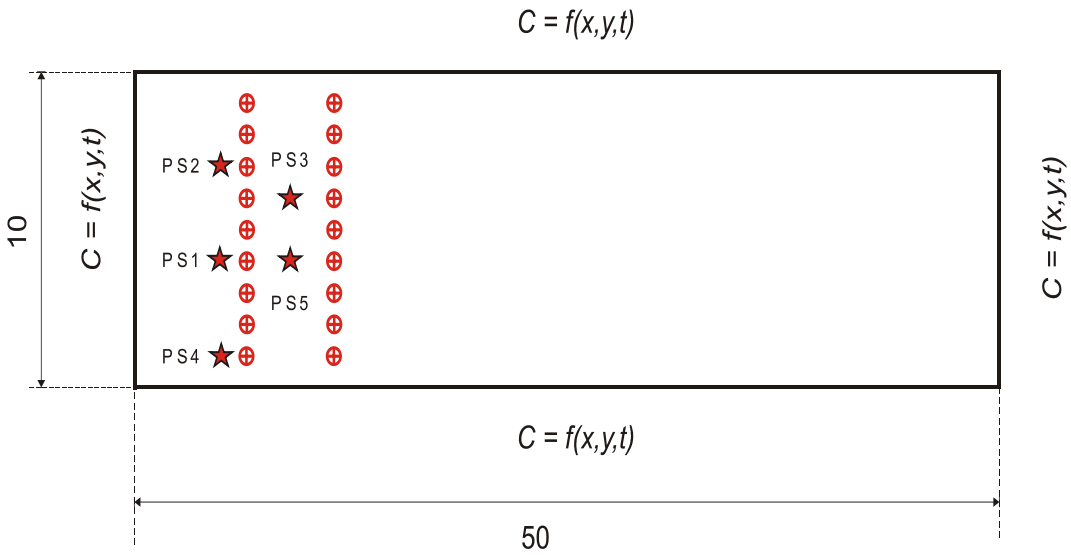


Figure 5.75: Schematic representation of the aquifer system in Test case 2. The location of the instantaneous sources is shown by the red stars and the sampling points are shown using the red crossed circle.

Table 5.17: Actual source strengths of the instantaneous sources for Test case 2.

Source number	Source strength and location	Values
PS1	Source strength $C_1^{'}$ and location (x_1, y_1)	100 (5,4)
PS2	Source strength $C_2^{'}$ and location (x_2, y_2)	200 (5,7)
PS3	Source strength $C_3^{'}$ and location (x_3, y_3)	0.0 (8.75, 6)
PS4	Source strength $C_4^{'}$ and location (x_4, y_4)	75 (5,1)
PS5	Source strength $C_5^{'}$ and location (x_5, y_5)	0.0 (8.75,4)

Figure 5.76 shows the exact and the computed source strengths using exact observation data. It is observed that Model 1 estimates the source strengths better with an average error of 2.413% as compared to Model 2 which has an average error of 12.621%. In both cases the dummy sources are estimated with negligible concentration values. The computed concentration at time $t = 10$ in Figure 5.77 shows that the computed solution matches well with the exact solution for Model 1, while Model 2 results show a trailing pattern of the plume although the magnitude is excellently estimated. The mean error for the computed concentration in Figure 5.78 shows that Model 1 performs better than Model 2 as time increases. The computation time for Model 2 was 463.8 seconds for a single run, compared to 8.39 seconds for Model 1.

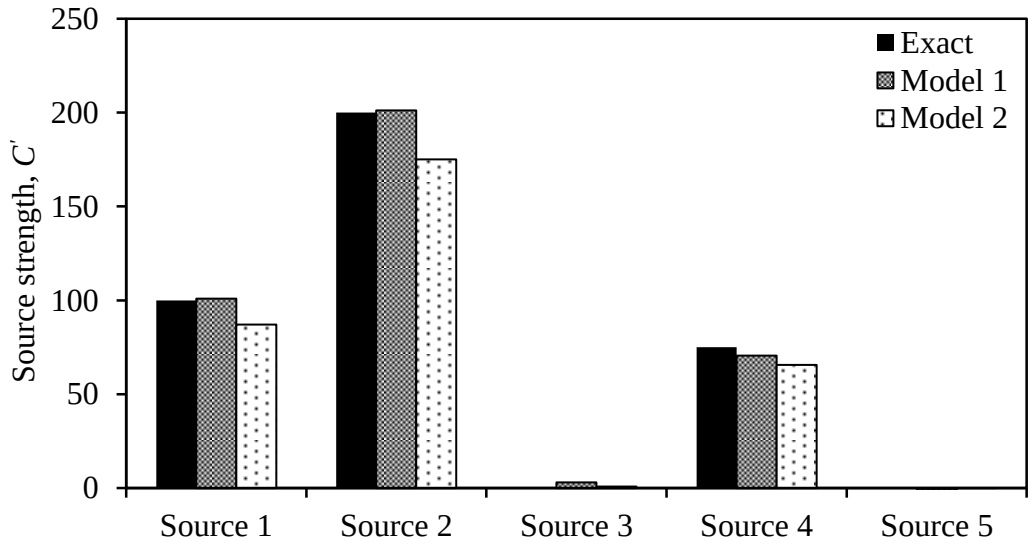


Figure 5.76: Exact, Model 1, and Model 2 computed source strength with exact observation data.

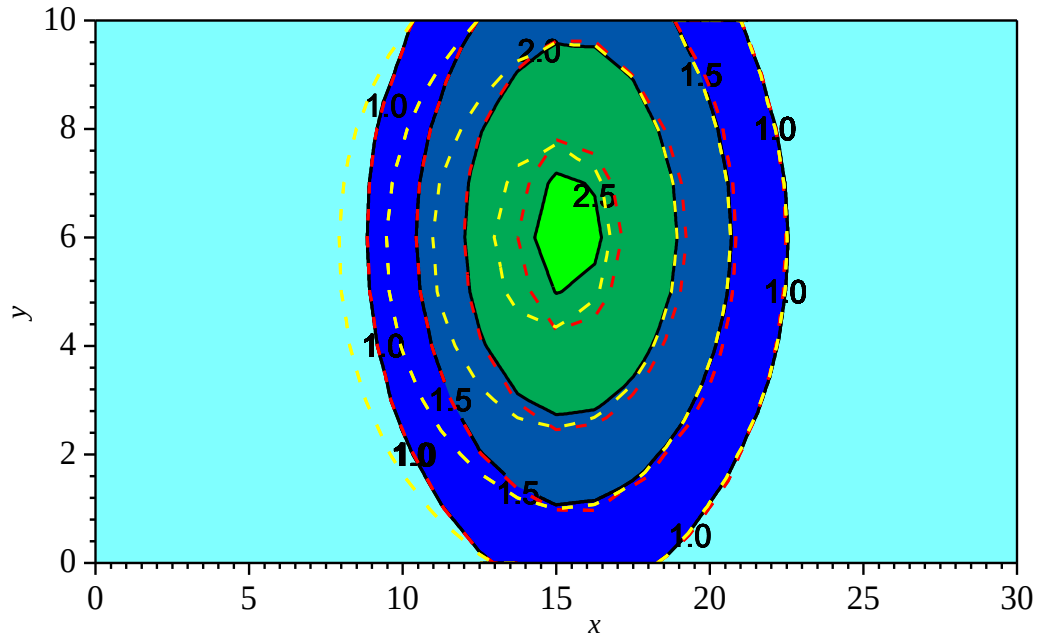


Figure 5.77: Contour plots of the concentration distribution at time (t=10), graded colour shows the exact solution, the dash red line shows the Model 1 solution, while the dash yellow line shows Model 2 solution.

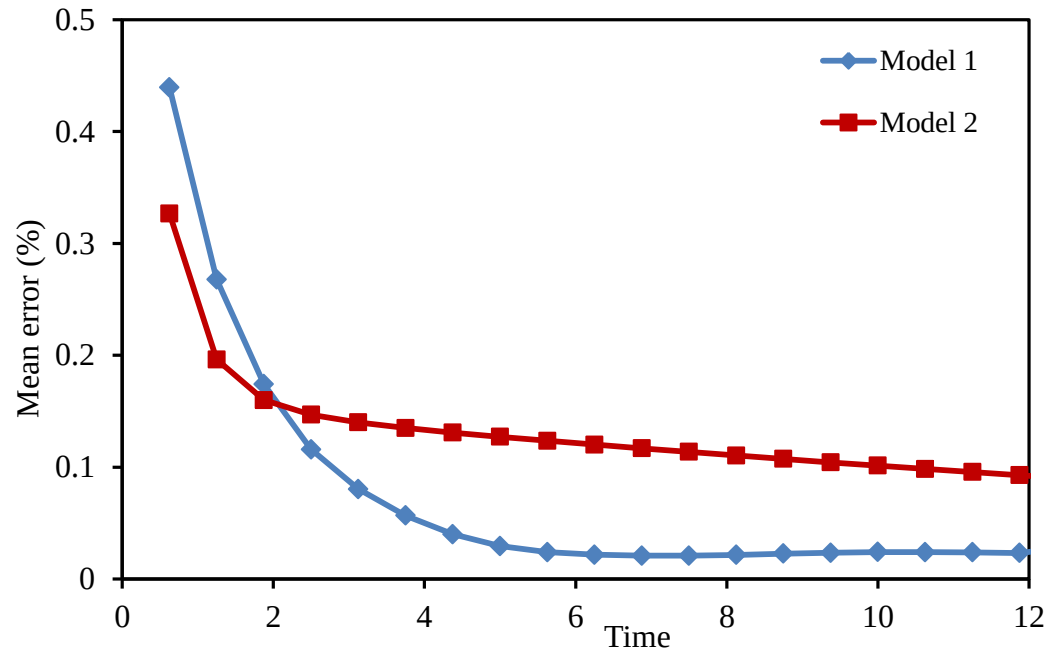


Figure 5.78: Mean error for the computed concentration using Model 1 and 2 with multiple instantaneous sources.

Random errors in observation data of Test case 2

Randomly perturbed observation data were utilized to compute the source strength. The computed source strengths are presented in Table 5.18 and Figure 5.79. It is observed that a good prediction of the source strength is obtained even in the presence of observation errors. The average errors relative to the exact source strengths using observation data with $\varepsilon = 0.0\%, \varepsilon = 1\%, \varepsilon = 3\%,$ and $\varepsilon = 5\%$ are 2.4134%, 2.7181%, 3.328%, and 3.9381% respectively. The errors increase with increase in the noise levels in the observation data. The computed concentration distribution at time $t = 10$ for noise levels $\varepsilon = 0.0\%$ and 5% are presented in Figure 5.80. The results indicate an excellent reconstruction of the plume even in the presence of observation errors.

Table 5.18: The exact and computed source strengths using randomly perturbed observation data.

Pollutant source location	Exact source strength	Computed source strength, C'			
		$\varepsilon = 0.00$	$\varepsilon = 0.01$	$\varepsilon = 0.03$	$\varepsilon = 0.05$
PS1	100	100.877	100.841	100.769	100.697
PS2	200	201.129	201.632	202.638	203.645
PS3	0	3.119	2.984	2.713	2.442
PS4	75	70.651	70.127	69.078	68.029
PS5	0	-1.154	-0.741	0.084	0.909

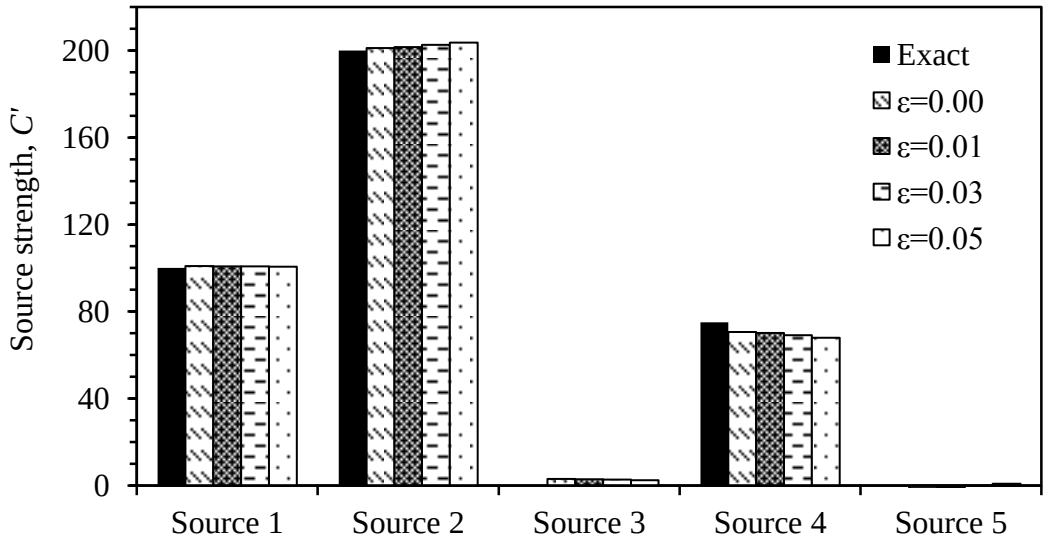


Figure 5.79: Exact and computed source strength using noisy observation data for Test case 2.

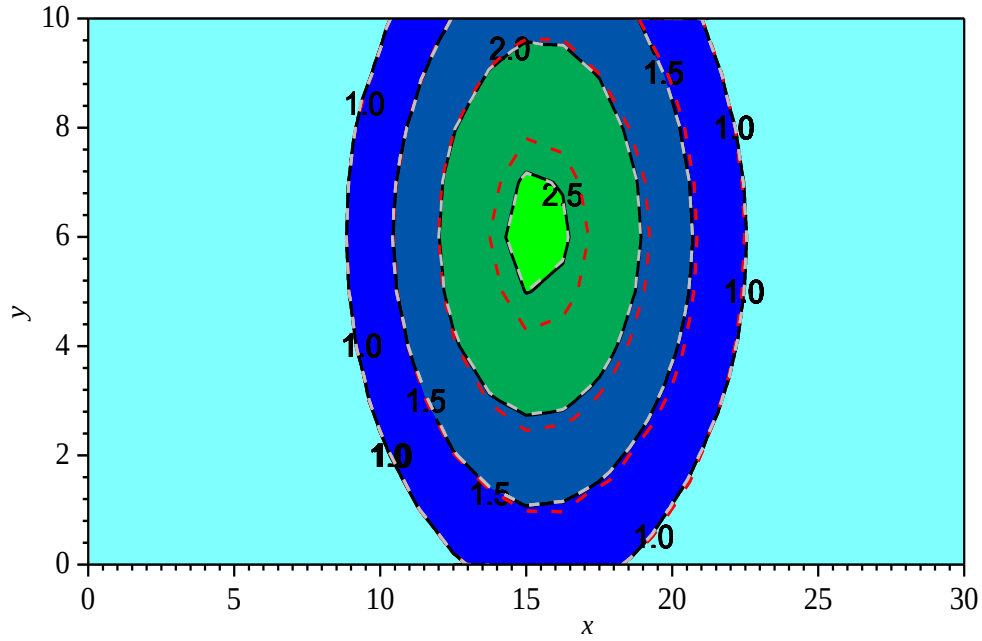


Figure 5.80: Contour plots of the concentration at time $t = 10$, graded colour shows the exact solution, dashed red line-Model 1 solution with $\varepsilon = 0\%$ and the grey dashed line - solution with $\varepsilon = 5\%$ in observation data.

Random errors in parameter data of Test case 2

The influence of errors in flow and medium parameters is evaluated by varying the error magnitudes of the velocity and dispersion by ±5%, ±10%, and ±15%. The simulations are carried out by first considering errors in velocity, then dispersion, and finally both velocity and dispersion. The computed source strengths with velocity errors are presented in Table 5.19. It is observed, that the computed source strengths decrease with higher negative errors of the velocity (except for $C_5^{'}$), whereas they increase with higher positive errors. The concentration distribution of the contaminant plume at time, $t = 10$ with positive 10% error in velocity is presented in Figure 5.81, and it shows a concentration plume that is shifted in the direction of the velocity error.

The influence of dispersion errors on source strength recovery is presented in Table 5.20. The only consistent trend in the numerical results of the source strength is that positive errors in the dispersion produce opposite effects to negative errors. In other words, source strengths reduce with higher positive dispersion errors and increase with higher negative errors. Figure 5.82 shows the

computed concentration distribution at $t = 10$ with 10% error in the dispersion coefficient, and the results indicate that the peak of the concentration is underestimated and more smeared.

Table 5.19: Model 1 computed source strength with error in velocity

Pollutant Source	Percentage error in velocity (- %)			Percentage error in velocity (+ %)		
	15	10	5	5	10	15
PS1	98.048	99.009	99.952	101.780	102.660	103.516
PS2	195.674	197.546	199.365	202.834	204.475	206.049
PS3	2.807	2.912	3.016	3.224	3.329	3.436
PS4	66.343	67.838	69.270	71.989	73.290	74.562
PS5	2.438	1.123	-0.068	-2.146	-3.058	-3.899

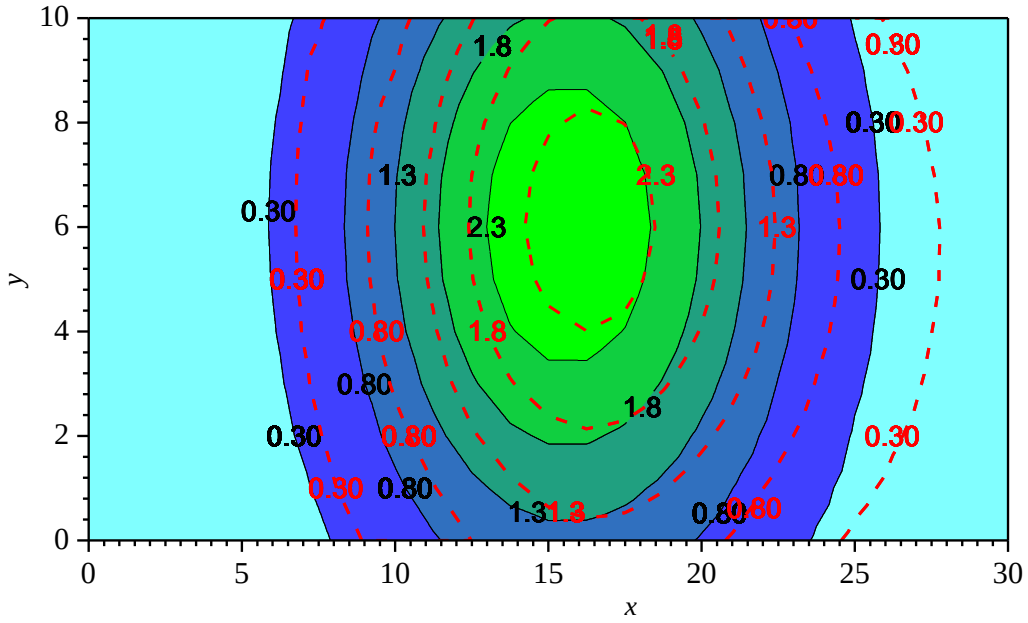


Figure 5.81: The exact in the graded colour and the Model 1 computed concentration with velocity, $u = u + 10\%u$ at time $t = 10$ in the red dashed line.

Table 5.20: Model 1 computed source strength with error in dispersion

Pollutant Source	Percentage error in dispersion (- %)			Percentage error in dispersion (+ %)		
	15	10	5	5	10	15
PS1	103.160	102.392	101.628	100.142	99.427	98.736
PS2	208.330	205.902	203.499	198.801	196.518	194.283
PS3	1.823	2.275	2.708	3.510	3.879	4.227
PS4	65.354	67.167	68.939	72.293	73.857	75.337
PS5	-3.584	-2.584	-1.782	-0.673	-0.0319	-0.071

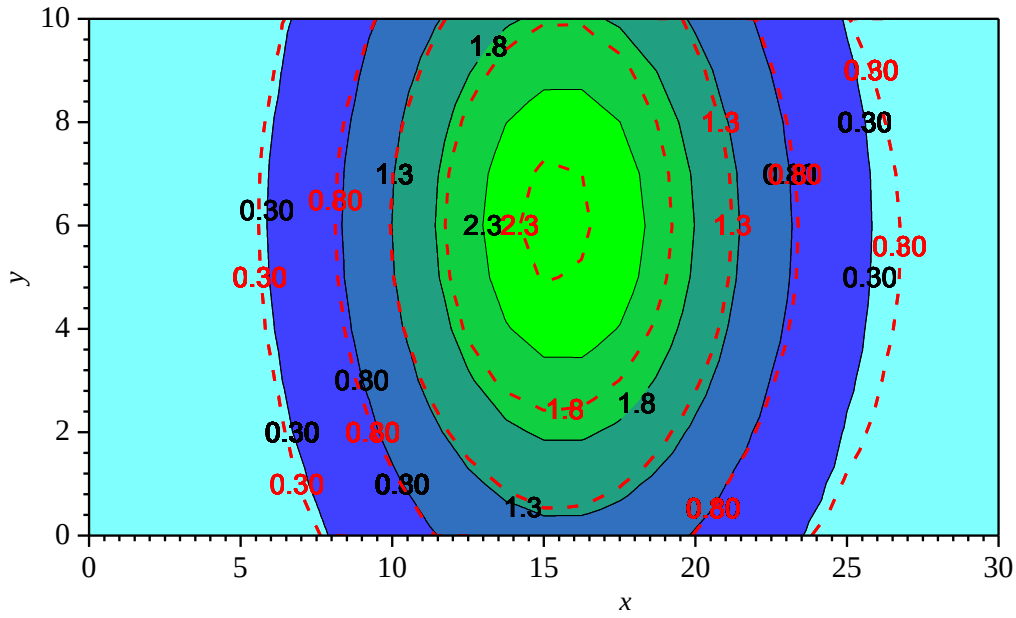


Figure 5.82: The concentration contours for the exact and computed solutions, the black solid line shows the exact, the red dashed line shows Model solution with 10% error in dispersion.

The effect of having both velocity and dispersion errors is presented in Table 5.21. When both the velocity and dispersion parameters have negative errors the source strength decreases with increase in the magnitude of the error; however a mixed trend is exhibited when there are positive errors. The computed concentration distribution in Figure 5.83 shows a shifted plume in the direction of the error and a diminished peak.

Table 5.21: Computed source strength with error both in velocity and dispersion.

Pollutant Source	Percentage error in velocity and dispersion (- %)			Percentage error in velocity and dispersion (+ %)		
	15	10	5	5	10	15
PS1	99.599	100.223	100.634	100.984	100.982	100.892
PS2	201.310	201.668	201.582	200.371	199.364	198.150
PS3	1.548	2.081	2.607	3.616	4.092	4.548
PS4	60.946	64.238	67.516	73.569	76.230	78.614
PS5	-0.429	-0.439	-0.718	-1.670	-2.221	-2.773

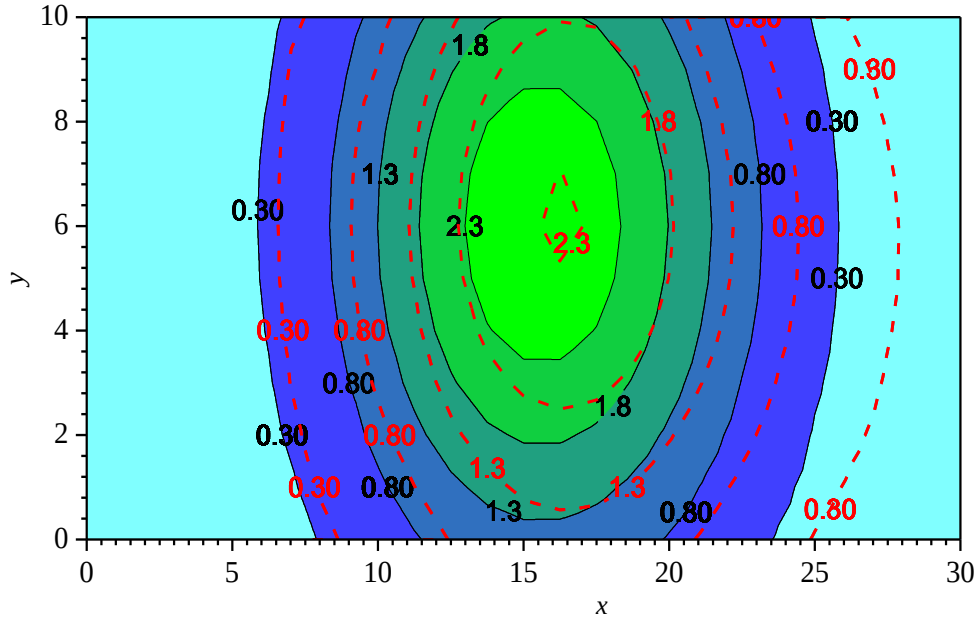


Figure 5.83: The exact in the graded colour and the Model 1 computed concentration with velocity, $u = u + 10\%u$ and dispersion, $D = D + 10\%D$ at time $t = 10$ in the red dashed line.

Table 5.22 shows the counter effects of having opposite errors in velocity and dispersion. It is observed that when the velocity has positive errors and dispersion has negative errors the computed source strengths increase with increase in the error magnitude, except for $C_3^{'}$ and $C_4^{'}$. On the contrary when there are negative velocity errors and positive dispersion errors the source magnitude decreases with increase in the errors for $C_1^{'}$ and $C_2^{'}$ on the contrary for $C_3^{'}$ and $C_5^{'}$ an increase in the source strength is observed. The combined effect of velocity and dispersion errors on the reconstructed plume is shown in Figures 5.84, and 5.85. A replicate of the individual effects is observed, where the plume is shifted in the direction of the error for velocity and the peak is diminished when positive errors in dispersion are present. Figure 5.86 shows the exact solution of the concentration fronts with time at three locations $x = 7.5, x = 13.75$, and $x = 22.5$ along $y = 4$ and computed solutions with 10% error in the velocity and in the dispersion coefficient. Higher concentration peaks are observed in the Model 1 solution with error in the velocity than in the dispersion coefficient.

Table 5.22: Computed source strength with opposite error both in velocity and dispersion

Pollutant Source	Percentage error in velocity (+ %) and dispersion (- %)			Percentage error in velocity (- %) and dispersion (+ %)		
	15	10	5	5	10	15
PS1	106.535	104.478	102.602	99.278	97.786	96.384
PS2	214.723	209.872	205.352	197.173	193.458	189.960
PS3	2.126	2.478	2.810	3.404	3.663	3.898
PS4	69.393	69.921	70.318	70.976	71.341	71.783
PS5	-5.904	-4.347	-2.751	0.414	1.922	3.348

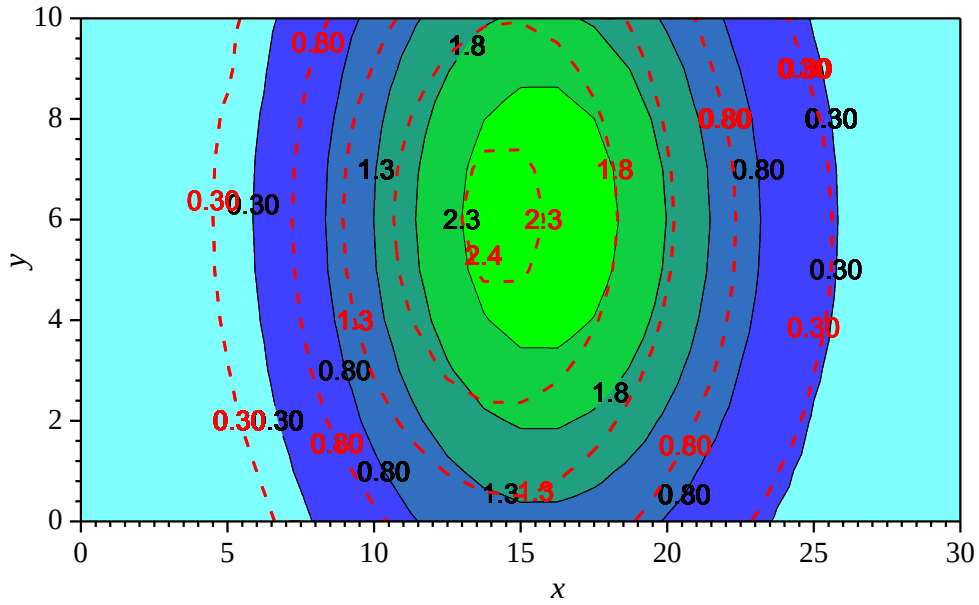


Figure 5.84: The exact and the computed concentration distribution with velocity, $u = u\ - 10\%u$ and dispersion, $D = D\ + 10\%D$.

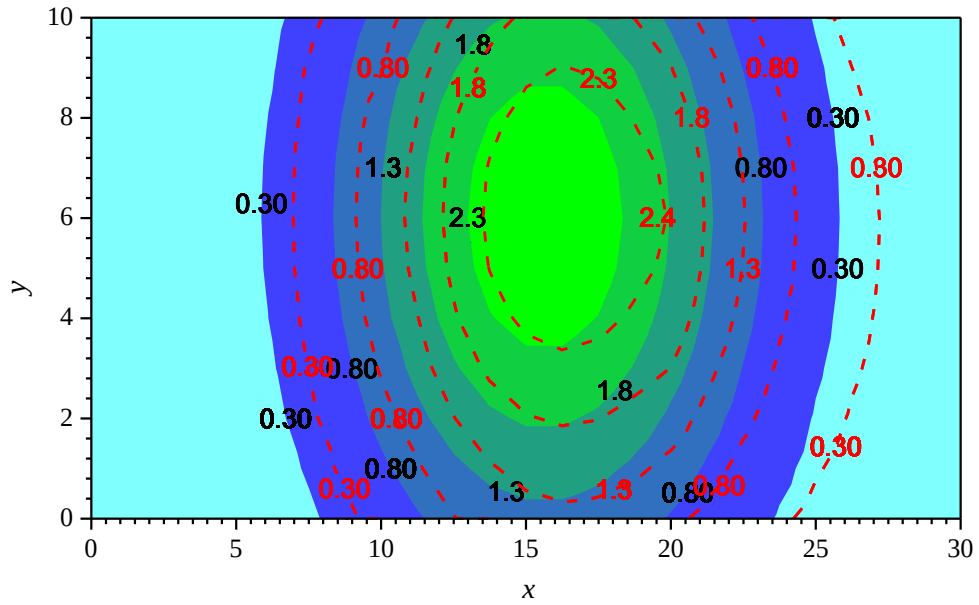


Figure 5.85: The exact and the computed concentration distribution with velocity, $u = u\ + 10\%u$ and dispersion, $D = D\ - 10\%D$.

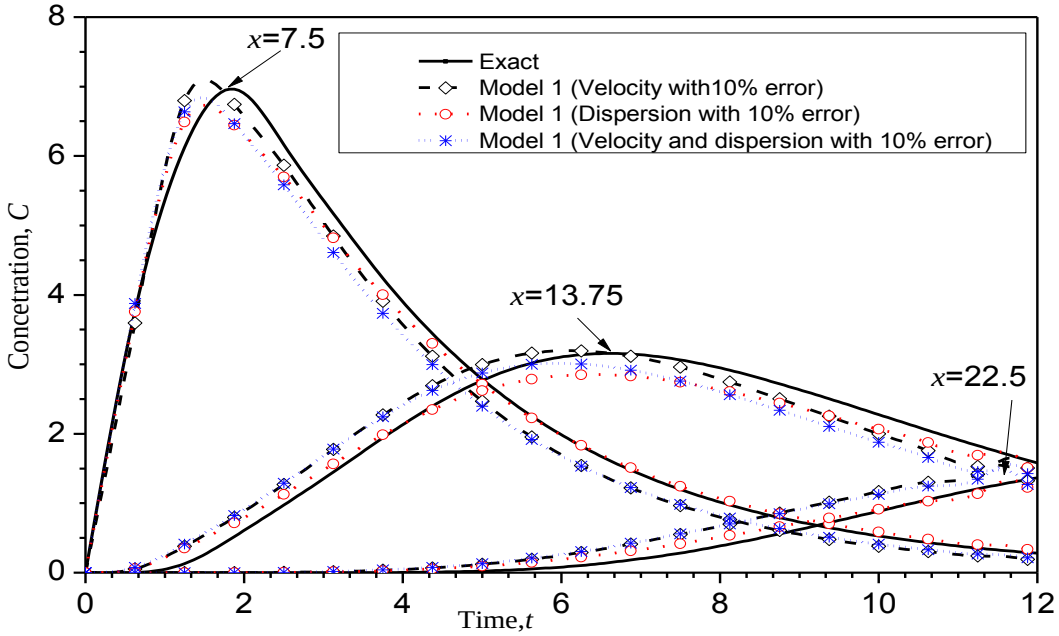


Figure 5.86: Exact and computed concentration fronts for velocity with 10% error, dispersion with 10% error, and both velocity and dispersion 10% error along $y = 4$.

5.4 Continuous point source problems

In this section we consider point sources, in which the fluid containing the pollutant is injected continuously starting at time $t = 0$ at a rate W_v. We utilize three test cases to demonstrate the potential of the developed methodology for contaminant source identification. These test cases have analytical solutions for benchmarking.

The analytical solution for the concentration distribution in a saturated, 2-dimensional, homogeneous aquifer under uniform flow in the *x*-direction for a continuous source under transient conditions is given as (Bear, 1972);

$$C(x,y,t) = \frac{C^{'}W_v}{4\pi\eta D}\exp\left(\frac{ux}{2D}\right)W(\Phi, z/\beta) \tag{5.20}$$

where $W(\Phi,z/\beta)$ is the Hantush well function that is given by

$$W(\Phi, z/\beta) = \int_{\Phi}^{\infty} e^{\left(-\xi-\frac{z^2}{4\beta^2\xi}\right)}\frac{d\xi}{\xi} \tag{5.21}$$

in which $\Phi = [(x-x_s)^2+(y-y_s)^2]/(4Dt)$, $z^2/\beta^2 = [(x-x_s)^2+(y-y_s)^2]u^2/D^2$, and (x_s,y_s) is the location of the pollutant source. Letting time to infinity steady state conditions are achieved. The analytical solution for the steady-state concentration distribution from a point source is given as;

$$C(x,y) = \frac{C^{'}W_v}{2\pi D}\exp\left(\frac{u(x-x_s)}{2D}\right)K_0\left[\left\{\frac{u^2}{4D}\left(\frac{(x-x_s)^2}{D}+\frac{(y-y_s)^2}{D}\right)\right\}^{0.5}\right] \tag{5.22}$$

where, K_0 is the modified Bessel function of second kind and zero order, and (x_s, y_s) is the position where the pollutant is injected.

5.4.1 Test case 1: Injection of a pollutant at a point into a uniform steady flow.

This first example in this section is a 2D problem with a point source of strength, C'=100, injected into a uniform flow field under steady state conditions. The pollutant is advected with uniform velocity in the direction of the flow, and dispersed equally in the longitudinal and transverse directions. The governing equation is given in Equation (2.4), and restated here for convenience as;

$$\nabla\cdot(D\nabla C) = \mathbf{V}\cdot\nabla C - Q(x,y). \tag{5.23}$$

The pollution point source is expressed as $Q = C^{'}\delta(x-x_s,y-y_s)$, where $C^{'}$ is the strength of the source located at (x_s,y_s). The inverse problem seeks to determine the unknown source strength, C'. The GEM simulations were carried out in a 2-D rectangular domain [40×10] using the parameters given in Table 5.23. Dirichlet boundary conditions were prescribed on all boundaries and additional information was obtained from an observation point located at (11.25, 5) by solving Equation (5.22).

Table 5.23: Parameter values used for simulation of the steady state case with point source.

Parameter	Parameter values
Spatial discretization, Δx, Δy	1.25,1
Source Location	(8,4.5)
Longitudinal /Transverse dispersion (D)	1
Velocity, *u*	0.5

In the simulations, Model 1 was implemented while accounting for observation errors and the regularization parameter was determined by the L-curve automatically. Model 2 was implemented with the following parameters $n_o = 1, p_o = 10, q_o = 2, m_o = 3, \alpha_{opt} = 1, \beta_{opt} = 3$. The number of decision variables for this case is one, because the problem is not time dependent, and there is only one source with unknown source strength. The convergence behaviour of the objective function from several runs is shown in Figure 5.87. The obtained minimized objective function is 5.836×10^{-5}.

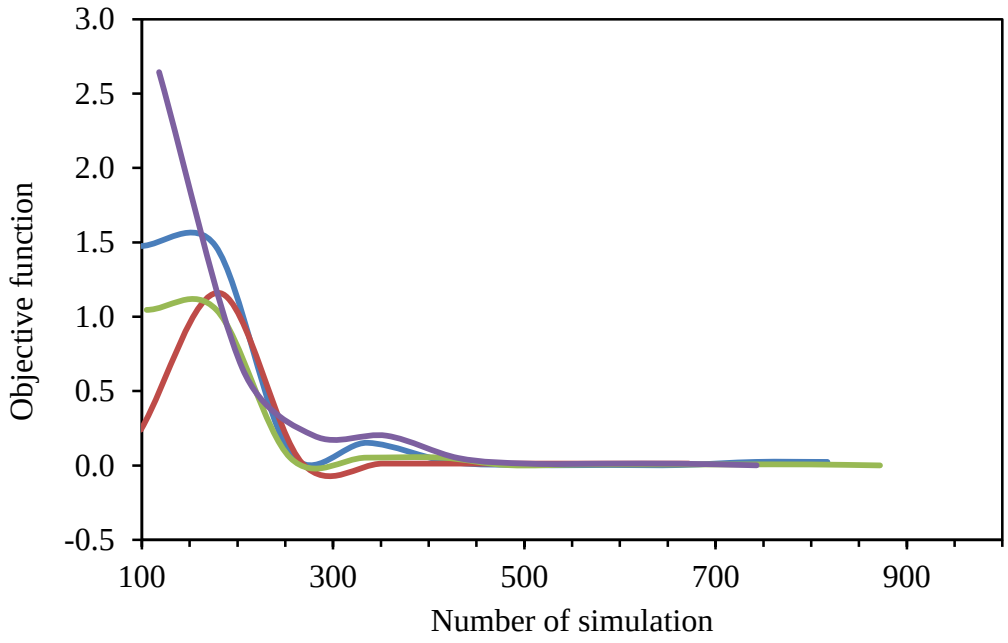


Figure 5.87: A plot of the objective function versus the number of simulations by Model 2 for Test case 1with point sources.

Table 5.24 shows the computed source strength results by Model 1 with error free and noisy observation data, and Model 2 with error free observation data. It is observed that both Model 1 and 2 estimate the source correctly with error free observation data. However, as the magnitude of the noise levels increase the accuracy of the computed source strength decreases in Model 1. The relative error for Model 1 when accounting for observation errors increases with increase in noise levels. Model 2 has the least relative error of the computed to the true source strength when compared to Model 1 for noise free observation data. On the other hand, the computation time for Model 2 is higher than Model 1.

Table 5.24: Model 1 and 2 computed source strength for Test case 1 with point source.

Model	Source strength, C'	Relative error (%)	Regularization parameter, α	Computation time (s)
Model 1 ($\varepsilon = 0\%$)	101.239	1.239	5.83×10^{-6}	1.14
Model 1 ($\varepsilon = 1\%$)	102.015	2.015	2.14×10^{-5}	1.15
Model 1 ($\varepsilon = 3\%$)	103.568	3.568	7.74×10^{-6}	1.14
Model 1 ($\varepsilon = 5\%$)	105.121	5.121	1.67×10^{-5}	0.84
Model 2 ($\varepsilon = 0\%$)	100.581	0.419	-	21.13

Figure 5.88 shows the contour plots for the exact, the computed concentration distribution by Model 1 and Model 2 for error free observation. It is observed that the recovered concentration distribution is excellent matching the exact solution. Figure 5.89 shows the contour plots of the exact and the computed concentration distribution simulated by Model 1 with ε=0% and ε=5% error in the observation data. It is observed that the spatial distribution of the concentration is not greatly influenced by observation errors, as the mean error for the computed concentration with ε=0% and ε=5% was obtained as 0.0284% and 0.0409% respectively.

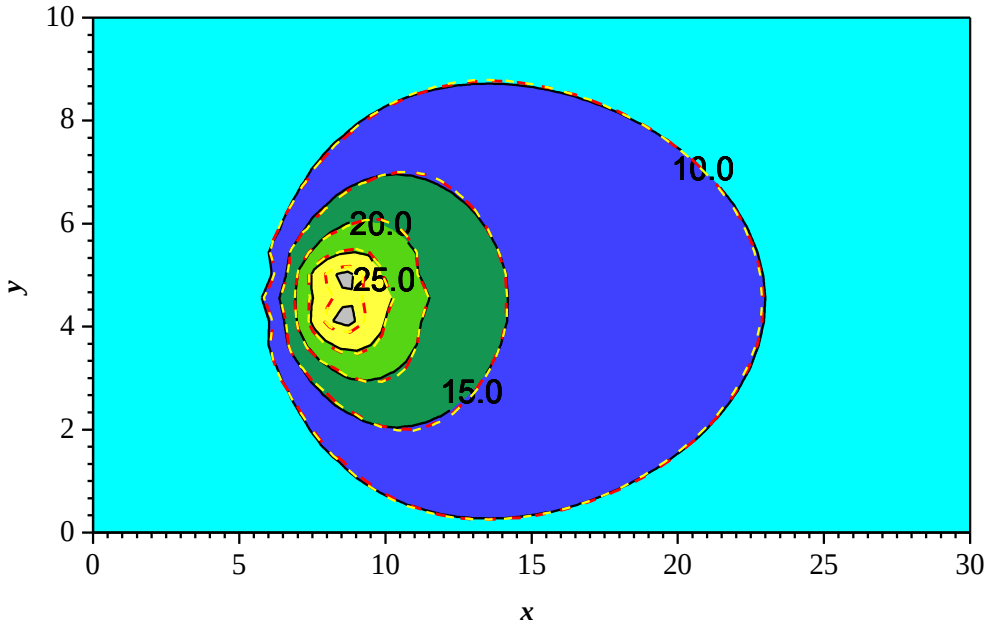


Figure 5. 88: Contour plots of the concentration distribution of Test case 1 simulated with exact observation data. The exact solution -graded colour, Model 1 solution -dashed red line, and Model 2 solution - dashed yellow line.

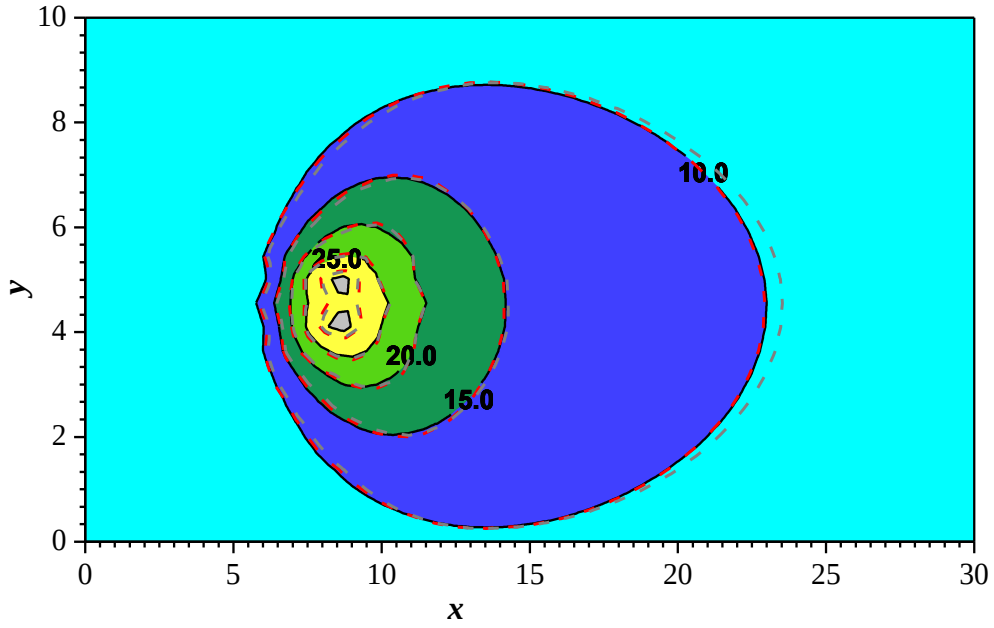


Figure 5. 89: Contour plots of the concentration distribution with error free and 5% observation error. Exact solution -Graded colour, Model 1 computed solution with ε=0% - red dashed line, and Model 1 computed solution with ε=5% - grey dashed line.

The influence of errors in flow and medium parameters was evaluated by varying the error magnitudes on the velocity and dispersion by ±5%. The Model 1 simulations were carried out with the same parameters in Table 5.23 but the

velocity was taken as $u = u \pm 0.05u$, and the dispersion coefficient was taken as $D = D \pm 0.05D$. It should be noted that observation errors were not considered.

Table 5.25 shows the computed source strengths using erroneous velocity and dispersion. It is observed that the computed source strengths with erroneous velocity are recovered with a lower relative error compared to dispersion errors.

Table 5.25: Computed source strength with 5% errors in velocity or dispersion.

Parameter	Percentage error (-5 %)			Percentage error (+5 %)		
	Computed source strength, *C'*	Relative error (%)	α	Computed source strength, *C'*	Relative error (%)	α
Velocity	99.363	0.637	1.08×10^{-5}	103.402	3.402	7.38×10^{-6}
Dispersion	97.228	2.772	8.51×10^{-6}	105.322	5.322	7.74×10^{-6}

Figure 5.90 shows the plume spatial distribution for the exact and the computed concentration with velocity errors ($\pm 5\%$). It is observed that the concentration fronts are shifted in the direction of the velocity errors. Figure 5.91 shows the plume distribution for the exact and the computed concentration with dispersion errors ($\pm 5\%$). No major trend is observed for this case. The mean error for the computed concentration with +5% velocity errors and +5% dispersion errors were obtained as 0.0686% and 0.316% respectively. It is therefore observed that the dispersion coefficient has higher influence on source recovery and plume reconstruction.

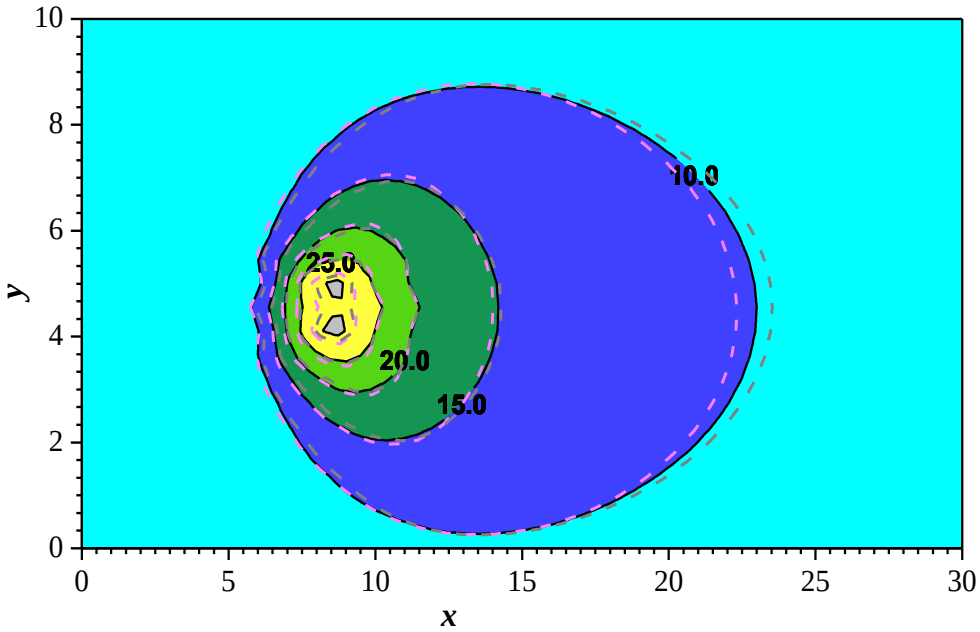


Figure 5.90: A Contour plot of the concentration distribution with velocity errors. Graded colour- exact solution, Model 1 solution with -5% errors in velocity – pink dashed line, and solution with +5% errors in velocity – grey dashed line.

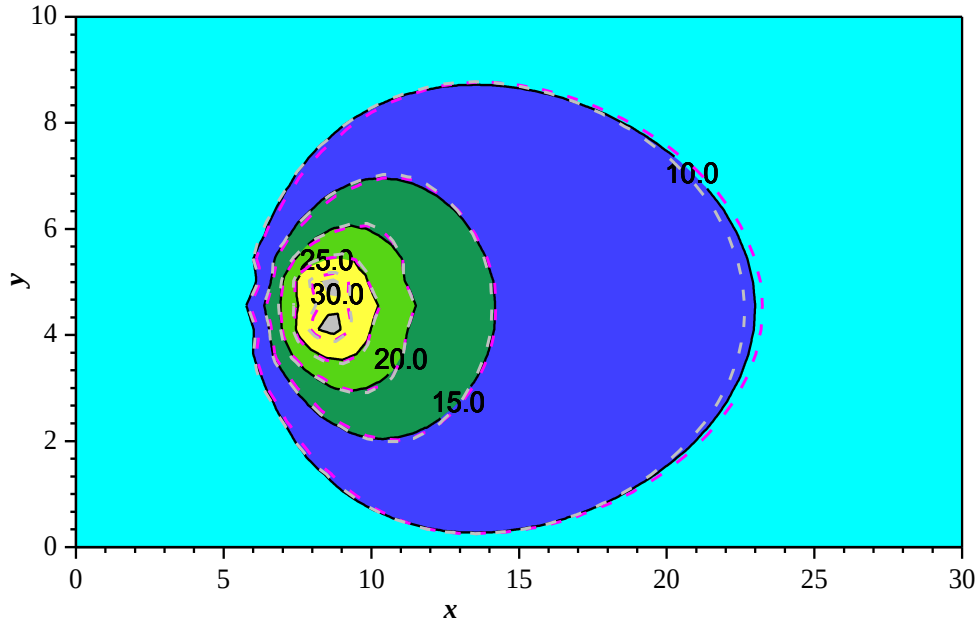


Figure 5.91: A contour plot of the computed concentration distribution with dispersion errors. Graded colour -exact solution, Model 1solution with -5% errors in dispersion data pink dashed line and the solution with +5% errors dispersion – grey dashed line.

5.4.2 Test case 2: A continuous injection at multiple points into a uniform steady flow

This is a 2-D contaminant transport problem in an infinitely extensive domain that arises from pollution point sources that are dispersed in two dimensions and advected in the *x*-direction under steady state conditions. Each pollution point source is expressed as $Q = C'\delta(x\text{-}x_s, y\text{-}y_s)$, where C' is the strength of the source located at (x_s,y_s). The exact solution for the spatial concentration distribution is

$$C(x,y) = \sum_{s=1}^{K} \frac{C'}{2\pi D} \exp\left(\frac{u(x-x_s)}{2D}\right) K_0\left[\frac{u}{2D}\left((x-x_s)^2 + (y-y_s)^2\right)^{0.5}\right] \qquad (5.24)$$

where K_0 is the modified Bessel function of second kind and zero order, and K is the number of pollution sources.

The inverse modelling of this problem is carried out in a rectangular domain [30×10] with three pollution sources (K =3) of unknown strengths. The sources are located at (x_1=5.5, y_1=4.5), (x_2=10.5, y_2=2.5) and (x_3=15.5, y_3=6.5), while the velocity $u = 0.5$, and dispersion coefficient $D = 1.0$. The 2-D domain is discretized into uniform rectangular elements $[\Delta x = 1 \times \Delta y = 1]$, while the concentration is specified on all external boundaries and at three observation points located at (6,5), (11,3) and (16,7), as illustrated in Figure 5.92. The specified concentration values are obtained from Equation (5.24) using the pollution source strengths 20, 10, and 4, for Source 1, 2, and 3 respectively.

The parameters used in Model 2 simulations include $n_o = 3, p_o = 10, q_o = 2, m_o = 7, \alpha_{opt} = 1, \beta_{opt} = 7$. The number of decision variables for this case is equal to the number of the unknown source strengths. The obtained minimized objective function is 9.729×10^{-4}.

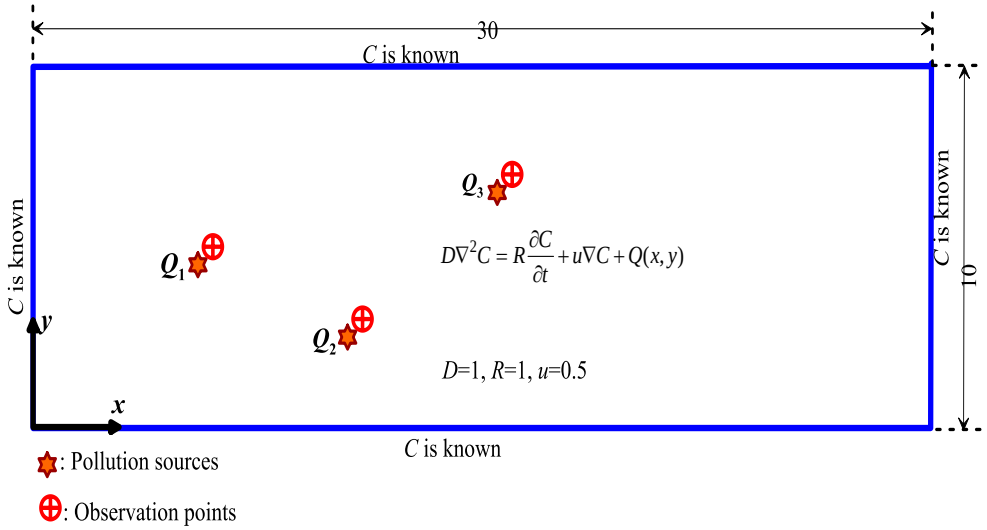


Figure 5.92: Schematic representation of aquifer for Test case 2 with point sources.

Table 5.26 shows the recovered pollution strengths by Model 1 with and without noise in the observation data, and Model 2 with error free observation data. The average relative error for the computed source strength by Model 1 is 1.47% and 6.28% for data with noise levels of $\varepsilon = 0\%$ and $\varepsilon = 5\%$ respectively, which shows an increase of relative error with increase in noise levels. Model 2 gives a better estimate of the source strengths, with a relative error of 1.24% for the error free case.

Table 5.26: Computed source strengths by Model 1 and Model 2 for Test case 2.

	Model 1				**Model 2**
	$\varepsilon = 0\%$	$\varepsilon = 1\%$	$\varepsilon = 3\%$	$\varepsilon = 5\%$	$\varepsilon = 0\%$
C_1'=20	19.447	19.584	19.858	20.132	19.374
C_2'=10	10.065	9.946	9.707	9.469	9.955
C_3'=4	4.040	3.929	3.707	3.485	4.006

Figure 5.93 shows the concentration plumes obtained by the exact solution are compared to those obtained by Model 1 and Model 2. From Figure 5.93 it is revealed that both Model 1 and 2 give good prediction of the concentration plume with mean errors for the computed concentration for Model 1 equal to 0.0248% and 0.0235% for Model 2. Figure 5.94 shows the spatial distribution of the recovered contaminant concentration by Model 1 with 5% observation error,

which is not significantly influenced by observation errors. The mean error for the computed concentration with 5% observation errors was obtained as 0.0296%.

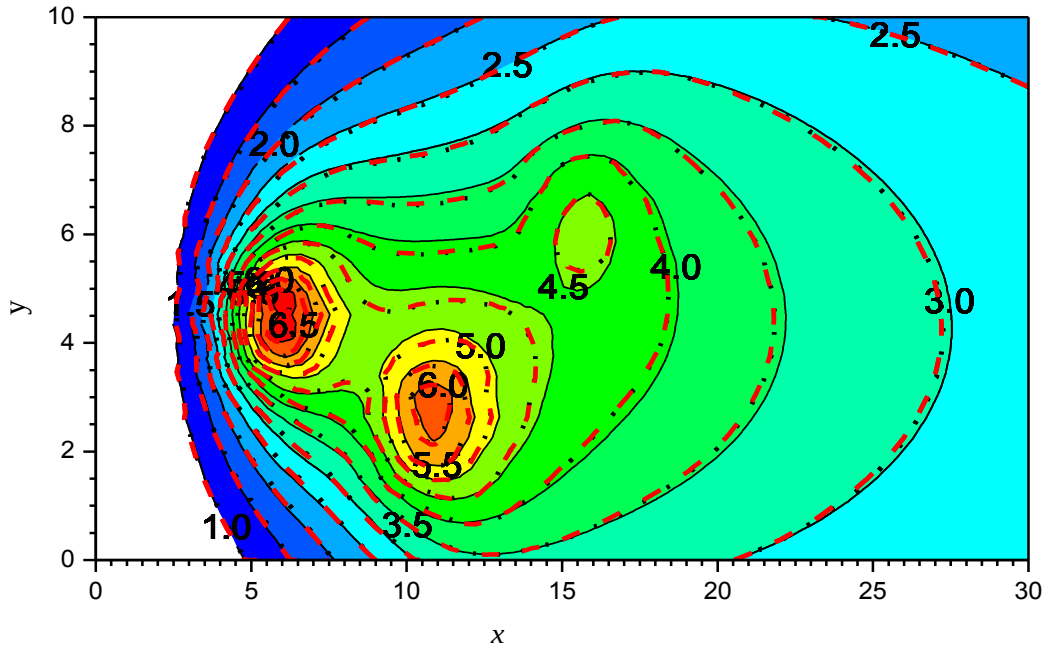


Figure 5.93: Spatial distribution of contaminant plume of Test case 2 with exact data: exact solution-graded colour and solid black line, Model 1 solution- Model 2 solution - dashed red lines Model 2 solution.

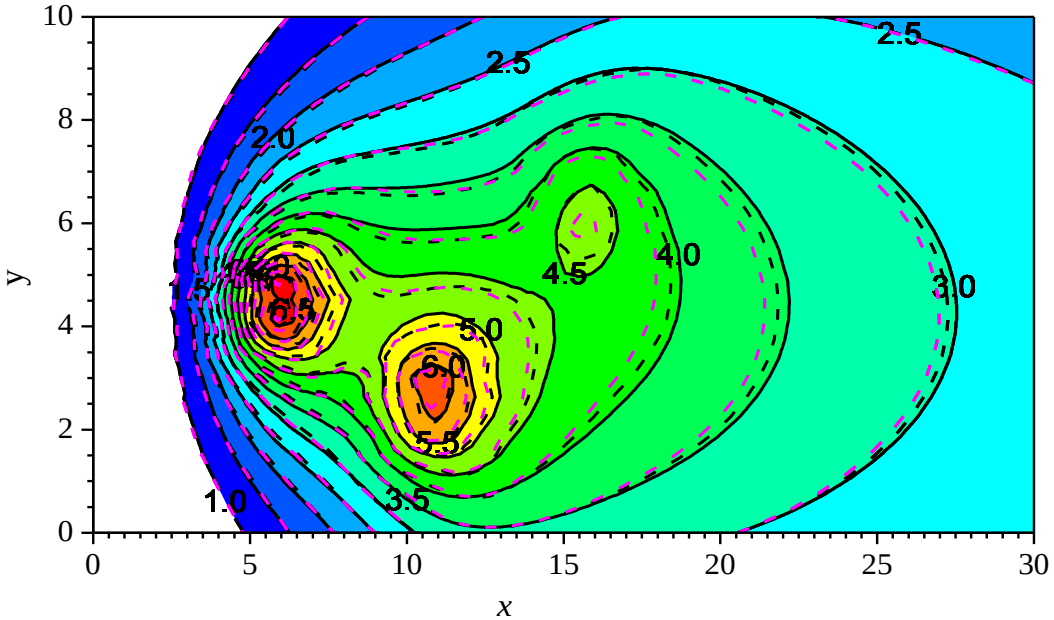


Figure 5.94: Spatial distribution of contaminant plume of Test case 1 with observation errors: exact solution-graded colour and solid black lines, Model 1 solution with no noise -black dashed lines, Model 1 solution with 5% observation error-pink dash lines.

Numerical simulations were carried out on this test case with no noise in the observation data but the parameters u and D were varied by ±5% of their prescribed values. The results of those simulations in predicting the pollution source strengths are summarized in Table 5.27. It is observed that the error in the dispersion coefficient has greater influence on the prediction of the pollution source strength than the error in the velocity. The average error for the computed source strength with dispersion errors (-5% and +5%) was 4.453% and 3.778% while for velocity errors (-5% and +5%) it was obtained as 2.283% and 1.47%, suggesting a higher influence of dispersion errors on the source strength than velocity errors. The mean error for the computed concentration when velocity errors are considered ranges from 0.0547% to 0.0794% while for dispersion errors the range is 0.23% to 0.236%, implying a good estimate of the concentration.

Table 5.27: Computed source strengths by Model 1 while accounting for parameter errors.

	Velocity		Dispersion	
	-5% of u	+5% of u	-5% of D	+5% of D
C_1'=20	18.858	20.045	18.773	20.124
C_2'=10	9.931	10.216	9.635	10.499
C_3'=4	4.018	4.081	3.857	4.229
Average relative Error (%)	**2.283**	**1.470**	**4.453**	**3.778**

5.4.3 Test case 3: Transient continuous point source located at the origin

This test case is a transient contaminant transport problem in 2-D for which the exact solution is given by Equation (5.20). The pollutant, which is continuously injected at a rate, W_v into the flow medium from a point source at the origin (0,0), is advected by uniform velocity in the x-direction and equally dispersed in the longitudinal and transverse directions. The problem is mathematically described by Equation (2.4) with the following initial and boundary conditions:

Initial conditions;

$$C = 0.0 \qquad x \geq -0.05 \quad y \geq 0 \text{ for } t = 0 \tag{5.25}$$

Boundary conditions;

$$\begin{aligned} &C = f(x,y,t) \quad \text{along } x = -0.05,\ y \geq 0 \\ &\frac{\partial C}{\partial y} = 0 \qquad x \geq -0.05 \text{ and } y = 0 \\ &C = f(x,y,t) \quad \text{along } x = 1 \text{ and } y \geq 0,\ x \geq -0.05 \text{ and } y = 1 \end{aligned} \tag{5.26}$$

In this work, the analytical solution for the transient case in Equation (5.20) with the Hantush well function is implemented using the series that were developed by Hunt, 1977. Thus, the Hantush well function is rewritten as

$$W(\Phi, z/\beta) = 2K_0\left(2\sqrt{\varpi}\right) - \sum_{nn=0}^{\infty} \frac{(-\Phi)^{nn}}{nn!} E_{nn+1}\left(\varpi/\Phi\right) \qquad (\varpi = z^2/4\beta^2) \tag{5.27}$$

Finally, Equation (5.20) is expressed as;

$$C(x,y,t) = \frac{C'W_v}{4\pi D} \exp\left(\frac{ux}{2D}\right) \times \left[2K_0\left(2\sqrt{\varpi}\right) - \sum_{nn=0}^{\infty} \frac{(-\Phi)^{nn}}{nn!} E_{nn+1}\left(\varpi/\Phi\right)\right]. \tag{5.28}$$

The inverse simulation is carried out in a rectangular domain [1.05×1] with the pollution source of unknown strength located at the origin, that is (x_s=0, y_s=0). Due to the influence of singularity around the source location, the GEM discretization is implemented in such a way that a non-uniform domain is adopted in the *x*-direction with element sizes of 0.1, 0.05, 0.1, 0.1, 0.1, 0.1, 0.1, 0.1, 0.1, 0.1, and 0.1. In the *y*-direction a uniform discretization of 0.1 is employed, thus, a total of 110 non-uniform rectangular elements are used for simulations. The parameters used for simulation are presented in Table 5.28, and a uniform time step of 0.05 is employed in all calculations. Figure 5.95 shows the computational domain with boundary conditions, the location of the contaminant and the location of the observation point.

Table 5.28: Transport parameters used in the simulation of Test case 3.

Pe	**D**	***u***	Δx	W_v	C'
0.1	1.0	1.0	0.1	1.0	10

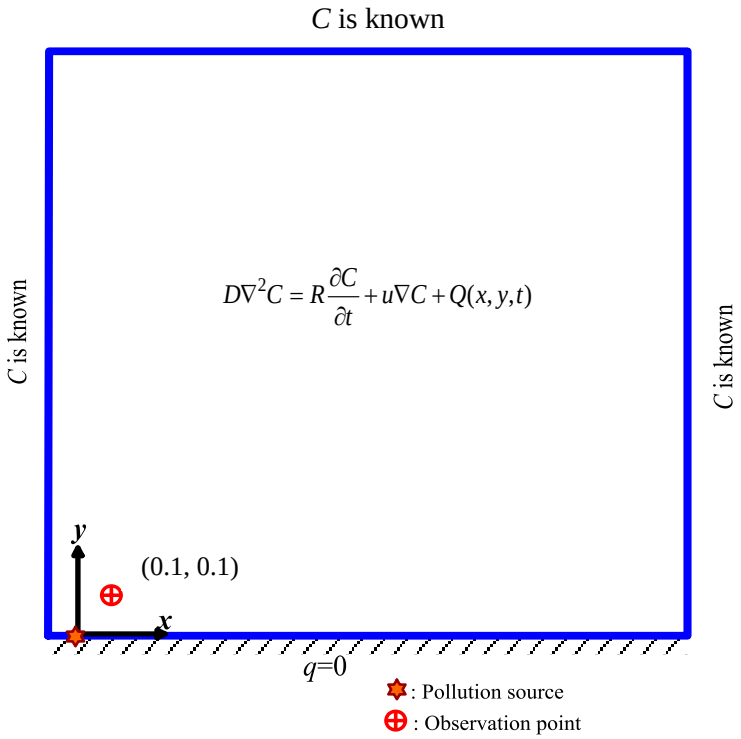


Figure 5.95: Computational domain of Test case 3 with a point source.

The parameters used for Model 2 simulation include $n_o = 20, p_o = 10, m_o = 41, q_o = 21, \alpha_{opt} = 1,$ and $\beta_{opt} = 41$. The number of decision variables in this case is equal to the number of unknown source strengths which is one times the number of time steps (20). Figure 5.96 shows the convergence of various runs, the minimized objective function was 7.571×10^{-4} after approximately 23000 simulations.

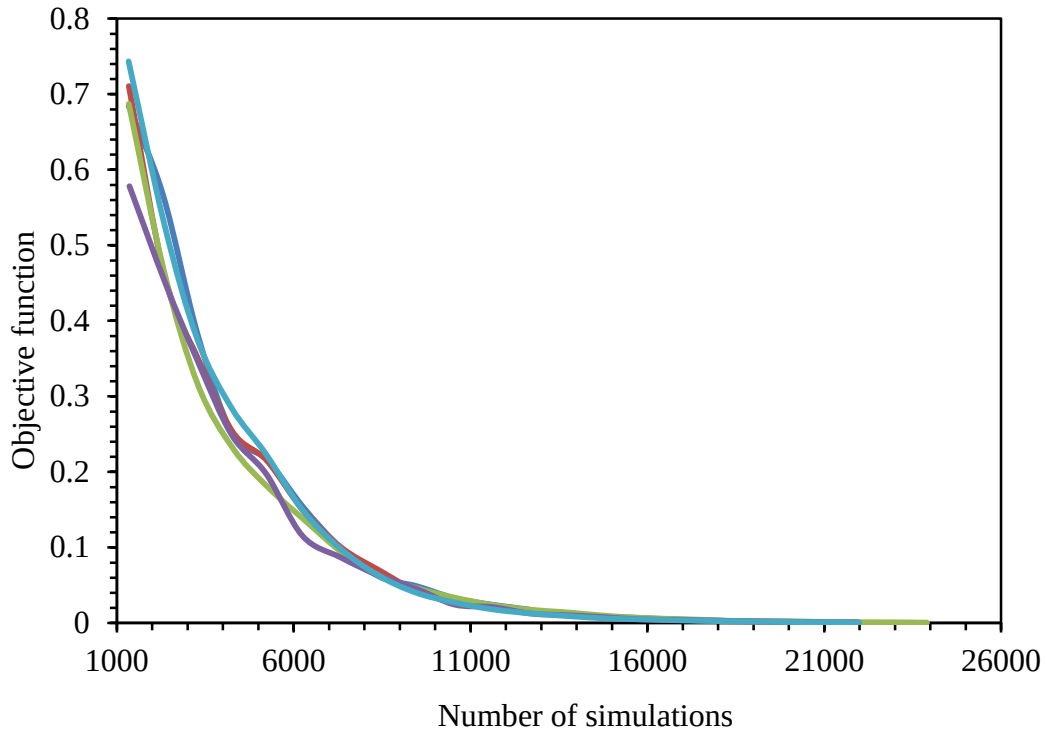


Figure 5. 96: A plot of the objective function versus the number of simulations of Test case 3 in Model 2.

Figure 5.97 shows the predicted pollution source strength throughout the simulation time by Model 1 and Model 2 when there is no noise in the observation data. It is observed that Model 1 gives a good prediction of the source strength compared to Model 2. The values of the regularization parameter used in the Model 1 simulations are obtained automatically by identifying the point of maximum curvature of the L-curve at each time step, and they were found to be in the range between 2.31×10^{-7} to 5.66×10^{-7}. Model 2 overestimates the source strength and it does not improve with time, except for the first time step.

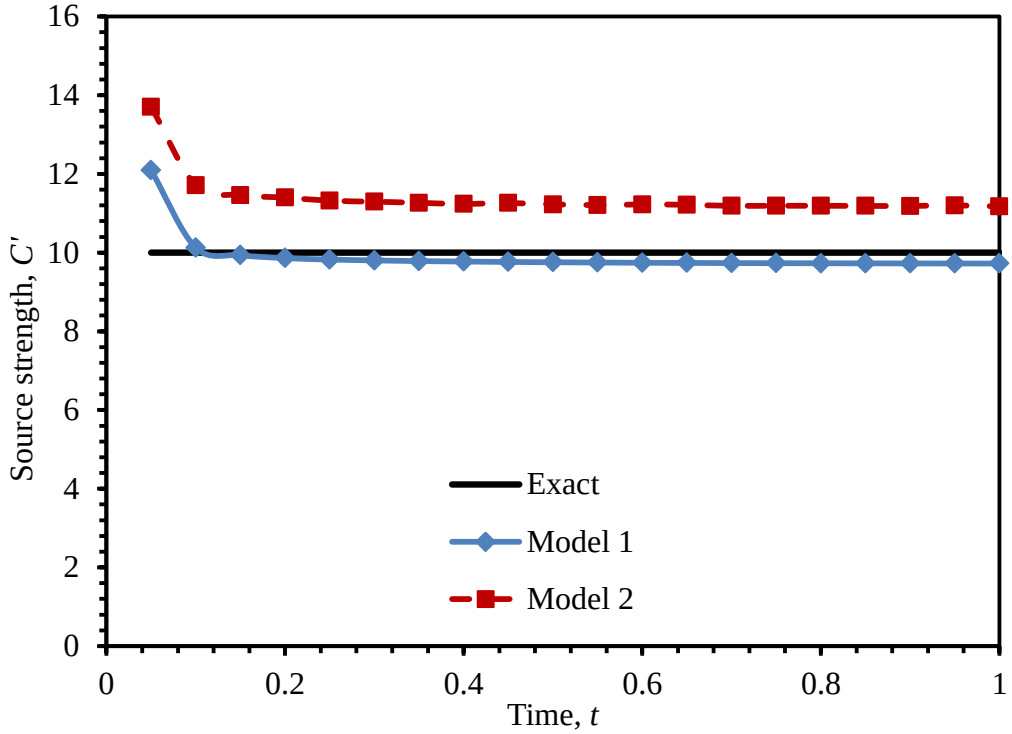


Figure 5.97: Model 1 and Model 2 computed source strength of Test Case 3 with point sources.

Figure 5.98 shows the temporal variation of the error for the computed pollution source strength relative to the exact source strength. It is revealed that except for the first time step, Model 2 has an average error of approximately 13%, while Model 1 has an error of less than 3%. The computation time for Model 1 was obtained as 6.0 seconds, while Model 2 as 1045.9 seconds. Thus, it is gathered that Model 1 achieves better estimates of the source strength, and is computationally efficient compared to Model 2 for this case.

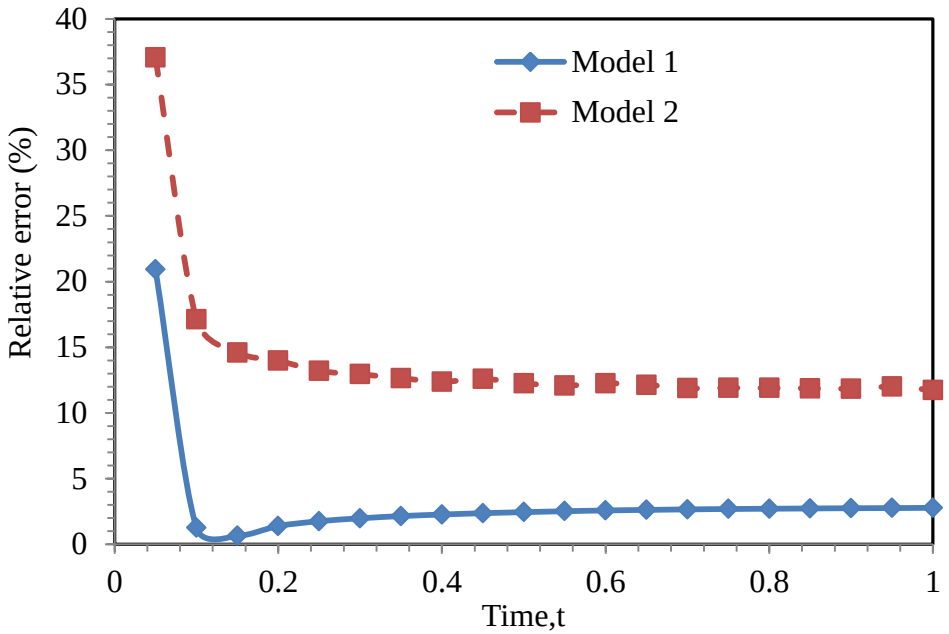


Figure 5.98: Temporal variation of the relative error of the computed source strength by Model 1 and 2 for test case 3.

Both Model 1 and Model 2 give a good prediction of the computed historical distribution of concentration as shown by the contour plots in Figures 5.99(a), (b), and (c) for time $t = 0.2$, $t = 0.5$, and $t = 1.0$ respectively. It is observed that as time increases from $t = 0.2$ to $t = 1.0$ the plume is advected and dispersed as it covers more area in the computation domain. An excellent prediction of the spatial contaminant concentration is observed at all times, this can be alluded to the fact that as time increases more observation data is made available for the inversion problem.

The mean error for the computed concentration by Model 1 and Model 2 relative to the exact solution is shown in Figure 5.100. It is observed that in both models the mean error reduces with time. However, Model 1 performs slightly better than Model 2.

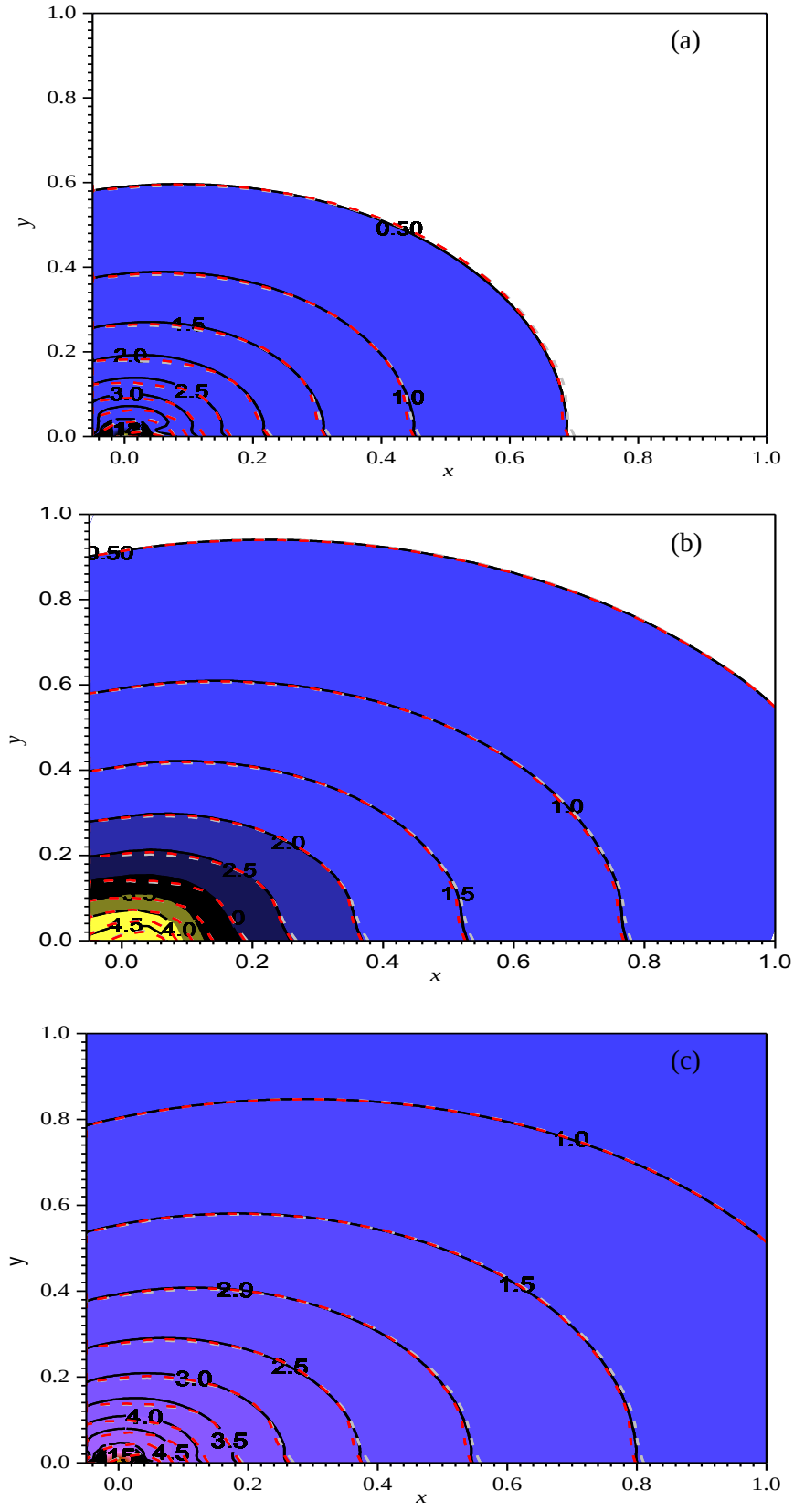


Figure 5.99: The exact concentration distribution is shown in graded colour, the computed solution of Model 1 in red dash line, and the computed Model 2 solution in grey dashed line (a) $t = 0.2$, (b) $t = 0.5$, and (c) $t = 1.0$.

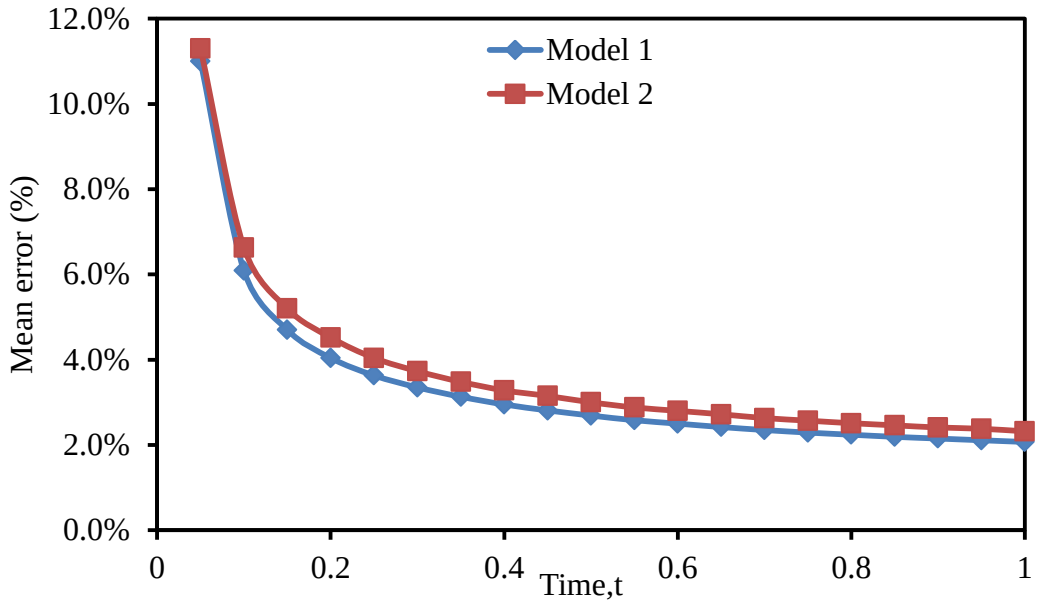


Figure 5.100: Temporal variation of the mean relative error of the computed concentration by Mode1 and 2 for test case 3.

To evaluate the influence of noise in observation data Model 1 is utilized. For simulations the data given in Table 5.28 is utilized and the observation data is perturbed randomly with noise levels of $\varepsilon = 1\%, \varepsilon = 3\%$ and $\varepsilon = 5\%$. Figure 5.101 shows the computed pollution source strength using Model 1 with noisy data. It is observed that the computed source strength with noise levels of $\varepsilon = 0\%$, and $\varepsilon = 1\%$ do not exhibit major oscillations. However, for $\varepsilon = 3\%$, and $\varepsilon = 5\%$ oscillates are exhibited about the true solution, with amplitudes increasing with increase in error magnitude.

The temporal variation of the relative error for the computed source strength for the various noise levels simulated is shown in Figure 5.102. From Figure 5.102 it is observed that the average relative error for the various noise levels increases with increase in the noise magnitude.

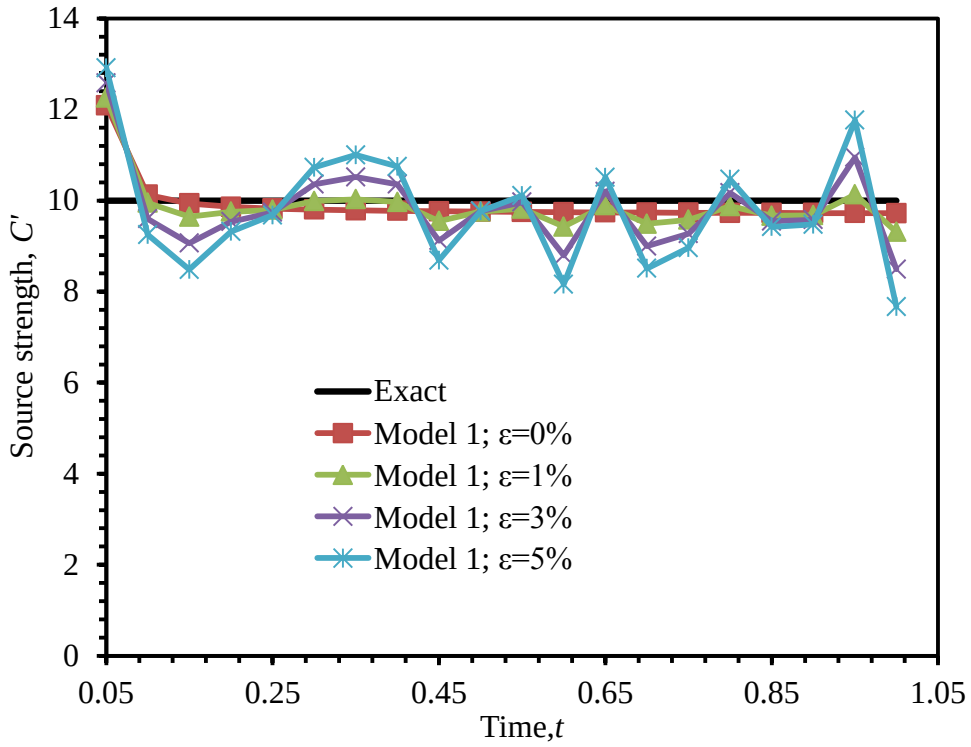


Figure 5.101: Model 1 computed source strength with time of Test case 3 using noisy observation data.

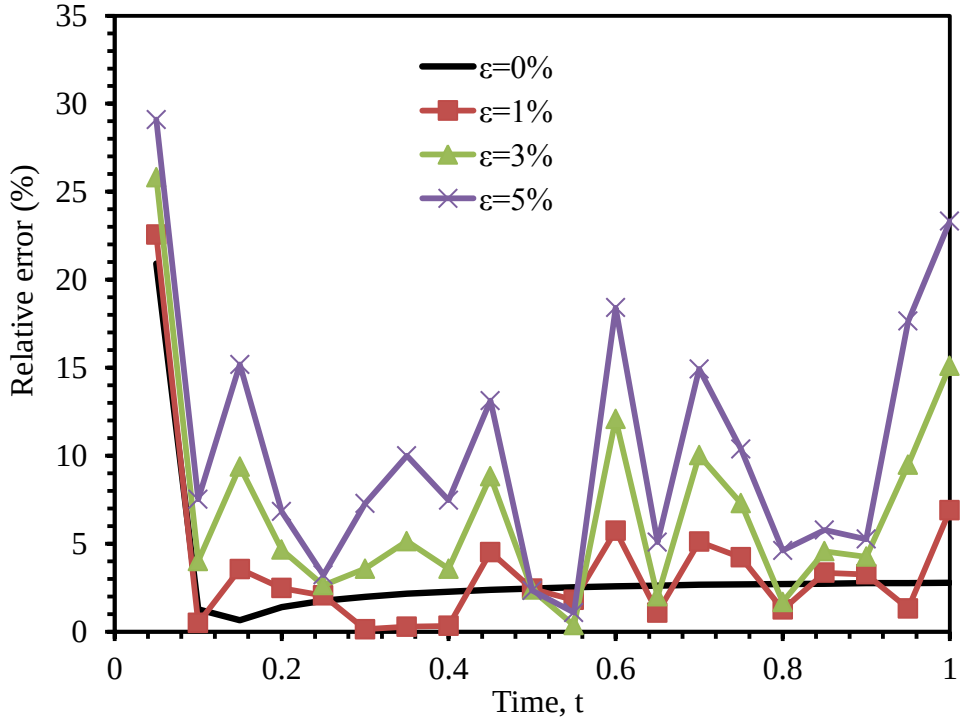


Figure 5.102: Temporal variation of the relative error of the computed source strength for test case 3.

The contour plot of the exact and the computed concentration distribution obtained by Model 1 with observation data with noise levels of $\varepsilon = 0\%$ and $\varepsilon = 5\%$ is given in Figure 5.103. It is observed that observation errors of up to 5% do not significantly influence the spatial concentration distribution. The mean relative error is calculated at each time step for noise levels $\varepsilon = 0\%$, $\varepsilon = 1\%$, $\varepsilon = 3\%$ and $\varepsilon = 5\%$, and the results are presented in Figure 5.104 which shows that the noise in the observed data has minimal influence on the calculated nodal concentrations, although as the noise level increases the mean error increases with oscillations.

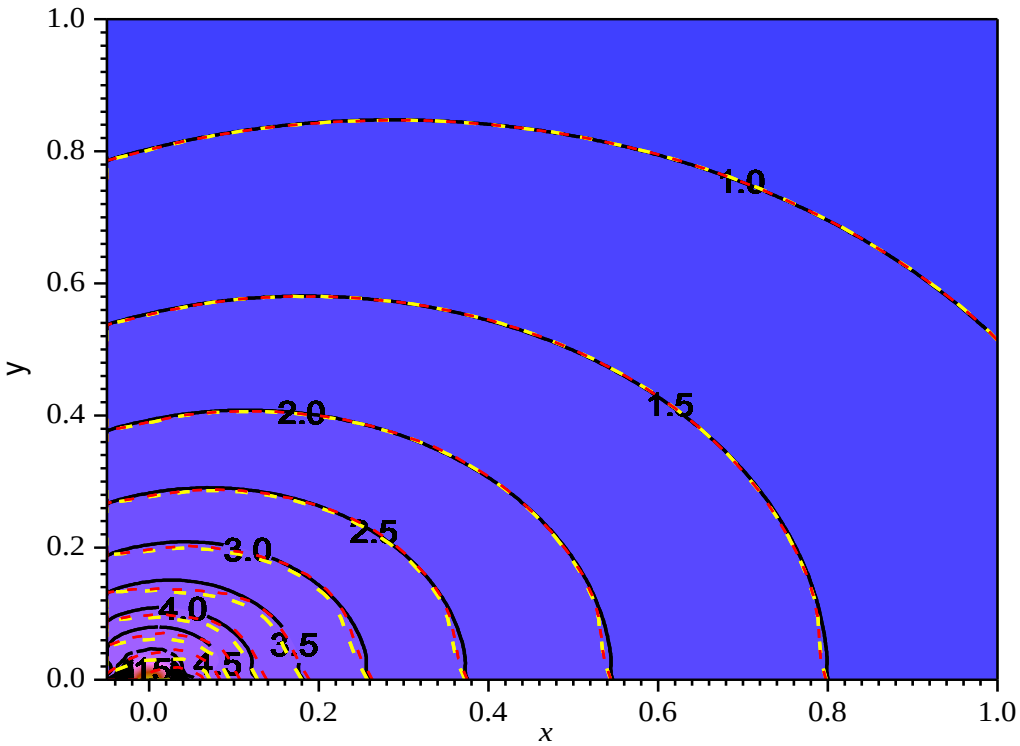


Figure 5.103: Model 1 computed concentration distribution at time, $t = 1$ of Test case 3. Graded colour shows the exact solution, the red dash line shows the error free solution, and the yellow dash line shows the solution for 5% error in the observation data.

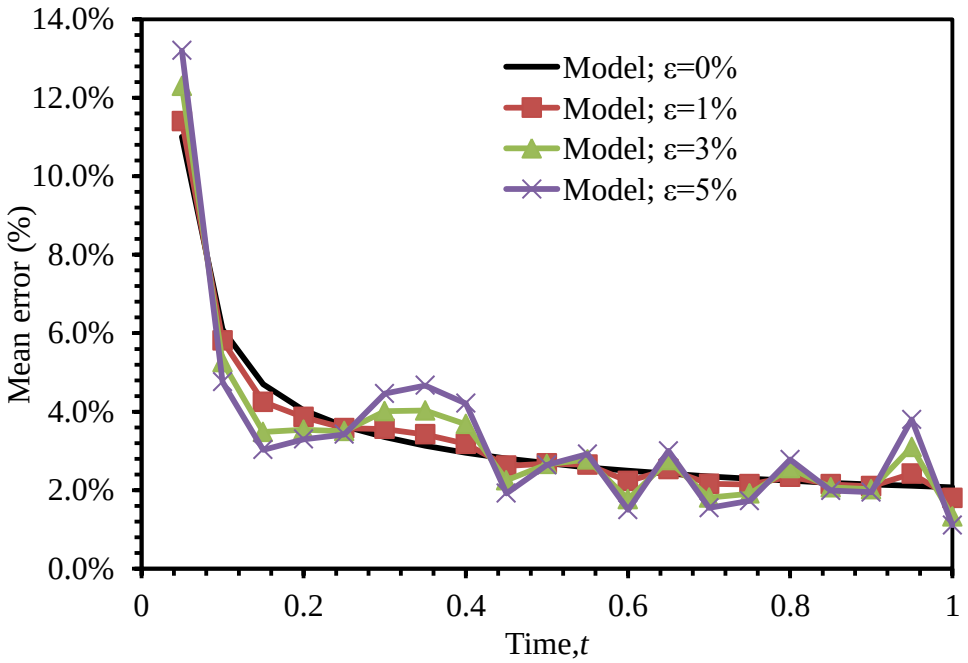


Figure 5.104: Temporal variation of the relative error of the computed concentration for test case 3.

5.5 Case study

To evaluate our proposed methodology, we consider an isotropic hypothetical aquifer system with dimensions of (1300 m × 800 m), using the problem considered in Mahar and Datta (2000) as illustrated in Figure 5.105. The aquifer consists of two active sources which are located at (250,250) and (250,550) and a pumping well located at (550,450). In the aquifer there is a network of eight observation wells (N_γ=8) represented as $\gamma_1, \gamma_2 \ldots \gamma_8$.

The north and south boundary conditions are no flow boundaries. The east and west boundary conditions are Dirichlet boundary conditions where the hydraulic head and concentration are known in the flow and the contaminant transport equations respectively. The hydraulic head varies linearly along the constant head boundaries while the concentration is assumed to be zero. The initial hydraulic head distribution is interpolated from the constant head boundaries, while the initial concentration is taken as zero in the whole computation domain.

The aquifer is discretized into elements of 100m × 100 m. The aquifer flow and contaminant transport parameter values are given in Table 5.29, while the pumping well rate and the source fluxes are given in Table 5.30 and Table 5.31, respectively. It should be noted that the source volume is considered not to significantly influence the hydraulic head, thus the source flux is the product of the concentration of the source and the volume rate of flux from the source of pollution.

Table 5.29: Flow and transport parameter values

Parameter	Parameter value
K_{xx} (m/month)	518.4
K_{yy} (m/month)	518.4
Porosity, η	0.25
Longitudinal dispersivity, α_L (m)	40
Transverse dispersivity, α_T (m)	40
Aquifer depth, b (m)	30.5
Δt (months)	3.0
S	0.002

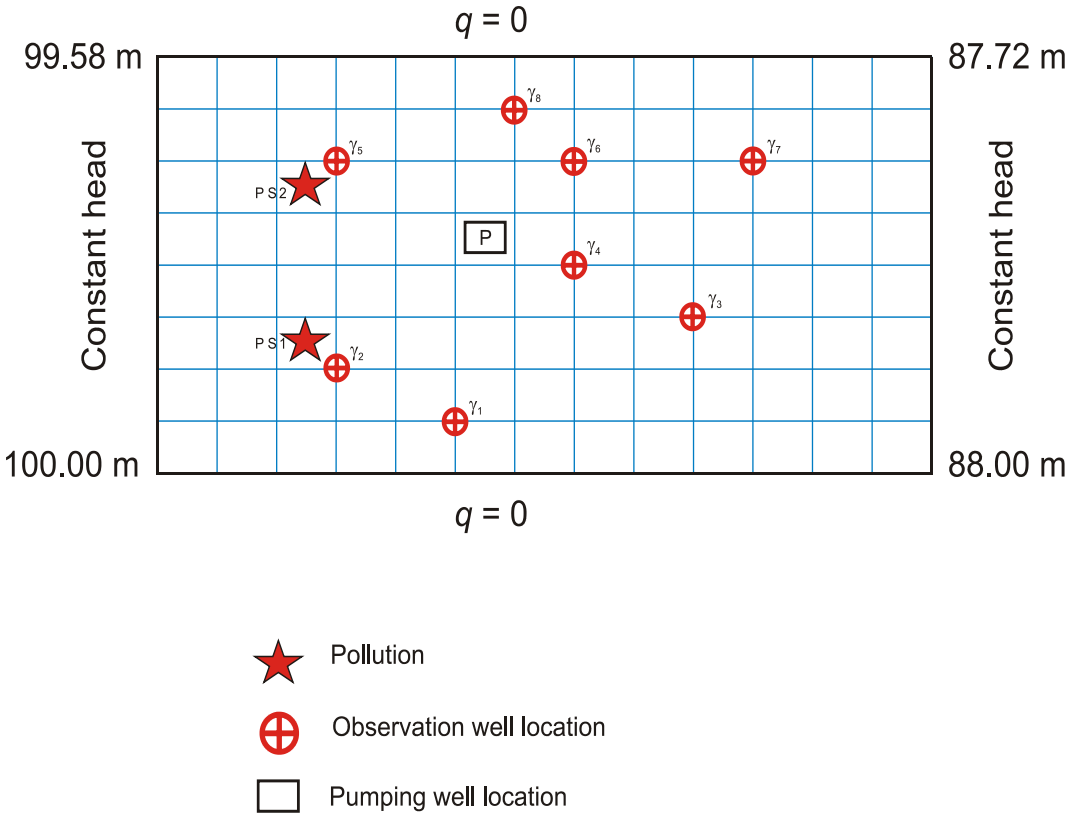


Figure 5. 105: Schematic representation of the aquifer.

Table 5.30: Pumping well rates

Time period	Pumping rate(m^3/month)
1	8190.72
2	4898.88
3	9823.68
4	4898.88
5	8190.72
6	9823.68
7	4898.88
8	8190.72
9	11430.72
10	6531.84
11	4898.88
12	9823.68
13	8190.72
14	4898.88
15	11430.72
16	6531.84
17	8190.72
18	4898.88
19	9823.68
20	6531.84

Table 5.31: Actual source fluxes for case study.

Time step	Source flux (g/s)	
	Source 1 (PS1)	Source 2 (PS2)
1	47.0	30.0
2	15.0	58.8
3	47.0	0.0
4	0.0	35.0

Simulation of measured concentrations

In order to obtain concentration measurements, the governing flow equation (Equation 2.1) and the contaminant transport equation (Equation 2.4) - restated here as Equation (5.29) and (5.30) respectively) - are solved by the direct GEM with the appropriate initial and boundary conditions.

$$\nabla \cdot (T \nabla h) = S \frac{\partial h}{\partial t} + Q_w \tag{5.29}$$

$$R \frac{\partial C}{\partial t} = \nabla \cdot (D \nabla C) - \mathbf{V}.\nabla C - \mu C - \frac{C' W_v}{b \eta} \tag{5.30}$$

This direct simulation computes the flow equation (5.29) to obtain the velocities required to transport the contaminant. The source fluxes given in Table 5.31 are used to compute the concentration distribution in the aquifer. The direct simulation results are provided as concentration contours in Figure 5.106 (a), (b), (c), and (d) for four time steps. Figure 5.106(a) shows the plume at 3 months, two distinct sources are observed to be active, and the pollutant is observed to be advected along the flow direction and with equal dispersion in the *x* and *y* directions. Figure 5.106(b) shows the plume at 12 months, source PS_2 is still active and this is the last pollution episode, the two sources have mixed and the plume is being advected and dispersed. Figure 5.106(c) shows the plume at 30 months, it is observed that there is no more release of the pollutant and the plume has been advected past the pumping well. Figure 5.106(d) shows the plume at the last time of 60 months, the plume has been advected and dispersed through the aquifer and much of the pollutant has left the aquifer. We utilise these concentration values for the inverse problem. There are eight observation wells as

shown in Figure 5.105, and the breakthrough curves for four of these wells are shown in Figure 5.107.

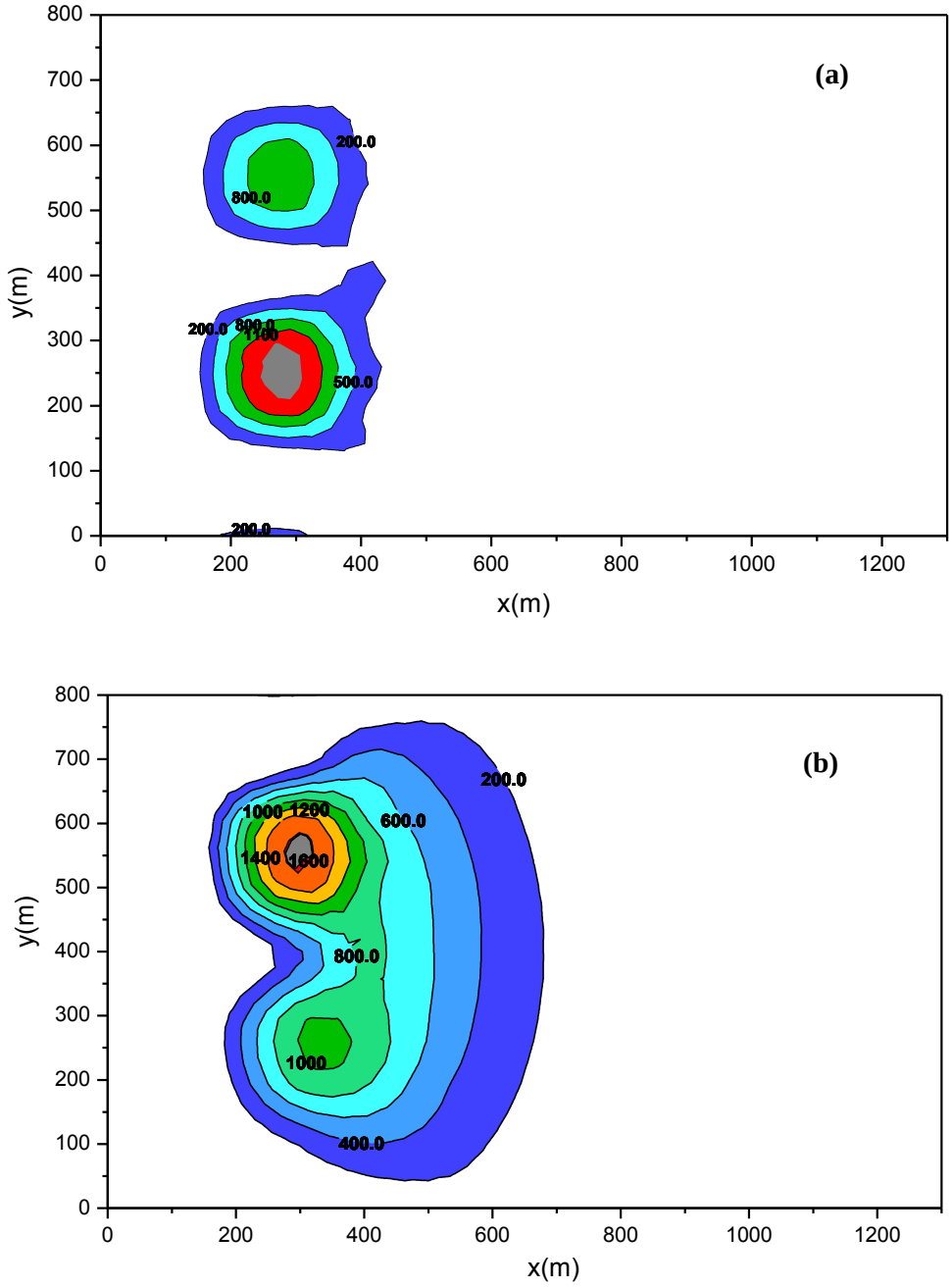


Figure 5.106: Concentration distribution contour in the aquifer at various time steps: (a) 3months (b) 12 months.

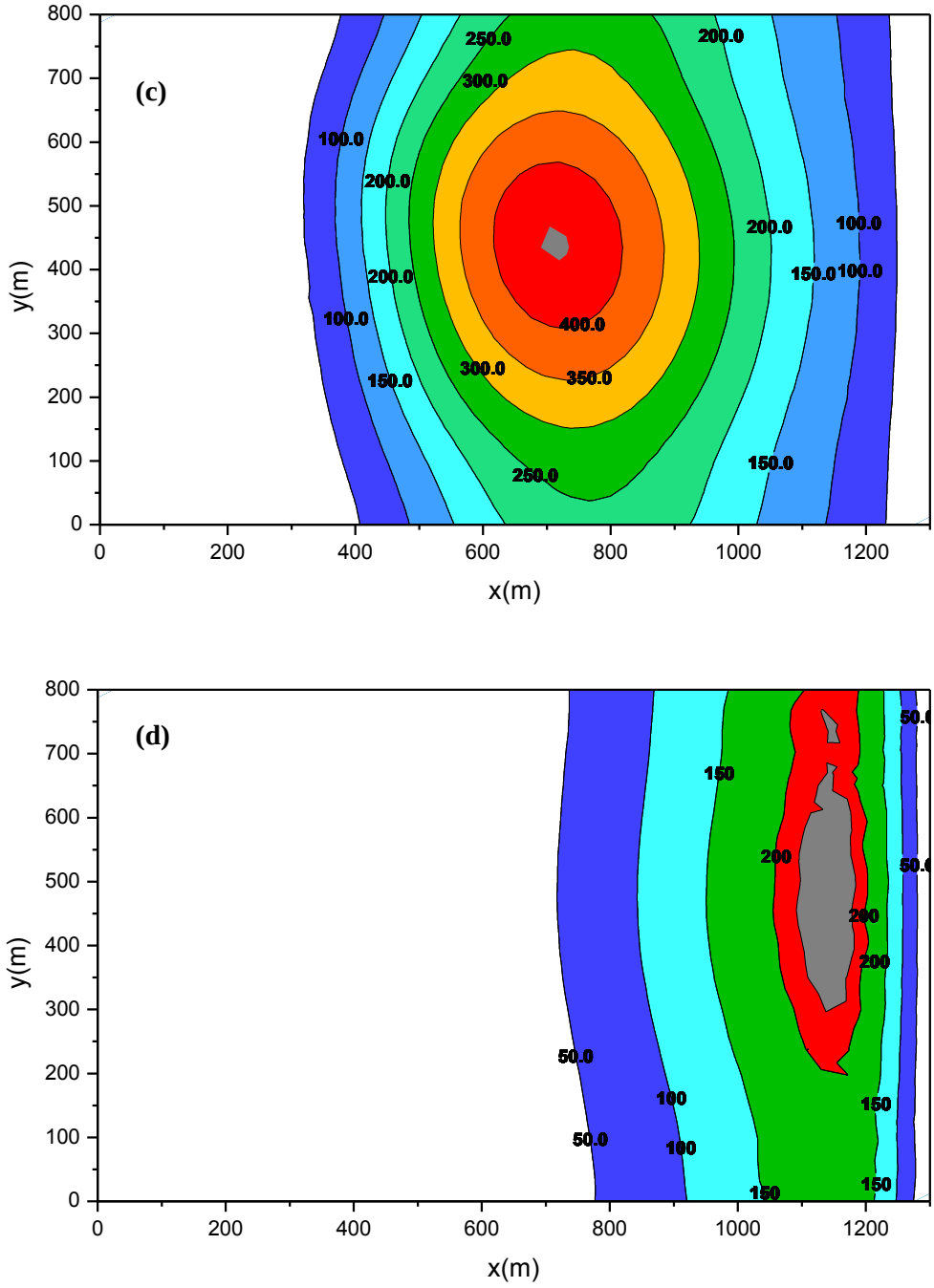


Figure 5.106(Continued): Concentration distribution contour in the aquifer at various time steps: (c) 30 months (d) 60 months.

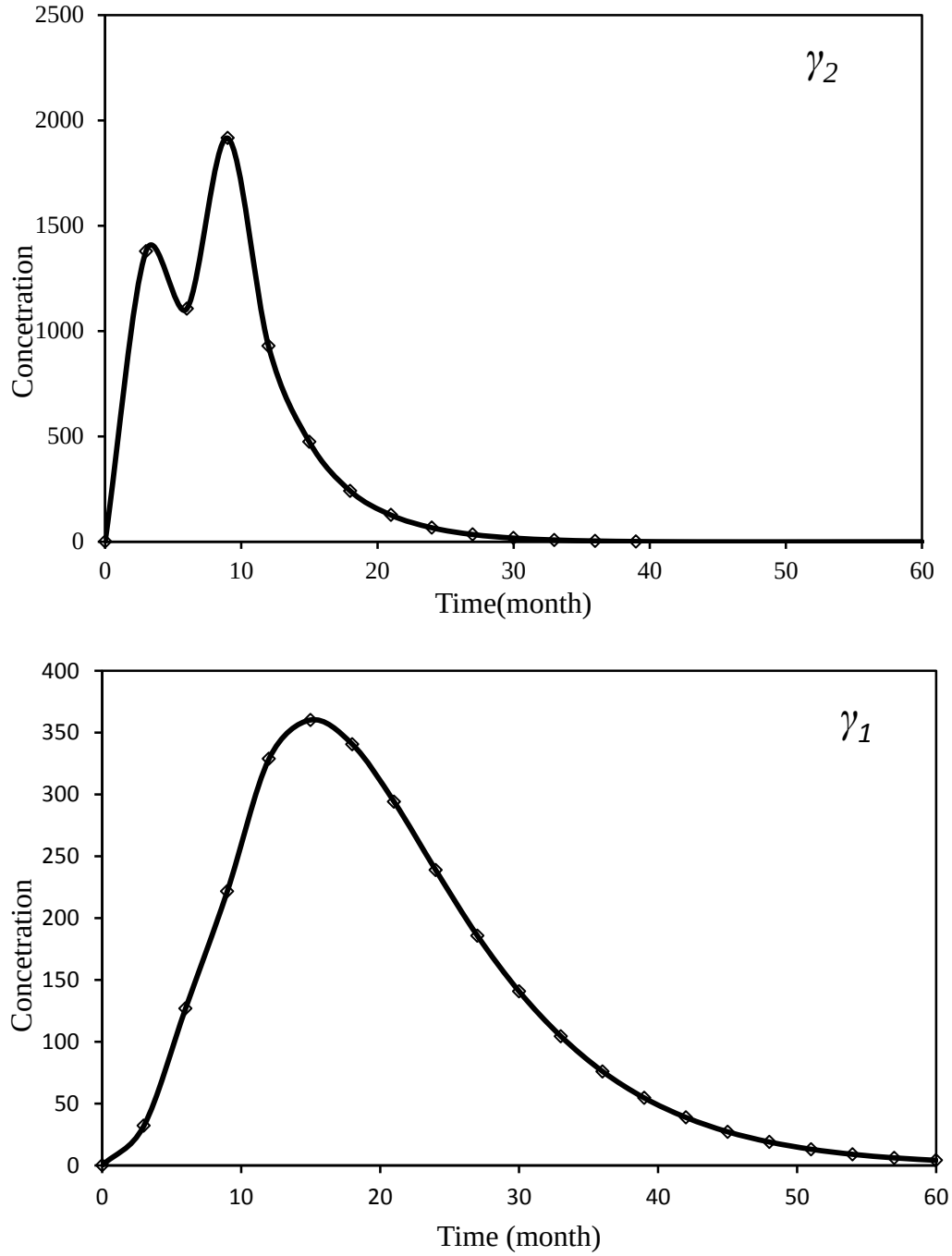
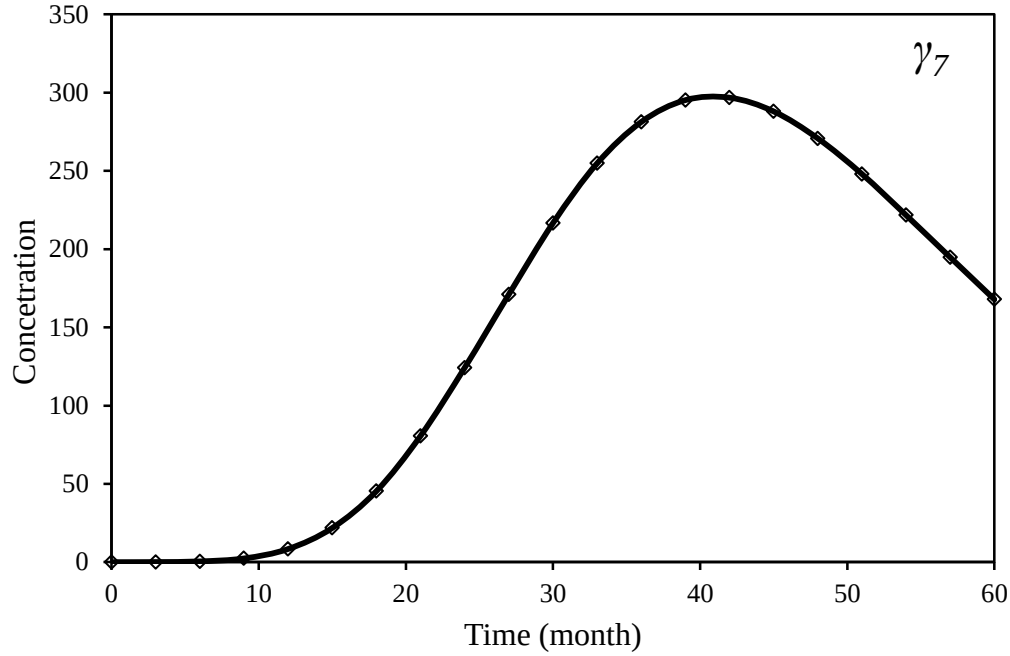


Figure 5.107: Breakthrough curves for observation points γ_2 and γ_1.



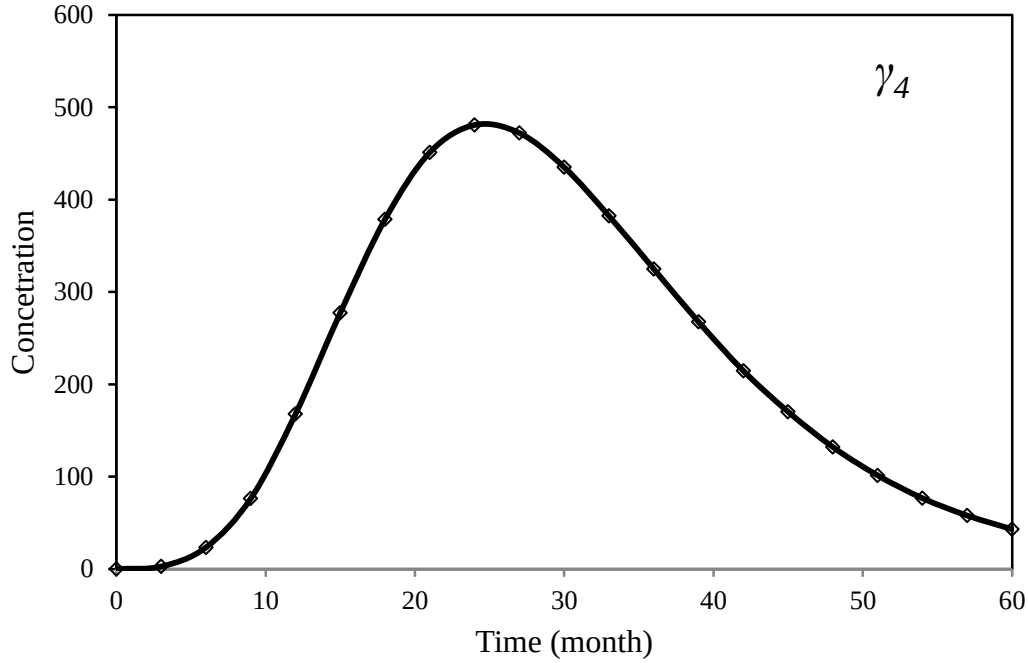


Figure 5.107(continued) Breakthrough curves for observation points γ_7 and γ_4.

5.5.1 Identification of source fluxes using data with measurement error

In this evaluation we utilize Model 1 and Model 2 to estimate the unknown source strengths for sources PS_1 and PS_2 represented as $C_1^{'}$ and $C_2^{'}$ respectively. To start with, we compare the performance of Model 1 and Model 2 using error free observation measurements. The values of the regularization parameter used in the Model 1 simulations were obtained automatically at each time step, and for this case study a value of 1.99×10^{-9} was obtained for all time steps. For Model 2, the simulation parameters were taken as; $n_o = 40, p_o = 10, m_o = 81, \beta_{opt} = 41, \alpha_{opt} = 1, q_o = 81$. The decision variables in this case were the two unknown strengths times the number of the computation time steps which were twenty. The obtained minimized objective function was 0.235 from 36703 simulations.

Table 5.32 shows the computed pollution source fluxes by Model 1 and Model 2 using noise free observation data. It is realised that using noise free observation data results in excellent estimates of the source fluxes by Model 1 with an average error of 0.58%, while Model 2 estimates have an average error of 13.00%. The computation time required for Model 2 was 2043.1 seconds while Model 1 was 60.24 seconds.

Table 5.32: Case study computed source fluxes by Model 1 and Model 2.

Time step	Source location	Actual value	Computed source flux(g/s)	
			Model 1	**Model 2**
1	PS1	47.0	46.99	49.95
	PS2	30.0	30.01	34.96
2	PS1	15.0	15.07	19.93
	PS2	58.8	59.57	59.97
3	PS1	47.0	46.80	49.91
	PS2	0.0	0.09	0
4	PS1	0.0	0.08	0
	PS2	35.0	35.43	39.95
Average relative error (%)			**0.5808**	**13.00**

To evaluate the influence of measurement errors, the additional data obtained from internal observation wells was randomly perturbed with noise levels of $\varepsilon = 1\%, \varepsilon = 3\%$ and $\varepsilon = 5\%$ using Equation 3.27. The computed source fluxes using Model 1 with randomly perturbed observed data are given in Table 5.33, while the corresponding relative error of each estimated source flux is illustrated in Figure 5.108. Detailed solutions including all time steps are given in Appendix A. From Table 5.33 it is observed that the computed source fluxes are excellent, even in the presence of observation errors. The average relative error for the computed source strengths is seen to increase from 0.58% to 3.32% as observation errors increase from 0% to 5%. From Figure 5.108, it is seen that the relative error for the computed source strength for each source at every time step increases with increase in observation errors, as previously observed.

Table 5.33: Model 1 computed source fluxes using observation data with random error.

Time step	Source location	Actual value	Computed source flux (g/s)			
			$\varepsilon = 0\%$	$\varepsilon = 1\%$	$\varepsilon = 3\%$	$\varepsilon = 5\%$
1	PS1	47.0	46.99	47.34	48.11	48.84
	PS2	30.0	30.01	29.86	29.56	29.27
2	PS1	15.0	15.07	14.76	14.14	13.52
	PS2	58.8	59.57	59.61	59.65	59.72
3	PS1	47.0	46.80	46.80	48.80	46.80
	PS2	0.0	0.09	0.07	0.04	0.00
4	PS1	0.0	0.08	0.09	0.13	0.16
	PS2	35.0	35.43	35.47	35.53	35.60
Average relative Error (%)			**0.5808**	**0.9893**	**2.1579**	**3.3199**

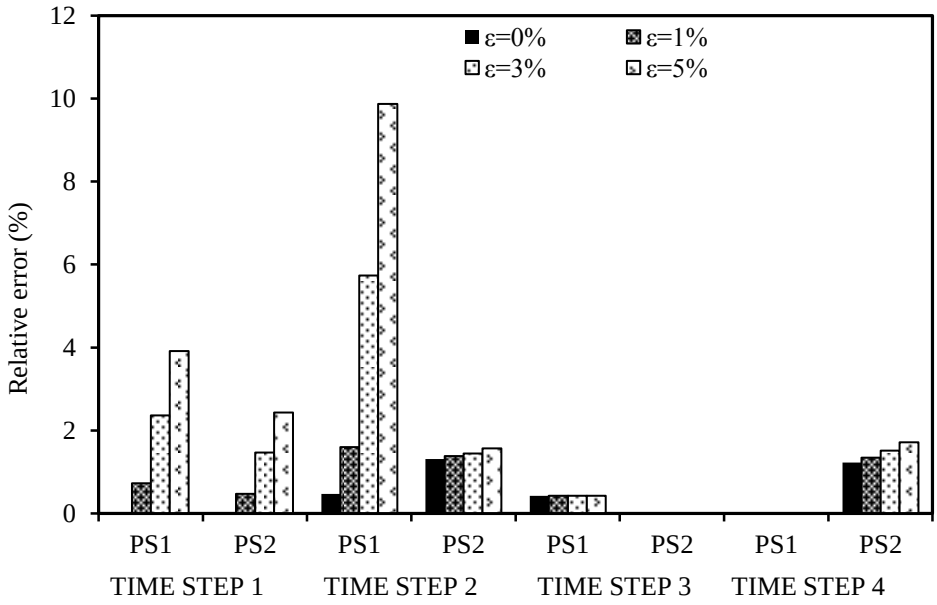


Figure 5.108: Relative error of computed source fluxes at different time steps.

Figure 5.109 shows the reconstructed concentration distribution plotted for 12 months and 30 months for observation data with errors of $\varepsilon = 0\%$, and $\varepsilon = 5\%$. It is observed that observation errors do not significantly influence the computed concentration distribution. The mean deviation for the computed nodal concentration (Figure 5.110) is found to be under 0.03% for all cases, which implies excellent recovery of the concentration. Generally, it is observed that Model 1 estimates the source fluxes and the spatial concentration accurately.

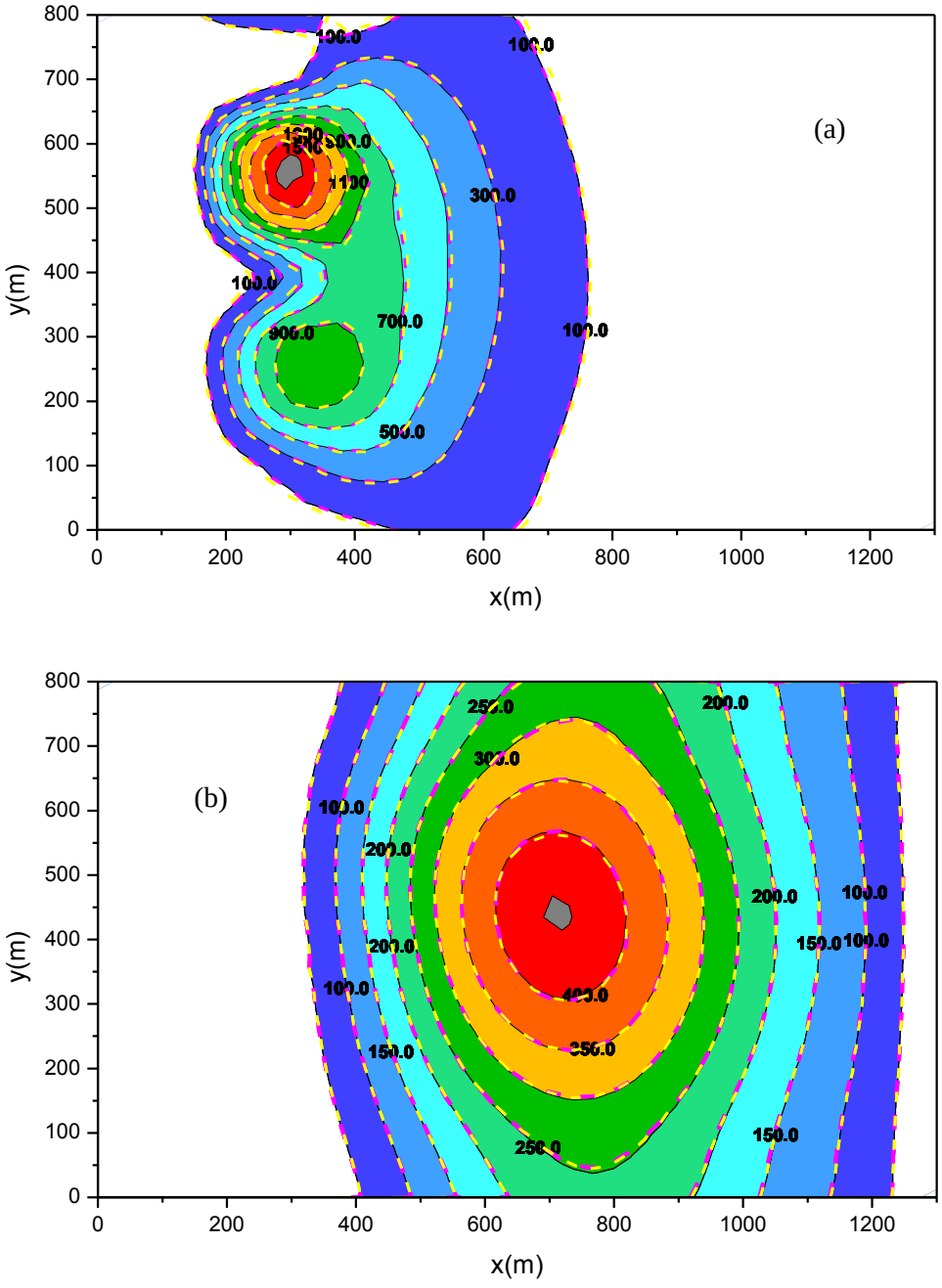


Figure 5.109: Concentration distribution, graded colour with black continuous line shows the direct solution, pink line shows the computed concentration with $\boldsymbol{\varepsilon = 0}$%, and yellow line shows the concentration distribution with $\boldsymbol{\varepsilon = 5}$% (a) 12 months (b) 30 months.

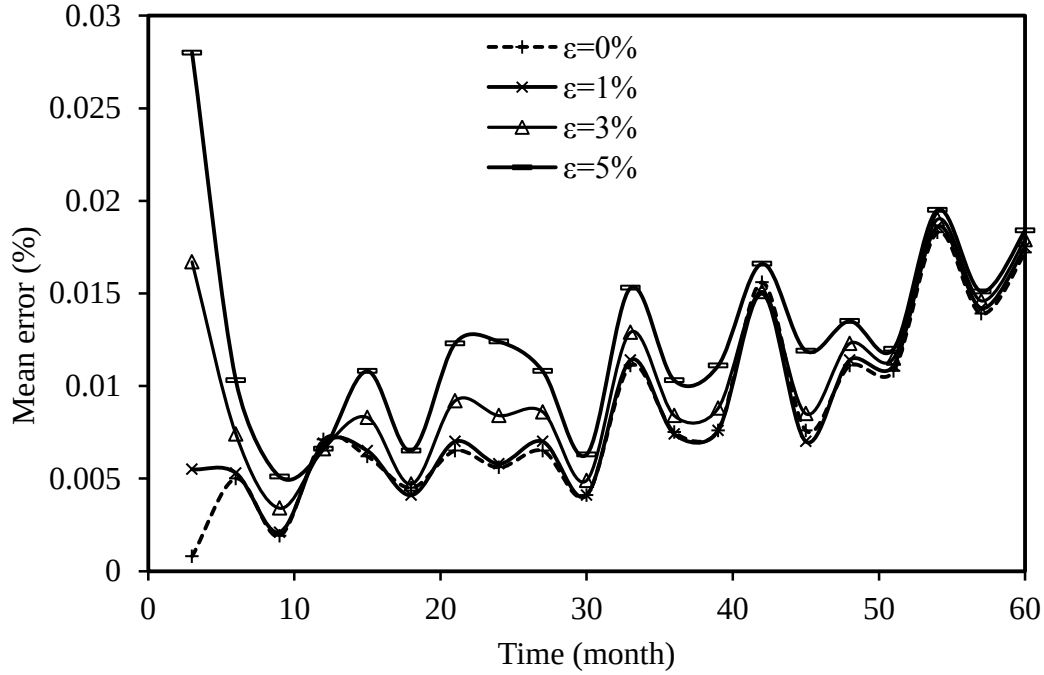


Figure 5.110: Temporal variation of the mean error for the concentration distribution.

5.5.2 Identification of source fluxes using data with parameter error

In order to evaluate the influence of parameter errors, the velocity was simulated with +5% errors such that the velocity in the *x* and *y* directions were represented as $u = u + 5\%u$ and $v = v + 5\%v$ respectively, while the dispersion coefficient was represented as $D = D + 5\%D$. The computed source fluxes while accounting for parameter errors are given in Table 5.34. The average error relative to the exact source flux is 1.6608 %, and 2.8605 % when considering velocity and dispersion errors respectively. It is observed that dispersion errors have a higher influence on the recovery of the source strength compared to velocity errors. Figure 5.111 shows the mean deviation for the computed concentration with velocity and dispersion errors which is less than 0.1% in both cases, implying a good estimate. It is also observed that the mean deviation with velocity errors increases with time while the mean deviation with dispersion errors tends to decrease with time.

Table 5.34: Model 1 computed source fluxes considering parameter errors.

Time step	Source location	Actual value	Computed source flux(g/s)	
			Velocity, $u = u + 5\%u$ and $v = v + 5\%v$)	Dispersion, $D = D + 5\%D$
1	P1	47.0	47.07	48.11
	PS2	30.0	30.05	30.74
2	PS1	15.0	15.51	15.53
	PS2	58.8	59.95	61.11
3	PS1	47.0	47.42	47.84
	PS2	0.0	0.88	0.17
4	PS1	0.0	0.76	0.2
	PS2	35.0	36.19	36.08
Average relative error (%)			**1.6608**	**2.8605**

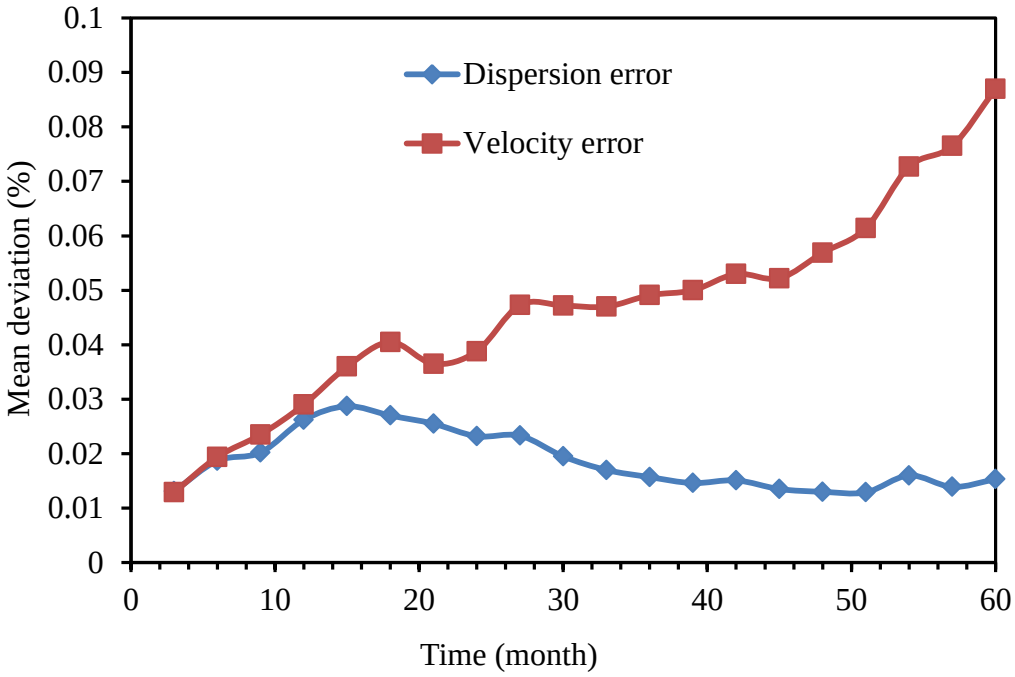


Figure 5.111: Temporal variation of the mean deviation for the concentration distribution computed with velocity and dispersion errors.

5.5.3 Identification of source fluxes considering multiple potential sources

In this simulation, the number of potential source locations was assumed higher than the actual source locations. Three potential sources PS_1, PS_2, and PS_3 were considered, sources PS_1 and PS_2 are active and their source strengths are given in

Table 5.31, while PS_3 is a dummy source which is located at (250,350) in the aquifer. The simulations were carried out using error free observation data, $\varepsilon = 0\%$ and observation data with a noise level of $\varepsilon = 5\%$. Table 5.35 shows the computed pollution source strengths, which are excellently estimated when concentration measurements from the direct solution with no observation error ($\varepsilon = 0\%$)are utilized. The computed source fluxes with $\varepsilon = 5\%$ observation errors have higher relative errors of 2.924% compared to those computed with no noise ($\varepsilon = 0\%$) which were obtained as 0.5%. It is observed that Model 1 estimates the dummy source (PS_3) correctly with negligible source fluxes when simulated concentration data with no noise is utilized. It can therefore be deduced that observation errors will inevitably affect the recovery of inactive sources.

Table 5.35: Model 1 computed source fluxes considering multiple potential sources.

Time step	Source location	Actual value	Computed source flux(g/s)	
			$\varepsilon = 0\%$	$\varepsilon = 5\%$
1	PS_1	47.0	46.99	48.42
	PS_2	30.0	30.01	29.26
	PS_3	0.0	0.24	4.85
2	PS_1	15.0	14.99	14.25
	PS_2	58.8	59.57	59.61
	PS_3	0.0	0.51	1.20
3	PS_1	47.0	46.84	48.26
	PS_2	0.0	0.08	0.09
	PS_3	0.0	0.20	16.98
4	PS_1	0.0	0.03	3.17
	PS_2	35.0	35.43	36.05
	PS_3	0.0	0.75	10.03
Average relative error (%)			**0.5000**	**2.9244**

5.5.4 The influence of time discretization on identification of source fluxes

Time discretization plays a dual role as discussed on section 5.2, Test case 1. First, it determines the sampling frequency for the inverse problem and secondly it determines the stability of the numerical scheme. In the previous simulations of this case study the computation time was taken as 3 months. In this scenario, simulations are carried out using a finer time discretization of $\Delta t = 0.25$ months. Table 5.36 shows the computed pollution source fluxes when a time discretization of $\Delta t = 0.25$ is utilized. The computed source fluxes are averaged for the finer time step of $\Delta t = 0.25$ and presented for 3 months. From Table 5.36, the computed source fluxes are excellent, and the relative error of the source fluxes increases with increase in observation error. It should be noted that source PS_1 at time step 2 exhibits a unique trend compared to all sources and time steps, thus its relative error has not been averaged. From Figure 5.112 it is observed that the relative error for the computed source fluxes for Source PS_1 at time step 2 decreases with increase in observation error, contrary to all other time steps. However, it should be noted that the influence of a finer time discretization for this case study is insignificant.

Table 5.36: Model 1 computed source fluxes using time discretization of Δt=0.25.

Time step	Source location	Actual value	Computed source flux (g/s)			
			$\varepsilon = 0\%$,	$\varepsilon = 1\%$,	$\varepsilon = 3\%$,	ε= 5%,
1	PS_1	47.0	46.72	46.53	46.15	45.77
	PS_2	30.0	29.63	29.62	29.60	29.58
2	PS_1	15.0	14.07	14.24	14.59	14.93
	PS_2	58.8	56.58	56.59	56.59	56.59
3	PS_1	47.0	48.55	48.55	48.55	48.55
	PS_2	0.0	1.84	1.84	1.84	1.84
4	PS_1	0.0	1.03	1.04	1.04	1.04
	PS_2	35.0	35.32	35.33	35.33	35.33
Average relative error* (%)			**1.6368**	**1.7120**	**1.8582**	**2.0035**

*Average relative error for active sources except source PS_1 at time step 2.

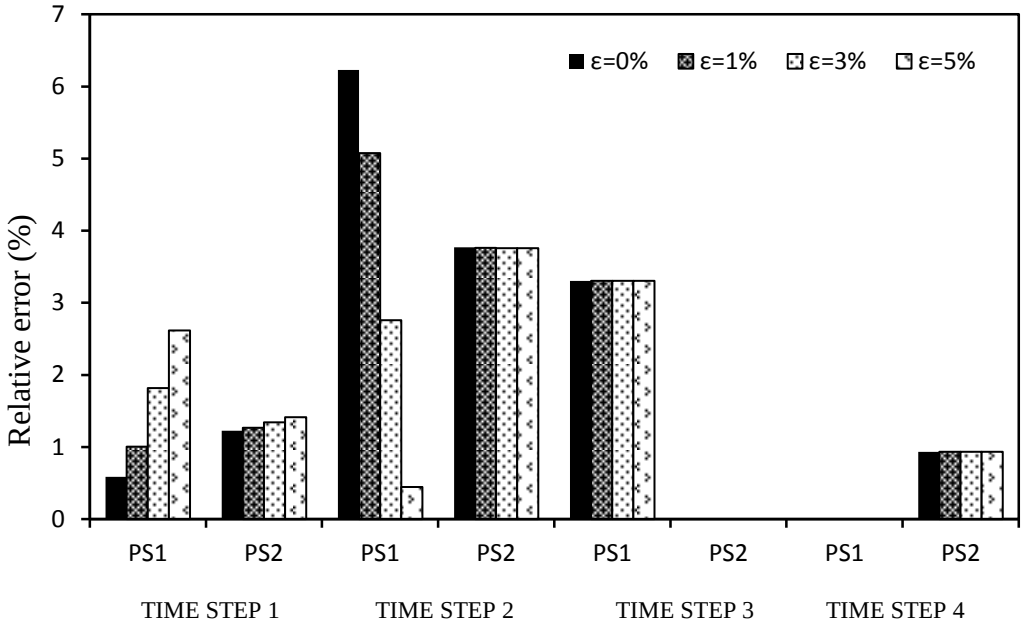


Figure 5.112: Relative error of computed source fluxes at different time steps using time discretization $\Delta \boldsymbol{t} = \mathbf{0.25}$.

6 CONCLUSIONS & RECOMMENDATIONS

Inverse modelling of groundwater contaminant transport has received much attention in the last few decades. The inverse contaminant transport problem entails identification and characterization of known or unknown pollution sources as well as the concentration for the resultant plume. Of importance are the methods used to tackle the ill-posed nature of this inverse problem. Thus, the development of methods that best solve inverse problems is of major interest to researchers.

Various techniques for the solution of the inverse contaminant problem have been reviewed in this work. It is observed that typically a numerical technique or an analytical technique is used in conjunction with an optimization method, or a stochastic, or even a regularization technique for the solution of the inverse problem. The numerical technique is applied for the solution of the partial differential equations that govern the transport of contaminants, while the optimization for example is used to guide the search in obtaining the source strength or the location of the source.

The objective of this research project was to develop a numerical formulation based on the Green element method for inverse groundwater contaminant transport problems. A hypothesis was raised that it is possible to develop an inverse formulation for the Green element method in conjunction with a regularization methodology and an optimization technique, and in the event that this is developed, it was the objective of the study to test various cases on the performance of the methodologies.

In this work, two methodologies have been developed. The first method consists of inverse GEM, of which the over-determined ill-conditioned discrete equations arising from solving an inverse problem are decomposed with the SVD and solved by the least square with Tikhonov regularization (Model 1). The second method utilizes the direct GEM and the SCE optimization method (Model 2). An

assessment on the performance of these methodologies on a number of contaminant transport problems for which analytical solutions are available as well as those that have appeared in literature is conducted. From the test cases that were used to demonstrate the potential of our methodologies the following conclusions have been deduced;

(i) The prediction capability of the source strength by both Model 1 and 2 is enhanced by having observation points located in close proximity of the source locations.

(ii) The amount of observation data available for inversion does influence the recovery of the source strength.

(iii) Spatial discretization of GEM does influence the inverse solutions; a relatively coarse discretization gives good estimates.

(iv) The Model 1 and Model 2 prediction of the source strength is generally better with more dispersion dominant transport than with the advection dominant one; for transient transport, oscillations are observed in the numerical solution at small times but they die out at later times.

(v) The two-fold influence of the Courant number *Cr* on the Model 1 solutions, namely numerical stability and frequency of available sampling data, makes it difficult to determine which influence will be dominant in any particular transport case. However, small values of *Cr* in the GEM simulations generally produce oscillatory solutions at early simulation times when concentration information are not available at observation points, but give accurate solutions at later times when they are available frequently at those points. The oscillations are more pronounced in the solutions for advection-dominant transport than for dispersion-dominant one.

(vi) For the simulated noise levels in the data at observation points, their influence on the recovery of the source strength is significant and, as expected, the influence on the inverse solutions increases with increased noise in the data.

(vii) The prediction of the concentration as the source strength is better handled by both Model 1 and Model 2 than the flux.

(viii) Errors in observation measurements have greater influence on the recovery of the source strength than on the historical concentration distribution.

(ix) For instantaneous sources, errors in the velocity and the dispersion coefficient do not have significant influence on the source strength recovery but the former causes a shift in historical concentration distribution while the latter causes a more smeared distribution with lower peak.

(x) In general, Model 1 and Model 2 perform fairly equally, however Model 2 is computationally expensive. It is worth mentioning that the Shuffled Complex evolutionary approach (Model 2) does many evaluations of the fitness function, which is computationally very expensive as it requires repeated solution of the simulation model. Again, the computation time required by this evolutionary approach increases exponentially with the increase in the number of decision variables. Ways to improve the computational efficiency of the methodology are highly recommended.

(xi) In this work, 1D and 2D groundwater contaminant problems have been extensively evaluated, future work on the application of the proposed methodology to 3D aquifer systems is highly recommended.

(xii) This Thesis has presented a novel application of GEM to inverse groundwater contaminant problems, future work to compare other numerical methods for example FEM, FDM, FVM available in the literature in terms of computational time, accuracy, stability and convergence of the inverse solutions is recommended.

REFERENCES

Agyei, E and Hatfield, K. (2006) Enhancing gradient-based parameter estimation with an evolutionary approach, *Journal of Hydrology*, Vol 316, pp. 266–80.

Ajami, K N, Gupta, H V, Wagener, T and Soroshian, S. (2004) Calibration of a semi-distributed model for streamflow estimation along a river system, *Journal of Hydrology*, Vol 298, pp. 112-135.

Alapati, S and Kabala, Z J. (2000) Recovering the release history of a groundwater contaminant using a non-linear least squares method, *Hydrological processes*, Vol 14, pp. 1003-1016.

Andersses, R S and Bloomfield P. (1974) Numerical differentiation procedures for non exact data, *Numerical mathematics*, Vol 22, pp.157-182.

Aral, M M, Guan, J and Maslia, M L. (2001) Identification of contaminant source location and release history in aquifers, *Journal of Hydrologic Engineering*,Vol. 6, no 3, pp. 225-234.

Atmadja, J and Bagtzoglou, A C. (2001) State of the Art Report on Mathematical Methods for Groundwater Pollution Source Identification, *Environmental Forensics*, Vol. 2, pp. 205-214.

Atmadja, J. (2001) The marching-jury backward beam equation method and its application to backtracking non-reactive plumes in ground-water, *Ph.D. Dissertation, Columbia University*, New York,121 pp.

Atmadja, J and Bagtzoglou A C. (2000) Groundwater Pollution Source Identification Using the Backward Beam Equation Method in Bentley L. (eds). *Computational Methods for Subsurface Flow and Transport*, Balkema Publishers, Rotterdam, Netherlands, pp.397-404.

Atmadja, J and Bagtzoglou, A C. (2001) Pollution Source Identification in Heterogeneous Porous Media, *Water Resources Research*, Vol.37, pp. 2113-2125.

Ayvaz, M T. (2007) Simultaneous determination of aquifer parameters and zone structures with fuzzy c-means clustering and meta-heuristic harmony search algorithm, *Advances in Water Resources*, vol. 30, pp. 2326–2338.

Ayvaz, M T. (2010) A linked simulation–optimization model for solving the unknown groundwater pollution source identification problems, *Journal of Contaminant Hydrology*, Vol. 117, pp. 46–59.

Backus, G and Gilbert, F. (1970) Uniqueness in the inversion of inaccurate gross Earth data, *Philos. Trans. R. Soc. London*, ser A, Vol. 266, pp. 123-192.

Bagtzoglou, A C, Dougherty, D E and Tompson, A F B. (1992), Application of particle methods to reliable identification of groundwater pollution sources, *Water Resources Management*, Vol 6, pp.15-23.

Bagtzoglou, A C and Atmadja, J. (2003), Marching-jury backward beam equation and quasi-reversibility methods for hydrologic inversion: Application to contaminant plume spatial distribution recovery, *Water Resources Research*,Vol. 39, no. 2, 1038.

Batu, V.(1993) A generalized two-dimensional analytical solute transport model in bounded media for flux-type finite multiple sources, *Water Resources Research*, Vol. 29, no. 8, pp. 2881-2892.

Bear, J.(1972) *Dynamics of fluids in porous media*, Elsevier Science publishing Co., New York, USA.

Bear, J. (1979) *Hydraulics of Groundwater*, McGraw-Hill, New York.

Beck, J, Blackwell, B, and Clair, C R. (1985) *Inverse Heat Conduction, Illposed problems*, Wiley Interscience, New York, USA.

Bell, L S, Binning, P J, Kuczera, G and Kau, P M. (2002), Rigorous uncertainty assessment in contaminant transport inverse modelling: a case study of floride diffusion through clay liners, *Journal of Contaminant Hydrology*, Vol. 57, pp. 1-20.

Brebbia, C. A. (1978) *The Boundary Element Method for engineers*, Pentech press , Great Britain.

Brezinski, C, Rodriguez, G and Seatzu, S. (2008) Error estimates for linear systems with applications to regularization, *Numerical Algorithms*, Vol. 49, pp.85–104.

Chu, W, Gao, X, and Sorooshian, S. (2010) Improving the shuffled complex evolution scheme for optimization of complex nonlinear hydrological systems: Application to the calibration of the Sacramento soil moisture accounting model, *Water Resources Research*, Vol. 46, W09530.

Contractor, D N and Jenson, J W.(2000) Simulated effect of vadose infiltration on water levels in the Northern Guam lens aquifer, *Journal of Hydrology*, Vol. 229, pp. 232–245.

Cooper, V A, Nguyen, V T, and Nicell, J A. (1997) Evaluation of global optimisation methods for conceptual rainfall-runoff model calibration, *Water Science Technology*, Vol 36, no.5, pp. 53–60.

Craven, P, and Wahba, G.(1979) Smoothing noisy data with spline functions: estimating the correct degree of smoothing by the method of generalized cross validation, *Numerical Mathematics*, Vol. 31, pp.377–403.

Datta, B, Chakrabarty, D, and Dhar, A. (2009) Simultaneous identification of unknown groundwater pollution sources and estimation of aquifer parameters, *Journal of Hydrology*, Vol. 376, pp.48-57.

Dechaumphai P. (2010) *Finite Element Method: Fundamentals and Applications*, Alpha Science International Ltd, United Kingdom.

Domenico, P A. (1987) An analytical model for multidimensional transport of a decaying contaminant species, *Journal of Hydrology*, Vol. 91, pp.49-58.

Domenico, P A and Schwartz, F W. (1998) *Physical and Chemical Hydrogeology*, Wiley, New York, USA.

Duan, Q, Sorooshian, S, and Gupta, V K.(1992) Effective and efficient Global optimisation for conceptual rainfall runoff models, *Water Resources Research* , Vol. 28, pp.1015-1031.

Duan, Q, Gupta V K, and Sorooshian S.(1993) A shuffled complex evolution approach for effective and efficient global minimisation, *Journal of Optimisation Theory Application*, Vol. 76, no.3, pp.501-521.

Duan, Q A, Sorooshian, S, and Gupta, V K. (1994) Optimal use of the SCE-UA global optimization method for calibrating watershed models, *Journal of Hydrology*, Vol. 158, pp. 265–284.

Engl H W, Hanke M and Neubauer A. (1996) *Regularization of inverse problems*. Mathematics and its applications, vol. 375. Kluwer Academic Publishers, Dordrecht.

Eusuff, M M and Lansey, K E. (2004) Optimal operation of artificial groundwater recharge systems considering water quality transformations, *Water Resources Management*, Vol.18, no. 4, pp. 379-405.

Floudas, C A and Gounaris, C E.(2009) A review of recent advances in global optimization, *Journal of Global Optimization*, Vol.45, pp.3–38.

Freeze, R A and Cherry, J A. (1979) *Groundwater*, Prentice-Hall, New Jersey.

Gan, T Y, Dlamini, E M and Biftu, G F. (1997) Effects of model complexity and structure, data quality, and objective functions on hydrologic modelling, *Journal of Hydrology*, Vol. 192, pp.81-103.

Golub, G H, Heath, M and Wahba, G. (1979) Generalized cross-validation as a method for choosing a good ridge parameter, *Technometrics* ,Vol. 21, no.2, pp. 215–223.

Goldberg, D E. (1989) *Genetic Algorithms in Search, Optimization and Machine Learning*, Addison-Wesley-Longman, Reading, Mass, USA.

Gomulka, J.(1978) Deterministic Versus Probabilistic Approaches to Global Optimization, Toward Global Optimization 2, in Dixon L. C. W. and Szego G. P.(Eds.), North-Holland, Amsterdam, Netherland, pp. 19-29.

Goncharskii, A V, Leonov, A S and Yagola, A G. (1972), A generalized discrepancy principle, *Zh. Vychisl. Mat. Mat. Fiz.* Vol. 2, no. 13, pp. 294-302.

Gorelick, S M, Evans, B, and Remson, I. (1983) Identifying sources of groundwater pollution:An optimisation approach, *Water Resources Research*, Vol.19, no. 3 , pp.779-790.

Gupta, H V, Bastidas, L, Vrugt, J A and Sorooshian S. (2003) Multiple criteria global optimization for watershed model calibration, in Duan Q. (Ed.) *Calibration of Watershed Models*, Water Science and Application, vol. 6, pp. 125– 132, AGU, Washington, D. C.

Hansen, P C.(1992) Analysis of discrete ill-posed problems by means of the L curve, *SIAM Review*, Vol. 34, no.4, pp. 561-580.

Hansen, P C and O'Leary D P.(1993) The use of the L-curve in the regularization of discrete ill-posed problems, *SIAM Journal on Scientific Computing*, Vol.14, no. 6, pp.1487–1503.

Hansen, P C.(2000) The L-curve and its use in the numerical treatment of inverse problems. In: Johnston P, ed. *Computational inverse problems in electrocardiology. Advances in computational bioengineering series*, vol. 4, Southampton, WIT Press.

Harbaugh, A W and McDonald M G. (1996) User's documentation for MODFLOW-96: An update to the U.S. Geological Survey modular finite-difference ground-water flow model, U.S. Geol. Surv. Open File Rep., 96-485, 56 pp.

Harbaugh, A W, Banta, E R, Hill, M C and McDonald, M G. (2000) MODFLOW-2000, the US Geological Survey Modular Ground-Water Model. US Geological Survey Open-File Report 00-92, US Geological Survey, Reston.

Harrouni, K E, Ouazar, D, Walters, G A, and Cheng, A H.-D. (1996) Groundwater optimization and parameter estimation by genetic algorithm and DRBEM, *Engineering analysis with boundary elements*,Vol. 18, pp.287-296.

Harrouni K E, Ouazar, D, Wrobel, L C and Cheng, A H.-D. (1997) Groundwater parameter estimation by optimization and DRBEM, *Engineering analysis with boundary elements* , Vol. 19, pp. 97-103.

Harrouni, K E, Ouazar, D, Wrobel, L C and Cheng, A H.-D. (1997) Aquifer parameter estimation by extended Kalman filtering and boundary elements, *Engineering analysis with boundary elements*, Vol.19, pp.231-237.

He, B, Takase, K and Wang, Y. (2007) Regional groundwater prediction model using automatic parameter calibration SCE method for a coastal plain of Seto Inland Sea, *Water Resources Management* , Vol. 21, pp. 947–959.

Holland, J. (1975) *Adaptation in natural and artificial systems*, Ann Arbor Michigan: University of Michigan press.

Huang, C-H, Li J-X, Kim S. (2008) An inverse problem in estimating the strength of contaminant source for groundwater systems, *Applied mathematical modelling*, Vol.32, pp. 417-431.

Hunt, B. (1977) Calculation of the leaky aquifer function, *Journal of Hydrology*, Vol.33, pp.179–183.

IMSL: 1989, User's Manual, Stat/Library, Version 1.1, IMSL, Inc., Houston, Texas, USA.

Jha, M and Datta, B. (2013) Three-Dimensional Groundwater Contamination Source Identification Using Adaptive Simulated Annealing, *Journal of Hydrologic Engineering*, Vol. 18, pp. 307—317.

Kabanikhin, S I. (2008) Definitions and examples of inverse and ill-posed problems, *Journal of Inverse & Illposed problems*, Vol.16, pp.317-357.

Katsifarakis, K L, Karpouzos, D K and Theodossiou, N. (1999) Combined use of BEM and genetic algorithms in groundwater flow and mass transport problems, *Engineering Analysis with Boundary Element*, Vol. 23, pp. 555–565.

Laloy, E, and Vrugt, J A. (2012) High-dimensional posterior exploration of hydrologic models using multiple-try DREAM and high-performance computing, *Water Resources Research*,Vol. 48, W01526.

Lesnic, D, Elliot, L and Ingham, D B.(1998) A boundary element method for the determinantion of the transimissivity of a heterogenous aquifer in groundwater flow systems, *Engineering Analysis with Boundary Elements*, Vol 21, pp. 223-234.

Li, Z and Mao, X. (2011) Global multiquadric collocation method for groundwater contaminant source identification, *Environmental Modelling & Software*, vol. 26, pp.1611-1621.

Liu, C and Ball, W P. (1999) Application of inverse methods to contaminat source identification from aquitard diffusion profiles at Dover AFB,Delaware, *Water Resources Research*, Vol.35, no.7, pp. 1975-1985.

Mahar, P S and Datta, B. (1997) Optimal monitoring network and ground-water-pollution source identification, *Journal of Water Resource Planning and Management. ASCE*, Vol.123, no.4, pp.199–207.

Mahar, P S and Datta, B. (2000) Identification of pollution sources in transient groundwater system, *Water Resources Management,* Vol.14, pp.209-227.

Mahar, P S and Datta, B. (2001) Optimal Identification of Ground-Water Pollution Sources and Parameter Estimation, *Journal of Water Resources Planning and Management*. Vol.127, 20-29.

Michalak, A M and Kitanidis P K.(2003) A method for enforcing parameter nonnegativity in Bayesian inverse problems with an application to contaminant source identification, *Water Resources Research*, Vol. 39, no.2, 1033, doi:10.1029/2002WR001480.

Michalak, A M and Kitanidis, P K. (2004) Estimation of historical groundwater contaminant distribution using the adjoint state method applied to geostatistical inverse modeling, *Water Resources Research*, Vol.40, W08302, doi:10.1029 /2004WR003214.

Madsen, H. (2000) Automatic calibration of a conceptual rainfall-runoff model using multiple objectives, *Journal of Hydrology*, Vol. 235, pp. 276-288.

Mahinthakumar, G. and Sayeed, M. (2005) Hybrid genetic algorithm- Local search methods for solving groundwater source identification inverse problems, *Journal of water resources planning and management.* Vol.131, pp.45-57.

Mariani, V C and Coelho, L S. (2011) A hybrid shuffled complex evolution approach with pattern search for unconstrained optimization, *Mathematics and Computers in Simulation*, Vol.81, pp. 1901-1909.

Mariño, M. A. (1974) Longitudinal dispersion in saturated porous media, *Journal of the Hydraulics Division, ASCE,* Vol.100, pp.151-157.

Natalini, B, and Popov R.(2004) An alternative approach for calculation of the first and higher order derivatives in the DRM-MD, *Engineering Analysis with Boundary Elements*, Vol.28,pp.61-78 (2004).

National Research Council(1990) Groundwater models-Scientific and Regulatory Applications, National Academy Press, Washington D.C.,USA.

Nardini, D and Brebbia, C. A. (1983) A new approach to free vibration analysis using boundary elements, *Applied Mathematical Modelling*, Vol.7, pp.157–162.

Ndiritu, J. G. (2009) Automatic calibration of the Pitman model using the Shuffled complex evolution method, WRC KV 229/09.

Ndiritu, J G and Daniell, T M. (2001) An improved genetic algorithm for rainfall-runoff model calibration and function optimization, *Mathematical and Computer Modelling*, Vol. 33, pp. 695–706.

Nelder, J A and Mead, R. (1965) A simplex method for function minimization, *Journal of Computing*, Vol. 7, pp. 308–313.

Neuman, S P (1973) Calibration of distributed parameter groundwater flow models viewed as multiple-objective decision process under uncertainty, *Water Resources Research*, Vol.9, no. 4, pp. 1006-1021.

Neupauer, R M and Wilson J L. (2001) Adjoint-derived location and travel time probabilities for a multi-dimensional groundwater system, *Water Resources Research*, Vol.37, no.6, pp. 1657-1668.

Neupauer, R M and Wilson J L. (2004) Numerical implementation of a backward probabilistic model of groundwater contamination, *Ground Water*, Vol.42, no.2, pp.175–189.

Neupauer, R M and Lin R. (2006) Identifying sources of a conservative groundwater contaminant using backward probabilities conditioned on measured concentrations, *Water Resources Research*, Vol. 42, W03424, doi:10.1029/2005WR004115.

Neupauer, R M, Borchers B and Wilson, J L. (2000) Comparison of inverse methods for reconstructing the release history of a groundwater contamination source, *Water Resources Research*, Vol.36, no.9, pp.2469– 2475.

Ogata, A and Banks, R B.(1961) A solution of the differential equation of longitudinal dispersion in porous media, *U.S Geological Survey Professional Paper*, 411-A, pp. A1-A9.

Onyejekwe, O O, Toolsi, S.(2001) Certain aspects of Green element computational model for BOD-DO Interaction, *Advances in Water Resources*, Vol. 24, pp.125-131.

Popov, V, and Power H.(1999) The DRM-MD integral equation method: An efficient approach for the numerical solution of domain dominant problems, *International Journal for Numerical methods in Engineering*, Vol. 44, no.3, pp. 327-353.

Prakash, O and Datta, B.(2014) Characterization of groundwater pollution sources with unknown release time history, *Journal of Water Resource and Protection*, Vol. 6, pp.337-350.

Price, W. L.(1978) A Controlled Random Search Procedure for Global Optimization, Toward Global Optimization 2, Edited by L. C. W. Dixon and G. P. Szego, North-Holland, Amsterdam, Holland, pp. 71-84.

Price, W. L.(1983) Global Optimization by Controlled Random Search, *Journal of Optimization Theory and Applications*, Vol. 40, pp. 333-348.

Price, W. L.(1987) Global Optimization Algorithms for a CAD Workstation, *Journal of Optimization Theory and Applications*, Vol. 55, pp. 133-146.

Qiu, Z H,Wrobel, L C and Power, H. (1998) Numerical solution of the convection-diffusion problems at high Peclet number using Boundary elements, *International journal for numerical methods in engineering*, Vol. 41, pp. 899-914.

Sidauruk, P, Cheng, A H-D and Ouazar, D. (1998)Ground water contaminant source and transport parameter identification by correleration coefficient optimization, *GROUND WATER* Vol.36, no.2, pp. 208-214.

Singh, R M, Datta, B and Jain, A.(2004) Identification of unknown groundwater pollution sources using artificial neural networks, *Journal of Water Resources Planning Management*, Vol.130, no. 6, pp. 506–514.

Singh, R M and Datta, B.(2006) Identification of groundwater pollution sources using GA-based linked simulation optimization model, *Journal of Hydrologic Engineering*, Vol.11, no.2, pp. 101–109.

Skaggs, T H and Kabala, Z J. (1994) Recovering the release history of a groundwater contaminant, *Water Resources Research*, Vol. 30, no.1, pp. 71-79.

Skaggs, T H and Kabala, Z J. (1995) Recovering the history of a groundwater contaminant plume: Method of Quasi-Reversibility, *Water Resources Research*, Vol.31, no.11, pp. 2669-2673.

Solomatine, D P, Dibike, Y B and Kukuric, N. (1999) Automatic calibration of groundwater models using global optimization techniques, *Hydrological Sciences–Journal–des Sciences Hydrologiques*, Vol. 44, no.6, pp. 879-894.

Sorooshian, S, Duan, Q, and Gupta, VK. (1993) Calibration of Rainfall-Runoff Models: Application of Global Optimization to the Sacramento Soil Moisture Accounting Model, *Water Resources Research*, Vol. 29, no.4, pp. 1185-1194.

Snodgrass, M F and Kitanidis, P K.(1997) A geostatistical approach to contaminant source identification, *Water Resources Research*, Vol. 33, pp.537-546.

Sun, N-Z. (1996) *Mathematical modelling of Groundwater pollution*, New York, USA: Springer-Verlag.

Sun, N-Z. (1999) *Inverse problems in Groundwater Modelling:Theory and applications of transport in porous media*, The Netherlands: Kluwer Academic publishers.

Sun A Y, Painter S L and Wittmeyer G W. (2006) A constrained robust least squares approach for contaminant release history identification, *Water Resources Research*,Vol.42, W04414.

Taigbenu A E and Liggett J. (1985) Boundary Element calculations of Diffusion Equation, *Journal of Engineering mechanics*, Vol. 111, no.3, pg. 311-328.

Taigbenu A E. (1995) The Green element method, *International Journal for Numerical Methods in Engineering*, Vol.(38), pp.2241-2263.

Taigbenu, A E. (1999) Three Green Element Models for the Diffusion-Advection Equation and their Stability Characteristics, *Engineering Analysis Boundary Elements*, Vol. 23, pg. 577-589.

Taigbenu, A.E. (2001) Unsaturated-Flow Simulation with Green Element Models, *Journal of Hydraulic Engineering ASCE*, Vol. 127, pp.307–312.

Taigbenu, A.E. (2001) Simulations of unsaturated flow in multiply zoned media by Green element models, *Transport Porous Media*, Vol.45, pp.387–406.

Taigbenu, A.E. (2003a) Features of a time-dependent fundamental solution in the Green Element Method, *Applied Mathematical Modeling*, Vol. 27, no.2, pp.125–143.

Taigbenu, A.E. (2003c) A time-dependent Green's function-based model for stream-unconfined aquifer flows, *Water SA*, Vol. 29, no.3, pp. 257–265.

Taigbenu A. E. (2007) Convection-dominant transport simulations with the flux Green element method, Advances in Boundary Element Techniques VIII.

Taigbenu, A E and Onyejekwe, O O (2000) A flux-correct Green element model of quasi three-dimensional multiaquifer flow, *Water Resources Research*, Vol. 36, no.12, pp. 3631–3640.

Taigbenu, A. E. (2010) *The Green Element Method*, The Netherlands: Kluwer Academic Publishers.

Taigbenu, A.E. (2012) Enhancement of the accuracy of the Green element method: Application to potential problems, *Engineering Analysis Boundary Elements*, Vol. 36, pp.125-136.

Taigbenu, A. E. (2015) Inverse solutions of temperature, heat flux and heat source by the Green element method, *Applied Mathematical modelling* , Vol. 39, pp. 667-681.

Taigbenu, A E and Ndiritu J G. (2012) Green element solutions to inverse heat conduction problems, 13th International Conference on Boundary Element and Meshless Techniques,3-5 September, Prague, Czech Republic.

Tanakamaru, H and Burges, S J. (1996) Application of global optimization to parameter estimation of the TANK model, *Proc., Int. Conference, Water Resour. and Environ. Res.* Kyoto Japan, 39-46.

Tang, Y, Reed, P and Wagener, T. (2006) How effective and efficient are multiobjective evolutionary algorithms at hydrologic model calibration? *Hydrol. Earth Syst. Sci.,* Vol.10,pp. 289-307.

Tian, N, Jun, S, Wenbo, X and Choi-Hong, L. (2011) An improved quantum behaved particle swarm optimization with perturbation operator and its application in estimating groundwater contaminant source, *Inverse Problems in Science and Engineering*, Vol. 19, no.2,pp. 181-202.

Tikhonov, A N and Arsenin, VY. (1977) *Solutions of Ill-Posed Problems*, Washington, DC, V.H. Winston & Sons.

Thyer, M, Kuczera, G and Bates, B C. (1999) Probabilistic optimization for conceptual rainfall-runoff models: A comparison of the Shuffled complex evolution and simulated annealing algorithms, *Water Resources Research*. Vol. 35, no.3,pp. 767-773.

Torn, A, (1978) A Search Clustering Approach to Global Optimization, Toward Global Optimization 2, Edited by L. C. W. Dixon and G. P. Szeg6, North-Holland, Amsterdam, Holland, pp. 49-62.

Tung, C P, Tang, C C, and Lin, Y P.(2003) Improving groundwater-flow modelling using optimal zoning methods, *Environmental Geology*, Vol. 44, no.6, pp. 627–38.

Van Genuchten M. Th. (1981) Analytical solutions for chemical transport with simultaneous adsorption, zero order production and first order decay, *Journal of Hydrology*, Vol. 49, pp. 213-233.

Voss, C I (1984) A finite element simulation model for saturated-unsaturated fluid density dependent groundwater flow with energy transport or chemically reactive single species solute transport, U. S. Geological Survey Water Resources Investment Report, pp.84-4369.

Vrugt, J A, Gupta, H V, Bouten, W and Sorooshian S.(2003) A Shuffled Complex Evolution Metropolis algorithm for optimization and uncertainty assessment of hydrologic model parameters, *Water Resources Research*, Vol.39, no.8,1201.

Vrugt, J A, Gupta H V, Bastidas L A, Bouten W and Sorooshian S.(2003) Effective and efficient algorithm for multiobjective optimization of hydrologic models, *Water Resources Research*, Vol. 39, no.8, 1214, doi:10.1029/2002WR001746.

Wagner, B. J. (1992) Simultaneous parameter estimation and contaminant source characterisation for coupled groundwater flow and contaminant flow and contaminant transport modelling, *Journal of Hydrology*, Vol.135, pp. 275-303.

Wang, Y, Yu, P and Yang, T. (2010) Comparison of genetic algorithms and shuffled complex evolution approach for calibrating distributed rainfall-runoff model, *Hydrological processes*, Vol. 24 , pp.1015-1026.

Wilson, J L and Liu J. (1994), Backward tracking to find the source of pollution, in Waste Management: From Risk to Remediation, vol. 1, edited by R. Bhada *et al.*, pp. 181– 199.

Woodbury, A D and Ulrych T J. (1996) Minimum relative entropy inversion: Theory and application to recovering the release history of a groundwater contaminant, *Water Resources Research*, Vol. 32, no. 9, pp. 2671–2681.

Yapo P O, Gupta H V and Sorooshian S. (1998) Multi-objective global optimization for hydrologic models, *Journal Hydrology*,Vol. 204, pp. 83–97.

Yeh, W-G. (1986) Review of parameter identification procedures in groundwater hydrology: The inverse problem, *Water Resources Research*, Vol. 22, no.2, pp. 95-108.

Yeh, H. D, Chang T H., and Lin Y C. (2007) Groundwater contaminant source identification by a hybrid heuristic approach, *Water Resources Research*, vol.43, W09420, doi:10.1029/2005WR004731.

Zhijia, L, Penglei, X and Jiahui, T. (2013) Study of the Xinanjiang model parameter calibration, *Journal of hydrologic Engineering*, Vol.18, pp. 1513-1521.

APPENDICES

Appendix A: Detailed solutions for Case study in Section 5.5 with $\Delta t = 3$.

Table A1: Model 1 computed pollution source strength with exact data.

Time (months)	Regularization parameter	Mean error (%)	Computed source strength (ε=0%)	
			Source 1	Source 2
3	1.99E-09	0.0008	46.99	30.01
6	1.99E-09	0.005	15.07	59.57
9	1.99E-09	0.0019	46.80	0.09
12	1.99E-09	0.0071	0.08	35.43
15	1.99E-09	0.0062	0.00	0.02
18	1.99E-09	0.0045	0.02	0.06
21	1.99E-09	0.0065	0.00	0.01
24	1.99E-09	0.0056	0.01	0.01
27	1.99E-09	0.0065	0.02	0.03
30	1.99E-09	0.0041	0.01	0.01
33	1.99E-09	0.0111	0.00	0.00
36	1.99E-09	0.0075	0.01	0.01
39	1.99E-09	0.0076	0.00	0.00
42	1.99E-09	0.0156	0.00	0.00
45	1.99E-09	0.0076	0.00	0.00
48	1.99E-09	0.0111	0.00	0.00
51	1.99E-09	0.0108	0.00	0.00
54	1.99E-09	0.0183	0.00	0.00
57	1.99E-09	0.0139	0.00	0.00
60	1.99E-09	0.0172	0.00	0.00

Table A2: Model 1 computed source strength with ε=1% in observation data.

Time (months)	Regularization parameter	Mean error (%)	Computed source strength (ε=1%)	
			Source 1	Source 2
3	1.99E-09	0.0055	47.34	29.86
6	1.99E-09	0.0053	14.76	59.61
9	1.99E-09	0.0021	46.80	0.07
12	1.99E-09	0.0069	0.09	35.47
15	1.99E-09	0.0065	0.01	0.10
18	1.99E-09	0.0041	0.03	0.05
21	1.99E-09	0.007	0.01	0.03
24	1.99E-09	0.0058	0.00	0.01
27	1.99E-09	0.007	0.02	0.04
30	1.99E-09	0.0041	0.01	0.01
33	1.99E-09	0.0114	0.01	0.00
36	1.99E-09	0.0074	0.00	0.01
39	1.99E-09	0.0076	0.01	0.00
42	1.99E-09	0.015	0.00	0.00
45	1.99E-09	0.007	0.00	0.00
48	1.99E-09	0.0114	0.00	0.00
51	1.99E-09	0.0111	0.00	0.00
54	1.99E-09	0.0186	0.00	0.00
57	1.99E-09	0.0142	0.00	0.00
60	1.99E-09	0.0175	0.00	0.00

Table A3: Model 1 computed source strength with ε=3% in observation data.

Time (months)	Regularization parameter	Mean error (%)	Computed source strength (ε=3%)	
			Source 1	Source 2
3	1.99E-09	0.0167	48.11	29.56
6	1.99E-09	0.0074	14.14	59.65
9	1.99E-09	0.0034	46.80	0.04
12	1.99E-09	0.0066	0.13	35.53
15	1.99E-09	0.0083	0.02	0.27
18	1.99E-09	0.0047	0.04	0.03
21	1.99E-09	0.0092	0.02	0.06
24	1.99E-09	0.0084	0.01	0.07
27	1.99E-09	0.0086	0.03	0.05
30	1.99E-09	0.0049	0.00	0.00
33	1.99E-09	0.0129	0.01	0.01
36	1.99E-09	0.0084	0.00	0.01
39	1.99E-09	0.0088	0.01	0.00
42	1.99E-09	0.0151	0.01	0.01
45	1.99E-09	0.0085	0.00	0.00
48	1.99E-09	0.0123	0.00	0.00
51	1.99E-09	0.0115	0.00	0.00
54	1.99E-09	0.019	0.00	0.00
57	1.99E-09	0.0146	0.00	0.00
60	1.99E-09	0.0179	0.00	0.00

Table A4: Model 1 computed source strength with ε=5% in observation data.

Time (months)	Regularization parameter (α)	Relative error (%)	Computed source strength (ε=5%)	
			Source 1	Source 2
3	1.99E-09	0.028	48.84	29.27
6	1.99E-09	0.0103	13.52	59.72
9	1.99E-09	0.0051	46.80	0.00
12	1.99E-09	0.0066	0.16	35.60
15	1.99E-09	0.0108	0.03	0.44
18	1.99E-09	0.0065	0.05	0.02
21	1.99E-09	0.0123	0.04	0.09
24	1.99E-09	0.0124	0.03	0.12
27	1.99E-09	0.0108	0.05	0.07
30	1.99E-09	0.0063	0.00	0.00
33	1.99E-09	0.0153	0.01	0.02
36	1.99E-09	0.0103	0.01	0.01
39	1.99E-09	0.0111	0.02	0.00
42	1.99E-09	0.0166	0.01	0.01
45	1.99E-09	0.0119	0.00	0.00
48	1.99E-09	0.0135	0.00	0.00
51	1.99E-09	0.012	0.00	0.00
54	1.99E-09	0.0195	0.00	0.00
57	1.99E-09	0.0151	0.00	0.00
60	1.99E-09	0.0184	0.00	0.00